FIRAT UNIVERSITY
GRADUATE SCHOOL OF NATURAL AND APPLIED SCIENCES
TÜRKİYE

SYNTHESIS, THERMAL AND ELECTROCHEMICAL PROPERTIES OF NEW DIPEPTIDE SUBSTITUTED PHTHALOCYANINE COMPLEXES

Sunusi IDRIS

Doctoral Thesis

DEPARTMENT OF CHEMISTRY

FEBRUARY 2025

FIRAT UNIVERSITY
GRADUATE SCHOOL OF NATURAL AND APPLIED SCIENCES
TÜRKİYE

Department of Chemistry

Doctoral Thesis

SYNTHESIS, THERMAL AND ELECTROCHEMICAL PROPERTIES OF NEW DIPEPTIDE SUBSTITUTED PHTHALOCYANINE COMPLEXES

Author
Sunusi IDRIS

Supervisor
Prof. Dr. Sinan SAYDAM

Co-Supervisor
Assoc. Prof. Dr. Eray ÇALIŞKAN

FEBRUARY 2025
ELAZIG

FIRAT UNIVERSITY
GRADUATE SCHOOL OF NATURAL AND APPLIED SCIENCES
TÜRKİYE

Department of Chemistry

Doctoral Thesis

Title:	Synthesis, Thermal and Electrochemical Properties of New Dipeptide Substituted Phthalocyanine Complexes
Author:	Sunusi IDRIS
Submission Date:	13 January 2025
Defense Date:	12 February 2025

THESIS APPROVAL

This thesis, which was prepared according to the thesis writing rules of the Graduate School of Natural and Applied Sciences, Fırat University, was evaluated by the committee members who have signed the following signatures and was unanimously approved after the defense exam made open to the academic audience.

		Signature
Supervisor:	Prof. Dr. Sinan SAYDAM Firat University, Faculty of Science	Approved
Chair:	Prof. Dr. Dursun ÖZER Fırat University, Engineering Faculty	Approved
Member:	Prof. Dr. Mustafa SÜLÜ İnönü University, Faculty of Science and Arts	Approved
Member:	Prof. Dr. Ahmet Orhan GÖRGÜLÜ Marmara Üniversity, Faculty of Science	Approved
Member:	Prof. Dr. Kenan KORAN Fırat University, Faculty of Science	Approved

This thesis was approved by the Administrative Board of the Graduate School on

..... / ..... / 20 .....

Signature

Prof. Dr. Burhan ERGEN
Director of the Graduate School

DECLARATION

I hereby declare that I wrote this Doctoral Thesis titled “Synthesis, Thermal and Electrochemical Properties of New Dipeptide Substituted Phthalocyanine Complexes” in consistent with the thesis writing guide of the Graduate School of Natural and Applied Sciences, Firat University. I also declare that all information in it is correct, that I acted according to scientific ethics in producing and presenting the findings, cited all the references I used, express all institutions or organizations or persons who supported the thesis financially. I have never used the data and information I provide here in order to get a degree in any way.

12 February 2025

Sunusi IDRIS

PREFACE

Phthalocyanines are aromatic, macromolecular, intensely blue-green heterocyclic compounds with an innermost ring system consisting of 18 π-electrons configurations from 8 carbons and 8 nitrogen atoms forming four iminoisoindoline groups of pyrrole unit linked by four aza (—N=C—) groups at the α-carbon of pyrrole unit to form **four** aza bridges and four phenylene rings.

These compounds possess properties of being easily modified with various substituents and forming or generating diverse properties depending on the substituents, electronic structure, and the type of metal ion coordinated into the central cavity of the compound coursing it acquired wide applications in several scientific and technological areas. The structures and characterization of the synthetic compounds were analyzed by various spectroscopies techniques such as ^{1}H-NMR, ^{13}C-NMR, UV-Vis, and FT-IR spectroscopy

I want to express my gratitude to almighty Allah for making this thesis on phthalocyanines a reality. However, it would not have been possible without the kind support and help of many individuals, we would like to extend our sincere thanks to all of them. I would also like to thank my esteemed advisor Prof. Dr. Sinan SAYDAM and Assoc. Dr. Eray ÇALIŞKAN who's Never withholding their interest and support for me during my thesis studies. My profound gratitude also goes to Prof. Dr. Kenan KORAN and Assoc. Prof. Dr. Fatih BİRYAN of which all the dipeptides synthesis was conducted from their research laboratory. I also extend my thanks to my former advisor Prof. Dr. A. Orhan GÖRGÜLÜ, who transferred his service from Firat University to Marmara University, Istanbul, and Prof. Dr. Süleyman SERVİ and Prof. Dr. Fikret KARATAS.

Finally, my regards to my dear wife, Bilkisu Muhammad, RUDWAN for her patience, and prayers and for overseeing the affairs of the family in my absence. I am indebted to my late mother Zainab IDRIS and father Idris MUSA; whose prayers keep me going throughout my life.

Sunusi IDRIS
ELAZIG, 2025

TABLE OF CONTENTS

ABSTRACT

Synthesis, Thermal and Electrochemical Properties of New Dipeptide Substituted Phthalocyanine Complexes

Sunusi IDRIS

Doctoral Thesis

FIRAT UNIVERSITY
Graduate School of Natural and Applied Sciences

Department of Chemistry

February 2025, Page: xxi + 115

Phthalocyanines are macrocyclic compounds with 18-π electrons delocalization consisting of four iminoisoindoline units. These compounds have application potential in many scientific and technological fields due to their interesting electronic structures, stability, physical and chemical properties. In view of this great feature, studies on the synthesis and properties of phthalocyanine and its derivatives are increasing exponentially among many research groups.

The purpose of this study is to synthesize a series of novel tetra substituted dipeptide amino acid phthalocyanines complexes bearing Tyrosine base dipeptide amino acid as substituent such as methyl (tert-butoxycarbonyl)-*L*-tyrosyl-*D*-phenylalaninate, methyl(tert-butoxycarbonyl)-*L*-tyrosyl-*D*-alaninate, methyl(tert-butoxycarbonyl)-*L*-tyrosylglycinate and Methyl (tert-butoxycarbonyl)-*L*-tyrosyl-*L*-valinate were synthesis through peptide coupling reaction. These compounds was reacted with 4-nitrophthalonitrile to form methyl ((*S*)-2-((tert-butoxycarbonyl) amino)-3-(4-(3,4-dicyanophenoxy) phenyl) propanoyl)-*D*-phenylalaninate, methyl ((*S*)-2-((tert-butoxycarbonyl) amino)-3-(4-(3,4-dicyanophenoxy) phenyl) propanoyl)-*D*-alaninate, methyl ((*S*)-2-((tert-butoxycarbonyl) amino)-3-(4-(3,4-dicyanophenoxy) phenyl) propanoyl)glycinate and methyl ((*S*)-2-((tert-butoxycarbonyl) amino)-3-(4-(3,4-dicyanophenoxy) phenyl) propanoyl)-*L*-valinate ligands respectıvely. The structures of the synthesized dipeptides were elucidated by elemental analysis, melting point, FT-IR, ^{1}H NMR, ^{13}C NMR, and mass spectroscopies methods while the ligands were verified by only FT-IR and ^{1}H NMR spectroscopies methods. The synthesized ligands undergo cyclotetramerization reactions in the presence of Cr(III), Mn(II), Fe(II), Co(II), Ni(II), Cu(II), or Zn(II) acetate salts respectively to form the complexes. IR and UV-visible spectroscopies methods clarified the formation of these synthesized complexes. The thermal behavior of the complexes was investigated by thermogravimetric analysis (TGA) and differential thermal analysis (DTA). Furthermore, Electrochemical properties of phthalocyanine complexes were conducted by Cyclic and Square wave voltammetry analysis techniques in non-aqueous solvent.

Keywords: Phthalocyanine, Dipeptide, Tyrosine, Alanine, Valine, Glycine, Phenylalanine, Macromolecule, Thermal analysis, Electrochemistry.

ÖZET

Yeni Dipeptit Sübstitüe Ftalosiyanin Komplekslerinin Sentezi, Termal ve Elektrokimyasal Özellikleri

Sunusi IDRIS

Doktora Tezi

FIRAT ÜNİVERSİTESİ
Fen Bilimleri Enstitüsü

Kimya Anabilim Dalı

Şubat 2025, Sayfa: xxi + 115

Ftalosiyaninler, dört iminoizoindolin biriminden oluşan 18-π elektron delokalizasyonuna sahip makrosiklik bileşiklerdir. Bu bileşikler, ilginç elektronik yapıları, termal kararlılıkları, fiziksel ve kimyasal özellikleri nedeniyle birçok bilimsel ve teknolojik alanda uygulama potansiyeline sahip bileşiklerdir. Bu önemli özellik göz önüne alındığında, ftalosiyanin ve türevlerinin sentezi ve özellikleri üzerine yapılan çalışmalar katlanarak artmaktadır.

Bu çalışmanın amacı, metil (tert-butoksikarbonil)-*L*-tirozil-*D*-fenilalaninat, metil (tert-butoksikarbonil)-*L*-tirozil-*D*-alaninat, metil (tert-butoksikarbonil)-*L*-tirozilglisinat ve metil (tert-butoksikarbonil)-L-tirozil-*L*-valinat gibi tirozin bazlı dipeptit amino asidini ikame edici olarak kullanan bir dizi yeni tetra dipeptit amino asit sübstitüentli ftalosiyanin komplekslerini sentezlemektir. Dipeptit bileşiklerinin 4-nitroftalonitril ile reaksiyonu sonucu sırasıyla metil ((S)-2-((tert-butoksikarbonil) amino)-3-(4-(3,4-disiyanofenoksi) fenil) propanoil)-*D*-fenilalaninat, metil ((S)-2-((tert-butoksikarbonil) amino)-3-(4-(3,4-disiyanofenoksi) fenil) propanoil)-*D*-alaninat, metil ((S)-2-((tert-butoksikarbonil) amino)-3-(4-(3,4-disiyanofenoksi) fenil) propanoil)glisinat ve metil ((S)-2-((tert-butoksikarbonil) amino)-3-(4-(3,4-disiyanofenoksi) fenil) propanoil)-*L*-valinat ligandları oluşturuldu. Sentezlenen yeni dipeptit ftalonitril bileşiklerinin yapıları elementel analiz, erime noktası, FT-IR, ^{1}H NMR, ^{13}C NMR ve kütle spektroskopisi yöntemleri ile karekterize edildi. Sentezlenen ligandların, birinci sıra geçiş metali ftalosiyanin komplekslerini oluşturmak için sırasıyla Cr(III), Mn(II), Fe(II),Co(II), Ni(II), Cu(II) ve Zn(II) asetat tuzlarının varlığında siklotetramerizasyon reaksiyonlarına tabi tutuldu. Sentezlenen komplekslerin oluşumu IR ve UV-görünür spektroskopi yöntemleri ile açıklığa kavuşturuldu. Komplekslerin termal davranışı termogravimetrik analiz (TGA) ve diferansiyel termal analiz (DTA) ile incelendi. Ayrıca, ftalosiyanin komplekslerinin elektrokimyasal özellikleri susuz ortamda Dönüşümlü ve Kare dalga voltametri teknikleri kullanılarak gerçekleştirildi.

Anahtar Kelimeler: Ftalosiyanin, Dipeptit, Tirosin, Alanin, Valin, Glisin, Fenilalanin, Makromolekül, Termal analiz, Elektrokimya

LIST OF FIGURES

Page

LIST OF TABLES

Page

LIST OF APPENDICES

Page

LIST OF APPENDICES

SYMBOLS AND ABBREVIATIONS

Abbreviations

(1) : Phthalimide

(2) : 4-Nitrophthalimide

(3) : 4-Nitrophthalamide

(4) : 4-Nitrophthalonitrile

(5) : (tert-butoxycarbonyl)-*L*- tyrosine **(Boc-Tyr-OH)**

(6) : **(Boc-Tyr-Phe-OCH_3)** Methyl (tert-butoxycarbonyl)-*L*- tyrosyl-*D*-phenylalaninate

(7) : methyl ((S)-2-((tert-butoxycarbonyl) amino)-3-(4-(3,4-dicyanophenoxy) phenyl) propanoyl)-*D*- phenylalaninate **(Boc-Tyr-Phe-OCH_3-O-PN) (7)**

(8) : **(Boc-Tyr-Ala-OCH_3)** Methyl (tert-butoxycarbonyl)-*L*- tyrosyl-*D*-alaninate

(9) : methyl ((S)-2-((tert-butoxycarbonyl) amino)-3-(4-(3,4-dicyanophenoxy) phenyl) propanoyl)-*D*- alaninate **(Boc-Tyr-Ala-OCH_3-O-PN) (9)**

(10) : **(Boc-Tyr-Gly-OCH_3)** Methyl (tert-butoxycarbonyl)-*L*- tyrosyl glycinate

(11) : methyl ((S)-2-((tert-butoxycarbonyl) amino)-3-(4-(3,4-dicyanophenoxy) phenyl) propanoyl) glycinate **(Boc-Tyr-Gly-OCH_3-O-PN) (11)**

(12) : **(Boc-Tyr-Val-OCH_3)** Methyl (tert-butoxycarbonyl)-*L*- tyrosyl-*L*-valinate

(13) : methyl ((S)-2-((tert-butoxycarbonyl) amino)-3-(4-(3,4-dicyanophenoxy) phenyl) propanoyl)-*D*- valinate **(Boc-Tyr-Val-OCH_3-O-PN) (13**

Pc : Phthalocyanine

MPc : Metallic Phthalocyanine

CrPc : Chromium Phthalocyanine

MnPc : Manganese Phthalocyanine

FePc : Iron Phthalocyanine

CoPc : Cobalt Phthalocyanine

NiPc : Nickel Phthalocyanine

CuPc : Copper Phthalocyanine

ZnPc : Zinc Phthalocyanine

$LnPc_2$: Lanthanum Bisphthalocyanines

$LuPc_2$: Lutetium Bisphthalocyanines

H_2Pc : Metal-Free Phthalocyanine

HOMO : Highest occupied molecular orbital

LUMO : Lowest unoccupied molecular orbital

PDT : Photodynamic Therapy

NIR : Near-infrared

ROS : Reactive Oxygen Species

VOC : Volatile Organic Compounds

GOx : Glucose Oxidase

ORR : Oxygen Reduction Reaction

HER : Hydrogen Evolution Reaction

CO_2RR : Carbon-dioxide Reduction

OPVs : Organic Photovoltaics

EDOT : 3,4-ethylene dioxythiophene

DMF : Dimethylformamide

DMAE : Dimethylaminoethanol

DMSO : Dimethyl sulfoxide

CDMT : 2-Chloro-4,6-dimethoxy-1,3,5-triazine

NMM : N-methyl morpholine

THF : Tetrahydrofuran

TEA : Triethanolamine

SI-L1 : methyl ((S)-2-((tert-butoxycarbonyl) amino)-3-(4-(3,4-dicyanophenoxy) phenyl) propanoyl)-*D*- phenylalaninate (Boc-Tyr-Phe-OCH_3-O-PN) **(7)**

SI-L2 : methyl ((S)-2-((tert-butoxycarbonyl) amino)-3-(4-(3,4-dicyanophenoxy) phenyl) propanoyl)-*D*- alaninate (Boc-Tyr-Ala-OCH_3-O-PN) **(9)**

SI-L3 : methyl ((S)-2-((tert-butoxycarbonyl) amino)-3-(4-(3,4-dicyanophenoxy) phenyl) propanoyl) glycinate (Boc-Tyr-Gly-OCH_3-O-PN) **(11)**

SI-L4 : methyl ((S)-2-((tert-butoxycarbonyl) amino)-3-(4-(3,4-dicyanophenoxy) phenyl) propanoyl)-*D*- valinate (Boc-Tyr-Val-OCH_3-O-PN) **(13**

Fe/Fe^+ : Ferrocene/Ferrocenium pair

TBAFB : Tetra butyl ammonium tetrafluoroborate

DMF : Dimethyl formamide

DMSO : Dimethyl sulfoxide

THF : Tetrahydrofuran

NMR : Nuclear Magnetic Resonance

FT-IR : Infrared

UV : Ultraviolet

TGA : Thermo Gravimetric Analysis

DTA : Differential Thermal Analysis

CV : Cyclic Voltammetry, Cyclic Voltammogram

SWV : Square Wave Voltammetry, Square Wave Voltammogram

1. INTRODUCTION

Phthalocyanines (Pcs) have been the subject of a wide range of research for over 100 years. This has led to the synthesis of both metal and non-metal varieties of substituted Pcs [1]. Given that, the main purpose for these substitutions was to enhance the properties and diversify the applications of Pcs into broader scientific and technological aspects. Pcs with an 18-π electron configuration from 8 carbons and 8 nitrogen-containing atoms in the innermost ring, are stable and useful chemical substances [2, 3]. Pcs have several applications in materials science, including gas sensor, biosensors and chemical sensors, molecular solar cells, industrial catalytic systems, photodynamic cancer therapy [4], optical data storage, printer inks, nonlinear optic, nanotechnology, electrochromic displays, electrochemical and electrical applications [1, 5, 6, 7, [8, [9].

The spectroscopic characteristics of phthalocyanines can vary significantly on account of the difference in substituent attachment [3, 10, 11]. Therefore, Pc possesses properties of being easily modified with various substituents and forming or generating diverse properties depending on the substituent [12, 13]. Because the bulk properties of a Pcs macromolecule are substantially tied to the characteristics of distinct molecules, different alterations to these individual compounds have been attempted to increase their efficiency as advanced materials [7, 14].

In recent years, dipeptide substitutions have become a noteworthy strategy to improve the solubility, biocompatibility, thermal stability [12, 15], photophysical, photochemical, and electrochemical properties of phthalocyanines. The combination of different dipeptides such as alanine, glycine, valine, and tyrosine-phenylalanine with phthalocyanines offers new ways to improve the properties of these macrocyclic compounds [16, 17, 18, 19]. Research has focused on developing novel functional structures employing peptides and their derivatives, taking into account the function of both amino acids and peptides [20]. The growing use of Pcs as advanced materials has encouraged us to research the synthesis of new derivative materials that differ in the central metal ion or the peripheral substituents. For this reason, our attention has been focused on the synthesis of phthalocyanine with new substituents like amino acid derivatives such as dipeptides [21].

The synthesis of functional group substituted metallo-phthalocyanines initiates by substituting the phthalocyanine core with suitable functional groups. These functional groups enable the coupling of dipeptides at peripheral or axial positions of the phthalocyanine core. The synthesis involves a combination of organic and inorganic synthesis methods and is optimized based on the chemical structure of the compounds. These strategic modifications significantly affect the solubility and chemical stability of the compounds [1, 18, 22, 23].

The goal of assembling peptides into Pc is to enhance the effectiveness of the desired molecules. The usage of peptide conjugates in macro molecule design has increased in recent years, making the synthesis of these families of molecules crucial [12, 24, 25].

The objective of this study is to synthesize a new tetra dipeptide substituted metallo phthalocyanines using a cyclotetramerization approach [24, 25, 26, 27] and characterize and evaluate their thermal and electrochemical properties. The characterization of the complex can be successfully achieved through FT-IR and UV-vis spectroscopies [28]. Generally, two characteristic peaks are usually seen in the UV-visible spectrum of phthalocyanine complexes with or without metals. The presence of these peaks can be used to estimate whether a phthalocyanine complex is formed and whether the complex possesses a metal or non-metal form. The first UV-vis absorption bands of phthalocyanine known as Soret or **B**-band occurs around 320-450 nm due to transitions from the deeper **n** level to the lowest unoccupied molecular orbital (LUMO) (**n→π***) [29]. While the second absorption peak (**Q**-band) occurs around 650-700 nm as a result of transition **(π→π*)** from the highest occupied molecular orbital (HOMO) to (LUMO) [30, 31].

In this work, first-row transition metals Cr, Mn, Fe, Co, Ni, Cu, and Zn were selected to coordinate with four Tyrosine base dipeptides substituted phthalonitrile compounds. The dipeptide was obtained from the coupling reaction [32, 33] of tyrosine amino acid (Boc-Tyr-OH) with methyl esters of phenylalanine (methyl-*L*-phenylalaninate hydrochloride), alanine (methyl-*L*-alaninate hydrochloride), glycine (methyl-*L*-glycinate hydrochloride) and valine (methyl-*L*-valinate hydrochloride) in the presence of coupling reagent 2-chloro-4,6-dimethoxy-1,3,5-triazine (CDMT) and N-Methyl Morpholine (NMM) base as a catalyst as shown by Koran and his co-workers [12] in **Figure 1.1** below**.** The dipeptide was later treated with 4-nitrophthalonitrile in Argon atmosphere with the action of K_2CO_3 to form the dipeptide substituted phthalonitrile. Although there are a few numbers of reports where peptides link as substituents on phthalocyanine [19, 22, 34, 35] there was none of such record published in the literature for dipeptide derivatives.

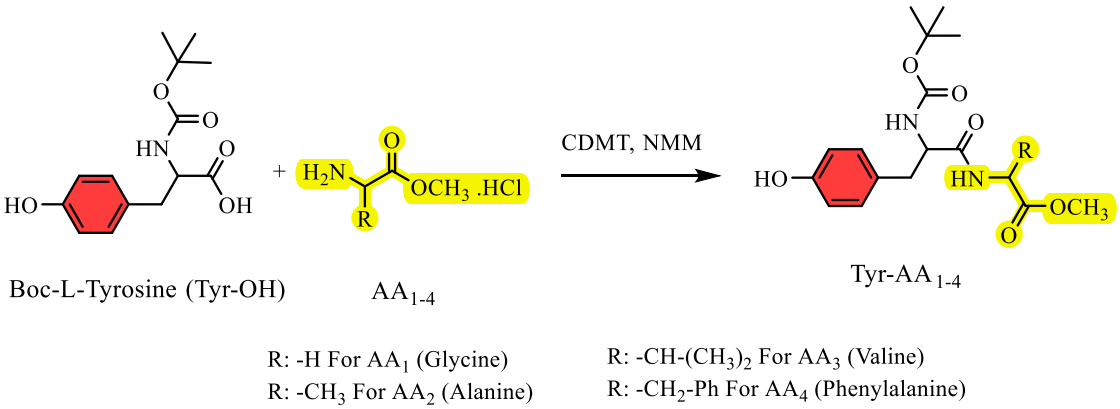

Figure 1.1 Synthetic route for Dipeptide compounds [12]

2. LITERATURE REVIEW

In this chapter, the general information on the historical development, properties, synthetic pathways, and applications of phthalocyanines and some information on dipeptides were described and previous studies in the literature were accessed and reported.

2.1 Historical discoveries of phthalocyanines

Phthalocyanines Pc is an aromatic macromolecular intensely blue-green heterocyclic compound with the general molecular formula $(C_8H_4N_2)_4H_2$. It is composed of four pyrroles units' structures linked by four aza (—N=C—) groups at the α-carbon of pyrrole unit to form four aza bridges and four phenylene rings with 18 π-electron systems configuration, are chemically and thermally stable compounds that exhibit extraordinary optical and electrical behavior. The original name of phthalocyanines (Pc) is a combination of the Greek words meaning mineral oil (naphtha) and dark blue meaning (cyanine), and their color can vary from blue to yellowish green. Phthalocyanine was first obtained from phthalimide and acetic anhydride as an unwanted by-product during the synthesis of o-cyanobenzamide from phthalimide and acetic acid by two researchers named Braun and Tcherniac in London working at South Metropolitan Gas Company in 1907 [36, 37].

Copper-phthalocyanine was later synthesized in 1927 by de Diesbach and Von der Wied from the reaction of copper (I) cyanine and,2-di bromobenzene refluxing in pyridine [38]. Furthermore, in 1928 a Scottish dye LTD reported the synthesis of Iron phthalocyanine from a reaction of ammonia phthalimide and phthalic anhydride accidentally by chance, and since then used as a powerful pigment [36, 38].

After 1928, phthalocyanine was presented as the most versatile industrial product used as colour and dyes in printing, dyeing plastics, aluminium surfaces, and textiles [39]. The term phthalocyanines (Pc) was first used by Linstead in 1933. Between 1929 and 1939, Linstead elucidated and clarifie phthalocyanines structures and developed synthetic methods for various metallic phthalocyanines complexes (MPc) [37]. Since their accidental discovery in 1907 and subsequent structure identification, phthalocyanines have been one of the most studied classes of organic materials [40]. Due to their commercial importance, phthalocyanines have formed the synthetic dyestuff class that has been the most researched after 1928.

2.2 Structure and Nomenclature of Phthalocyanines

There are two basic structural forms of phthalocyanines, the metal-free phthalocyanines (H_2Pc) and metal phthalocyanines (MPc) as shown in **Figure 2.1** below.

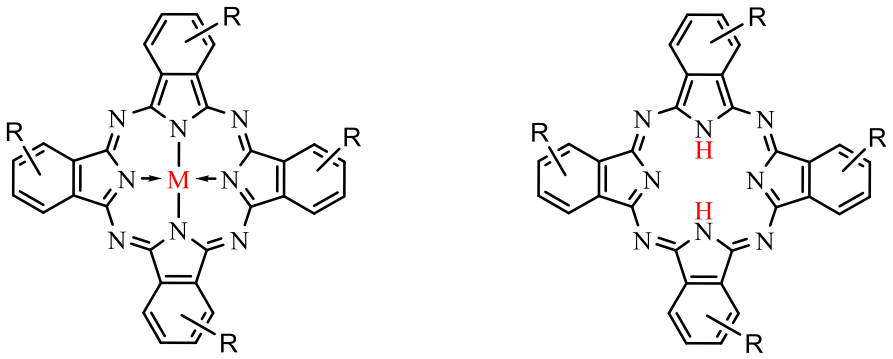

Figure 2.1. Structure of Metal Phthalocyanines (MPc) and Non-metal Phthalocyanines (H_2Pc)

They are a class of bivalent compounds like porphyrins, phthalocyanines are tetra dentate, planar, and consist of an 18-π electronic configuration system from **8** carbons and 8 nitrogen atoms making two-dimensional geometry of an aromatic macrocyclic compound as indicated in **Figure 2.2** below. Phthalocyanines consist of four isoindole units joined by four aza (—N=) groups at the α-carbon of the pyrrole unit to form four aza bridges connected as porphyrizing ring shown in **Figure 2.2** below. Pc has a two-dimensional geometry (Planner) with an innermost ring system.

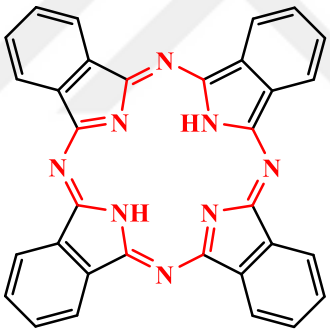

Figure 2.2. Structure of non-metal Phthalocyanine H_2Pc indicating the innermost ring system

There is a generally accepted numbering system on the phthalocyanine ring. There are 16 positions for macrocyclic substitution on the four benzo units, 8 of these locations (carbon atoms 2, 3, 9, 10, 16, 17, 23, 24) are peripheral (p) positions and the remaining 8 carbon positions are (1, 4, 8, 11, 15, 18, 22, 25) are called nonperipheral (np) positions [38]. Schematic nomenclature of phthalocyanine compounds is given in **Figure 2.3 [38]**.

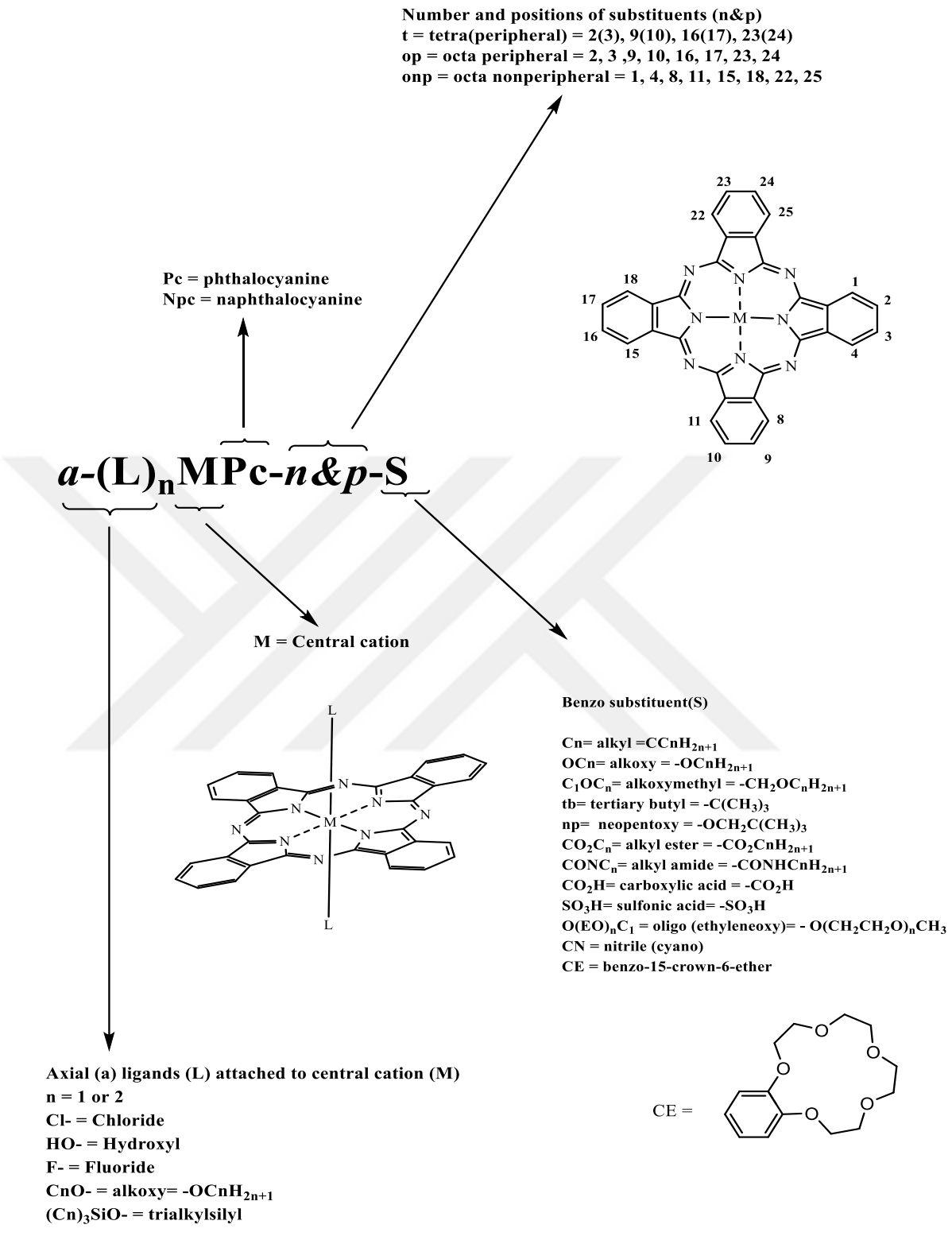

Figure 2.3. Schematic nomenclature of phthalocyanines [38]

2.3. Properties of phthalocyanine

Generally, physical and chemical properties of phthalocyanines are attributed to their efficient electron transfer abilities of 18 π-electrons configuration system from **8** carbons and **8** nitrogen atoms in the central cavity of phthalocyanines, metal ions, coordinated in the central cavity and the kind of substituent attached to the phthalocyanines core.

2.3.1 Chemical properties of phthalocyanine

Phthalocyanines can be obtained from aromatic o-dicarboxylic acid or amide, imide, and nitrile derivatives of these acids. However, phthalocyanine synthesis is not possible if the carboxyl groups are not directly attached to the unsaturated aromatic group. Furthermore, another condition required for the synthesis of phthalocyanine is the presence of double bonds between carbon atoms carrying carboxyl or cyano groups.

The directing effect of the metal ion in the production of metal-containing phthalocyanines increases the product yield. Therefore, the product yield of metal-containing phthalocyanines is higher than metal-free phthalocyanines. Studies indicate that metal-containing variants, such as zinc(II) phthalocyanine [41], can be prepared in good yields and demonstrate better performance in terms of properties like fluorescence and singlet oxygen quantum yield compared to their metal-free counterparts.

The stability of metal-containing phthalocyanines depends on the metal ion diameter [42]. Metal atoms can be easily separated from phthalocyanines when the cavity diameter of the phthalocyanine molecule is significantly larger or smaller than 1.35 Å.

Metal phthalocyanines can be categorized into two types based on the nature of the bonding which is covalent and electrovalent (also known as ionic). Covalent phthalocyanine complexes are more stable than electrovalent ones. Such phthalocyanines are difficult to remove ring-containing metals by treating them with acids. This increase in stability can be attributed to the stronger bonding interactions present in covalent complexes compared to the ionic interactions of electrovalent complexes. covalent complexes can sublimate in a vacuum at 400-500 °C without decomposition [43]. Due to the strong bond between metal and phthalocyanine and the aromatic character of the whole molecule, there is no deterioration in their structure when treated with inorganic acids other than nitric acid. All phthalocyanines are oxidized to phthalimide when treated with strong oxidants such as nitric acid and potassium permanganate.

Electrovalent phthalocyanines are a class of phthalocyanine compounds that have been modified to exhibit ionic characteristics, typically by incorporating charged functional groups into the phthalocyanine structure. Electrovalent phthalocyanines generally contain alkaline earth and alkaline earth metals and are insoluble in organic solvents. Electrovalent phthalocyanines represent a versatile group of compounds with significant potential in various fields of science and

technology, particularly in medical applications and materials science. They cannot sublime at high temperatures in a vacuum. When treated with dilute inorganic acids [44], aqueous alcohol, or even water, the metal ion is easily separated from the molecule and metal-free phthalocyanine is obtained 45]. Unlike others, lithium phthalocyanine dissolves in alcohol at room temperature [46, 47, 48], and when treated with other metal salts, lithium replaces the cation of the salt and new metalized phthalocyanine is formed.

2.3.2. Physical properties of phthalocyanine

Unsubstituted phthalocyanines exist in three forms of crystal structures. These are the α-form, β-form, and x-form. Of these crystal structures, the x-form is obtained by grinding the α-form [49, 50]. **Figure 2.4** shows the α- and β-form crystal structures of unsubstituted CuPc schematically.

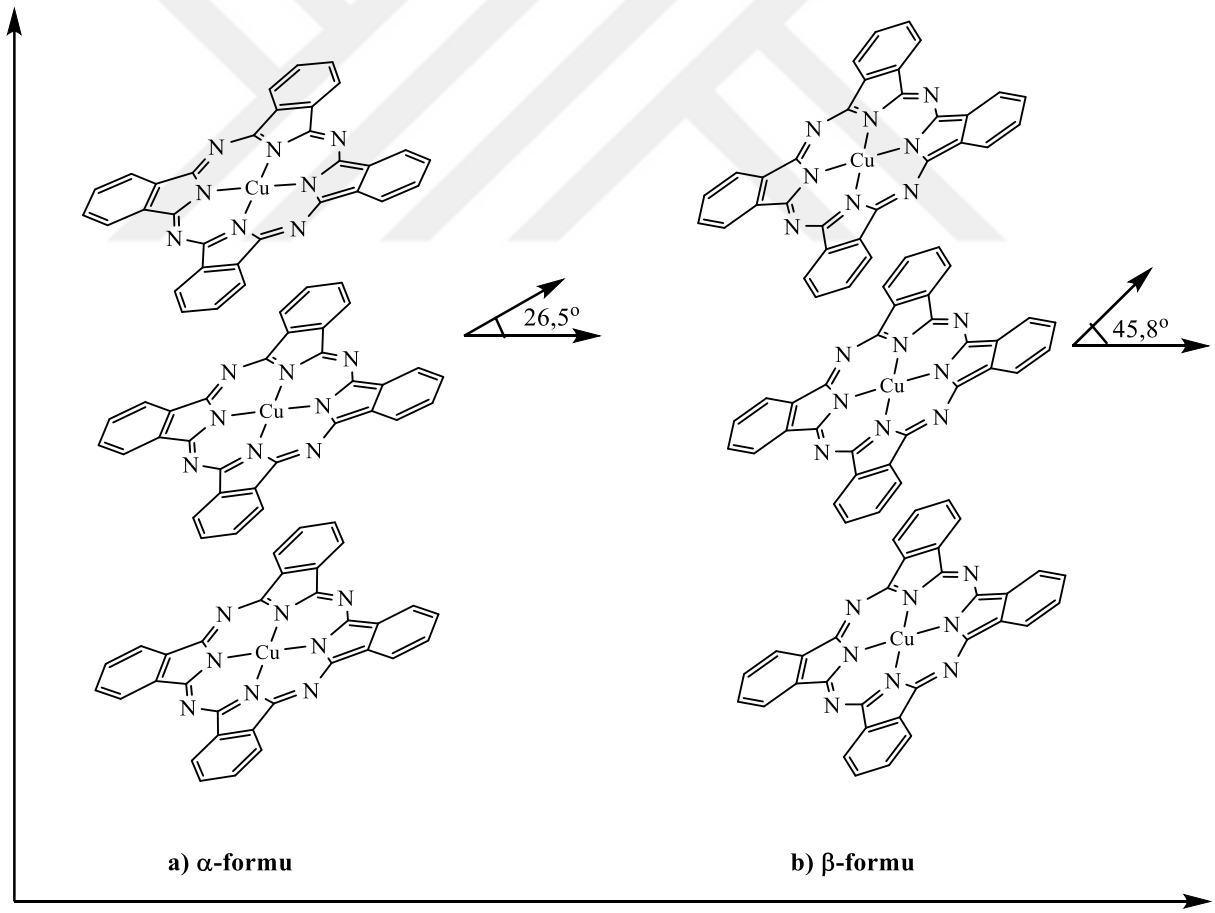

Figure 2.4. Schematic representation of the crystal structures of unsubstituted CuPc in a) α-form and b) β-form.

These crystal structures differ in solubility, color, and stability, the β-form is more stable than the α-form and is the most common structure. The α-form can be obtained during synthesis using polar solvents [51]. An example of this is the precipitation of the α-form with the rapid dilution of phthalocyanine dissolved in concentrated sulfuric acid. The more stable β-form is formed when the organic solvent is used during synthesis [52, 53]. If the α-form is treated with aromatic organic solvents or heated to high temperatures, the β-form is obtained

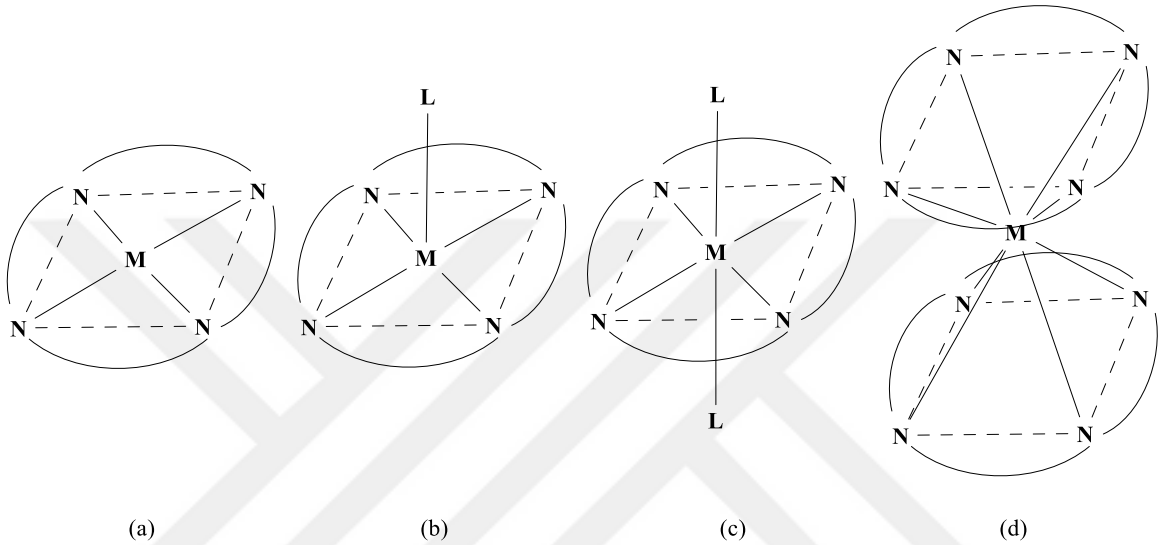

Figure 2.5. Schematic representation of the geometric structure of the phthalocyanine molecule a) Square planar, four-coordinated b) Square-based pyramid, five-coordinated c) Octahedral, six-coordinated d) Octahedral, Eight coordination

Many phthalocyanine compounds differ in color depending on their chemical and crystalline structural form. For instance, the color of copper phthalocyanine shifts from blue to green as the number of substituted chlorine atoms on the surface increases. Since most phthalocyanine compounds decompose before reaching their melting point, they do not have a specific melting point. In some cases, they do not undergo significant degradation up to 400–500º in the air [54, 55] this shows how copper phthalocyanine has high thermal stability [56].

2.3.3. Spectral properties of phthalocyanine

UV/visible spectrum of phthalocyanine compounds reported two characteristic peaks with metals or without metals. These peaks can be used to justify the formation of phthalocyanine complex synthesis. The first peak occurs due to the transition (n→π*) around 320-370 nm and is called the B band or Soret band. While the second peak occurs due to the transition by $\pi \rightarrow \pi^*$ transition from the highest occupied molecular orbital (HOMO) to the Pc ring's lowest unoccupied molecular orbital (LUMO) (π→π*) around 650-700 nm and is called the Q band. In addition, a

shoulder-shaped peak is seen around 600-650 nm. The characteristic of the Q band is that the molecule is shaped according to its symmetry. Electronic transitions in the UV / visible region [57], are shown in **Figure 2.8.**

Furthermore, a single peak is seen attributed to the metal phthalocyanine complex (MPc) in D_{4h} symmetry, while a double peak is observed in the metal-free phthalocyanine complex molecule (H_2Pc) in D_{2h} symmetry. UV/visible spectrum for metal-free phthalocyanine derivatives with such transitions is given in **Figure 2.6.** Then for metalized phthalocyanine derivatives, the UV/visible spectrum is accounted for in **Figure 2.7** below.

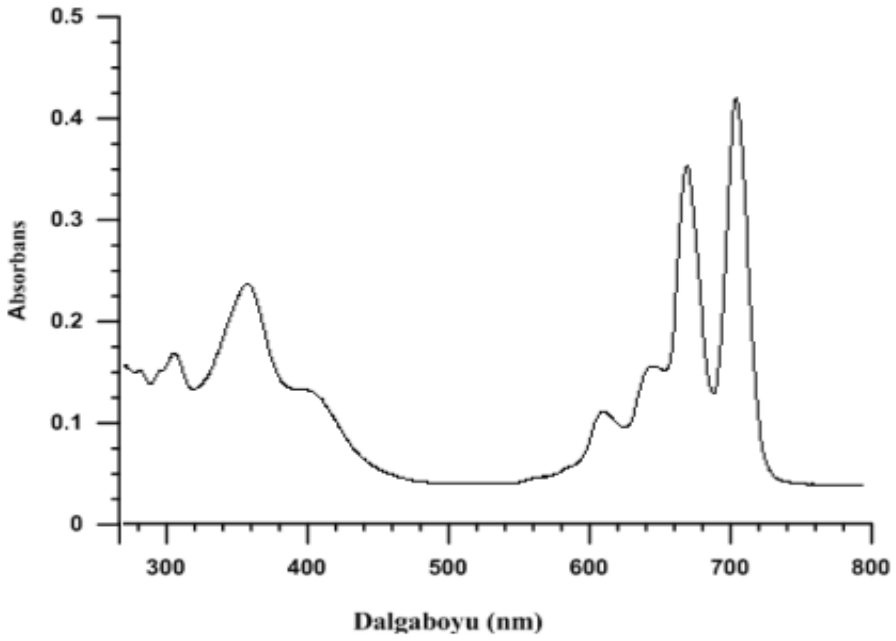

Figure 2.6. General expected UV/visible spectrum for metal-free phthalocyanine [57]

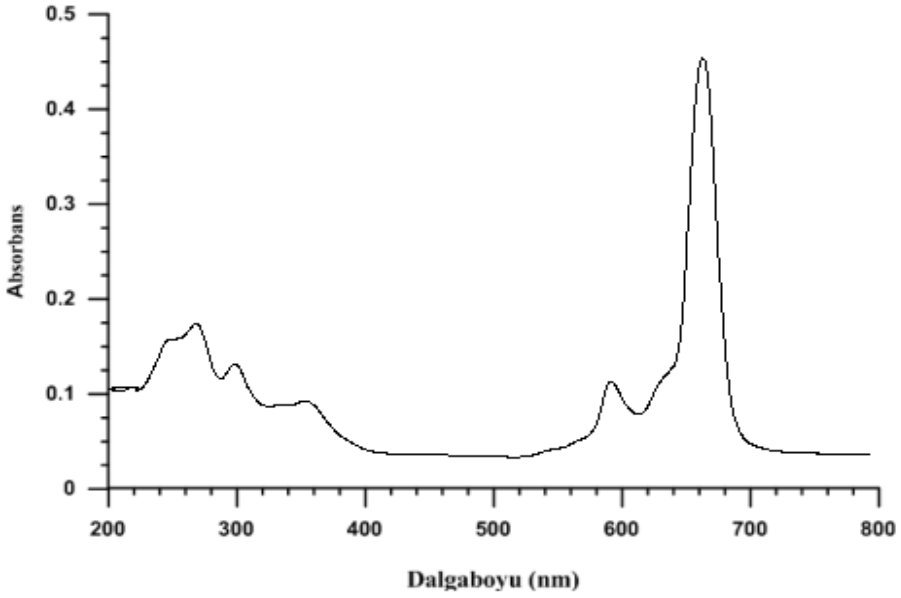

Figure 2.7. General expected UV / visible spectrum for metal phthalocyanine [57].

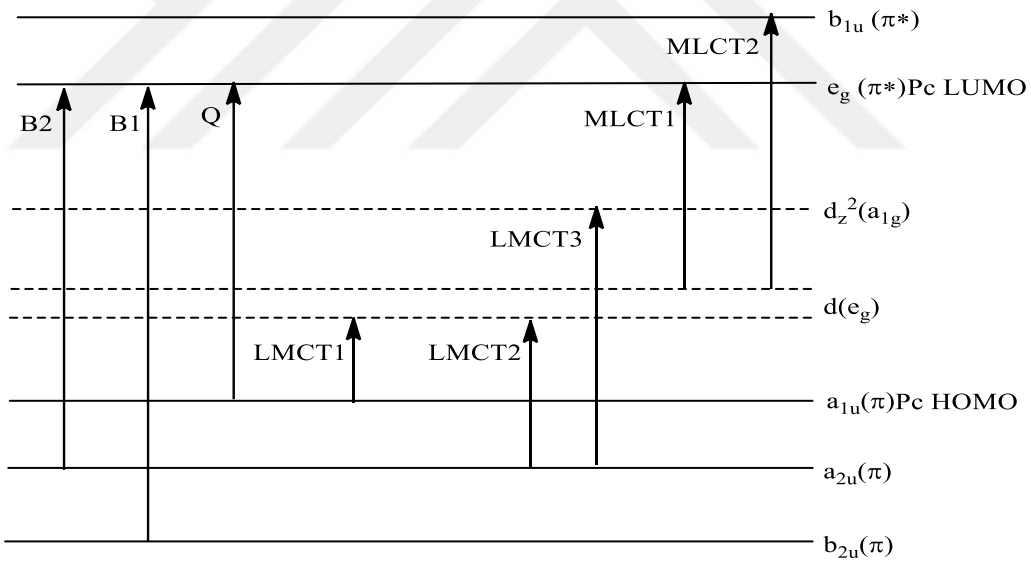

Figure 2.8. Electronic transitions of energy levels in the UV/visible region (Q and B bands and Ligand to Metal (LMCT) and Metal to Ligand (MLCT) charge transfer transition bands) [58]

2.4. Applications of Phthalocyanines

The application of Pc is largely attributed to its electronic properties that are intricately connected to its structural features, including its π-electronic conjugated system, metal coordination, functionalization, solvent effects, and aggregation behavior all these features contributed toward the wider application of Pc complexes. Understanding these relationships is

crucial for optimizing phthalocyanine for various applications in electronics, photonics, and materials science.

2.4.1 Dyes and Pigments Applications of Phthalocyanines

Phthalocyanines are used as pigments as well as in many types of dyes [36]. Industrial production of copper phthalocyanine started in 1953 under the trade name Monastral Fast Blue [59]. The brightness of the copper phthalocyanine pigment was further increased by producing particles with α-form by dissolving and reprecipitating in sulfuric acid. Phthalocyanines are often vibrant in color due to their extensive π-conjugation which influences the absorption ability of light in visible regions particularly by the dyes and pigments. This makes them useful in coloring applications as dyes in textiles and as pigments in paints and plastics due to their intense color and stability. There is a wide range of applications of phthalocyanines based on their remarkable properties. Pcs strongly absorb light in the low-energy region of the visible spectrum to give bright blue or green colours [60, 61].

Today copper phthalocyanine pigments are used in the colouring of detergents, soaps, and other cleaners, and the colouring of polymers coated on woven or non-woven glass fibre. Thousands of tons of phthalocyanine are produced as blue and green dyestuffs per year to meet the increasing demand of the industry [62]. These are some examples of copper phthalocyanine pigment and dyes presented in **Figure 2.9.** below.

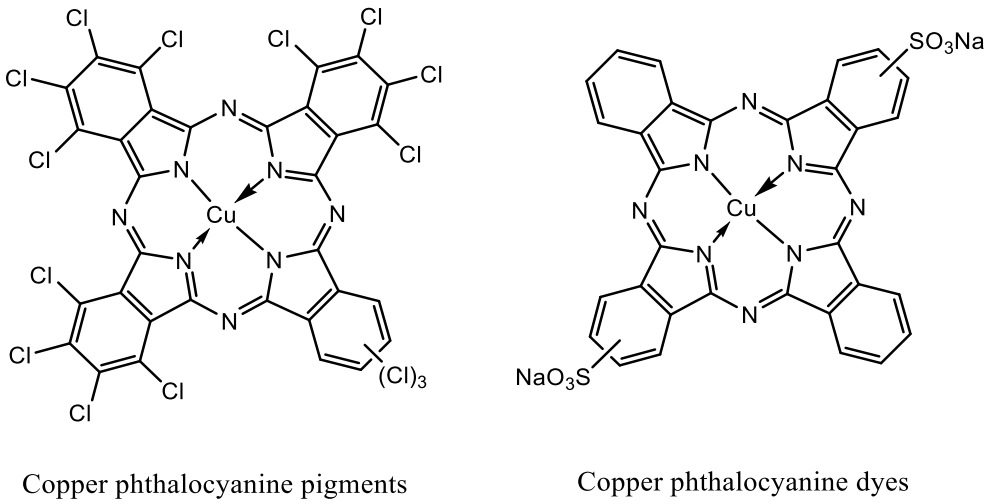

Copper phthalocyanine pigments Copper phthalocyanine dyes

Figure 2.9. Copper phthalocyanines pigment and dyes

Phthalocyanines with excellent blue-green colours are used in inkjet, fountain pen inks, the paper industry, plastic and metal surfaces as well as the textile industry [63].

2.4.2. Photodynamic Therapy (PDT) Application of Phthalocyanines

Photodynamic therapy (PDT) is a therapeutic approach that uses photosensitizing agents, like phthalocyanines, combined with light to produce reactive oxygen species (ROS) that can kill malignant cells. Phthalocyanines have significant potential in photodynamic therapy, offering an effective treatment modality for various cancers and other diseases through their ability to generate reactive oxygen species upon light activation [64, 65, 66, 67]. Ongoing research aims to improve phthalocyanine formulations, enhance targeting strategies (like conjugating them with antibodies or nanoparticles), and explore new applications in disease treatment beyond oncology.

In summary, phthalocyanines have significant potential in photodynamic therapy, offering an effective treatment modality for various cancers and other diseases through their ability to generate reactive oxygen species upon light activation.

Here's an overview of how phthalocyanines are utilized in PDT, their mechanisms of action, and their specific applications

1. **Photosensitization:** Phthalocyanines, when administered to a patient, accumulate in target tissues, including tumors. They possess a strong absorbance in the visible and near-infrared (NIR) regions, making them effective light-absorbing agents.
2. **Light Activation:** After administration, the localized application of light activates the accumulated phthalocyanines. When exposed to specific wavelengths of light, phthalocyanines transition to an excited state.
3. **Reactive Oxygen Species Generation:** The transition to the excited state facilitates energy transfer, leading to the production of reactive oxygen species (such as singlet oxygen). These ROS can damage cellular components, such as proteins, lipids, and DNA, ultimately leading to cell death.
4. **Cellular Effects:** The generated ROS can induce apoptosis (programmed cell death) and necrosis, targeting malignant cells while minimizing damage to surrounding healthy tissues Photodynamic therapy (PDT) is widely used in medicine in the following areas

    - ***Cancer Treatment: Phthalocyanines are primarily explored for treating various types of cancers, including:***
    - ***Skin cancers (e.g., basal cell carcinoma, squamous cell carcinoma)***
    - ***Head and neck cancers***
    - ***Breast cancer***
    - ***Other solid tumors***
    - ***Tumor Imaging: Besides their therapeutic use, phthalocyanines can also serve as imaging agents due to their fluorescence properties. They can help in visualizing tumors during PDT, assisting in treatment planning and monitoring***

- ***Combination Therapies: Phthalocyanines can be used in combination with other treatment modalities, such as chemotherapy or immunotherapy, to enhance overall treatment efficacy.***
- ***Vascular Targeting: Phthalocyanines can be designed to target the tumor vasculature, causing vascular shutdown and thereby starving tumors of oxygen and nutrients in addition to direct cell killing.***
- ***Infection Treatment: Beyond cancer, phthalocyanines have potential applications in treating infections, as they can also target bacteria and fungi when activated by light.***

Phthalocyanines offer several advantages in photodynamic therapy (PDT), including selective accumulation in tumor tissues, which enhances the therapy's targeting accuracy. Their strong light absorption in the visible and near-infrared spectrum allows for deeper tissue penetration, improving treatment efficacy. Additionally, phthalocyanines are chemically stable and can be synthesized with various metal centers to further enhance their therapeutic potential. PDT with phthalocyanines also tends to have minimal side effects, causing less damage to surrounding healthy tissues compared to traditional therapies like chemotherapy and radiotherapy. However, there are challenges and considerations to be addressed, including increased skin sensitivity to light in patients during and after treatment. The effectiveness of PDT also depends on the presence of oxygen, making hypoxic tumor regions less responsive. Furthermore, as with any therapy, there is a potential for cancer cells to develop resistance, highlighting the need for ongoing research into new phthalocyanine derivatives and combination therapies [68, 69].

2.4.3. Optical Data Storage application of phthalocyanines

High-density optical data storage on compact discs (CD), which was first produced in 1982, has revolutionized the computer and music industries. Research in this area has focused on developing IR-absorbing dyes suitable for use in inexpensive semiconductor diode lasers [70]. Phthalocyanines have become very interesting materials for long-term optical data storage on write-once-read-many discs due to their excellent chemical stability and suitability for semiconductor diode lasers. Point laser heating applied on the phthalocyanine material made into thin films for optical data storage sublimates this material pointwise. By optically detecting the hole that appears in this way, reading or writing is accomplished [71]. The CD-ROM (compact disk read-only memory), stores text, sound, as well as images; in WORM (writing-once read-many), a form of a disk that can once be stored and read every time; and in new disks which are rewritable entirely. This is the newest compact record technology [72]. Recordable CDs (CD-R) disks have a polycarbonate sheet with a spiral groove that directs the laser beam as it writes and reads data. The

spiral groove is covered with a thin layer of paint and then with a thin layer of gold (Au) or silver (Ag).

2.4.4. Sensors application of phthalocyanines

Phthalocyanine derivatives are increasingly utilized in sensor applications due to their unique electronic properties, stability, and ability to respond to the presence of various analytes. Here are some key aspects of their use in sensors:

1. Gas Sensors

Phthalocyanines can detect volatile organic compounds (VOCs) [73, 74]and gases such as ammonia, nitrogen dioxide, and acetone. Their sensing mechanism typically relies on changes in electrical conductivity or optical properties upon interaction with target gas molecules. The modification of metal ions in the phthalocyanine structure can tailor their sensitivity and selectivity toward specific gases for example nickel phthalocyanine (NiPc) thin films used in a chemiresistor-type nitric oxide gas sensor [75, 76].

2. Chemical Sensors

Chemical sensors are devices that can convert chemical information in the environment, the type and amount of gas or gases in the environment into measurable electronic information depending on physical variables such as mass, conductivity, and frequency [71].

Phthalocyanines are employed in chemical sensors for the detection of small molecules, including biomolecules. These sensors often utilize electrochemical methods [77, 78] to measure changes in current or voltage in response to the analyte binding, allowing for sensitive detection.

3. Biosensors

Modified phthalocyanines can be used as components in biosensors [79] that detect biomolecules, such as glucose, DNA, or proteins. They can facilitate electron transfer in the biosensor's electrocatalytic processes, enhancing the sensitivity and specificity of the sensor. For example, phthalocyanine derivatives can be coupled with enzymes [80] or antibodies to create highly selective biosensors. Phthalocyanine self-assembled monolayer was then evaluated as a mediator for glucose oxidase (GOx)-based biosensor [81, 82].

4. Optical Sensors

Phthalocyanines exhibit strong absorption in the visible and near-infrared regions [83, 84], making them suitable for optical sensing applications. Changes in their absorption spectra in response to the presence of certain substances can be measured to determine concentrations of analytes [85].

Non-linear optics is a branch of optics that studies the behavior of light in a nonlinear medium. After the 1960s, the invention of very intense light sources with laser mechanisms made it necessary to conduct research for the protection of optical sensors and the human eye from lasers. Today, some materials and devices related to this subject have been developed. Among these materials, organic and organometallic compounds with nonlinear optical properties are very suitable for reducing the intensity of laser light. Examples of such materials are porphyrins, phthalocyanines, fullerenes, and organometallic compounds. Particularly, porphyrins and phthalocyanines are much more useful because nonlinear optical properties can be changed with some structural modifications, fast response times, low absorption losses, low dielectric constants, and resistance to heat and environmental conditions [86].

5. Environmental Monitoring

Due to their ability to detect pollutants at low concentrations, phthalocyanine-based sensors are used in environmental monitoring to track air quality and detect hazardous substances in water or soil. A zinc phthalocyanine (ZnPc) based microporous device was fabricated and its capacitance was utilized as the sensing mechanism for a humidity sensor [87, 88].

6. Electronic Nose Technology

Phthalocyanines can be incorporated into electronic nose devices that mimic the human sense of smell. These sensors can differentiate between complex mixtures of odors by analyzing the changes in electrical signals upon exposure to different volatile compounds (VOCs) [89, 90, 91].

Advantages of Phthalocyanine Sensors:

- **High Sensitivity**: The extensive π-electron system and the ability to form complexes with various analytes enhance detection sensitivity.
- **Selectivity**: The functionalization of phthalocyanines allows for tailoring the sensors to specific target analytes.
- **Stability**: Phthalocyanine derivatives are known for their thermal and chemical stability, which is advantageous for long-term sensor applications.
- **Cost-Effectiveness**: Many phthalocyanine materials can be synthesized relatively inexpensively, making them attractive for widespread use in sensors.

In summary, phthalocyanines have promising applications in various types of sensors, capitalizing on their unique properties to detect and quantify a wide range of substances.

2.4.5. Catalysts Application of Phthalocyanines

Phthalocyanines (Pcs) have garnered significant attention for their use as catalysts in various chemical reactions due to their structural properties, stability, and ability to facilitate electron transfer processes. Here are some key applications of phthalocyanines as catalysts:

1. Oxidation Reactions

Phthalocyanine complexes, especially those containing transition metals (like cobalt, copper, or nickel), are effective catalysts for oxidation reactions [78, 87, 92, 93]. They can promote the oxidation of alcohols to aldehydes or ketones and the oxidation of a wide range of substrates, including hydrocarbons, using various oxidants such as hydrogen peroxide or molecular oxygen.

2. Electrocatalysis

Phthalocyanines are used in electrocatalytic processes, such as:

- **Oxygen Reduction Reaction (ORR)**: Metal-phthalocyanines are employed as catalysts in fuel cells to enhance the efficiency of the ORR at the cathode [13, 94, 95].
- **Hydrogen Evolution Reaction (HER)**: Some phthalocyanine derivatives can catalyze the generation of hydrogen from water, a promising process for renewable energy production. The electrochemical polarization can be reduced by the usage of efficient **electrocatalysts** in the electrochemical or **HER process** e.g. Cobalt phthalocyanine as an efficient catalyst for hydrogen evolution reaction [96, 97, 98].

3. Photocatalysis

Phthalocyanines can act as photocatalysts when exposed to light, facilitating various photoreactions [99]. They can absorb light and generate reactive species that can initiate chemical transformations, such as the photodegradation of pollutants or the conversion of carbon dioxide into useful chemicals [100].

4. Polymerization Reactions

Phthalocyanines have been explored as catalysts for polymerization processes, promoting the polymerization of various monomers [89, 101]. Their catalytic activity can be advantageous in producing polymers with specific properties. Recent advancements include the development of porous polymer networks using commercial phthalocyanines, such as iron phthalocyanine (FePc), as monomers. These networks enhance catalytic efficiency, particularly in carbon dioxide reduction (CO_2 RR) applications.

Innovative methodologies have been introduced to synthesize phthalocyanine-containing polymers, which improve the catalytic activity for CO_2 fixation. For instance, a one-pot synthesis of copper phthalocyanine polymers has shown promise as an efficient catalyst for CO_2 reduction. The structural arrangement of phthalocyanines, including cofacial arrangements, plays a significant

role in their catalytic performance, highlighting the potential of integrating both organic and inorganic materials in this system [88].

5. Cyanation Reactions

Some metal-phthalocyanines are capable of catalyzing cyanation reactions [102], which involve the introduction of cyano groups into organic compounds. This is particularly valuable in organic synthesis for producing nitriles. Metal-phthalocyanines have been shown to catalyze various reactions, including cyanation reactions, due to their redox-active properties and ability to mediate transformations in organic synthesis. Specifically, metal complexes like iron-phthalocyanines are noted for their ability to catalyze a range of reactions effectively [103, 104, 105].

6. Heterogeneous Catalysis

Phthalocyanines can be immobilized onto solid supports to create heterogeneous catalysts. This approach enhances their utility in continuous flow reactions or easy separation after the reaction. Supported phthalocyanine catalysts can be used in various reactions, including carbon-carbon coupling reactions. Phthalocyanines, particularly metallo-phthalocyanines, are explored as heterogeneous catalysts due to their notable electronic properties and ability to facilitate various chemical reactions, including the electrochemical reduction of CO_2. However, a significant challenge in utilizing them effectively in heterogeneous catalysis is achieving a high surface area, which can often be addressed by anchoring them onto suitable supports [98, 105].

7. Degradation of Pollutants

Phthalocyanines can be employed to catalyze the degradation of environmental pollutants, such as dyes and phenolic compounds, through oxidation reactions [106]. This application is essential for wastewater treatment and environmental remediation. Among the new strategies for wastewater treatment, photocatalysis has attracted considerable interest for its ability to break down organic contaminants in water, particularly when used alongside sunlight and a recoverable photocatalyst. Heterogeneous photocatalysts offer specific benefits, as they can be collected and reused without a notable decrease in effectiveness across multiple cycles [22, 107, 108, 109].

Advantages of Phthalocyanine Catalysts:

a) **High Activity**: Metalized phthalocyanines exhibit excellent catalytic activity due to the presence of coordinated metal centers that facilitate electron transfer processes.

b) **Stability**: Their chemical stability under various reaction conditions allows for prolonged usage without significant deactivation.

c) **Selectivity**: Catalysts based on phthalocyanines can be designed or modified to provide high selectivity for specific reactions.

2.4.6. Organic Photovoltaics Application of Phthalocyanines

Phthalocyanines are a class of organic pigments that have shown promising applications in organic photovoltaics (OPVs) due to their strong light absorption, good charge transport properties, and high stability [110, 111]. These compounds are used in organic solar cells to enhance light absorption and charge transport, contributing to developing more efficient solar energy conversion systems. Recent studies, including advancements in various silicon and germanium phthalocyanines, have highlighted their effectiveness in enhancing the efficiency of solar cells. These compounds can be integrated into mesoscopic structures to improve energy conversion efficiencies significantly. Their tunable electronic properties also allow for optimization in different solar cell architectures.

A phthalocyanine macrocycle tends to form clusters in which neighboring atoms can be of smaller size as they interact with each other in the large π-system. Normally, pure phthalocyanines are insulators mainly because they have a band gap of 2 eV. The aggregation required for the desired π-π interaction in good conductivity is achieved by chemical or electrochemical means by adding extra electrons or holes to the conduction or valence band. Molecular semiconductors are gaining value day by day in the manufacture of electronic devices. All these properties make phthalocyanines attractive in molecular semiconductor materials.

2.4.7. Electrochromic imaging application of phthalocyanines

Phthalocyanines (Pcs) are utilized in electrochromic imaging applications due to their ability to undergo reversible colour changes when an electrical potential is applied. These compounds can be tailored by changing their central metal ions, enhancing their ionic and electronic conductivity contributing to their electrochromic properties. For instance, metal phthalocyanines with redox-active groups exhibit significant electrochromic responses, making them suitable for applications such as sensors and smart windows.

The colour change of the substance in oxidized and reduced states when a certain voltage is applied in the electrical environment is called electrochromism, and the substances that change colour with the voltage change in this way are called electrochromic substances. Electrochromic materials are used in the production of materials such as display panels, rearview mirrors and roof glasses of cars, sunglasses, and watch screens eg. electro polymerizable double-decker lutetium(III) phthalocyanine, functionalized with 3,4-ethylene dioxythiophene (EDOT) is a significant electrochromic substance which is potentially used in electronic display technologies. Furthermore, phthalocyanine complexes with electrochromic properties are the bis phthalocyanine complexes of the rare earth metals lanthanides as shown in (**Figure 2.11)** below. Synthesis of these complexes

produces a neutral green product with the general formula $LnPc_2$. The dianion-shaped structure of $[Pc_2\text{-}Ln_3{+}Pc_2\text{-}]$- anion, which is the reduction product observed in electrochemical studies of this neutral product $LnPc_2$, gives lanthanide bis phthalocyanine many electrochemical, electrochromic, magnetic, spectral and structural properties. These properties result from both the sandwich structure of the molecule and the interplanetary interaction between the π-electron systems in both phthalocyanine rings. Electrochromic transformations of a $LnPc_2$ molecule can be represented in **Figure 2.10** shown below [112, 113, 114].

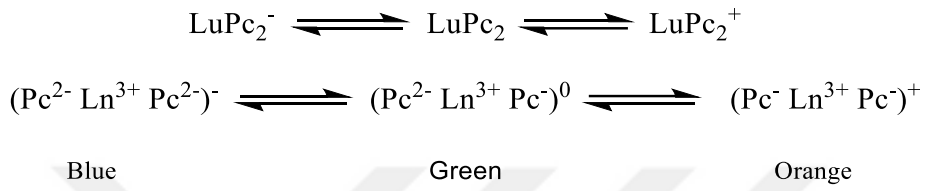

Figure 2.10. Electrochromic transformations of the $LuPc_2$ molecule.

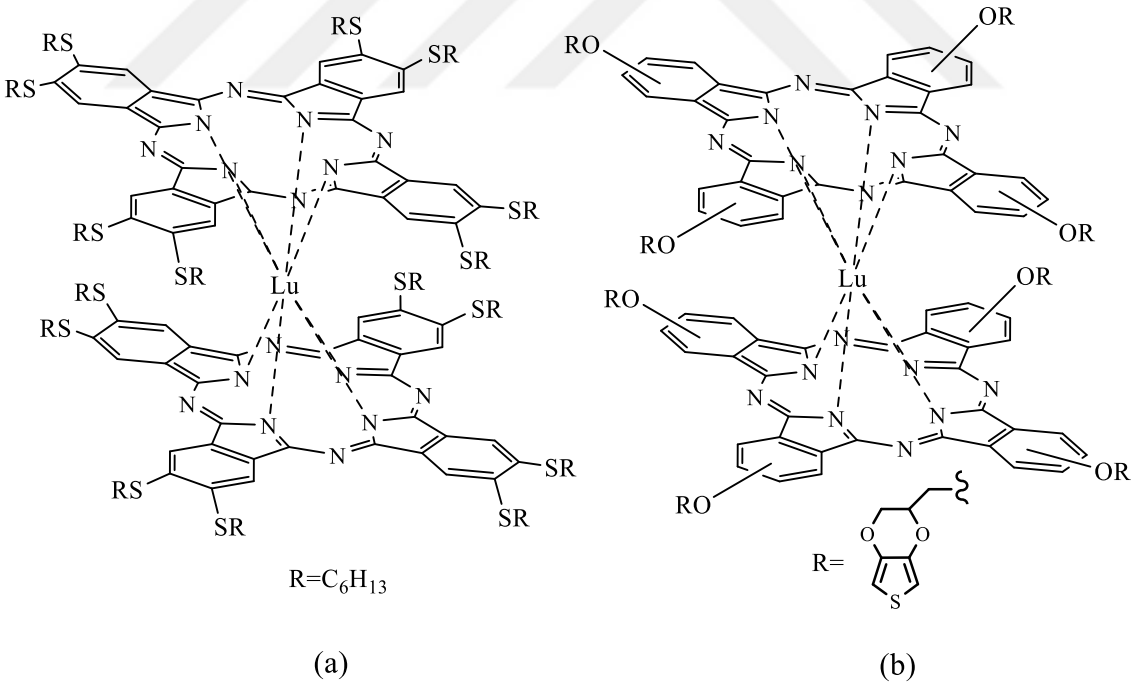

Figure 2.11. a) Octa substituted [113], b) Tetra substituted [114] Lutetium bisphthalocyanines ($LuPc_2$) (double-decker phthalocyanine)

2.4.8. Electrophotography application of phthalocyanines

Phthalocyanines are used in electrophotography primarily as photosensitive recording materials. Their ability to efficiently absorb light and produce charge carriers makes them suitable as photoconductors in imaging applications. This property is essential in rendering images on photoconductive surfaces when exposed to laser light. Additionally, phthalocyanine derivatives have demonstrated significant effectiveness in capturing and holding electric charges, which enhances image quality in photocopying and printing processes. Phthalocyanines have also found extensive use in many of the modern high technologies, e.g. are highly effective as cyan dyes for inkjet printing due to their vibrant color and stability and are also utilized in electrophotography as charge generation materials for laser printers, enhancing the printing process through their strong electronic properties and light absorption capabilities and as colorants for cyan toners. Their versatility makes them a popular choice in various printing applications [115].

2.5. General Synthetic Methods of Phthalocyanines

Phthalocyanines can be synthesized using several methods, primarily starting from phthalic acid, phthalic anhydride, phthalimide, o-cyanobenzamide, phthalonitrile, isoiminoindoline, or 1,2-dibromobenzene derivatives. The synthesis typically involves high boiling organic solvents like dimethylformamide (DMF) or dimethylaminoethanol (DMAE) etc. To enhance solubility, functional groups such as tertiary butyl, hexyl, amide, or carboxylic acid groups can be added to the phthalocyanine structure. These modifications assist in customizing the characteristics of the resultant compounds for diverse applications [58].

3. MATERIALS AND METHODS

Common glassware and other general laboratory equipment were used during the synthesis, purification, and identification of the synthesized compounds. In the laboratory, commonly used glassware and other laboratory tools were used.

3.1. Chemicals Used

N-methyl morpholine (NMM) (Sigma-Aldrich) (99 %), Acetonitrile (Labkim), Acetone (Merck) (99.5 %), Chloroform (Merck), n-Hexane (Merck) (95%), Ethyl acetate (Acros Organics) (99 %), Anhydrous Magnesium sulphate (Horasan Kimya) (99 %) and 2-Chloro-4,6-dimethoxy-1,3,5-triazine (CDMT) (99.9 %), Boc-L-Tyrosine (Boc-L-Tyr-OH) (99.26 %), L-Phenylalanine methyl ester hydrochloride (L-Phe-OMe**.** HCl) (99.91 %), L-Alanine methyl ester hydrochloride (L-Ala-OMe**.** HCl) (99.92 %), L-Glycine methyl ester hydrochloride (L-Gly-OMe**.** HCl) (99.69 %), L-Valine methyl ester hydrochloride (L-Val-OMe**.** HCl) (99.38 %) all obtain from CHEM-IMPEX INT'L INC.

Phthalimide (Acros organics) (99 %), Nitric acid (Merck) (65 %), Sulfuric acid (Merck), (98%), ammonium hydroxide (Merck) (25%), potassium carbonate (Merck), thionyl chloride (Merck), chromium(III) acetate (Merck), manganese (II) acetate (Merck), iron (II) acetate (Merck), cobalt (II) acetate (Merck), Nickel (II) acetate (Merck), Copper (II) acetate (Merck), zinc (II) acetate (Merck), argon gas. dimethylformamide (DMF) (CHEM SOLUTE) (99.9%), dimethyl sulfoxide (DMSO) (Carlo Erba) (99%), tetrahydrofuran (THF) (Merck) (99%), acetone (Carlo Erba), diethaylacetate.

3.2. Equipment Used

The FT-IR spectra of the samples were conducted in the Department of Chemistry, Faculty of Arts and Sciences, Fırat University. The spectra of the intermediate step products and complexes were formed into discs with KBr, and their spectra were obtained in the range of 4000-400 cm^{-1} with the Perkin Elmer Spectrum one Series FT-IR spectrometer.

Nuclear magnetic resonance (^{1}H and ^{13}C NMR) spectra were obtained using a Bruker Avance III 400 MHz NMR Spectrometer with deuterated dimethyl sulfoxide (DMSO-d_6) as the solvent and tetramethylsilane (TMS) as the internal standard at the (Chemistry Department, Fırat University). Chemical shifts are reported in δ [ppm].

Elemental analyses were performed by Leco CHNS 932 instrument.

The UV spectra were analyzed with UV-1900i SHIMADZU UV-VIS Spectrophotometer which have wavelength ranges between 200 and 900 nm, using 1.0 cm path length quartz cell in DMF solvent**.**

Thermal analysis was taken with Shimadzu TA-60WS (TGA/DTA) with 20 °C/min scan rate in the Fırat University Chemistry Department.

Electrochemical measurements were done by Gamry Interface 1010 B, in DMF, with glassy carbon electrode as working electrode, Pt electrode as counter electrode tetra butyl ammonium tetrafluoro borate (TBTFB) as supporting electrolyte using ferrocene/ferrocenium as sudo reference electrode in Chemistry Department, Firat University

3.3. Synthesis of Starting Material

3.3.1. Synthesis of 4-Nitrophthalimide (2)

4-Nitrophthalimide was prepared in a three-neck round bottom flask equipped with a magnetic stirrer, thermometer, and dropper placed in ice mixed with salt to lower the temperature between 0 to -5 °C. 280ml of Conc. H_2SO_4 acid was added to the flask followed by the addition of cold 80 ml of 69 % nitric acid dropwise below 0 °C. After, 50.0 g (0.340 mol) of phthalimide **(1)** was added in portions while dissolving in the mixture within the spend of 2 hours under constant stirring and the temperature was maintained at below 0 °C until the phthalimide was completely added in the mixture. Then, the reaction mixture was removed from the ice bath in which it was placed and allowed to stand for 24 hours at room temperature on constant stirring.

After 1 day, the mixture was cooled to 0 °C and precipitated by pouring about 1 kg of crushed ice. The precipitated very light-yellow product was filtered under vacuum and washed with cold distilled water. It was crystallized in about 850-900 ml of ethyl alcohol. The bright yellow crystals formed were filtered under a vacuum and washed with cold ethyl alcohol. It was dried in an oven at 45-50 °C. The product of the reaction as shown in **Figure 3.1** below was light yellow shiny small crystals with FT-IR symmetric stretching peak at 1539 $cm^{-1}$and asymmetric stretching peak at 1355 cm^{-1} as shown in **Appendix 1.1**, yield: 31g (47.5%), MP: 195°C.

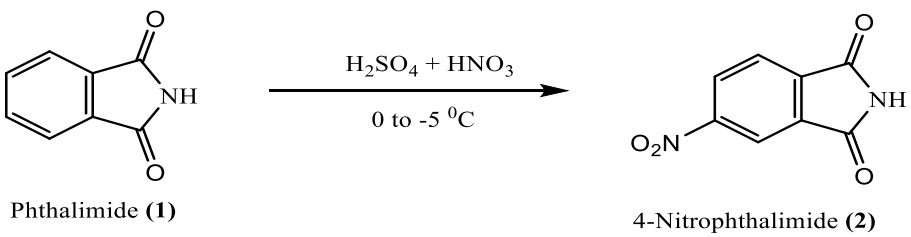

Figure 3.1. Synthesis of 4-Nitrophthalimide [116]

3.4.2. Synthesis of 4-Nitrophthalamide (3)

The 250 ml of ethyl alcohol was added to the three-neck plate bottom flask fitted with a thermometer and rubber tube supplying NH_3 gas. The flask was placed on a hot magnetic stirrer, stirring at 40 °C. 20 ml of THF solvent was introduced after 30.0 g (0.204 mol) of 4-nitro phthalimide (2) was added to facilitate the dissolution of the solid. The reaction as shown in **Figure 3.2** below was allowed to continuous for 40 minutes, in the meantime, the FT-IR spectrum of the samples was regularly taken from the reaction system at 10-minute intervals, until the appearance of a medium N-H stretching peak belonging to amides at 3440 cm^1 and strong bond stretching vibration of amide carbonyl (C=O) peak at 1663 cm^1were formed as seen in **Appendix 1.2**. The ammonia gas permeation process was terminated and the white milky colour precipitate was filtered under vacuum, washed with plenty of cold water and finally with cold ethanol [116]. It was air-dried at room temperature for 1 day. The product was a white powder, yield: 28.75g (88.02%), MP: 197 °C.

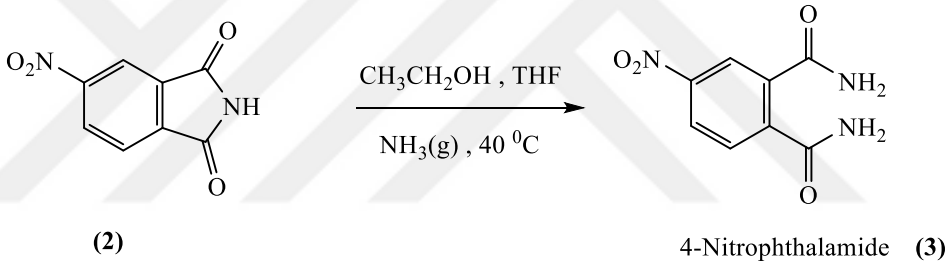

(2) 4-Nitrophthalamide **(3)**

Figure 3.2. Synthesis of 4-Nitrophthalamide [46]

3.4.3. Synthesis of 4-Nitrophthalonitrile (4)

170 ml of dry N, N-dimethyl formamide (DMF) cooled to 0 °C in a three-neck round bottom flask fitted with a thermometer, magnetic stirrer, and dropper placed in a salt-ice bath. 30 ml of thionyl chloride ($SOCl_2$) was added dropwise slowly so that the temperature of the reaction mixture did not exceed 5 °C. The mixture was allowed to be continuously stirred for 20 minutes after the addition of $SOCl_2$ before the introduction of 25.8 g (0.123 mol) of 4-nitro phthalimide **(3)** in portions for about 50 minutes, while the temperature was maintained between 0-5 °C. Then, the reaction mixture was allowed to be stirred at room temperature for 20 hours by removal of the ice bath. The mixture was precipitated by stirring in 250 g of breaking ice and vacuum filtered, washed first with water about three times, then with 250 ml of 5 % sodium bicarbonate ($NaHCO_3$) solution and finally with distilled water [46, 116]. The product of the reaction as indicated in **Figure 3.3** below is a white pale yellow after being dried in an oven at 60 °C to a constant weight. The FT-IR

spectrum of the product indicates the presence of a sharp single weak peak signal of nitrile C≡N at 2238.18 cm^{-1} as seen in **Appendix 1.3,** yield**: 1**8.5 g (71%), MP: 141 °C.

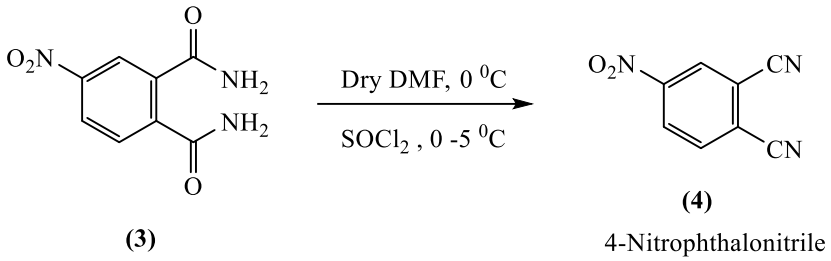

(3) **(4)**

4-Nitrophthalonitrile

Figure 3.3. Synthesis of 4-Nitrophthalonitrile (4) [46]

3.4. Synthesis of Tyrosine- Phenylalanine Dipeptide Amino Acids Substituents and Complexes

All the amino acids, coupling reagent 2-Chloro-4,6-dimethoxy-1,3,5-triazine (CDMT), and the catalysts N-methyl morpholine (NMM) used in the dipeptide synthesis were directly used as received pure from a manufacturing company. The solvents acetonitrile, acetone, ethyl acetate, chloroform, and n-hexane were all obtained pure and used in the process.

3.4.1. Methyl (tert-butoxycarbonyl)-*L*-tyrosyl-*D*-phenylalaninate (Boc-Tyr-Phe-OCH_3) (6)

The reaction as indicated by **Figure 3.4** below was conducted by the addition of 2.00 g (7.11 mmol) of Tyrosine amino acid **(**Boc-Tyr-OH) (1.0 equivalent) **(5)** with the amine group protected, 1.53 g (7.11 mmol) of phenylalanine methyl ester (NH_2-Phe-OCH_3.HCl) (1.0 equivalent) and 1.37 g (7.82 mmol) of (CDMT) (1.10 equivalent) as coupling agent in 250 ml plate bottom flask. An appropriate amount of 25 ml of Acetonitrile solvent was added into the reaction flask at room temperature with constant stirring. On continuous stirring, 1.95 ml (17.77 mmol) of (NMM) Base was added to the reaction mixture dropwise. The reaction was allowed to continuous stirring for 16 to 24 hours with sequences of thin layer chromatography (TLC) tests to monitor the completion of the reaction using free-coated aluminum TLC paper as stationary phase and a mixture of ethyl acetate and n-hexane solvent system in a ratio of 3:4 as mobile phase.

On completion of the reaction, then the solution of the mixture was filtered to remove any unreacted residue and the solvent in the filtrate was evaporated under a reduced pressure using a vacuum rotary evaporator. The residue was dissolved in 10 ml acetone and precipitated in 200 ml of water in a baker. The precipitate was filtered and dried at room temperature. The product is a white powder weight of 2.84 g with a percentage yield of 90.16 %, molecular weight of 442.5 and molecular formula $C_{24}H_{30}N_2O_6$. The FT-IR, ^{1}H-NMR, ^{13}C-NMR, Mass spectroscopy peaks and

Elemental Analyses results were presented in **Table 3.1a** below and the FT-IR, ^{1}H-NMR, ^{13}C-NMR, Mass spectroscopy Spectrum were given in **Appendix Section.**

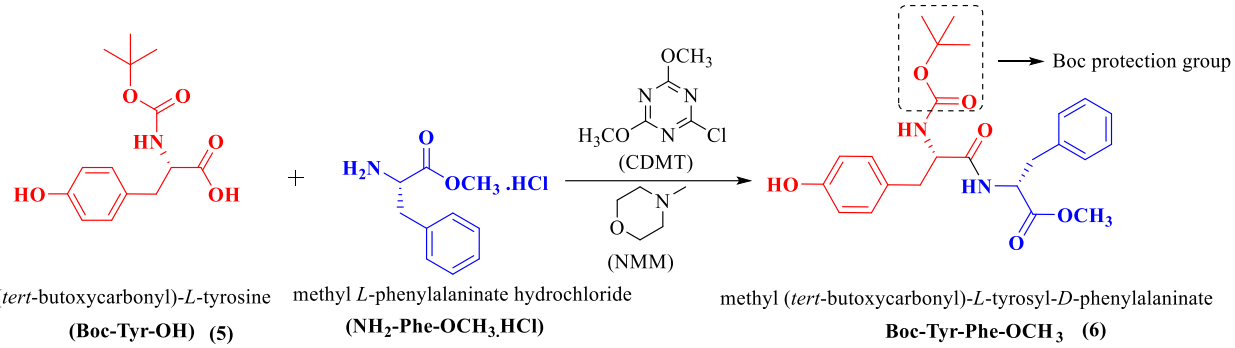

Figure 3.4 Synthesis of methyl (tert-butoxycarbonyl)-*L*- tyrosyl-*D*-phenylalaninate (Boc-Tyr-Phe-OCH_3)

Table 3.1. Spectroscopies and elemental analysis values of methyl (tert-butoxycarbonyl)-*L*-tyrosyl-*D*-phenylalaninate (Boc-Tyr-Phe-OCH_3) compound.

FT-IR (cm-1)	**^{1}H-NMR (ppm)**	**13C –APT NMR (ppm)**
ν_{N-H}, ν_{OH} 3214, 3304, 3339 **$\nu_{C-H(Aromatic)}$, $\nu_{C-H(Aliphatic)}$** 3030, 3064, 3087 2855, 2932, 2963 **$\nu_{C=C}$** 1518, 1536, 1597, 1615 **$\nu_{C=O}$** 1660 (Amide C=O) 1686 (Boc Protection Group C=O), 1706 (Ester C=O),	1.31 (9H, s, H^{11}), 2.56-2.59 and 2.74-2.79 (2H, H^{6}), 2.96-3.07 (2H, m, H^{17}), 4.08-4.09 (1H, q, H^{14}), 4.49-4.53 (1H, q, H^{7}), 6.63-6.65 (2H, d, J=8.4 Hz, H^{2}), 6.81-6.83 (1H, d, H^{8} (-NH)), 7.0-7.02 (2H, d, J=8.8 Hz, H^{3}), 7.23-7.30 (5H, m, H^{19}, H^{20} and H^{21}), 8.32-8.34 (1H, d, H^{13} (-NH)), 9.19 (1H, s, H^{5} (-OH))	155.57 C^{1} , 172.48 C^{12}, 115.24 C^{2} , 053.97 C^{14}, 128.74 C^{3} , 172.31 C^{15}, 128.50 C^{4} , 052.32 C^{16}, 037.09 C^{6} , 037.18 C^{17}, 056.35 C^{7} , 137.49 C^{18}, 156.18 C^{9} , 129.61 C^{19} 074.44 C^{10} , 130.54 C^{20} 028.61 C^{11}, 127.05 C^{21} **DMSO-d_6** **^{13}C –APT:** 39 **^{1}H-NMR :** 2.51 and 3.36
MALDI-TOF MS	**Elemental Analyse (%)**	
Theoretical **Mw:** 442.51 g/mol **Experimental** **[M]:** 442.548 m/z **[M-C(CH_3)$_3$]:** 386.609 m/z **[M-Boc] :** 342.542 m/z	**$C_{24}H_{20}N_2O_6$ (Mw: 442.51 g/mol)** **Theoretical:** C, 65.14; H, 6.83; N, 6.33 **Experimental:** C, 65.20; H, 6.88; N, 6.30	

3.4.2. Synthesis of Methyl ((*S*)-2-((tert-butoxycarbonyl) amino)-3-(4-(3,4-dicyanophenoxy) phenyl) propanoyl)-*D*-phenylalaninate (Boc-Tyr-Phe-OCH_3-O-PN) (7)

In a 250 ml three-neck bottom flask placed on hot plate fitted with magnetic stirrer, thermometer and rubber tube supplying Argon gas, 1.96 g (11.30 mmol) of dried 4-nitrophthalonitrile (**4**) and 5.0 g (11.30 mmol) of dried methyl (tert-butoxycarbonyl)-*L*-tyrosyl-*D*-phenylalaninate (**6**) was dissolved in 60 ml of DMF solvent at room temperature forming a light yellow solution. Then, the temperature was raised to 80 °C and 3.12 g of dried powder K_2CO_3 was added to the reaction mixture in a portion over 1.5 hours while maintaining the temperature between 80 – 95 °C. On the addition of K_2CO_3 the colour of the reaction medium gradually changed to dark brown. The reaction as shown in **Figure 3.5** below proceeded for 48 hours on constant stirring and supplied of Argon gas at 90 °C with regular checking of FT-IR spectral of the reaction mixture at certain intervals for monitoring a complete disappearance of strong stretching peaks of $–NO_2$ around 1538 cm^{-1} and 1355 cm^{-1}. The mixture was cooled to room temperature and precipitated in 600 ml of distilled water with the addition of a few drops of 1.0 M HCl (to bring down the pH of the medium from basic to pH 6) and salt solution all to facilitate a good precipitation of the product. The precipitated product was filtered, washed with plenty of water and air-dried at room temperature. The colour of the resulting product methyl ((*S*)-2-((tert-butoxycarbonyl) amino)-3-(4-(3,4-dicyanophenoxy) phenyl) propanoyl)-*D*-phenylalaninate **(7)** is light brown, the yield is 4.35g (67.65%). The molecular formula, molecular weight, weight of the product and % yield of the compound **(7)** are given in **Table 2.1b**, and the FT-IR spectral peaks values are given in **Table 2.1c**

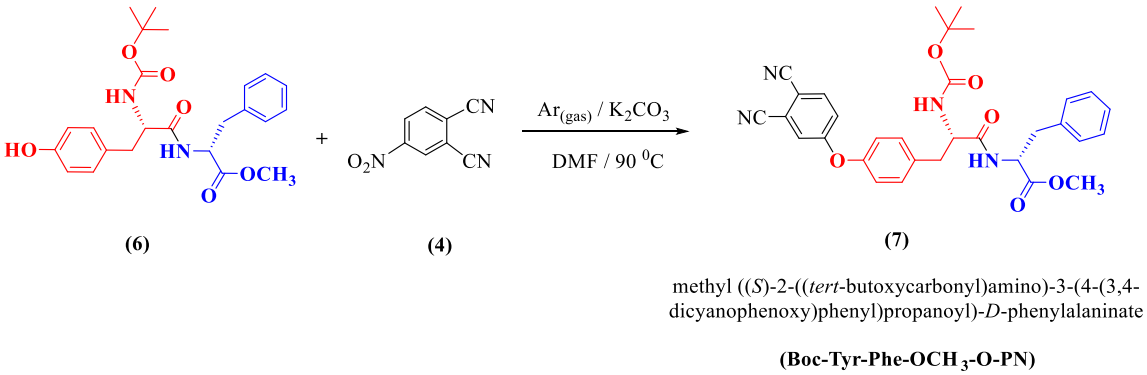

Figure 3.5. Synthesis of methyl ((S)-2-((tert-butoxycarbonyl) amino)-3-(4-(3,4-dicyanophenoxy) phenyl) propanoyl)-D-phenylalaninate **(Boc-Tyr-Phe-OCH_3-O-PN) (7)**

3.4.3. Synthesis of Phthalocyanine complexes of Methyl ((*S*)-2-((tert-butoxycarbonyl) amino)-3-(4-(3,4-dicyanophenoxy) phenyl) propanoyl)-*D*-phenylalaninate compounds (7a,7b,7c,7d,7e 7f)

An Argon gas was passed through 3 ml of DMF at 130 °C in a Borosilicate Glass Vacuum Cold Trap Glass Bubbler with a 10 mm serrated Hose, 225 mm length below the 29/42 joint reaction tube. 0.204 g (0.3588 mmol) of **(7)** was added into each of the reaction tubes followed by addition of 0.0270 g (0.0897mmol) of $Cr(Ac)_3 4H_2O$, 0.02198 g (0.0897 mmol) of $Mn(Ac)_2 4H_2O$, 0.0188 g (0.0897 mmol) of $Fe(Ac)_2 2H_2O$, 0.0223 g (0.0897 mmol) of $Co(Ac)_2 4H_2O$, 0.0223 g (0.0897 mmol) of $Ni(Ac)_2 4H_2O$, 0.0204 g (0.0897 mmol) of $Cu(Ac)_2 4H_2O$, and 0.0197 g (0.0897mmol) of $Zn(Ac)_2 2H_2O$ respectively. After 1 hour, if there was no colour change, 3 drops of triethanolamine (TEA) were added to the reaction medium and the temperature was increased to 150 °C. The product **7a**-CrPc was refluxed for 48 hours, **7b**-MnPc for 4 hours, **7c**-FePc for 4 hours, **7d**-CoPc for 2 hours, **7e**-NiPc for 2 hours and **7f**-ZnPc was reflux for 3 hours. The blue or green colour products obtained as indicated in **Figure 3.6** below were precipitated in 200 ml of water and filtered to dry at 60 °C in the oven. These were later purified by stirring in hot ethanol for 1 hour, filtered and dried in a vacuum oven at 60 °C. The molecular formula, molecular weight, weight of product and % yield results of the synthesized phthalocyanine compounds are given in **Table 3.2,** and FT-IR and UV-visible spectrum peaks are presented in **Table 3.3**.

FT-IR spectra of the ligand **(7)** and its complexes as well as the UV-visible spectral of the complexes are given in the **Appendix Section.**

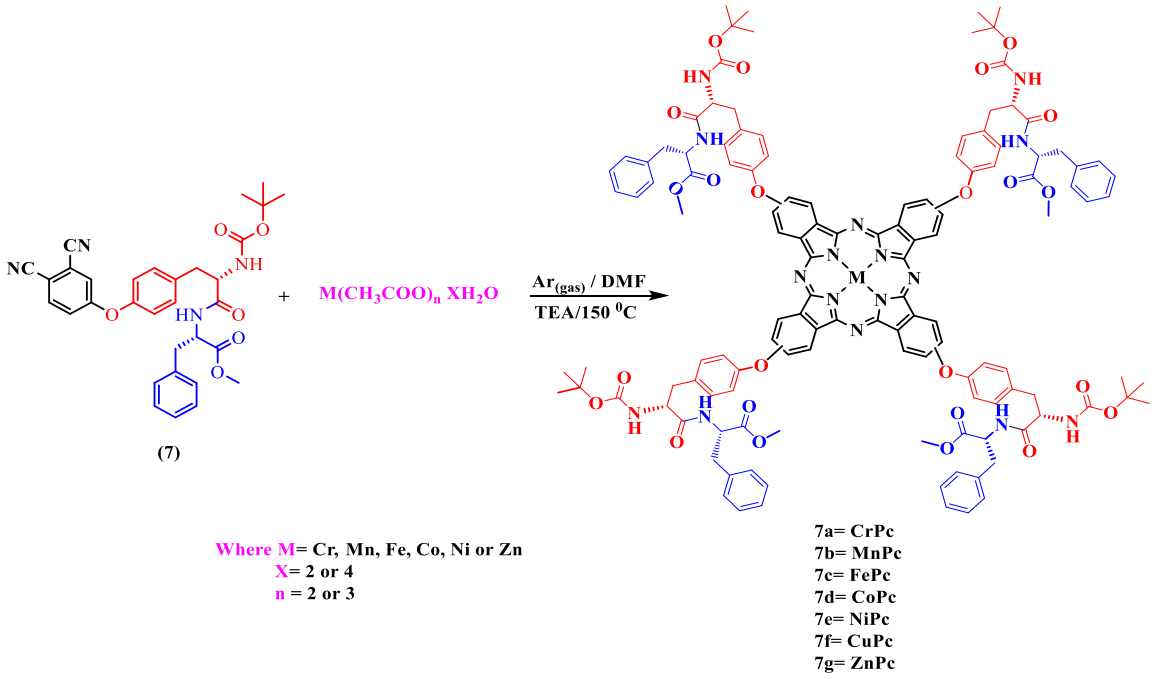

Figure 3.6. Synthesis Tyr-Phe Dipeptide Substituted Metallo Phthalocyanine complexes

Table 3.2. Molecular formula, molecular weight, weight of products and % yield results of compounds **7** and **(7a, 7b, 7c, 7d, 7e, 7f and 7g**) phthalocyanine complexes

Compounds	Molecule Formula	Molecular Weight (g/mol)	Weight obtained (g)	% Yield
7	$C_{32}H_{32}N_4O_6$	568.63	4.35	67.64
7a-CrPc	$C_{128}H_{128}CrN_{16}O_{24}$	2326.52	0.167	80.03
7b-MnPc	$C_{128}H_{128}MnN_{16}O_{24}$	2329.46	0.156	74.67
7c-FePc	$C_{128}H_{128}FeN_{16}O_{24}$	2330.37	0.143	68.42
7d-CoPc	$C_{128}H_{128}CoN_{16}O_{24}$	2333.45	0.176	84.10
7e-NiPc	$C_{128}H_{128}NiN_{16}O_{24}$	2333.21	0.176	84.10
7f-CuPc	$C_{128}H_{128}CuN_{16}O_{24}$	2338.07	0.140	66.76
7g-ZnPc	$C_{128}H_{128}ZnN_{16}O_{24}$	2339.90	0.205	97.68

Table 3.3. Major FT-IR and UV-visible spectrum peaks of compound **7** and **(7a, 7b, 7c, 7d, 7e, 7f** and **7g)** phthalocyanine complexes.

Compounds	FT-IR Peaks (cm^{-1})	UV-Visible Bands (nm)
7	3146-3020, 2979-2832, 1716,1662,2232,1591,1248,1245,1167,1021	-
7a-CrPc	2864, 1767, 1710, 1597, 1504, 1394, 1232, 1167, 10682	676, 630, 608, 587, 313
7b-MnPc	2885, 1769, 1707, 1599, 1505, 1394, 1232, 1165, 1077, 744	721, 590, 254
7c-FePc	2877, 1765, 1709, 1598, 1504, 1391, 1231, 1164, 1052, 747	664, 618, 600, 583, 262, 227
7d-CoPc	3312, 1768, 1710, 1652, 1596, 1506, 1387, 1231, 1164, 1095, 751	669, 521, 268, 229
7e-NiPc	3331, 1716, 1668, 1602, 1506, 1367, 1234, 1163, 1093, 750	669, 647,627, 521, 258, 238, 233, 226
7f-CuPc	3312,2949-2830,1767,1708,1661,1504,1394,1231,1169,1033	675, 658, 332
7g-ZnPc	3279, 1770, 1712, 1599, 1506, 1393, 1231, 1164, 1064, 747	677, 625, 611, 553, 260, 239, 235

3.4.4. Electrochemistry experimental of tyrosine- phenylalanine dipeptide substituted phthalocyanine complexes.

The solvents were purified following the standard technique reported in [117, 118] and stored over molecular sieves. Cyclic voltammetry (CV) experiments were conducted in a non-aqueous reagent employing tetra butyl ammonium tetra fluoro borate (TBAFB) (Fluka) as the supporting electrolyte and a Gamry Interface 1010 B Potentiostat/Galvanostat/ZRA. For CV measurements in dimethylformamide (DMF), a three-electrode setup was employed, consisting of a glassy carbon working electrode, a platinum wire counter, and a platinum wire quasi-reference electrode. The ferrocene/ferrocenium pair (Fc/Fc^+) was employed as an internal standard, and potentials were reported in relation to Fc/Fc^+ in non-aqueous solutions. Square wave voltammetry analysis was performed at a frequency of 5 or 10 Hz, amplitude of 40 mV, and step potential of 4 mV. High-purity Argon is used to de-oxygenate the cell at least 10 minutes before conducting electrochemical tests, and the solution is shielded from air by an argon throughout the entire process

[6]. A wide potential range (-2.5 to +1.5 V versus Fc/Fc^{+}) was employed to explore the electrochemical characteristics of all the phthalocyanine complexes. **Table 3.4** gives the summary of redox potential values of both the reduction and oxidation processes for tyrosine-phenylalanine dipeptide substituted phthalocyanine complexes.

Table 3.4. Redox potential (Volt, against Fc/Fc^{+}, calculated from midpoint of anodic and cathodic peak potentials of SWV) of tyrosine- phenylalanine dipeptide substituted phthalocyanine complexes.

Complexes	R4	R3	R2	R1	Mr	Mo	O1	O2
7a-CrPc	-2.36	-2.13	-1.86	-1.32	-1.12	-0.52	0.31	0.60
7b-MnPc	-2.32	-1.89	-1.22			0.14	0.4	0.88
7c-FePc	-2.41	-2.15	-1.91	-1.3		-0.24	0.5	0.92
7d-CoPc	-2.37	-2.12	-1.89	-1.31	-0.88	0.45	0.59	0.93
7e-NiPc	-2.27	-2.07	-1.64	-1.26			0.48	1.41
7f-CuPc	-2.35	-2.04	-1.80	-1.21			0.64	0.96
7g-ZnPc	-2.27	-1.92	-1.73	-1.14			0.31	0.73

3.5. Synthesis of Tyrosine-Alanine Dipeptide Amino Acid Substituent and complexes

3.5.1. Methyl (tert-butoxycarbonyl)-*L*-tyrosyl-*D*-alaninate (Boc-Tyr-Ala-OCH_3) (8)

The reaction was conducted by addition of 2.50 g (8.89 mmol) of Tyrosine amino acid (Boc-Tyr-OH) (1.0 equivalent) **(5)** with the amine group protected, 1.24 g (8.89 mmol) of Alanine methyl ester (NH_2-Ala-OCH_3.HCl) (1.0 equivalent) and 1.72 g (9.78 mmol) of (CDMT) (1.2 equivalent) as coupling agent in 250 ml plate bottom flask. An appropriate amount of 25 ml of Acetonitrile solvent was added into the reaction flask at room temperature with constant stirring. On continuous stirring, 2.44 ml (22.2 mmol) of N-methyl morpholine (NMM) Base was added to the reaction mixture dropwise. The reaction as reported in **Figure 3.7** below was allowed to continuously stirring for 16 to 24 hours with sequences of Thin Layer Chromatography (TLC) tests to monitor the completion of the reaction using free-coated aluminium TLC paper as stationary phase and a mixture of Ethyl acetate and n-Hexane solvent system in a ratio of 3:4 as mobile phase. On completion of the reaction, then the solution of the mixture was filtered to remove any unreacted residue and the solvent in the filtrate was evaporated under a reduced pressure using a vacuum rotary evaporator. The residue was dissolved in 10 ml Acetone and precipitated in 200 ml of water in a Baker. The precipitate was filtered and dried at room temperature. The product **(8)** is white powder weight 2.52 g with a percentage yield of 77.3 %, molecular weight of 366.41 and molecular formula $C_{18}H_{26}N_2O_6$. The FT-IR, ^{1}H-NMR, ^{13}C-NMR, mass spectroscopy peaks and elemental analysis values are presented in **Table 3.5** below and the FT-IR, ^{1}H-NMR, ^{13}C-NMR, mass spectroscopy spectrum were given in **Appendix section.**

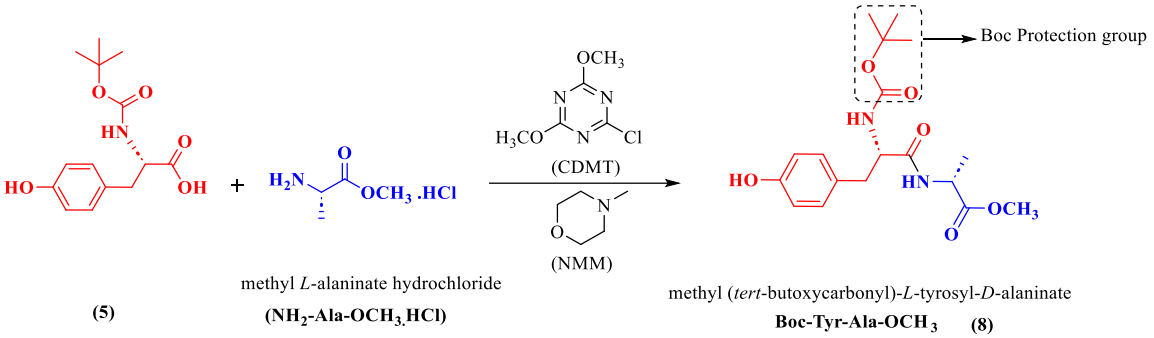

Figure 3.7. Synthesis of methyl (tert-butoxycarbonyl)-*L*- tyrosyl-*D*-alaninate (Boc-Tyr-Ala-OCH_3) **(8)**

Table 3.5. Spectroscopies and Elemental analysis values of methyl (tert-butoxycarbonyl)-*L*- tyrosyl-*D*-alaninate **(Boc-Tyr-Ala-OCH_3)** compound.

FT-IR (cm^{-1})	**^{1}H-NMR (ppm)**	**^{13}C –APT NMR (ppm)**
ν_{N-H}, ν_{OH} 3278, 3331, 3402 **$\nu_{C-H(Aromatic)}$, $\nu_{C-H(Aliphatic)}$** 3005, 3028 2933, 2959 **$\nu_{C=C}$** 1514, 1527, 1599, 1614 **$\nu_{C=O}$** 1645 (Amide C=O) 1685 (Belongs to the Boc protection group C=O), 1742 (Ester C=O),	1.26-1.30 (3H, d, H^{17}), 1.32 (9H, s, H^{11}), 2.56-2.65 and 2.84-2.88 (2H, H^6), 3.64 (3H, s, H^{16}), 4.08-4.13 (1H, m, H^{14}), 4.29-4.32 (1H, q, H^7), 6.65-6.67 (2H, d, J=8.4 Hz, H^2), 6.74-6.76 (1H, d, H^8 (-NH)), 7.06-7.08 (2H, d, J=8.8 Hz, H^3), 8.29-8.31 (1H, d, H^{13} (-NH)), 9.14 (1H, s, H^5 (-OH))	155.70 C^1 , 078.40 C^{10}, 115.26 C^2 , 028.63 C^{11}, 130.57 C^3 , 172.33 C^{12}, 128.63 C^4 , 047.99 C^{14}, 037.06 C^6 , 173.47 C^{15}, 056.17 C^7 , 052.32 C^{16}, 156.19 C^9 , 017.46 C^{17}, **DMSO-d_6** **^{13}C –APT:** 39 **^{1}H-NMR :** 2.51 and 3.36
MALDI-TOF MS	**Elemental Analyse (%)**	
Theoretical **Mw:** 366.41 g/mol **Experimental** **[M]:** 366.445 m/z **[M-C(CH_3)$_3$] :** 310.310 m/z	**$C_{18}H_{26}N_2O_6$ (Mw: 366.41 g/mol)** **Theoretical:** C, 59.0; H, 7.15; N, 7.65 **Experimental:** C, 59.07; H, 7.19; N, 7.61	

3.5.2. Synthesis of Methyl ((*S*)-(2-[(tert-butoxycarbonyl) amino)-3-(4-(3,4-dicyanophenoxy) phenyl) propanoyl)-*D*- alaninate (Boc-Tyr-Ala-OCH_3-O-PN) (9)

In a 250 ml three-neck bottom flask placed on hot plate fitted with magnetic stirrer, thermometer and rubber tube supplying Argon gas, 2.36 g (13.65 mmol) of dried 4-Nitrophthalonitrile (**4**) and 5.0 g (13.65 mmol) of dried methyl (tert-butoxycarbonyl)-*L*- tyrosyl-*D*-alaninate (**8**) was dissolved in 60 ml of DMF solvent at room temperature forming a light-yellow

solution. Then, the temperature was raised to 80 °C and 3.77 g (27.3 mmol) of dried powder K_2CO_3 was added to the reaction mixture in portions over 1.5 hours while maintaining the temperature between 80 – 95 °C. On the addition of K_2CO_3 the colour of the reaction medium gradually changed to dark brown. The reaction as shown in **Figure 3.8** below proceeded for 48 hours on constant stirring and supplied of Argon gas at 90 °C with regular checking of FT-IR spectral of the reaction mixture at certain intervals for monitoring a complete disappearance of $–NO_2$ peak at 1538 cm^{-1} and 1355 cm^{-1}. The mixture was cooled to room temperature and precipitated in 600 ml of distilled water with the addition of a few drops of 1.0 M HCl (to bring down the pH of the medium from basic to pH 6) and salt solution all to facilitate a good precipitation of the product. The precipitated product was filtered, washed with plenty of water and air-dried at room temperature. The colour of the resulting product methyl ((*S*)-2-((tert-butoxycarbonyl) amino)-3-(4-(3,4-dicyanophenoxy) phenyl) propanoyl)-*D*-alaninate **(9)** is light brown, the yield is 4.90 g (72.9 %). The molecular formula, molecular weight, weight of product and % yield results of the compound **(9)** are given in **Table 3.6**, and the FT-IR spectral peaks values are given in **Table 3.7**.

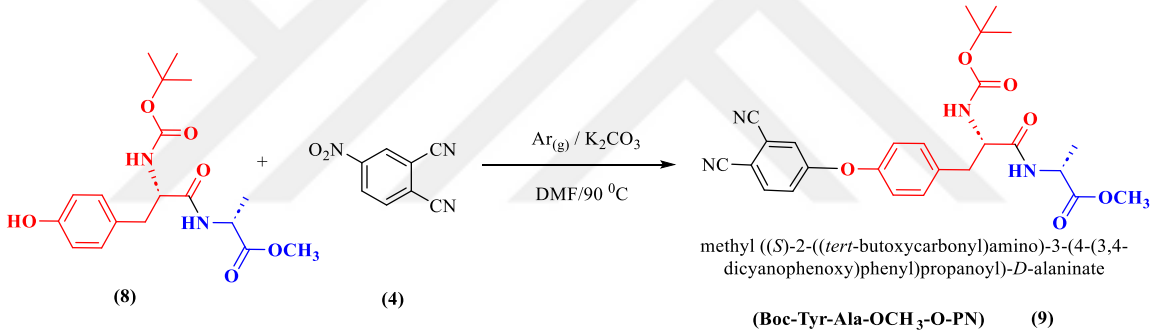

Figure 3.8. Synthesis of methyl ((S)-2-((tert-butoxycarbonyl) amino)-3-(4-(3,4-dicyanophenoxy) phenyl) propanoyl)-*D*-alaninate **(Boc-Tyr-Ala-OCH$_3$-O-PN) (9)**

3.5.3. Synthesis of Phthalocyanine complexes of Methyl ((S)-2-((tert-butoxycarbonyl) amino)-3-(4-(3,4-dicyanophenoxy) phenyl) propanoyl)-*D*-alaninate compounds (9a, 9b, 9c, 9d, 9e, 9f 9g)

An Argon gas was passed through 3 ml of DMF at 130 °C in a Borosilicate Glass Vacuum Cold Trap Glass Bubbler with a 10 mm serrated Hose, 225 mm length below the 29/42 joint reaction tube. 0.204 g (0.4142 mmol) of **(9)** was added into each of the reaction tubes followed by the addition of 0.0312 g (0.1036mmol) of $Cr(Ac)_34H_2O$; 0.0254 g (0.1036 mmol) of $Mn(Ac)_24H_2O$; 0.0217 g (0.1036 mmol) of $Fe(Ac)_22H_2O$; 0.0258 g (0.1036 mmol) of $Co(Ac)_24H_2O$; 0.0258 g (0.1036 mmol) of $Ni(Ac)_24H_2O$; 0.0225 g (0.1036 mmol) of $Cu(Ac)_22H_2O$ and 0.0227 g (0.1036mmol) of $Zn(Ac)_22H_2O$ respectively. After 1 hour, if there was no colour change, 3 drops of triethanolamine (TEA) were added to the reaction medium and the temperature was increased to

150 °C. The product of the reactions shown below in **Figure 3.9** as **9a**-CrPc was refluxed for 23 hours, **9b**-MnPc for 20 hours, **9c**-FePc for 4 hours, **9d**-CoPc for 2 hours, **9e**-NiPc for 3 hours, **9f**-CuPc for 22 hours and **9g**-ZnPc was reflux for 7 hours. The blue or green colour products were precipitated in 200 ml of water and filtered to dry at 60 °C in the oven. These were later purified by stirring in hot ethanol for 1 hour, filtered and dried in a vacuum oven at 60 °C. The molecular formula, molecular weight, weight of product and % yield results of the synthesized phthalocyanine compounds are given in **Table 3.6,** and FT-IR and UV-visible spectrum peaks are presented in **Table 3.7.** FT-IR spectra of the ligand **(9)** and its complexes as well as the UV-visible spectral of the complexes are given in the **Appendix Section.**

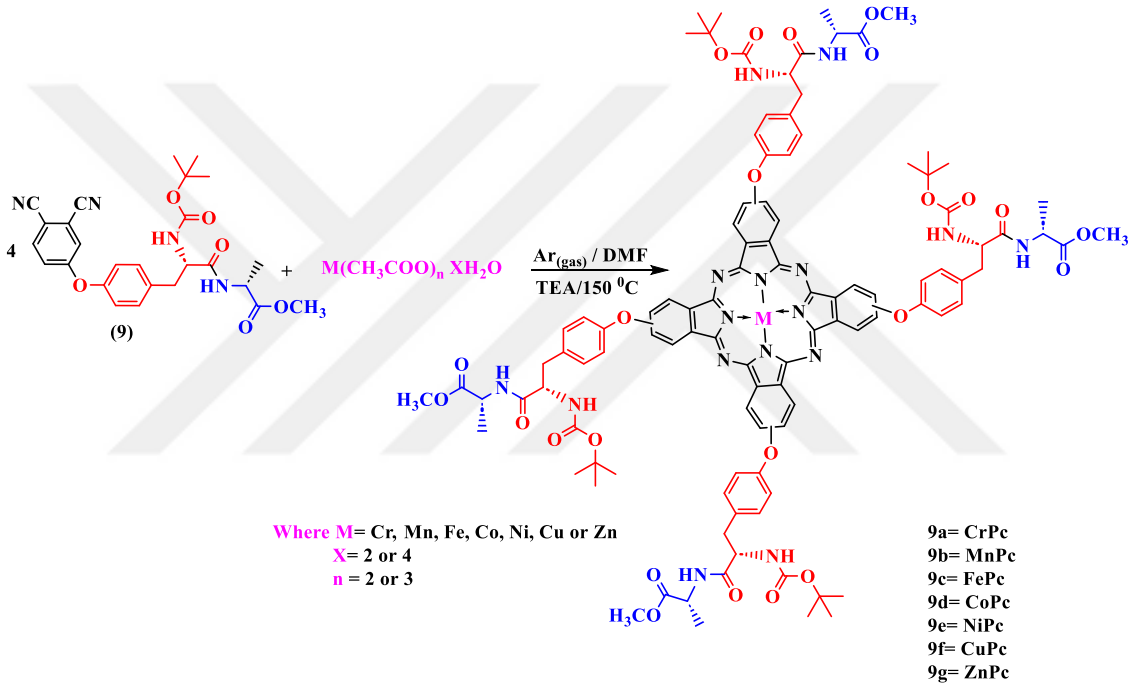

Figure 3.9. Synthesis Tyr-Ala Dipeptide Substituted Metallo Phthalocyanine complexes

Table 3.6. Molecular formula, molecular weight, weight of products and % yield results of compounds **9** and **(9a, 9b, 9c, 9d, 9e, 9f** and **9g**) phthalocyanine complexes.

Compounds	Molecule Formula	Molecular Weight (g/mol)	Weight obtained (g)	% Yield
9	$C_{26}H_{28}N_4O_6$	492.52	4.90	72.91
9a-CrPc	$C_{106}H_{117}CrN_{16}O_{24}$	2051.19	0.106	49.91
9b-MnPc	$C_{106}H_{117}MnN_{16}O_{24}$	2054.13	0.151	70.99
9c-FePc	$C_{106}H_{117}FeN_{16}O_{24}$	2055.04	0.139	65.32
9d-CoPc	$C_{106}H_{117}CoN_{16}O_{24}$	2058.12	0.149	69.92
9e-NiPc	$C_{106}H_{117}NiN_{16}O_{24}$	2057.88	0.162	76.03
9f-CuPc	$C_{106}H_{117}CuN_{16}O_{24}$	2062.74	0.161	75.38
9g-ZnPc	$C_{106}H_{117}ZnN_{16}O_{24}$	2064.57	0.084	39.29

Table 3.7. Major FT-IR and UV-visible spectrum peaks of compound **9** and (**9a, 9b, 9c, 9d, 9**e**, 9f and 9g**) phthalocyanine complexes.

Compounds	FT-IR Peaks (cm^{-1})	UV-Visible Bands (nm)
9	3320, 3100-3000, 2986-2860, 2232, 1717, 1657, 1591, 1486, 1419, 1394, 1250, 1169, 1020	-
9a-CrPc	3285, 2938-2869, 1769, 1709, 1656, 1597, 1504, 1395, 1231, 1068	676, 628, 609, 575, 305, 299, 253
9b-MnPc	3238, 2937-2850, 1766, 1700, 1662, 1595, 1504, 1394, 1230, 1167, 1071	718, 654, 647, 616, 423, 390, 252
9c-FePc	3309, 2982-2845, 1764, 1701, 1657, 1593, 1506, 1394, 1233, 1166, 1057	667, 626, 599, 592, 313, 264, 260
9d-CoPc	3317, 2978-2859, 1766, 1714, 1658, 1600, 1506, 1476, 1365, 1230, 1162, 1093	664, 612, 606, 529, 324, 315, 294, 275, 264, 217, 205
9e-NiPc	3312, 2977-2935, 1766, 1716, 1657, 1592, 1506, 1475, 1365, 1233, 1162, 1094	667, 648, 622, 509, 305
9f-CuPc	3238, 2936-2844, 1760, 1661, 1506, 1394, 1230, 1066, 1033	675, 628, 608, 586, 316, 296
9g-ZnPc	3269, 2973-2866, 1770, 1711, 1650, 1599, 1505, 1365, 1231, 1164, 1064, 747,700	674, 619, 612, 516, 341, 320, 260, 246

3.5.4. Electrochemistry experimental of tyrosine- alanine dipeptide substituted phthalocyanine complexes.

The solvents were purified following the standard technique reported in [117, 118] and stored over molecular sieves. Cyclic voltammetry (CV) experiments were conducted in a non-aqueous reagent employing tetra butyl ammonium tetra fluoro borate (TBAFB) (Fluka) as the supporting electrolyte and a Gamry Interface 1010 B Potentiostat/Galvanostat/ZRA. For CV measurements in dimethylformamide (DMF), a three-electrode setup was employed, consisting of a glassy carbon working electrode, a platinum wire counter, and a platinum wire quasi-reference electrode. The ferrocene/ferrocenium pair (Fc/Fc^+) was employed as an internal standard, and potentials were reported with Fc/Fc^+ in non-aqueous solutions. Square wave voltammetry analysis was performed at a frequency of 5 or 10 Hz, amplitude of 40 mV, and step potential of 4 mV. High-purity Argon is used to de-oxygenate the cell at least 10 minutes before conducting electrochemical tests, and the solution is shielded from air by an argon throughout the entire process [6]. A wide potential range (-2.5 to +1.5 V versus Fc/Fc^+) was employed to explore the electrochemical characteristics of all the phthalocyanine complexes. **Table 3.8** gives the summary of redox potential values of both the reduction and oxidation processes for tyrosine- alanine dipeptide substituted phthalocyanine complexes.

Table 3.8. Redox potential (Volt, against Fc/Fc^{+}, calculated from midpoint of anodic and cathodic peak potentials of SWV) of tyrosine- alanine dipeptide substituted phthalocyanine complexes.

Complexes	R4	R3	R2	R1	Mr	Mo	O1	O2
9a-CrPc	-2.42	-2.27	-1.82	-1.20		0.36	0.53	0.95
9b-MnPc	-2.39	-1.89	-1.61	-1.16			0.24	0.83
9c-FePc	-2.35	-1.98	-1.77	-1.12	-0.72	0.15	0.37	0.72
9d-CoPc	-2.43	-2.09	-1.91	-1.30	-0.89	0.08	0.38	0.62
9e-NiPc	-2.38	-2.06	-1.84	-1.42			0.29	0.67
9f-CuPc	-2.36	-2.05	-1.72	-0.84			0.43	0.86
9g-ZnPc	-2.48	-2.15	-2.00	-1.29			0.29	0.80

3.6. Synthesis of Tyrosine-Glycine Dipeptide Amino Acid Substituent and complex

3.6.1. Methyl (tert-butoxycarbonyl)-*L*-tyrosyl glycinate (Boc-Tyr-Gly-OCH_3) (10)

The reaction was conducted by addition of 3.75 g (13.33 mmol) of Tyrosine amino acid **(Boc-Tyr-OH)** (1.0 equivalent) **(5)** with the amine group protected, 1.67 g (13.33 mmol) of Glycine methyl ester (NH_2-Gly-OCH_3.HCl) (1.0 equivalent) and 2.57 g (14.66 mmol) of (CDMT) (1.10 equivalent) as coupling agent in 250 ml plate bottom flask. An appropriate amount of 35 ml of Acetonitrile solvent was added into the reaction flask at room temperature with constant stirring. On continuous stirring, 2.93 ml (26.66 mmol) of (NMM) as a base was added to the reaction mixture dropwise. The reaction as indicated in **Figure 3.10** below was allowed to be continuously stirred for 16 to 24 hours with sequences of Thin Layer Chromatography (TLC) tests to monitor the completion of the reaction using free coated Aluminum TLC Paper as stationary phase and a mixture of ethyl acetate and n-Hexane solvent system in a ratio of 3:4 as mobile phase.

On completion of the reaction, then the solution of the mixture was filtered to remove any unreacted residue and the solvent in the filtrate was evaporated under a reduced pressure using a vacuum rotary evaporator. The residue was dissolved in 10 ml Acetone and precipitated in 200 ml of water in a Baker. The precipitate was filtered and dried at room temperature. The product **(10)** is white powder weight 4.24 g (12.03 mmol) with a percentage yield of 90.26 %, molecular weight 352.39 and molecular formula $C_{17}H_{24}N_2O_6$. The FT-IR, ^{1}H-NMR, ^{13}C-NMR, Mass spectroscopy peaks and Elemental Analyse values are presented in **Table 3.9** below and the FT-IR, ^{1}H-NMR, ^{13}C-NMR, Mass spectroscopy Spectrum were given in **Appendix section.**

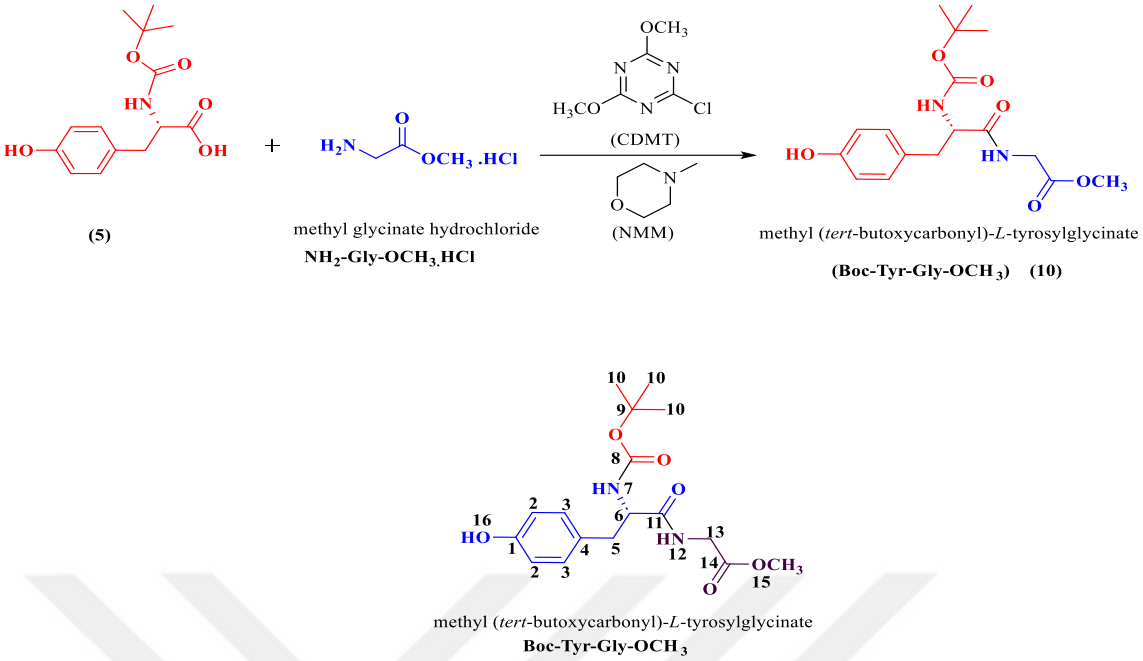

Figure 3.10. Synthesis of methyl (tert-butoxycarbonyl)-*L*- tyrosyl glycinate (Boc-Tyr-Gly-OCH_3) **(10)**

Table 3.9. Spectroscopies and Elemental analysis values of methyl (tert-butoxycarbonyl)-*L*- tyrosyl glycinate **(Boc-Tyr-Gly-OCH_3)** compound.

<table>
<tr><th>FT-IR (cm^{-1})</th><th>^{1}H-NMR (ppm)</th><th>^{13}C –APT NMR (ppm)</th></tr>
<tr><td rowspan="2">ν_{N-H}, ν_{OH}
3250, 3366, 3333
$\nu_{C-H(Aromatic)}$, $\nu_{C-H(Aliphatic)}$
3016 2924,2955
$\nu_{C=C}$
1516, 1595,
$\nu_{C=O}$
1637 (Amide C=O)
1688 (Belong to the Boc protection group C=O),
1744 (Ester C=O),</td><td rowspan="2">1.31 (9H, s, H^{10}),
2.61-2.64 and 2.85-2.90 (2H, H^5)
3.85-3.90 (2H, H^{13}),
4.09-4.12 (1H, q, H^6),
6.64-6.66 (2H, d, J=8.8 Hz, H^2),
6.89-6.91 (1H, d, H^7 (-NH)),
7.05-7.07 (2H, d, J=8.4 Hz, H^3),
8.38 (1H, t, H^{12} (-NH)),
9.19 (1H, s, H^{16} (-OH))</td><td>155.72 C^1 , 078.40 C^9,
115.25 C^2 , 028.63 C^{10},
130.55 C^3 , 172.99 C^{11},
128.70 C^4 , 041.06 C^{13},
037.09 C^5 , 170.77 C^{14},
056.34 C^6 , 052.17 C^{15},
156.16 C^8</td></tr>
<tr><td>DMSO-d_6
^{13}C –APT: 39
<b>^{1}H-NMR: 2.51 and 3.36</td></tr>
<tr><th>MALDI-TOF MS</th><th colspan="2">Elemental Analysis (%)</th></tr>
<tr><td>Theoretical Information
Mw: 352.39 g/mol
Experimental
[M]: 352.306 m/z
[M+Na]: 374.373 m/z
[M+K]: 390.429 m/z
[M-C(CH_3)$_3$] : 296.134</td><td colspan="2">$C_{17}H_{24}N_2O_6$ (Mw: 352.39 g/mol)
Theoretical: C, 57.94; H, 6.87; N, 7.95
Experimental: C, 57.99; H, 6.90; N, 7.99</td></tr>
</table>

3.6.2. Synthesis of Methyl ((S)-(2-[(tert-butoxycarbonyl) amino)-3-(4-(3,4-dicyanophenoxy) phenyl) propanoyl] glycinate (Boc-Tyr-Gly-OCH_3-O-PN) (11)

In a 250 ml three-neck bottom flask placed on a hot plate fitted with a magnetic stirrer, thermometer, and rubber tube supplying Argon gas, 2.26 g (13.05mmol) of dried 4-nitrophthalonitrile (**4**) and 4.60 g (13.05 mmol) of dried methyl (tert-butoxycarbonyl) tyrosyl glycinate (**10**) was dissolved in 60 ml of DMF solvent at room temperature forming a light-yellow solution. Then, the temperature was raised to 80 °C, and 3.61 g (26.11 mmol) of dried powder K_2CO_3 was added to the reaction mixture in portions over 1.5 hours while maintaining the temperature between 80 – 95 °C. On the addition of K_2CO_3 the colour of the reaction medium gradually changed to dark brown. The reaction as reported in **Figure 3.11** below proceeded for 48 hours on constant stirring and supplied of Argon gas at 90 °C with regular checking of FT-IR spectral of the reaction mixture at certain intervals for monitoring a complete disappearance of strong stretching signal of $–NO_2$ around 1538 cm^{-1} and 1355 cm^{-1}. The mixture was cooled to room temperature and precipitated in 400 ml of distilled water with the addition of a few drops of 1M HCl (to bring down the pH of the medium from basic to pH 6) and salt solution all to facilitate a good precipitation of the product. The precipitated product was filtered, washed with plenty of water, and air-dried at room temperature. The colour of the resulting product methyl ((*S*)-2-((tert-butoxycarbonyl) amino)-3-(4-(3,4-dicyanophenoxy) phenyl) propanoyl) glycinate **(11)** is light brown, the yield is 4.46 g (9.32 mmol) 71.4 %. The molecular formula, molecular weight, weight of the product, and % yield results of the compound **(11)** are given in **Table 2.3b**, and the FT-IR spectral peaks values are given in **Table 2.3c.**

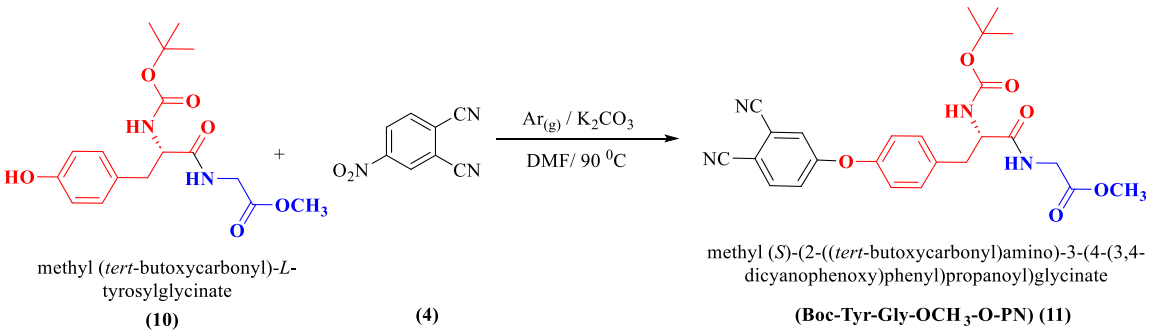

methyl (*tert*-butoxycarbonyl)-*L*-tyrosylglycinate **(10)**

(4)

methyl (*S*)-(2-((*tert*-butoxycarbonyl)amino)-3-(4-(3,4-dicyanophenoxy)phenyl)propanoyl)glycinate **(Boc-Tyr-Gly-OCH_3-O-PN) (11)**

Figure 3.11. Synthesis of methyl ((S)-2-((tert-butoxycarbonyl) amino)-3-(4-(3,4-dicyanophenoxy) phenyl) propanoyl) glycinate **(Boc-Tyr-Gly-OCH_3-O-PN) (11).**

3.6.3. Synthesis of Phthalocyanine complexes of Methyl ((S)-2-((tert-butoxycarbonyl) amino)-3-(4-(3,4-dicyanophenoxy) phenyl) propanoyl) glycinate complexes (11a, 11b, 11c, 11d, 11e, 11f 11g)

An Argon gas was passed through 3 ml of DMF at 130 °C in a Borosilicate Glass Vacuum Cold Trap Glass Bubbler with a 10 mm serrated Hose, 225 mm length below the 29/42 joint reaction tube. 0.204 g (0.4263 mmol) of **(9)** was added into each of the reaction tubes followed by the addition of 0.0321g (0.1066 mmol) of $Cr(Ac)_3 4H_2O$, 0.0261 g (0.1066 mmol) of $Mn(Ac)_2 4H_2O$, 0.0224 g (0.1066 mmol) of $Fe(Ac)_2 2H_2O$, 0.0266 g (0.1066 mmol) of $Co(Ac)_2 4H_2O$, 0.0265 g (0.1066 mmol) of $Ni(Ac)_2 4H_2O$, 0.0232 g (0.1066 mmol) of $Cu(Ac)_2 2H_2O$ and 0.0234 g (0.1066 mmol) of $Zn(Ac)_2 2H_2O$ respectively. After 1 hour, if there was no colour change, 3 drops of triethanolamine (TEA) were added to the reaction medium and the temperature was increased to 150 °C. The product of the reactions shown below in **Figure 3.12** as **11a**-CrPc was refluxed for 48 hours, **11b**-MnPc for 4 hours, **11c**-FePc for 4 hours, **11d**-CoPc for 2 hours, **11e**-NiPc for 2 hours, **11f**-CuPc for 2 hours and **11g**-ZnPc was reflux for 3 hours. The blue or green colour products were precipitated in 200 ml of water and filtered to dry at 60 °C in the oven. These were later purified by stirring in hot ethanol for 1 hour, filtered and dried in a vacuum oven at 60 °C. The molecular formula, molecular weight, weight of product and % yield results of the synthesized phthalocyanine compounds are given in **Table 3.10,** and FT-IR and UV-visible spectrum peaks are presented in **Table 3.11**.

FT-IR spectra of the ligand **(11)** and its complexes as well as the UV-visible spectral of the complexes are given in the **Appendix Section.**

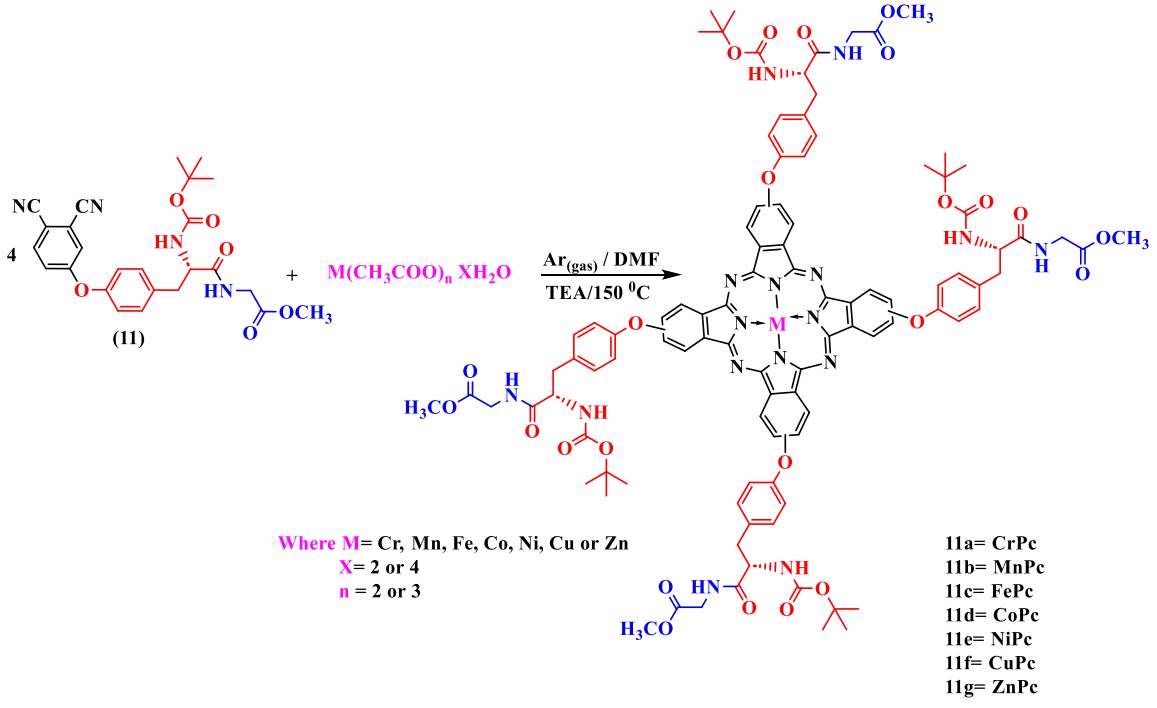

Figure 3.12. Synthesis Tyr-Gly Dipeptide Substituted Metallo Phthalocyanine complexes

Table 3.10. Molecular formula, molecular weight, weight of products and % yield results of compounds **11** and **(11a, 11b, 11c, 11d, 11e, 11f** and **11g)** phthalocyanine complexes.

Compounds	Molecule Formula	Molecular Weight (g/mol)	Weight obtained (g)	% Yield
11	$C_{25}H_{26}N_4O_6$	478.50	4.46	71.40
11a-CrPc	$C_{102}H_{109}CrN_{16}O_{24}$	1995.08	0.120	56.43
11b-MnPc	$C_{102}H_{109}MnN_{16}O_{24}$	1998.02	0.190	89.22
11c-FePc	$C_{102}H_{109}FeN_{16}O_{24}$	1998.93	0.110	51.63
11d-CoPc	$C_{102}H_{109}CoN_{16}O_{24}$	2002.02	0.135	63.27
11e-NiPc	$C_{102}H_{109}NiN_{16}O_{24}$	2001.78	0.158	74.06
11f-CuPc	$C_{102}H_{109}CuN_{16}O_{24}$	2006.63	0.169	79.02
11g-ZnPc	$C_{102}H_{109}ZnN_{16}O_{24}$	2008.46	0156	72.87

Table 3.11. Major FT-IR and UV-visible spectrum peaks of compound **11** and (**11a, 11b, 11c, 11d, 11**e**, 11f** and **11g**) phthalocyanine complexes.

Compounds	FT-IR Peaks (cm^{-1})	UV-Visible Bands (nm)
11	3331, 2985, 2233, 1711, 1660, 1597, 1486, 1368, 1250, 1169	-
11a-CrPc	3260, 2934-2868, 1768, 1711, 1657, 1593, 1386, 1232, 1069	680, 612, 332, 299, 632, 577, 325.
11b-MnPc	3261, 1766, 1708, 1662, 1595, 1389, 1233, 1163, 1075	723, 673, 263, 694, 625
11c-FePc	3260, 2941-2871, 1768, 1710, 1658, 1597, 1431, 1381, 1232,1163	667, 599, 335, 295, 626, 592, 313.
11d-CoPc	3312, 1769, 1711, 1657, 1597, 1506, 1473, 1390, 1232, 1162, 1096, 1057	674, 607, 292, 623, 557
11e-NiPc	3226, 1768, 1705, 1602, 1597, 1505, 1381, 1229, 1165, 1067	678, 599, 459, 637, 588, 434.
11f-CuPc	3306, 2941, 2846, 1766, 1704, 1658, 1593, 1506, 1436, 1380, 1231, 1143, 1067, 1032	676, 544, 321, 312, 236, 227, 544, 317, 205.
11g-ZnPc	3284, 2978-2936, 1769, 1706, 1597, 1476, 1393, 1231, 1164, 1088, 1044	680, 611, 353, 631, 531, 321

3.6.4. Electrochemistry experimental of tyrosine- glycine dipeptide substituted phthalocyanine complexes.

The solvents were purified following the standard technique reported in [117, 118] and stored over molecular sieves. Cyclic voltammetry (CV) experiments were conducted in a non-aqueous reagent employing tetra butyl ammonium tetra fluoro borate (TBAFB) (Fluka) as the supporting electrolyte and a Gamry Interface 1010 B Potentiostat/Galvanostat/ZRA. For CV measurements in dimethylformamide (DMF), a three-electrode setup was employed, consisting of a glassy carbon working electrode, a platinum wire counter, and a platinum wire quasi-reference

electrode. The ferrocene/ferrocenium pair (Fc/Fc^+) was employed as an internal standard, and potentials were reported with Fc/Fc^+ in non-aqueous solutions. Square wave voltammetry analysis was performed at a frequency of 5 or 10 Hz, amplitude of 40 mV, and step potential of 4 mV. High-purity Argon is used to de-oxygenate the cell at least 10 minutes before conducting electrochemical tests, and the solution is shielded from air by an argon throughout the entire process [6]. A wide potential range (-2.5 to +1.5 V versus Fc/Fc^+) was employed to explore the electrochemical characteristics of all the phthalocyanine complexes. **Table 3.12** gives the summary of redox potential values of both the reduction and oxidation processes for tyrosine- glycine dipeptide substituted phthalocyanine complexes.

Table 3.12. Redox potential (Volt, against Fc/Fc^+, calculated from midpoint of anodic and cathodic peak potentials of SWV) of glycine dipeptide substituted phthalocyanine complexes.

Complexes	R4	R3	R2	R1	Mr	Mo	O1	O2
11a-CrPc	-2.40	-2.10	-1.51	-1.23	-1.12	0.23	0.54	0.85
11b-MnPc	-2.39	-2.08	-1.65	-1.27		0.25	0.46	0.82
11c-FePc	-2.42	-2.16	-1.93	-1.30	-0.81	0.38	0.47	0.82
11d-CoPc	-2.44	-2.12	-1.49	-1.12	-0.88	0.14	0.43	0.78
11e-NiPc	-2.4	-2.11	-1.71	-1.3			0.41	0.71
11f-CuPc		-2.48	-2.07	-1.31			0.36	0.75
11g-ZnPc	-2.23	-1.97	-1.60	-1.18			0.36	0.65

3.7. Synthesis of Tyrosine-Valine Dipeptide Amino Acid Substituent and Complex

3.7.1. Methyl (tert-butoxycarbonyl)-L- tyrosyl-L- valinate (Boc-Tyr-Val-OCH3) (12)

The reaction was conducted by addition of 5.0 g (17.77 mmol) of Tyrosine amino acid **(Boc-Tyr-OH)** (1.0 equivalent) **(5)** with the amine group protected, 2.98 g (17.77 mmol) of valine methyl ester **(NH_2-Val-OCH_3.HCl)** (1.0 equivalent) and 3.43 g (19.55 mmol) of (CDMT) (1.1 equivalent) as coupling agent in 250 ml plate bottom flask. An appropriate amount of 50 ml of acetonitrile solvent was added into the reaction flask at room temperature with constant stirring. On continuous stirring, 4.88 ml (44.4 mmol) of N-methyl morpholine (NMM) Base was added to the reaction mixture dropwise. The reaction was allowed to continuous stirring for 16 to 24 hours with sequences of thin layer chromatography (TLC) tests to monitor the completion of the reaction using free-coated aluminum TLC paper as stationary phase and a mixture of ethyl acetate and n-hexane solvent system in a ratio of 3:4 as mobile phase.

On completion of the reaction as shown in **Figure 3.13** below, then the solution of the mixture was filtered to remove any unreacted residue and the solvent in the filtrate was evaporated under a reduced pressure using a vacuum rotary evaporator. The residue was dissolved in 10 ml

acetone and precipitated in 200 ml of water in a baker, but there was no formation of precipitate in water. Given that, the solution was then extracted with an equal quantity of volume of ethyl acetate in the separation funnel. The organic phase was dried with a dry $MgSO_4$, filter, and evaporate all the ethyl acetate. The remaining oily is the crude product. The product was later dissolved in 10 ml Chloroform and precipitated in 200 ml of n-hexane. The precipitate was decanted and vacuum-dried at 45 °C for 12 hours. The product **(12)** is white powder weight 5.56 g (14.11 mmol) with a percentage yield of 79.36 %, molecular weight of 366.4, and molecular formula $C_{20}H_{30}N_2O_6$. The FT-IR, ^{1}H-NMR, ^{13}C-NMR, Mass spectroscopy peaks and Elemental Analyse values are presented in **Table 3.13** and the FT-IR, ^{1}H-NMR, ^{13}C-NMR, Mass spectroscopy Spectrum was given in **Appendix section.**

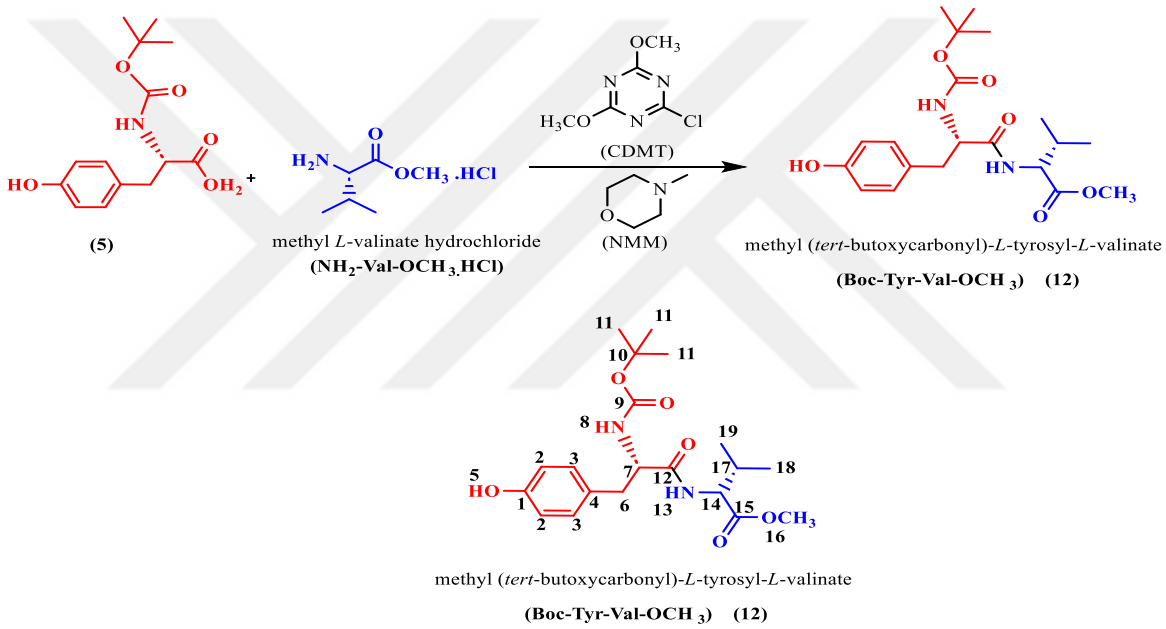

Figure 3.13. Synthesis of methyl (tert-butoxycarbonyl)-*L*- tyrosyl-*L*-valinate **(Boc-Tyr-Val-OCH$_3$) (12)**

3.7.2. Synthesis of Methyl((*R*)-(2-[(tert-butoxycarbonyl) amino)-3-(4-(3,4-dicyanophenoxy) phenyl) propanoyl] valinate (Boc-Tyr-Val-OCH$_3$-O-PN) (13)

In a 250 ml three-neck bottom flask placed on hot plate fitted with magnetic stirrer, thermometer and rubber tube supplying Argon gas, 1.43g (8.24 mmol) of dried 4-Nitrophthalonitrile (**4**) and 3.25 g (8.24 mmol) of dried methyl (tert-butoxycarbonyl)-*L*-tyrosyl-*L*-valinate (**12**) was dissolved in 45 ml of DMF solvent at room temperature forming a light yellow solution. Then, the temperature was raised to 80 °C, and 2.28 g (16.5 mmol) of dried powder K_2CO_3 was added to the reaction mixture in a portion over 1.5 hours while maintaining the temperature between 80 – 95 °C. On the addition of K_2CO_3 the colour of the reaction medium gradually changed

to dark brown. The reaction as indicated in **Figure 3.14** below proceeded for 48 hours on constant stirring and supplied of Argon gas at 90 °C with regular checking of FT-IR spectral of the reaction mixture at certain intervals for monitoring a complete disappearance of $–NO_2$ peak at 1538 cm^{-1} and 1355 cm^{-1}. The mixture was cooled to room temperature and precipitated in 400 ml of distilled water with the addition of a few drops of 1.0 M HCl (to bring down the pH of the medium from basic to pH 6) and salt solution all to facilitate good precipitation of the product. The precipitated product was filtered, washed with plenty of water, and air-dried at room temperature. The colour of the resulting product methyl ((*S*)-2-((tert-butoxycarbonyl) amino)-3-(4-(3,4-dicyanophenoxy) phenyl) propanoyl)-*L*-valinate **(13)** is light brown, the yield is 3.27g (6.28 mmol) 76.2 %. The molecular formula, molecular weight, weight of the product, and % yield results of the compound **(13)** are given in **Table 3.14,** and the FT-IR spectral peaks values are given in **Table 3.15.**

Table 3.13. Spectroscopies and Elemental analysis values of methyl (tert-butoxycarbonyl)-*L*- tyrosyl valinate **(Boc-Tyr-Val-OCH_3)** compound.

<table>
<tr><th>FT-IR (cm^{-1})</th><th>^{1}H-NMR (ppm)</th><th>^{13}C –APT NMR (ppm)</th></tr>
<tr><td rowspan="2">ν_{N-H}, $\nu_{OH(Acid)}$
3329, 3303, 3411
$\nu_{C-H(Aromatic)}$, $\nu_{C-H(Aliphatic)}$
3020, 2871, 2928,2965
$\nu_{C=C}$
1516, 1595, 1614
$\nu_{C=O}$
1656 (Amide C=O)
1691 (Belongs to the Boc protection group C=O),
1710 (Ester C=O),</td><td rowspan="2">0.88-0.92 (6H, m, H^{18}, H^{19}),
1.32 (9H, s, H^{11}),
2.04-2.06 (1H, m, H^{17}),
2.61-2.65 and 2.80-2.83 (2H, H^6),
3.64 (3H, s, H^{16}),
4.17-4.24 (2H, m, H^7, H^{14}),
6.65-6.67 (2H, d, J=8.4 Hz, H^2),
6.89-6.91 (1H, d, H^8 (-NH)),
7.06-7.08 (2H, d, J=8.4 Hz, H^3),
8.07-8.09 (1H, d, H^{13} (-NH)),
9.20 (1H, s, H^5 (-OH))</td><td>155.72 C^1 , 028.60 C^{11},
115.23 C^2 , 172.76 C^{12},
130.59 C^3 , 057.68 C^{14},
128.55 C^4 , 172.38 C^{15},
036.90 C^6 , 052.19 C^{16},
056.30 C^7 , 030.61 C^{17},
156.19 C^9 , 018.61 C^{18},
078.45 C^{10} , 019.36 C^{19}</td></tr>
<tr><td>DMSO-d_6
^{13}C –APT: 39
<b>^{1}H-NMR : 2.51 and 3.36</td></tr>
<tr><th>MALDI-TOF MS</th><th colspan="2">Elemental Analysis (%)</th></tr>
<tr><td>Theoretical
Mw: 394.47 g/mol
Experimental
[M]: 394.512 m/z
[M-C(CH_3)$_3$]: 338.361 m/z
[M-Boc] : 294.149 m/z</td><td colspan="2">$C_{20}H_{30}N_2O_6$ (Mw: 394.47 g/mol)
Theoretical: C, 60.90; H, 7.67; N, 7.10
Experimental: C, 60.93; H, 8.0; N, 7.14</td></tr>
</table>

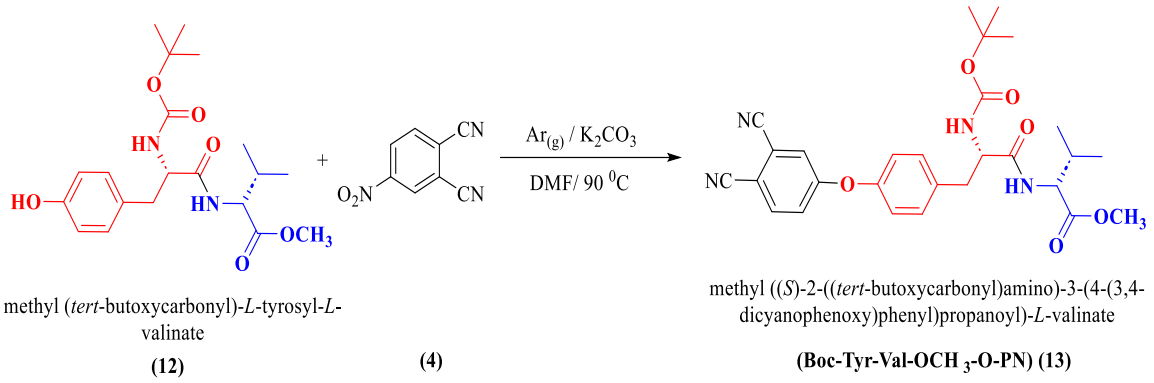

methyl (*tert*-butoxycarbonyl)-*L*-tyrosyl-*L*-valinate

(12)

(4)

methyl ((*S*)-2-((*tert*-butoxycarbonyl)amino)-3-(4-(3,4-dicyanophenoxy)phenyl)propanoyl)-*L*-valinate

(Boc-Tyr-Val-OCH $_3$-O-PN) (13)

Figure 3.14. Synthesis of methyl ((S)-2-((tert-butoxycarbonyl) amino)-3-(4-(3,4-dicyanophenoxy) phenyl) propanoyl)-*L*- valinate (Boc-Tyr-Val-OCH_3-O-PN) **(13).**

3.7.3. Synthesis of Phthalocyanine complexes of Methyl ((S)-2-((tert-butoxycarbonyl) amino)-3-(4-(3,4-dicyanophenoxy) phenyl) propanoyl)-*L*-valinate complexes (13a, 13b, 13c, 13d, 13e, 13f, 13g)

An Argon gas was passed through 3 ml of DMF at 130 °C in a Borosilicate Glass Vacuum Cold Trap Glass Bubbler with a 10 mm serrated Hose, 225 mm length below the 29/42 joint reaction tube. 0.204 g (0.3919 mmol) of **(13)** was added into each of the reaction tubes followed by addition of 0.0295 g (0.0979 mmol) of $Cr(Ac)_3 4H_2O$, 0.0240 g (0.0979 mmol) of $Mn(Ac)_2 4H_2O$, 0.0206 g (0.0979 mmol) of $Fe(Ac)_2 2H_2O$, 0.0244 g (0.0979 mmol) of $Co(Ac)_2 4H_2O$, 0.0244 g (0.0979 mmol) of $Ni(Ac)_2 4H_2O$, 0.0213 g (0.0979 mmol) of $Cu(Ac)_2 2H_2O$ and 0.0215 g (0.0979 mmol) of $Zn(Ac)_2 2H_2O$ respectively. After 1 hour, if there was no colour change, 3 drops of triethanolamine (TEA) were added to the reaction medium, and the temperature was increased to 150 °C. The product of the reactions shown below in **Figure 3.15** as **13a-**CrPc was refluxed for 48 hours, **13b-**MnPc for 4 hours, **13c-**FePc for 4 hours, **13d-**CoPc for 2 hours, **13e-**NiPc for 2 hours, **13f-**CuPc for 2 hours and **13g-**ZnPc was reflux for 3 hours. The blue or green colour products were precipitated in 200 ml of water and filtered to dry at 60 °C in the oven. These were later purified by stirring in hot ethanol for 1 hour, filtered, and dried in a vacuum oven at 60 °C. The molecular formula, molecular weight, weight of the product, and % yield results of the synthesized phthalocyanine compounds are given in **Table 3.14,** and FT-IR and UV-visible spectrum peaks are presented in **Table 3.15.** FT-IR spectra of the ligand **(13)** and its complexes as well as the UV-visible spectral of the complexes are given in the **Appendix Section.**

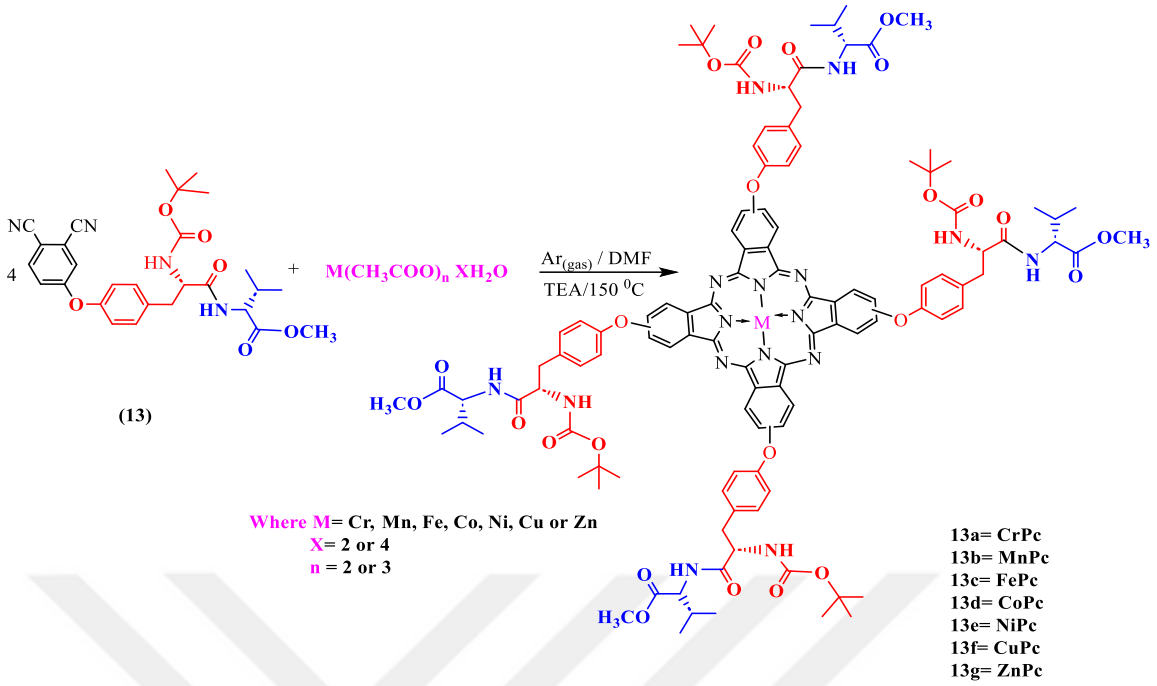

Figure 3.15. Synthesis Tyr-Val dipeptide substituted metallo phthalocyanine complexes

Table 3.14. Molecular formula, molecular weight, the weight of products, and % yield results of compounds **13** and (**13a**, **13b**, **13c**, **13d**, **13e, 13f,** and **13g**) phthalocyanine complexes

Compounds	Molecule Formula	Molecular Weight (g/mol)	Weight obtained (g)	% Yield
13	$C_{28}H_{32}N_4O_6$	520.59	3.27	76.24
13a-CrPc	$C_{114}H_{133}CrN_{16}O_{24}$	2163.40	0.120	56.62
13b-MnPc	$C_{114}H_{133}MnN_{16}O_{24}$	2166.34	0.190	89.53
13c-FePc	$C_{114}H_{133}FeN_{16}O_{24}$	2167.25	0.120	58.87
13d-CoPc	$C_{114}H_{133}CoN_{16}O_{24}$	2170.34	0.152	71.49
13e-NiPc	$C_{114}H_{133}NiN_{16}O_{24}$	2170.10	0.165	77.61
13f-CuPc	$C_{114}H_{133}CuN_{16}O_{24}$	2174.95	0.135	63.36
13g-ZnPc	$C_{114}H_{133}ZnN_{16}O_{24}$	2176.79	0.136	63.77

3.7.4. Electrochemistry experimental of tyrosine- valine dipeptide substituted phthalocyanine complexes.

The solvents were purified using standard techniques referenced in [117, 118] and were subsequently stored over molecular sieves. Cyclic voltammetry (CV) experiments were carried out in a non-aqueous reagent, employing tetra-n-butyl ammonium tetrafluoroborate (TBAFB) (Fluka) as the supporting electrolyte, with a Gamry Interface 1010 B Potentiostat/Galvanostat/ZRA used

for measurements. For CV analysis in dimethylformamide (DMF), a three-electrode configuration was utilized, which included a glassy carbon working electrode, a platinum wire counter electrode, and a platinum wire quasi-reference electrode. The ferrocene/ferrocenium (Fc/Fc^+) pair served as the internal standard, with potentials reported relative to Fc/Fc^+ in non-aqueous solutions. Square wave voltammetry was performed at frequencies of 5, 10 or 20 Hz, with an amplitude of 40 mV and a step potential of 4 mV. High-purity argon was employed to deoxygenate the cell for at least 10 minutes before conducting the electrochemical tests, with the solution being continually shielded from the air by argon throughout the entire process [6]. A broad potential range of -2.5 to +1.5 V versus Fc/Fc^+ was used to investigate the electrochemical properties of all the phthalocyanine complexes. **Table 3.16** summarizes the redox potential values associated with both the reduction and oxidation processes of the tyrosine-valine dipeptide-substituted phthalocyanine complexes.

Table 3.15. Major FT-IR and UV-visible spectrum peaks of compound **13** and (**13a**, **13b**, **13c**, **13d**, **13e, 13f** and **13g**) phthalocyanine complexes.

Compounds	FT-IR Spectrum Peaks (cm^{-1})	UV-Visible Bands (nm)
13	3353, 3279, 2966, 2233, 1739, 1656, 1592, 1486, 1391, 1366, 1249, 1205, 1168, 1018	-
13a-CrPc	3281, 2971-2958, 1769, 1713, 1594, 1505, 1391, 1231, 1043	679, 611, 263, 794, 632, 539, 226.
13b-MnPc	3268, 2966-2873, 1769, 1709, 1599, 1394, 1232, 1166, 1076	720, 651, 312, 661, 575, 232.
13c-FePc	3251, 2967-2871, 1768, 1713, 1662, 1599, 1476, 1365, 1232, 1163	749, 682, 612, 553, 331, 280, 758, 625, 575, 491, 301.
13d-CoPc	3313, 2967-2876, 1771, 1717, 1661, 1597, 1506, 1476, 1365, 1232, 1164, 1091, 1017	675, 609, 269, 626, 539.
13e-NiPc	3314, 2967-2876, 1770, 1717, 1658, 1592, 1486, 1381, 1229, 1165, 1067	672, 642, 647, 515.
13f-CuPc	3313, 2966-2876, 1770, 1716, 1661, 1602, 1506, 1476, 1363, 1231, 1164, 1088, 1041	678, 610, 311, 631, 575.
13g-ZnPc	3251, 2966-2876, 1769, 1713, 1602, 1506, 1476, 1231, 1164, 1089, 1042	679, 611, 321, 790, 631, 530, 299.

Table 3.16. Redox potential (Volt, against Fc/Fc^+, calculated from midpoint of anodic and cathodic peak potentials of SWV) of tyrosine- valine dipeptide substituted phthalocyanine complexes.

Complexes	R4	R3	R2	R1	Mr	Mo	O1	O2
13a-CrPc	-2.34	-2.97	-1.81	-1.31	-1.09	0.18	0.38	0.70
13b-MnPc	-2.40	-1.90	-1.36	-1.14		0.31	0.54	0.88
13c-FePc	-2.58	-2.29	-2.09	-1.46	0.76	-0.17	0.38	0.74
13d-CoPc	-2.25	-2.08	-1.86	-1.26	-0.83	0.20	0.44	0.94
13e-NiPc	-2.45	-2.06	-1.63	-1.18			0.41	0.65
13f-CuPc	-2.59	-2.35	-2.16	-1.65			0.33	0.51
13g-ZnPc	-2.53	-1.92	-1.40	-1.15			0.50	0.79

4. RESULTS AND DISCUSSION

4.1. Characterization of starting materials

The synthetic route followed for synthesizing 4-nitrophthalonitrile through its derivatives as the starting material for synthesizing dipeptides substituted phthalonitrile ligands and their phthalocyanine complexes are given in **Figure 3.1** above. The synthesis started with phthalimide to produce 4-nitrophthalimide **(2)** as seen in **Figure 4.1** below. A light yellow shiny small crystals powder characterized with FT-IR spectroscopy by appearances of the strong symmetric stretching peak at 1544 cm^{-1} and asymmetric stretching peak at 1346 cm^{-1} of nitro group $–NO_2$ as shown in **Appendix 1.1.** Other important peaks present are the N-H medium broad stretching peak of amine at 3316.4 cm^{-1}, the strong stretching peak of C=O (carbonyl group) at 1699 $cm^{-1,}$ and the strong sharp bending vibration signal of the C-H bond of the aromatic ring at 718 cm^{-1}. The percentage yield of product obtained after dying is (31g) 47.5 % and the melting point is 195 °C.

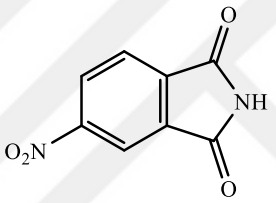

Figure 4.1. Structure of 4-nitrophthalimide **(2)**

The 4-nitrophthalimide was converted to 4-nitrophthalamide by passing a stream of ammonia gas into a solution of 4-nitrophthalimide dissolved in a mixture of ethanol and THF at 40 °C on constant stirring until the yellowish mixture turned up to a milky precipitated suspension solution. The formation of 4-nitrophthalamide in **Figure 4.2** below was validated by appearance of a medium N-H stretching peak belonging to amide group at 3426.9 cm^{-1} and strong bond stretching vibration of amide carbonyl (C=O) peak at 1661 cm^{-1} in addition to strong asymmetric and symmetric stretching peaks of $–NO_2$ group at 1347 cm^{-1} and 1538 cm^{-1} respectively as well as C-H strong bending vibration peak at 798 cm^{-1} of aromatic ring as shown in the **Appendix 1.2**. After dying, the product was a white powder, yield: 28.75 g (88.0 %), MP: 197 °C.

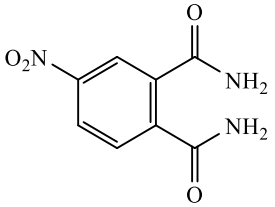

Figure 4.2. Structure of 4-nitrophthalamide **(3)**

The formation of 4-nitrophthalonitrile was achieved by dropwise slow addition of thionyl chloride in DMF solvent at a very low temperature below 5 °C with a constant stirring followed by the addition of 4-nitrophthalamide in portion while maintaining the temperature between 0-5 °C. The product obtained as shown in **Figure 4.3** below is a white pale yellow after drying in an oven at 60 °C to a constant weight. The product was confirmed by the appearance of a sharp single weak signal of the C≡N nitrile group at 2239 cm^{-1} and disappearances of both medium –NH stretching peaks belonging to the amide group at 3440 cm^{-1} as well as the C=O stretching signal of the carbonyl group at around 1760-1665 cm^{-1} as indicated at FT-IR spectrum in the **Appendix 1.3**. Other important signal presence in the spectrum is the asymmetric stretching peak at 1535.8 cm^{-1} and symmetric stretching peak at 1353 cm^{-1} of nitro group $–NO_2$ and C-H bending vibration peak at 744.4 cm^{-1}.

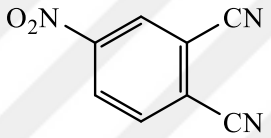

Figure 4.3. Structure of 4-nitrophthalonitrile **(4)**

4.2. Characterizations of tyrosine- phenylalanine dipeptide amino acids substituent and complexes.

The dipeptide amino acid substituent methyl (tert-butoxycarbonyl)-*L*-tyrosyl-*D*-phenylalaninate (Boc-Tyr-Phe-OCH_3) **(6)** was characterized using FT-IR, ^{1}H-NMR, ^{13}C-NMR, mass spectroscopies and elemental analysis while the ligand Methyl ((*S*)-2-((tert-butoxycarbonyl) amino)-3-(4-(3,4-dicyanophenoxy) phenyl) propanoyl)-*D*-phenylalaninate **(Boc-Tyr-Phe-OCH_3-O-PN) (7)** and complexes are characterized by FT-IR and UV-visible spectroscopies.

4.2.1. Characterisation of methyl (tert-butoxycarbonyl)-*L*-tyrosyl-*D*-phenylalaninate (Boc-Tyr-Phe-OCH_3) (6)

The FT-IR, ^{1}H-NMR, ^{13}C-NMR, and mass spectroscopies spectra of compound **(6)** are given in the **Appendix Section**. The carbons and hydrogens in compound **(6)** are numbered as in **Figure 4.4** below.

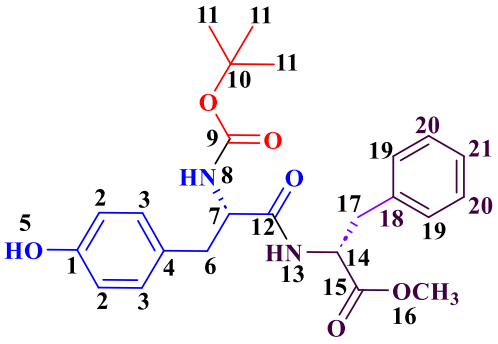

methyl (*tert*-butoxycarbonyl)-*L*-tyrosyl-*D*-phenylalaninate

Boc-Tyr-Phe-OCH$_3$ (6)

Figure 4.4. Numbering of carbons and hydrogens in methyl (tert-butoxycarbonyl)-*L*-tyrosyl-*D*-phenylalaninate **(6)** compound

a) FT-IR spectrum of compound (6)

Some of the most important FT-IR peak of methyl (*tert*-butoxycarbonyl)-*L*-tyrosyl-*D*-phenylalaninate dipeptide are medium broad stretching peaks of N-H bond for amide group at 3214 cm^{-1}, 3304 cm^{-1}and 3339 cm^{-1}, a weak broad stretching peaks of O-H bond (Aromatic) at 3030 cm^{-1}, 3064 cm^{-1} and 3087 cm^{-1}, a medium stretching peaks of C-H bonds (Aliphatic) at 2855 cm^{-1}, 2932 cm^{-1} and 2963 cm^{-1}, a medium stretching of C-C bonds (Aromatic) at 1435 cm^{-1}and 1447 cm^{-1}, a medium broad bending vibration signal of N-H (Amide) at 1597 cm^{-1}and 1616 cm^{-1}, a strong broad stretching peaks of carbonyl C=O at 1661 cm^{-1} and 1686 cm^{-1} (secondary amide C=O), and 1706 cm^{-1}(Ester C=O), a medium broad bending vibration signal of O-H bond (phenol) at 1367 cm^{-1}, a strong broad stretching peak of C-O (Ester) at 1304 cm^{-1}and 1259 cm^{-1}, medium broad stretching vibration signal of C-N (Aliphatic) at 1224 cm^{-1}, 1174 cm^{-1}, 1167 cm^{-1}, 1021 cm^{-1} and lastly a strong broad wagging vibration of N-H (secondary amine) at 699 cm^{-1} as shown in the **Appendix 2.**

b) ^{1}H-NMR spectrum of compound (6)

The ^{1}H-NMR of methyl (*tert*-butoxycarbonyl)-*L*-tyrosyl-*D*-phenylalaninate dipeptide **(6)** taken in DMSO-d$_6$, 298K: shown in (**Appendix 6.1**) indicated the presence of 1-proton singlet peak at 9.19 ppm belongs to H^5 (-OH). The doublet signals of 1 proton at 8.32-8.34 ppm belong to H^{13} (-NH). The multiple signals of 5 protons at 7.23-7.30 ppm belong to H^{19}, H^{20} and H^{21}. The 2 protons produce double signals belongs H^3 at 7.0-7.02 ppm with coupling constant value of (distance between the two peaks) J= 8.8 Hz. The proton generated double peaks at 6.81-6.83 ppm belong to H^8 (-NH). The double peak signals of 2 protons at 6.63–6.65 ppm occupy a distance of 8.4 Hz between the two peaks is belong to H^2. The quartet peaks of 1-proton at 4.49-4.53ppm

belong to H^7. The four signals at 4.08-4.09 ppm are produced by H^{14}. The presence of 3 protons produces a singlet peak at 3.06 ppm is belongs to H^{16}. The 2- protons produce multiple peaks at 2.96-3.07 belonging to H^{17}. The 2-proton split to produce double doublet peak at 2.59-2.59 ppm and 2.74-2.79 ppm belongs to proton H^6, the 9-proton given a singlet intense signal at 1.31 ppm belongs to H^{11} and lastly, a peak at 3.40 ppm belongs to DMSO-d6 water and the peak at 2.51 ppm belongs to DMSO-d6.

c) ^{13}C-NMR spectrum of compound (6)

The ^{13}C-NMR spectrum of methyl (*tert*-butoxycarbonyl)-*L*-tyrosyl-*D*-phenylalaninate dipeptide **(6)** taken in DMSO-d6, 298K is shown in **Appendix 6.2.** The peak C^1 at 155.57 ppm is an aromatic carbon that is attached to the phenol functional group. The peak C^2 at 115.24 ppm is an aromatic carbon, the peak C^3, the peak C^3 at 128.74 ppm**,** 128.50 C^4, 037.09 C^6, 056.35 C^7, 156.18 C^9, 074.44 C^{10}, 028.61 C^{11}, 172.48 C^{12}, 053.97 C^{14}, 172.31 C^{15}, 052.32 C^{16}, 037.18 C^{17}, 137.49 C^{18}, 129.61 C^{19}, 130.54 C^{20}, 127.05 C^{21}, (Figure 3).

d) Mass spectrum of compound (6)

The theoretically calculated molecular weight of the Boc-Tyr-Phe-OCH_3 compound is 442.51 g/mol. In the MALDI-TOF MS spectrum of compound **(6)** given in **Appendix 6.3**, the 442.548 [M] peak belongs to the compound. The peaks observed under this peak indicate the compound resulting from the groups leaving the structure. According to calculations, the peak at 386.61 corresponds to the rupture of the -$C(CH_3)_3$ group in the Boc protecting group, 386.61 [M-$C(CH_3)_3$]. The peak at 342.54 corresponds to the complete separation of the **Boc** group from the structure. 342.542 [M-Boc].

4.2.2. Characterizations of methyl ((S)-2-((tert-butoxycarbonyl) amino)-3-(4-(3,4-dicyanophenoxy) phenyl) propanoyl)-*D*-phenylalaninate (Boc-Tyr-Phe-OCH_3-O-PN) (7)

The characterization **(Boc-Tyr-Phe-OCH_3-O-PN) (7)** indicated in **Figure 4.5** below was done by FT-IR, ^{1}H NMR, ^{13}C NMR spectroscopies.

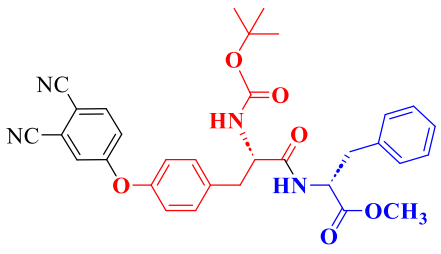

Figure 4.5. Methyl ((S)-2-((tert-butoxycarbonyl) amino)-3-(4-(3,4-dicyanophenoxy) phenyl) propanoyl)-*D*-phenylalaninate **(Boc-Tyr-Phe-OCH_3-O-PN) (7)**

a) FT-IR spectrum of compound (7)

The FT-IR (ATR, cm^{-1}) spectrum of compound **(7)** obtained is shown in **Appendix 2.1**. In the spectrum, the aromatic –CH bond peaks at 3146-3020 cm^{-1}, aliphatic –CH bond peaks at 2979-2832 cm^{-1}, a weak sharp nitrile C≡N peaks at 2232 cm^{-1}, the medium broad stretching peak signal at 1591 cm^{-1} is own by C=C aromatic (in-ring), a strong sharp stretching peak at 1245 cm^{-1} is belong to C–O–C (ether). Other peaks are medium broad stretching peaks of carbonyl C=O at 1662 cm^{-1}(amide C=O), 1716 cm^{-1}(ester C=O), and medium broad stretching vibration signal of C-N (aliphatic amine) at 1248 cm^{-1}, 1167 cm^{-1}, and 1021 cm^{-1}.

b) ^{1}H-NMR spectrum of compound (7)

The ^{1}H-NMR of methyl ((S)-2-((*tert*-butoxycarbonyl) amino)-3-(4-(3,4-dicyanophenoxy) phenyl) propanoyl)-*D*-phenylalaninate **(7)** taken in DMSO-d6, 400 MHz: shown in (**Appendix 6.4**) indicated the presence of 1-proton doublet peak at 8.14 ppm with coupling constant value of (distance between the two peaks) J= 8.7 Hz, a doublet signal of 1-proton with coupling constant value of (distance between the two peaks) J= 2.6 Hz, a multiplet signals of 8 protons observed at 7.23 ppm-7.27 ppm, a multiplet signals of 4 protons observed at 7.19 ppm-7.22 ppm, then 2-protons split to produce double doublet peaks signals at 4.52 ppm with coupling constant value of (distance between the peaks) J= 15.0 Hz and J= 7.7 Hz, 1-proton of split to produce triple doublet peaks signals at 4.23 ppm with coupling constant value of (distance between the peaks) J= 15.0 Hz and J= 7.7 Hz, 3-protons produces a singlet peak at 3.60 ppm, 9-proton given a singlet intense signal at 1.31 ppm and lastly a peak at 3.40 ppm belongs to DMSO-d6 water and the peak at 2.51 ppm belongs to DMSO-d_6.

4.2.2.1. Characterization of CrPc (7a) Complex

Characterization of phthalocyanine complex was performed by FT-IR spectra, UV-visible spectra, thermal analysis (TGA and DTA), and electrochemistry techniques (CV and SWV)

a) FT-IR spectrum of complex (7a) compound

The FT-IR spectrum of chromium tyrosine- phenylalanine dipeptide substituted phthalocyanine complex **(7a)** is shown in **Appendix 2.2.** revealed the absence of weak sharp nitrile C≡N peaks at 2232 cm^{-1} which qualified the cyclotetramerization [21] of the compound **(7)** in the formation of the complex compound **(7a)** and presence medium stretching peaks of C-H bonds (Aliphatic) at 2864 cm^{-1}, a strong medium peak of carbonyl carbon C=O at 1767 cm^{-1} and 1710 cm^{-1} (ester C=O), a medium broad bending vibration signal of N-H (Amide) at 1597 cm^{-1}, a medium

stretching peak of C-C (in-ring) aromatic at 1504 cm^{-1}, a medium broad bending vibration of C-H bond (methyl of protection group) at 1394 cm^{-1}, and a medium broad stretching peak of C-N bond (aliphatic amines) at 1068 cm^{-1} and a strong sharp stretching peak of C-O-C bond (ether) at 1232 cm^{-1}.

b) UV-visible spectrum of complex (7a) compound

The UV-visible spectrum of chromium tyrosine-phenylalanine dipeptide substituted phthalocyanine complex **(7a)** dissolved in DMF is shown in **Appendix 10.1**. in the spectrum, a single Q-band is seen at 680 nm and a B-band at 259 nm. The small shoulder at 612 nm is due to aggregation.

c) Thermal analysis of complex (7a) compound

It is seen in the TGA thermograms curve of the chromium tyrosine- phenylalanine dipeptide substituted phthalocyanine complex **(7a)** compound that the compound is thermally stable up to180 °C and undergoes two stages of degradation. A weight loss of 50 % was recorded between 180-420 °C in the first stage of degradation followed by a weight loss of 28 % in-between 420-460 °C in the second stage of degradation with leftover 22% non-decompose residue as shown in the **Appendix 14.1.** It is indicated from the DTA curves of the complexes that the compound decomposes without melting. Therefore, under normal conditions complex (**7a**) compounds do not have a melting point and all their stages of degradation follow exothermic decomposition.

d) Electrochemistry analysis of complex (7a) compound

The electrochemical analysis of chromium tyrosine- phenylalanine dipeptide substituted phthalocyanine complex **(7a)** compound was performed by both Cyclic and square wave voltammetry. A glassy carbon electrode is used as the working electrode while platinum Pt as a counter electrode, tetrabutylammonium tetrafluoroborate as the electrolyte, and ferrocene /ferrocenium (Fc/Fc^{+}) as a pseudo-reference electrode in DMF. A wide potential range (-2.5 to +1.5 V versus Fc/Fc^{+}) was employed to explore the phthalocyanine complexes' electrochemical characteristics [119, [120]. The complex **(7a)** possesses a redox-active metal (chromium) center that undergoes two oxidations ($\mathbf{O_1}$ 0.31 volt and $\mathbf{O_2}$ 0.60 volt) which involve $\mathbf{[Pc^{(-2)}\,Cr^{(2)}]^{0}}$ / $\mathbf{[Pc^{(-1)}Cr^{(3)}]^{+2}}$and $\mathbf{[Pc^{(-1)}\,Cr^{(2)}]^{+}}$ / $\mathbf{[Pc^{(0)}\,Cr^{(3)}]^{+3}}$ for first $\mathbf{O_1}$ and second $\mathbf{O_2}$ oxidatıon transitions related to the formation of cation radicals, four reductions ($\mathbf{R_4}$ -2.36 volt, $\mathbf{R_3}$ -2.13 volt, $\mathbf{R_2}$ -1.86 volt, and $\mathbf{R_1}$ -1.32 volt) these produce $\mathbf{[Pc^{(-5)}\,Cr^{(2)}]^{-3}}$ / $\mathbf{[Pc^{(-6)}\,Cr^{(2)}]^{-4}}$ for $\mathbf{R_4}$, $\mathbf{[Pc^{(-4)}\,Cr^{(2)}]^{-2}}$ / $\mathbf{[Pc^{(-5)}\,Cr^{(2)}]^{-3}}$ for $\mathbf{R_3}$, $\mathbf{[Pc^{(-3)}\,Cr^{(2)}]^{-1}}$ / $\mathbf{[Pc^{(-4)}\,Cr^{(2)}]^{-2}}$ for $\mathbf{R_2}$, and $\mathbf{[Pc^{(-2)}\,Cr^{(2)}]^{0}}$ / $\mathbf{[Pc^{(-3)}\,Cr^{(2)}]^{-1}}$ for $\mathbf{R_1}$ reductıon transition related to the formation of anion radicals from the redox reaction of the conjugated macrocycle Pc ring**.** The metal center redox reaction ($\mathbf{M_R}$ -1.12 and $\mathbf{M_O}$ -0.52) involves $\mathbf{[Pc^{(-2)}\,Cr}$

$^{(2)}]^{0}$ / **[Pc** $^{(-2)}$ **Cr** $^{(1)}]^{-1}$ for metal base reduction $\mathbf{M_R}$, and **[Pc** $^{(-2)}$ **Cr** $^{(2)}]^{0}$ / **[Pc** $^{(-2)}$ **Cr** $^{(3)}]^{+1}$ for metal base oxidation $\mathbf{M_O}$ to formed anion and cation radicals respectively. The redox activity is directly connected with oxidation by removing electrons from the highest occupied molecular orbital (HOMO) and adding electrons to the lowest unoccupied molecular orbital (LUMO) of phthalocyanines macrocyclic. The voltammograms of square wave and cyclic voltammograms of complex **(7a)** compound are both shown in **Appendix 18.1a** and **18.1b** respectively.

4.2.2.2. Characterization of MnPc (7a) Complex

Characterization of phthalocyanine complex was performed by FT-IR spectra, UV-visible spectra, thermal analysis (TGA and DTA), and electrochemistry techniques (CV and SWV)

a) FT-IR spectrum of complex (7b) compound

The FT-IR spectrum of manganese tyrosine- phenylalanine dipeptide substituted phthalocyanine complex **(7b)** shown in **Appendix 2.3** reported the absence of a weak sharp nitrile C≡N peaks at 2232 cm^{-1} which indicates the cyclotetramerization of the compound **(7)** in the formation of the complex compound **(7b)**. Other most important peaks presence are presence a medium stretching peaks of C-H bonds (Aliphatic) at 2885 cm^{-1}, a strong medium peak of carbonyl carbon C=O at 1769 cm^{-1} and 1709 cm^{-1} (ester C=O), a medium broad bending vibration signal of N-H (Amide) at 1599 cm^{-1}, a medium stretching peak of C-C (in-ring) aromatic at 1505 cm^{-1}, a medium broad bending vibration of C-H bond (methyl of protection group) at 1394 cm^{-1}, and a medium broad stretching peak of C-N bond (aliphatic amines) at 1165 cm^{-1} and 1077 cm^{-1}, a strong sharp stretching peak of C-O-C bond at 1232 cm^{-1} and a strong sharp bending vibration peak of C-H (Aromatic) at 744 cm^{-1}.

b) UV-visible spectrum of complex (7b) compound

The UV-visible spectrum of manganese tyrosine- phenylalanine dipeptide substituted phthalocyanine complex **(7b)** dissolved in DMF is shown in **Appendix 10.2**. in the spectrum, a single Q-band is seen at 721nm and a B-band at 254 nm. The small shoulder at 650 nm is due to aggregation.

c) Thermal analysis of complex (7b) compound

It is seen in the TGA thermograms curve of the manganese tyrosine- phenylalanine dipeptide substituted phthalocyanine complex **(7b)** that the compound is thermally stable up to 200 ^{0}C and undergoes a 5% weight loss up to this temperature. This weight loss is thought to be due to the moisture absorbed and lost at the bagging of heating of the complex **(7b)**. The complex undergoes two stages of degradation. A weight loss of 42.5% was recorded between 200- 400 ^{0}C in the first

stage of degradation followed by a weight reduction of 35.5 % occur between 400-430 ^{0}C in the second stage of degradation with leftover 17% of the material non-decompose as seen in the TGA thermogram curve in **Appendix 14.2.** The DTA curves of the complex indicate that the compound decomposes without melting. Therefore, under normal conditions complex **(7b)** compounds do not have a melting point and all their stages of degradation follow exothermic.

d) Electrochemistry analysis of complex (7b) compound

The electrochemical analysis of manganese tyrosine- phenylalanine dipeptide substituted phthalocyanine complex **(7b)** compound was performed by both Cyclic and square wave voltammetry. A glassy carbon electrode is used as the working electrode while platinum Pt as a counter electrode, tetrabutylammonium tetrafluoroborate as the electrolyte, and ferrocene /ferrocenium (Fc/Fc+) as a pseudo-reference electrode in DMF. A wide potential range (-2.5 to +1.0 V versus Fc/Fc+) was employed to explore the phthalocyanine complexes' electrochemical characteristics [119, 120]. The complex **(7b)** possesses a redox-inactive metal (manganese) center that undergoes two oxidations ($\mathbf{O_1}$ 0.40 volt and $\mathbf{O_2}$ 0.88 volt) which involve $\mathbf{[Pc^{(-2)}\,Mn^{(2)}]^0}$ / $\mathbf{[Pc^{(-1)}\,Mn^{(3)}]^{+2}}$and $\mathbf{[Pc^{(-1)}\,Mn^{(2)}]^{+}}$ / $\mathbf{[Pc^{(0)}\,Mn^{(3)}]^{+3}}$ for first $\mathbf{O_1}$ and second $\mathbf{O_2}$ oxidatıon electronic transitions related to the formation of cation radicals, three reductions ($\mathbf{R_3}$ -2.32 volt, $\mathbf{R_2}$ -1.89 volt, and $\mathbf{R_1}$ -1.22 volt) these produce $\mathbf{[Pc^{(-4)}\,Mn^{(2)}]^{-2}}$ / $\mathbf{[Pc^{(-5)}\,Mn^{(2)}]^{-3}}$ for $\mathbf{R_3}$, $\mathbf{[Pc^{(-3)}\,Mn^{(2)}]^{-1}}$ / $\mathbf{[Pc^{(-4)}\,Mn^{(2)}]^{-2}}$ for $\mathbf{R_2}$, and $\mathbf{[Pc^{(-2)}\,Mn^{(2)}]^0}$ / $\mathbf{[Pc^{(-3)}\,Mn^{(2)}]^{-1}}$ for $\mathbf{R_1}$ reduction transition related to the formation of anion radicals of the conjugated macrocycle Pc ring. The Pc undergoes a metal base redox oxidation reaction to produce a positive potential value of $\mathbf{M_O}$ 0.14 volt involves $\mathbf{[Pc^{(-2)}\,Mn^{(2)}]^0}$ / $\mathbf{[Pc^{(-2)}\,Mn^{(3)}]^{+1}}$ for metal base oxidation $\mathbf{M_O}$ to formed cation radicals [121].

The redox activity is directly connected with oxidation by removing electrons from the highest occupied molecular orbital (HOMO) and adding electrons to the lowest unoccupied molecular orbital (LUMO) of phthalocyanines macrocyclic[94, 122, 123]. The voltammograms of square wave and cyclic voltammograms of complex **(7b)** compound are both shown in **Appendix 18.2a** and **18.2b** respectively.

4.2.2.3. Characterization of FePc (7c) Complex

Characterization of phthalocyanine complex was performed by FT-IR spectra, UV-visible spectra, thermal analysis (TGA and DTA), and electrochemistry techniques (CV and SWV)

a) FT-IR spectrum of complex (7c) compound

The FT-IR spectrum of iron tyrosine- phenylalanine dipeptide substituted phthalocyanine complex **(7c)** shown in **Appendix 2.4** reported the absence of a weak sharp nitrile C≡N peaks at 2232 cm^{-1} which indicates the cyclotetramerization of the compound **(7)** in the formation of the complex

compound **(7c)**. Other most important peaks present in the spectrum are the appearance of a medium stretching peak of C-H bonds (Aliphatic) at 2877 cm^{-1}, a strong medium peak of carbonyl carbon C=O at 1765 cm^{-1} and 1709 cm^{-1} (ester C=O), a medium broad bending vibration signal of N-H (Amide) at 1598 cm^{-1}, a medium stretching peak of C-C (in-ring) aromatic at 1504 cm^{-1}, a medium broad bending vibration of C-H bond (methyl of protection group) at 1391 cm^{-1}, and a medium broad stretching peak of C-N bond (aliphatic amines) at 1164 cm^{-1} and 1052 cm^{-1}, a strong sharp stretching peak of C-O-C bond (ether) at 1231 cm^{-1} and a strong sharp bending vibration peak of C-H (Aromatic) at 747 cm^{-1}.

b) UV-visible spectrum of complex (7c) compound

The UV-visible spectrum of iron tyrosine-phenylalanine dipeptide substituted phthalocyanine complex **(7c)** dissolved in DMF is illustrated in **Appendix 10.3**. The spectrum features a distinct Q-band at 664 nm and a B-band at 262 nm, with a slight shoulder at 600 nm attributed to aggregation.

c) Thermal analysis of complex (7c) compound

The TGA and DTA thermogram curves of the iron tyrosine- phenylalanine dipeptide substituted phthalocyanine complex **(7c)** indicate that the compound remains thermally stable up to 190 °C with only 3% weight loss accounted due to loss of moisture after which it undergoes three stages of degradation. A weight loss of 21% occurs between 190-350 °C during the first stage, followed by a 28% weight loss between 350-525 °C in the second stage of degradation. The complex undergoes the third stage of degradation with weight loss of 21% between 525-800 °C leaving a residue of 19% that does not decompose as shown in **Appendix 14.3**. DTA curves reveal that the compound decomposes without a melting phase, suggesting that complex **(7c)** does not possess a melting point under normal conditions and exhibits exothermic degradation throughout its stages.

d) Electrochemistry analysis of complex (7c) compound

The electrochemical properties of iron tyrosine-phenylalanine dipeptide substituted phthalocyanine complex **(7c)** were examined using cyclic and square wave voltammetry techniques. Similar to previous analyses, a glassy carbon electrode served as the working electrode while platinum was used as a counter electrode. The electrolyte comprised tetrabutylammonium tetrafluoroborate with ferrocene/ferrocenium (Fc/Fc+) as a pseudo-reference electrode in DMF. The investigations were conducted over a potential range of -2.5 to +1.0 V versus Fc/Fc+. The complex **(7c)** exhibited two Pc base oxidation processes $\mathbf{O_1}$ at 0.50 volt and $\mathbf{O_2}$ at 0.92 volt) which involve $\mathbf{Pc^{(-2)}Fe^{(2)}}$ / $\mathbf{[Pc^{(-1)}Fe^{(3)}]^{+2}}$.and $\mathbf{[Pc^{(-1)}Fe^{(2)}]^{+}}$ / $\mathbf{[Pc^{(0)}Fe^{(3)}]^{+3}}$ for first $\mathbf{O_1}$ and second $\mathbf{O_2}$ oxidatıon transitions respectively

related to the formation of cation radicals, along with four reduction processes ($\mathbf{R_4}$ at -2.41 volt, $\mathbf{R_3}$ at -2.15 volt, $\mathbf{R_2}$ at -1.91 volt, $\mathbf{R_1}$ at -1.30 volt) that produce $\mathbf{[Pc^{(-5)}\ Fe^{(2)}]^{-3}}$ / $\mathbf{[Pc^{(-6)}\ Fe^{(2)}]^{-4}}$ for $\mathbf{R_4}$, $\mathbf{[Pc^{(-4)}\ Fe^{(2)}]^{-2}}$ / $\mathbf{[Pc^{(-5)}\ Fe^{(2)}]^{-3}}$ for $\mathbf{R_3}$, $\mathbf{[Pc^{(-3)}\ Fe^{(2)}]^{-1}}$ / $\mathbf{[Pc^{(-4)}\ Fe^{(2)}]^{-2}}$ for $\mathbf{R_2}$, and $\mathbf{[Pc^{(-2)}\ Fe^{(2)}]^{0}}$ / $\mathbf{[Pc^{(-3)}\ Fe^{(2)}]^{-1}}$ for $\mathbf{R_1}$ reductıon transition related to the formation of anion radicals. Iron metal is a redox-active metal that undergoes redox reaction to produce metal center oxidation $\mathbf{M_O}$ -0.24 with negative potential involving electronic transition related to the formation of cation radical $\mathbf{[Pc^{(-2)}\ Fe^{(2)}]^{0}}$ / $\mathbf{[Pc^{(-2)}\ Fe^{(3)}]^{+1}}$ [121, 124].

The redox activity is connected to the transfer of electrons from the highest occupied molecular orbital (HOMO) and the lowest unoccupied molecular orbital (LUMO) of the phthalocyanine macrocycle. The voltammograms for the square wave and cyclic voltammetry of complex **(7c)** can be found in **Appendix 18.3a** and **18.3b**, respectively.

4.2.2.4. Characterization of CoPc (7d) Complex

Characterization of phthalocyanine complex was performed by FT-IR spectra, UV-visible spectra, thermal analysis (TGA and DTA), and electrochemistry techniques (CV and SWV)

a) FT-IR spectrum of complex (7d) compound

The FT-IR spectrum of the cobalt tyrosine-phenylalanine dipeptide substituted phthalocyanine complex **(7d)** in **Appendix 2.5** reveals several noteworthy features that are significant for confirming the structural characteristics of the compound. Notably, the absence of the weak sharp nitrile C≡N peak at 2232 cm^{-1} supports the cyclotetramerization process of the precursor compound **(7)** in forming the complex **(7d).**

Key peaks in the spectrum include: A medium broad stretching peak for N-H bonds (Aliphatic amide) observed at 3312 cm^{-1}, indicating the presence of amide functionalities. A weak broad bending vibration peak of C-H (Aromatic) at 1768 cm^{-1}, suggests the involvement of aromatic structures. A strong broad stretching peak for the carbonyl bond C=O, with peaks at 1710 cm^{-1} (ester C=O) and 1652 cm^{-1} (amide C=O), highlighting the presence of both ester and amide groups in the structure. A medium bending vibration peak for the N-H bond (amide) at 1596 cm^{-1} confirms amide incorporation. A medium stretching peak for C-C bonds (aromatic) at 1506 cm^{-1}, emphasizing the aromatic character in the compound. A medium broad bending vibration of C-H (methyl of the protection group) at 1387 cm^{-1}, indicative of protective groups present in the structure. A strong sharp stretching peak for the C-O-C bond (ether) at 1231 cm^{-1}, confirms ether linkages. Medium sharp stretching peaks for C-N bonds (aliphatic amines) were observed at 1164 cm^{-1} and 1095 cm^{-1}. Lastly, a medium sharp bending vibration peak of C-H (Aromatic) at 751 cm^{-1} rounds out the distinctive spectral features of the complex.

These peaks combined provide a comprehensive understanding of the functional groups present in the complex **(7d)** and aid in characterizing its chemical structure**.**

b) UV-visible spectrum of complex (7d) compound

The UV-visible spectrum of cobalt tyrosine- phenylalanine dipeptide substituted phthalocyanine complex **(7d)** dissolved in DMF as solvent is shown in **Appendix 10.4**. In the spectrum, a single Q-band is seen at 669nm and a B-band at 387 nm. The small shoulder at 610 nm is due to aggregation.

c) Thermal analysis of complex (7d) compound

The TGA and DTA thermogram curves of cobalt tyrosine- phenylalanine dipeptide substituted phthalocyanine complex **(7d)** compound are presented in **Appendix 14.4.** As it was observed from the TGA thermogram the complex was thermally stable up to 180 ^{0}C with only 4% weight loss accounted for as a result of moisture loss absorbed by the complex. The complex undergoes two stages of degradation as seen in the thermogram. The first decomposition is noted between 180^{0}C-250^{0}C with a weight loss of 11%. However, the second degradation was recorded between 250^{0}C-500^{0}C given a weight loss of 80% and a 5% weight left of material as residue which may probably be the metal oxide CoO of the complex.

Conversely, the DTA thermogram curve of the complex shows that the complex decomposes without melting, this implies that under normal conditions the complex does not have a melting point and its degradation follows an exothermic pathway.

d) Electrochemistry analysis of complex (7d) compound

The electrochemical properties of cobalt tyrosine-phenylalanine dipeptide substituted phthalocyanine complex **(7d)** were examined using cyclic and square wave voltammetry techniques. Similar to previous analyses, a glassy carbon electrode served as the working electrode while platinum was used as a counter electrode. The electrolyte comprised tetrabutylammonium tetrafluoroborate with ferrocene/ferrocenium (Fc/Fc+) as a pseudo-reference electrode in DMF. The investigations were conducted over a potential range of -2.5 to +1.0 V versus Fc/Fc+. The complex **(7d)** exhibited two oxidation processes $\mathbf{O_1}$ at 0.59 volt and $\mathbf{O_2}$ at 0.93 volt) which involve $\mathbf{Pc^{(-2)}Co^{(2)}}$ **/** $\mathbf{[Pc^{(-1)}Co^{(3)}]^{+2}}$and $\mathbf{[Pc^{(-1)}Co^{(2)}]^{+}}$ **/** $\mathbf{[Pc^{(0)}Co^{(3)}]^{+3}}$ for first $\mathbf{O_1}$ and second $\mathbf{O_2}$ oxidatıon transitions respectively related to the formation of cation radicals, along with four reduction processes ($\mathbf{R_4}$ at -2.37 volt, $\mathbf{R_3}$ at -2.12 volt, $\mathbf{R_2}$ at -1.89 volt, $\mathbf{R_1}$ at -1.31 volt) that produce $\mathbf{[Pc^{(-5)}Co^{(2)}]^{-3}}$ **/** $\mathbf{[Pc^{(-6)}Co^{(2)}]^{-4}}$ for $\mathbf{R_4}$, $\mathbf{[Pc^{(-4)}Co^{(2)}]^{-2}}$ **/** $\mathbf{[Pc^{(-5)}Co^{(2)}]^{-3}}$ for $\mathbf{R_3}$, $\mathbf{[Pc^{(-3)}Co^{(2)}]^{-1}}$ **/** $\mathbf{[Pc^{(-4)}Co^{(2)}]^{-2}}$ for $\mathbf{R_2}$, and $\mathbf{[Pc^{(-2)}Co^{(2)}]^{0}}$ **/** $\mathbf{[Pc^{(-3)}Co^{(2)}]^{-1}}$ for $\mathbf{R_1}$ reduction transition related to the formation

of anion radicals for the redox reaction of the conjugated Pc ring. Cobalt metal is a redox-active metal exhibit metal center redox reaction **(M_R** -0.88 and **M_O** 0.45) involves **[Pc $^{(-2)}$ Co $^{(2)}$]^{0} / [Pc $^{(-2)}$ Co $^{(1)}$]$^{-1}$** for metal base reduction **M_R**, and **[Pc $^{(-2)}$ Co $^{(2)}$]^{0} / [Pc $^{(-2)}$ Co $^{(3)}$] $^{+1}$** for metal base oxidation **M_O** to formed anion and cation radicals respectively.

The redox activity is connected to the transfer of electrons from the highest occupied molecular orbital (HOMO) and the lowest unoccupied molecular orbital (LUMO) of the phthalocyanine macrocycle. The voltammograms for the square wave and cyclic voltammetry of complex (7c) can be found in **Appendix 18.4a** and **18.4b**, respectively.

4.2.2.5. Characterization of NiPc (7e) Complex

Characterization of phthalocyanine complex was performed by FT-IR spectra, UV-visible spectra, thermal analysis (TGA and DTA), and electrochemistry techniques (CV and SWV)

a) FT-IR spectrum of complex (7e) compound

The FT-IR spectrum of nickel tyrosine- phenylalanine dipeptide substituted phthalocyanine complex **(7e)** shown in **Appendix 2.6** recorded the absence of weak sharp nitrile C≡N peaks at 2232 cm^{-1} which confirmed the cyclotetramerization of the compound (7) in the formation of the complex **(7e)** compound. Among the most important peaks that appeared in the spectrum are the appearance of a medium broad stretching peak of N-H bonds (Aliphatic amide) at 3331 cm^{-1}, a weak broad bending vibration peak of C-H (Aromatic) at 1716 cm^{-1}, a medium broad stretching carbonyl bond C=O at 1668 cm^{-1} (secondary amide C=O)**,** a medium broad stretching peak of C=C bond (Aromatic) at 1602 cm^{-1}, a medium stretching peak (in-ring) of C-C bond (aromatic) at 1506 cm^{-1}, a medium broad bending vibration of C-H bond (methyl of protection group) at 1367 cm^{-1}, a strong broad stretching peak of C-O-C bond (ethers) at 1234 cm^{-1}, a medium sharp stretching peak of C-N bond (aliphatic amines) at 1163 cm^{-1} and a medium sharp bending vibration peak of C-H (Aromatic) at 750 cm^{-1}.

b) UV-visible spectrum of complex (7e) compound

The UV-visible spectrum of nickel tyrosine- phenylalanine dipeptide substituted phthalocyanine complex **(7e)** dissolved in DMF as solvent is shown in **Appendix 10.5**. In the spectrum, a single Q-band is seen at 665nm and a B-band at 450 nm. The pronouns shoulder at 620 nm are due to aggregation.

c) Thermal analysis of complex (7e) compound

As it was indicated, the TGA thermograms curve of the nickel tyrosine- phenylalanine dipeptide substituted phthalocyanine complex **(7e)** compound is thermally stable up to 200 °C with

only 3% weight loss against temperature due to moisture trapped in the complex and it undergoes three stages of degradation. A weight loss of 11 % was recorded between 200 °C - 240 °C in the first stage of degradation followed by a weight loss of 31 % between 240 °C - 425 °C in the second stage of degradation and finally, a weight loss of 46 % was accounted in the third stage of decomposition between 425 °C - 475 °C with the leftover of 12 % non-decompose residue as shown in the **Appendix 14.5**. It is indicated from the DTA curves of the complexes that the compound decomposes without melting this translated that under normal conditions complex **(7e)** compound does not have a melting point and all their stages of degradation follow exothermic decomposition.

d) Electrochemical analysis of complex (7e) compound

The electrochemical analysis of nickel tyrosine- phenylalanine dipeptide substituted phthalocyanine complex **(7e)** compound was performed by both Cyclic and square wave voltammetry. A glassy carbon electrode is used as the working electrode while platinum Pt as a counter electrode, tetrabutylammonium tetrafluoroborate as the electrolyte, and ferrocene /ferrocenium (Fc/Fc^{+}) as a pseudo-reference electrode in DMF. A wide potential range (-2.5 to +1.5 V versus Fc/Fc^{+}) was employed to explore the phthalocyanine complexes' electrochemical characteristics [119, [120]. The complex **(7e)** possesses a redox-inactive nickel metal center that undergoes two oxidation potentials $\mathbf{O_1}$ 0.48 volt and $\mathbf{O_2}$ 1.41 volt with the electronic transition of **[Pc $^{(-2)}$ Ni $^{(2)}$]^{0} / [Pc $^{(-1)}$ Ni $^{(2)}$]$^{+1}$** and **[Pc $^{(-1)}$ Ni $^{(2)}$] $^{+1}$ / [Pc ^{0} Ni $^{(2)}$] $^{+2}$** electronic transition of the Pc macrocycle ring to formed cation. It also exhibits four reductions reaction $\mathbf{R_4}$ -2.27 volt**,** $\mathbf{R_3}$ -2.07 volt, $\mathbf{R_2}$ -1.64 volt, and $\mathbf{R_1}$ -1.26 volt involves electrons transition as **[Pc $^{(-5)}$ Ni $^{(2)}$]$^{-3}$ / [Pc $^{(-6)}$ Ni $^{(2)}$]$^{-4}$**, **[Pc $^{(-4)}$ Ni $^{(2)}$]$^{-2}$ / [Pc $^{(-5)}$ Ni $^{(2)}$]$^{-3}$**, **[Pc $^{(-3)}$ Ni $^{(2)}$]$^{-1}$ / [Pc $^{(-4)}$ Ni $^{(2)}$]$^{-2}$**, and **[Pc $^{(-2)}$ Ni $^{(2)}$]^{0} / [Pc $^{(-3)}$ Ni $^{(2)}$]$^{-1}$** respectively of the conjugated Pc macrocycle ring formed cation and anion radicals. The redox activity is directly connected with oxidation by removing electrons from the highest occupied molecular orbital (HOMO) and adding electrons to the lowest unoccupied molecular orbital (LUMO) of phthalocyanines macrocyclic [94, 121, 122]. The voltammograms of square wave and cyclic voltammograms of complex **(7e)** compound are both indicated in **Appendix 18.5a** and **18.5b** respectively.

4.2.2.6. Characterization of CuPc (7f) Complex

Characterization of phthalocyanine complex was performed by FT-IR spectra, UV-visible spectra, thermal analysis (TGA and DTA), and electrochemistry techniques (CV and SWV)

a) FT-IR spectrum of complex (7f) compound

The FT-IR spectrum of copper tyrosine- phenylalanine dipeptide substituted phthalocyanine complex **(7f)** shown in **Appendix 2.7** reported the absence of weak sharp nitrile C≡N peaks at 2232 cm^{-1} which testified the cyclotetramerization of the compound **(7)** in the formation of the complex **(7f)**. Some of the most important peaks that appeared in the spectrum are a medium broad stretching peaks of N-H bonds (Aliphatic amide) at 3312 cm^{-1}, a medium broad stretching peaks of C-H bond (methyl group) between 2949-2830 cm^{-1}, a weak broad bend vibration peak of C-H (Aromatic) overtone at 1767 cm^{-1}**,** the medium broad peak of carbonyl carbon bond (ester C=O) and (amide C=O) between 1708 cm^{-1} and 1661 cm^{-1} respectively, a medium broad bending vibration peak of N-H (Amines) at 1597 cm^{-1}**,** a medium stretching (in-ring) of C-C bond (aromatic) at 1504 cm^{-1}, a medium broad bending vibration of C-H bond (methyl of protection group) at 1394 cm^{-1}, a strong broad stretching peak of C-O-C bond (ethers) at 1231 and C-O bond (ester) 1169 cm^{-1} and a medium broad stretching peak of C-N bond (aliphatic amine) at 1033 cm^{-1}.

b) UV-visible spectrum of complex (7f) compound

The UV-visible spectrum of copper tyrosine- phenylalanine dipeptide substituted phthalocyanine complex **(7f)** dissolved in DMF is shown in **Appendix 10.6** The spectrum recorded a single Q-band signal at 680 nm.

c) Thermal analysis of complex (7f) compound

The TGA and DTA thermogram curves of the copper tyrosine- phenylalanine dipeptide substituted phthalocyanine complex **(7f)** report that the compound remains thermally stable up to 200 °C with 2 % weight loss due to the moisture loss trapped by the complex, after which it undergoes three stages of degradation. A weight loss of 33 % occurs between 200-440 °C during the first stage, followed by a 43 % weight loss between 440-575 °C in the second stage. The third degradation is observed between 575-670 °C wıth a weight loss of 2 % leaving a residue of 20 % that does not decompose as indicated in **Appendix 14.6**. DTA curves reveal that the compound decomposes without a melting phase, suggesting that complex **(7f)** does not possess a melting point under normal conditions and exhibits exothermic degradation throughout its stages

d) Electrochemistry analysis of complex (7f) compound

The electrochemical analysis of copper tyrosine- phenylalanine dipeptide substituted phthalocyanine complex **(7f)** compound was performed by both Cyclic and square wave voltammetry. A glassy carbon electrode is used as the working electrode while platinum Pt as a counter electrode, tetrabutylammonium tetrafluoroborate as the electrolyte, and ferrocene /ferrocenium (Fc/Fc^{+}) as a pseudo-reference electrode in DMF. A wide potential range (-2.5 to +1.5 V versus Fc/Fc^{+}) was employed to explore the phthalocyanine complexes' electrochemical characteristics. The complex **(7f)** possesses a redox-active copper metal center that undergoes two oxidation with potential values of ($\mathbf{O_1}$ 0.64 volt and $\mathbf{O_2}$ 0.96 volt from the electronic transition of the redox oxidation reaction of $\mathbf{[Pc^{(-2)}\,Cu^{(2)}]^{0}}$ / $\mathbf{[Pc^{(-1)}\,Cu^{(2)}]^{+1}}$ and $\mathbf{[Pc^{(-1)}\,Cu^{(2)}]^{+}}$ / $\mathbf{[Pc^{(0)}\,Cu^{(2)}]^{+2}}$ respectively and four reductions reaction potential values of $\mathbf{R_4}$ -2.35 volt, $\mathbf{R_3}$ -2.04 volt, $\mathbf{R_2}$ -1.80 volt, and $\mathbf{R_1}$ -1.21 volt involves electrons transition as $\mathbf{[Pc^{(-5)}\,Cu^{(2)}]^{-3}}$ / $\mathbf{[Pc^{(-6)}\,Cu^{(2)}]^{-4}}$, $\mathbf{[Pc^{(-4)}\,Cu^{(2)}]^{-2}}$ / $\mathbf{[Pc^{(-5)}\,Cu^{(2)}]^{-3}}$, $\mathbf{[Pc^{(-3)}\,Cu^{(2)}]^{-1}}$ / $\mathbf{[Pc^{(-4)}\,Cu^{(2)}]^{-2}}$, and $\mathbf{[Pc^{(-2)}\,Cu^{(2)}]^{0}}$ / $\mathbf{[Pc^{(-3)}\,Cu^{(2)}]^{-1}}$ respectively for the reduction reaction of the conjugated Pc macrocycle ring formed cation and anion radicals.

The redox activity is directly connected with oxidation by removing electrons from the highest occupied molecular orbital (HOMO) and adding electrons to the lowest unoccupied molecular orbital (LUMO) of phthalocyanines macrocyclic [94, 121, 122]. The voltammograms of square wave and cyclic voltammograms of complex**(7f)** compound are both reported in **Appendix 18.6a** and **18.6b** respectively.

4.2.2.7. Characterization of ZnPc (7g) Complex

Characterization of phthalocyanine complex was performed by FT-IR spectra, UV-visible spectra, thermal analysis (TGA and DTA), and electrochemistry techniques (CV and SWV)

a) FT-IR spectrum of complex (7g) compound

The zinc tyrosine- phenylalanine dipeptide substituted phthalocyanine complex **(7g)** FT-IR spectrum shown in **Appendix 2.5** indicated the absence of weak sharp nitrile C≡N peaks at 2232 cm^{-1} which confirmed the cyclotetramerization of the compound (7) with $Zn(CH_3COO)_2$ in the formation of the complex **(7f)** compound. Some of the most important peaks appeared in the spectrum are the presence of a medium broad stretching peak of N-H bonds (Aliphatic amide) at 3279 cm^{-1}, a weak broad bend vibration peak of C-H (Aromatic) at 1770 c m^{-1}, a strong broad stretching carbonyl bond C=O at 1712 cm^{-1} (ester C=O), a medium stretching (in-ring) peak of C=C bond (Aromatic) at 1599 cm^{-1}, a medium stretching (in-ring) peak of C-C bond (Aromatic) at 1506 cm^{-1}, a medium broad bending vibration of C-H bond (methyl of protection group) at 1393 cm^{-1}, a strong sharp stretching peak of C-O-C bond (Aryl ether) at 1231 cm^{-1}, a medium broad

stretching peak of C-N bond (aliphatic amines) at 1164 cm^{-1} and a medium sharp bending vibration peak of C-H (Aromatic) at 747 cm^{-1} and 700 cm^{-1}.

b) UV-visible spectrum of complex (7g) compound

The UV-visible spectrum of zinc tyrosine- phenylalanine dipeptide substituted phthalocyanine complex **(7g)** dissolved in DMF is shown in **Appendix 10.7**. The spectrum revealed a single Q-band at 675nm and a B-band at 450 nm. The shoulder appeared at 613 nm due to aggregation.

c) Thermal analysis of complex (7g) compound

TGA thermogram curve of the zinc tyrosine- phenylalanine dipeptide substituted phthalocyanine complex **(7g)** compound as shown in **Appendix 14.7** indicates the complex is thermally stable up to 240 ^{0}C with 4 % weight loss against temperature due to the loss of moisture trapped in the complex. The complex undergoes two stages of degradation with a weight loss of 53 % recorded between 240 °C - 440 °C in the first stage of degradation followed by a weight loss of 22 % between 440 °C - 460 °C in the second stage of degradation and finally with leftover of 21 % remained as non-decompose residue as seen in the thermogram curve. Furthermore, the DTA curves indicate that the complex decomposes without melting and this implies that under normal conditions, the complex does not possess melting point and undergo decomposition exothermically.

d) Electrochemistry analysis of complex (7g) compound

The electrochemical analysis of zinc tyrosine- phenylalanine dipeptide substituted phthalocyanine complex **(7g)** compound was performed by both cyclic and square wave voltammetry similar to those performed for the above complexes. The complex **(7g)** possesses a redox-inactive zinc metal center that undergoes Pc base electronic redox reactıon. The complex observed two oxidation potentials at $\mathbf{O_1}$ 0.31 volt and $\mathbf{O_2}$ 0.73 volt with the electronic transition of $\mathbf{[Pc^{(-2)}\,Zn^{(2)}]^0 / [Pc^{(-1)}\,Zn^{(2)}]^{+1}}$ and $\mathbf{[Pc^{(-1)}\,Zn^{(2)}]^{+1} / [Pc^{(0)}\,Zn^{(2)}]^{+2}}$.respectively. The complex exhibit four reductions reaction with reduction potential as $\mathbf{R_4}$ -2.27 volt**,** $\mathbf{R_3}$ -1.92 volt, $\mathbf{R_2}$ -1.73 volt, and $\mathbf{R_1}$ -1.14 volt involves electrons transition as $\mathbf{[Pc^{(-5)}\,Zn^{(2)}]^{-3} / [Pc^{(-6)}\,Zn^{(2)}]^{-4}}$, $\mathbf{[Pc^{(-4)}\,Zn^{(2)}]^{-2} / [Pc^{(-5)}\,Zn^{(2)}]^{-3}}$, $\mathbf{[Pc^{(-3)}\,Zn^{(2)}]^{-1} / [Pc^{(-4)}\,Zn^{(2)}]^{-2}}$, and $\mathbf{[Pc^{(-2)}\,Zn^{(2)}]^{0} / [Pc^{(-3)}\,Zn^{(2)}]^{-1}}$ respectively for the conjugated Pc macrocycle ring formed cation and anion radicals. The redox activity is directly connected with oxidation by removing electrons from the highest occupied molecular orbital (HOMO) and adding electrons to the lowest unoccupied molecular orbital (LUMO) of phthalocyanines macrocyclic [94, 121, 122]. The voltammograms of square wave and cyclic

voltammograms of complex **(7g)** compound are both indicated in **Appendix 18.7a** and **18.7b** respectively

4.3. Characterisation of tyrosine- alanine dipeptide amino acids substituent and complexes

The dipeptide amino acid substituent methyl (tert-butoxycarbonyl)-*L*-tyrosyl-*D*-alaninate **(Boc-Tyr-Ala-OCH_3) (8)** was characterized using FT-IR, ^{1}H-NMR, ^{13}C-NMR, mass spectroscopies, and elemental analysis while the ligand Methyl ((*S*)-2-((tert-butoxycarbonyl) amino)-3-(4-(3,4-dicyanophenoxy) phenyl) propanoyl)-*D*-alaninate **(Boc-Tyr-Ala-OCH_3-O-PN) (9)** and complexes are characterized by FT-IR and UV-visible spectroscopies.

4.3.1. Characterization of methyl (tert-butoxycarbonyl)-*L*-tyrosyl-*D*-alaninate (Boc-Tyr-Ala-OCH_3) (8)

The FT-IR, ^{1}H-NMR, ^{13}C-NMR, and mass spectroscopies spectra of compound (8) are given in the **Appendix Section**. The carbons and hydrogens in compound (8) are numbered as in **Figure 4.6** below.

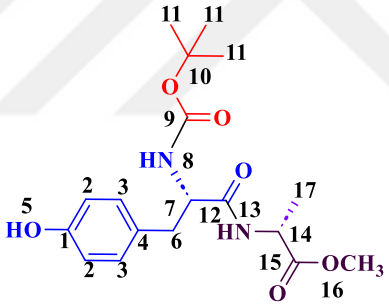

methyl (*tert*-butoxycarbonyl)-*L*-tyrosyl-*D*-alaninate

(Boc-Tyr-Ala-OCH_3) (8)

Figure 4.6. Numbering of carbons and hydrogens in methyl (tert-butoxycarbonyl)-*L*-tyrosyl-*D*-alaninate compound **(8)**

a) FT-IR spectrum of compound (8)

The FT-IR peak of methyl (*tert*-butoxycarbonyl)-*L*-tyrosyl-*D*-alaninate dipeptide indicates the presence of medium broad stretching peaks of N-H bond for amide group at 3403 $cm^{-1}$and 3339 cm^{-1}, a weak broad stretching peaks of O-H bond (Aromatic) at 2985 cm^{-1}, a medium stretching peaks of C-H bonds (Aliphatic) at 2935 cm^{-1}, a strong broad stretching peaks of carbonyl C=O at 1686 cm^{-1}(secondary amide C=O), a medium broad bending peak of N-H bond (amine) at 1645 cm^{-1}, a medium broad bending of C-H bonds (methyl group) at 1456 cm^{-1}, medium broad bending

vibration of O-H bonds (Aromatic) at 1365 cm^{-1} and 1338 cm^{-1}, a strong broad stretch of C-O bond (ester) at 1158 $cm^{-1}$and finally a last important signal is the medium broad stretching of C-N bond (amine) at 1058 cm^{-1} and 1023 cm^{-1} as it shown in the **Appendix 3**.

b) ^{1}H-NMR spectrum of compound (8)

The ^{1}H-NMR of methyl (*tert*-butoxycarbonyl)-*L*-tyrosyl-*D*-alaninate dipeptide **(8)** taken in DMSO-d6, 298K: shown in **Appendix 7.1** reported the presence of 1-proton singlet peak at 9.14 ppm belongs to H^{5} (-OH). The doublet signals of 1 proton at 8.29 -8.31 ppm belong to H^{13} (-NH). The 2 protons produce double signals belongs H^{3} at 7.06 -7.08 ppm with coupling constant value of (distance between the two peaks) J= 8.8 Hz. The proton generated double peaks at 6.74 -6.76 ppm belong to H^{8} (-NH). The double peak signals of 2 protons at 6.65 - 6.67 ppm occupy a distance of 8.4 Hz between the two peaks is belong to H^{2}. The quartet peaks of 1-proton at 4.29 - 4.32ppm belong to H^{7}. The multiple signals of 1- proton at 4.08 -4.13 ppm are produced by H^{14}. The presence of 3 proteins produces a singlet peak at 3.64 ppm is belongs to H^{16}. The 2- proton split to produce a double doublet peak at 2.56 -2.65 ppm and 2.84 -2.88 ppm belongs to proton H^{6}, the 9 protons given a singlet intense signal at 1.32 ppm belong to H^{11}. The 3 protons produce double peak signals at 1.26-1.30 ppm belonging to H^{17} and lastly, a peak at 3.36 ppm belongs to DMSO-d6 water and the peak at 2.51 ppm belongs to DMSO-d6.

c) ^{13}C-NMR spectrum of compound (8)

The ^{13}C-NMR spectrum of methyl (*tert*-butoxycarbonyl)-*L*-tyrosyl-*D*-alaninate dipeptide **(8)** taken in DMSO-d6, 298K is shown in **Appendix 7.2.** The peak C^{1} at 155.70 ppm is an aromatic carbon that is attached to the phenol functional group. The peak C^{2} at 115.26 ppm is an aromatic carbon, the peak C^{3}at 130.57 ppm,128.63 C^{4}, 037.06 C^{6}, 056.17 C^{7}, 156.19 C^{9}, 078.40 C^{10}, 028.63 C^{11}, 172.33 C^{12}, 047.99 C^{14}, 173.47 C^{15}, 052.32 C^{16}, 017.46 C^{17}.

d) Mass spectrum of compound (8)

The theoretically calculated molecular weight of the **Boc-Tyr-Ala-OCH_3** compound is 366.41 g/mol. In the MALDI-TOF MS spectrum of compound **(8)** given in **Appendix 7.3**, the 366.445 [M] peak belongs to the compound. The peaks observed below this peak indicate the compound resulting from the groups leaving the structure. According to calculations, the peak at 310.310 corresponds to the breakage of the -$C(CH_3)_3$ group in the Boc protecting group at 310.310 [M-$C(CH_3)_3$].

4.3.2. Characterization of methyl ((S)-2-((tert-butoxycarbonyl) amino)-3-(4-(3,4-dicyanophenoxy) phenyl) propanoyl)-*D*-alaninate (Boc-Tyr-Ala-OCH_3-O-PN) (9)

The characterization of (Boc-Tyr-Ala-OCH_3-O-PN) **(9)**, shown in **Figure 4.7** below, was done by FT-IR, ^{1}H-NMR, and ^{13}C-NMR spectroscopies

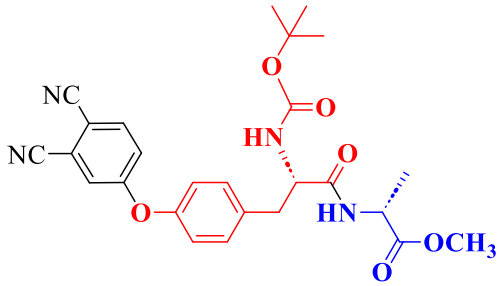

Figure 4.7. Methyl ((S)-2-((tert-butoxycarbonyl) amino)-3-(4-(3,4-dicyanophenoxy) phenyl) propanoyl)-*D*-alaninate **(Boc-Tyr-Ala-OCH_3-O-PN) (9)**

a) FT-IR spectrum of compound (9)

The FT-IR (ATR, cm^{-1}) spectrum of methyl ((*S*)-2-((tert-butoxycarbonyl) amino)-3-(4-(3,4-dicyanophenoxy) phenyl) propanoyl)-*D*-alaninate compound **(9)** obtained shown in **Appendix 3.1.** indicated the appearance of a weak sharp nitrile C≡N peak at 2232 cm^{-1} as one of the most important signal peaks in the ligand compound. Other important peaks in the spectrum are a medium broad stretching of the N-H bond (Secondary amine) at 3320 cm^{-1}, a -CH aromatic bond peak signal observed in the range of 3100-3000 cm^{-1}, and a -CH aliphatic bond signal presence between 2986-2860 cm^{-1}. There is also the presence of strong broad stretching peak signals of C=O (ester) bond at 1717 cm^{-1} and C=O (amide) at 1657 cm^{-1}, a medium broad bending peak signal of N-H (amine) at 1591 cm^{-1}**,** then a medium broad stretching peak of C-C aromatic (in-ring) at 1486 cm^{-1}, a medium broad bending signal of C-H bond (methyl protection group) at 1419 cm^{-1} and 1394 cm^{-1}, a strong broad stretching peak signal at 1250 cm^{-1} belong to C-O-C (ether), a medium broad stretching peaks signals of C-N bond (aliphatic amine) at 1169 cm^{-1} and 1020 cm^{-1}.

b) ^{1}H-NMR spectrum of compound (9)

The ^{1}H-NMR of methyl ((*S*)-2-((tert-butoxycarbonyl) amino)-3-(4-(3,4-dicyanophenoxy) phenyl) propanoyl)-*D*-alaninate **(9)** taken in DMSO-d6, 400 MHz: shown in (**Appendix 7.4**) observed the presence of 1-proton doublet peak at 8.45 ppm with coupling constant value of (distance between the two peaks) J= 7.0 Hz, a doublet signal of 1-proton with coupling constant value of (distance between the two peaks) J= 8.8 Hz, a doublet peak signal of 2-protons observed at 7.43ppm wıth coupling constant value of J= 8.4 Hz, 3-protons split to produce double triplet

peaks signals at 7.26 ppm with coupling constant value of (distance between the peaks) J= 9.5 Hz and J= 5.1 Hz, 2-protons doublet signals with coupling constant value of J= 8.8 Hz appeared at 7.15 ppm, moreover a 1-proton doublet is observed at 7.00 ppm with coupling constant value of J= 8.9 Hz, a triplet 1-proton with coupling constant value of J= 7.1 Hz appeared at 4.31 ppm, a multiplet peak signal of 1-proton observed between 4.27 ppm-4.18 ppm, 3-protons singlet observed at 3.64 ppm, 1-proton of split to produce double doublet peaks signal at 3.01 ppm with coupling constant value of (distance between the peaks) J= 13.8 Hz and J= 4.0 Hz, 2-protons split to produce double doublet peaks signals at 2.75 ppm with coupling constant value of (distance between the peaks) J= 13.6 Hz and J= 10.6 Hz, 1-proton doublet peak signal observed at 1.53 ppm with coupling constant value of J= 7.3 Hz, 9-proton given a singlet intense signal at 1.31 ppm, 3-protons doublet with coupling constant value of J= 9.0 Hz appeared at 1.26 ppm and lastly, a peak at 3.40 ppm belongs to DMSO-d6 water and the peak at 2.51 ppm belongs to DMSO-d6.

4.3.2.1 Characterisation of CrPc (9a) Complex

Characterization of phthalocyanine complex were performed by FT-IR spectra, UV-Visible spectra, thermal analysis (TGA and DTA) and electrochemistry techniques (CV and SWV)

a) FT-IR spectrum of complex (9a) compound

The FT-IR spectrum of chromium tyrosine- alanine dipeptide substituted phthalocyanine complex **(9a)** shown in **Appendix 3.2** indicated the absence of weak sharp nitrile C≡N peaks at 2232 cm^{-1} which confirmed the occurrence of cyclotetramerization of the compound **(9)** in the formation of the complex compound **(9a)**. Furthermore, some of the most important peaks present are medium broad stretching peaks of N-H bonds (Aliphatic amide) at 3285 cm^{-1}, a medium broad stretching peaks of C-H bond (aliphatic) between 2938-2869 cm^{-1}, a weak broad bend vibration peak of C-H (Aromatic) overtone at 1769 cm^{-1}**,** a strong broad peak signal of carbonyl carbon C=O at 1709 cm^{-1} (ester C=O) and 1656 cm^{-1} for (amide C=O), a medium broad bending vibration signal of N-H (Amide) at 1597 cm^{-1}, a medium stretching peak of C-C bond (in-ring) aromatic at 1504 cm^{-1}, a medium broad bending vibration of C-H bond (methyl of protection group) at 1395 cm^{-1}, a strong broad peak signal of C-O-C (ether) at 1231 cm^{-1} and a medium broad stretching peak of C-N bond (aliphatic amines) at 1068 cm^{-1}.

b) UV-visible spectrum of complex (9a) compound

The UV-visible spectrum of chromium tyrosine-alanine dipeptide substituted phthalocyanine complex **(9a)** dissolved in DMF is shown in **Appendix 11.1**. in the spectrum, a single Q-band is seen at 670 nm and a B-band at 440 nm. The pronouns shoulder at 612 nm are due to aggregation.

c) Thermal analysis of complex (9a) compound

TGA thermogram curve of the chromium tyrosine- alanine dipeptide substituted phthalocyanine complex **(9a)** compound as shown in **Appendix 15.1** indicates the complex is thermally stable up to 220 °C with 5 % weight loss against the temperature due to the loss of moisture trapped in the complex. The complex undergoes two stages of degradation with a weight loss of 50 % recorded between 220 - 415 °C in the first stage of degradation followed by a weight loss of 36 % recorded between 440 - 460 °C in the second stage of degradation. Finally, a leftover 9% remained as non-decompose residue which probably may consist of its metal oxide Cr_2O_3 as seen in the thermogram curve. Furthermore, the DTA curves reported that the complex decomposes without melting and this implies that under normal conditions, the complex does not possess a melting point and undergoes decomposition exothermically.

d) Electrochemistry analysis of complex (9a) compound

The electrochemical analysis of chromium tyrosine-alanine dipeptide substituted phthalocyanine complex **(9a)** compound was performed by both Cyclic and square wave voltammetry. A glassy carbon electrode is used as the working electrode while platinum Pt as a counter electrode, tetrabutylammonium tetrafluoroborate as the electrolyte, and ferrocene /ferrocenium (Fc/Fc^+) as a pseudo-reference electrode in DMF. A wide potential range (-2.5 to +1.5 V versus Fc/Fc^+) was employed to explore the phthalocyanine complexes' electrochemical characteristics [119, 120]. The complex **(9a)** possesses a redox-active chromium metal center that undergoes two oxidation potential values $\mathbf{O_1}$ 0.53 volt and $\mathbf{O_2}$ 0.95 which involves $\mathbf{[Pc^{(-2)}\,Cr^{(2)}]^0}$ / $\mathbf{[Pc^{(-1)}\,Cr^{(3)}]^{+2}}$ and $\mathbf{[Pc^{(-1)}\,Cr^{(2)}]^{+1}}$ / $\mathbf{[Pc^{(0)}\,Cr^{(3)}]^{+3}}$ for **O_1 and O_2 oxidation** electronic transition respectively related to the formation of cation radicals. The complex observed four reductions ($\mathbf{R_4}$ -2.42 volt, $\mathbf{R_3}$ -2.27 volt, $\mathbf{R_2}$ -1.82 volt, and $\mathbf{R_1}$ -1.20 volt) these produce $\mathbf{[Pc^{(-5)}\,Cr^{(2)}]^{-3}}$ / $\mathbf{[Pc^{(-6)}\,Cr^{(2)}]^{-4}}$ for $\mathbf{R_4}$, $\mathbf{[Pc^{(-4)}\,Cr^{(2)}]^{-2}}$ / $\mathbf{[Pc^{(-5)}\,Cr^{(2)}]^{-3}}$ for $\mathbf{R_3}$, $\mathbf{[Pc^{(-3)}\,Cr^{(2)}]^{-1}}$ / $\mathbf{[Pc^{(-4)}\,Cr^{(2)}]^{-2}}$ for $\mathbf{R_2}$, and $\mathbf{[Pc^{(-2)}\,Cr^{(2)}]^0}$ / $\mathbf{[Pc^{(-3)}\,Cr^{(2)}]^{-1}}$ for $\mathbf{R_1}$ reductıon electronic transitions related to the formation of anion radicals from the redox reaction of the conjugated macrocycle Pc ring**.** The complex exhibits a metal center redox reaction potential value $\mathbf{M_O}$ 0.36 volt involves the electronic transfer $\mathbf{[Pc^{(-2)}\,Cr^{(2)}]^0}$ / $\mathbf{[Pc^{(-2)}\,Cr^{(3)}]^{+1}}$ for metal base oxidation $\mathbf{M_O}$ to formed cation radicals.

The redox activity is directly connected with oxidation by removing electrons from the highest occupied molecular orbital (HOMO) and adding electrons to the lowest unoccupied molecular orbital (LUMO) of phthalocyanines macrocyclic. The voltammograms of square wave and cyclic voltammograms of complex **(9a)** compound are both shown in **Appendix 19.1a** and **19.1b** respectively.

4.3.2.2. Characterisation of MnPc (9b) complex

Characterization of phthalocyanine complex were performed by FT-IR spectra, UV-Visible spectra, thermal analysis (TGA and DTA) and electrochemistry techniques (CV and SWV)

a) FT-IR spectrum of complex (9b) compound

FT-IR spectrum of manganese tyrosine- alanine dipeptide substituted phthalocyanine complex **(9b)** shown in the **Appendix 3.3** observed the absence of a weak sharp nitrile C≡N bond peak signal at 2232 cm^{-1} which justified the formation cyclotetramerization reaction of the compound **(9)** in the complex **(9b)** compound making. Conversely, some of the presence of the most important peaks in the spectrum are medium broad stretching peaks of N-H bonds (Aliphatic amide) at 3238 cm^{-1}, a medium broad stretching peaks of C-H bond (methyl group) between 2937-2850 cm^{-1}, weak broad bend vibration peak of C-H (Aromatic) overtone at 1766 cm^{-1}**,** a strong broad peak signal of carbonyl carbon C=O at 1700 cm^{-1} (Ester C=O) and 1662 cm^{-1} for (Amide C=O), a medium broad bending vibration signal of N-H (Amide) at 1595 cm^{-1}, a medium stretching peak of C-C (in-ring) aromatic at 1504 cm^{-1}, a medium broad bending vibration of C-H bond (methyl of protection group) at 1394 cm^{-1}, a strong broad peak signal of C-O-C (ether) at 1230 cm^{-1} and a medium broad stretching peak of C-N bond (aliphatic amines) at 1167 cm^{-1} and 1071 cm^{-1}.

b) UV-visible spectrum of complex (9b) compound

Appendix 11.2 shows the UV-visible spectrum of a manganese tyrosine-alanine dipeptide substituted phthalocyanine complex **(9b)** dissolved in DMF. In the spectrum, a single Q-band is seen at 712 nm and a B-band at 437 nm. The small shoulder at 675 nm is due to aggregation.

c) Thermal analysis of complex (9b) compound

It was observed from the TGA thermograms curve of the manganese tyrosine-alanine dipeptide substituted phthalocyanine complex **(9b)** that the compound is thermally stable up to 150 °C with only 4% weight loss against the temperature due to moisture trapped in the complex and it undergoes three stages of degradation. A weight loss of 11 % was recorded between 150 -350 °C in the first stage of degradation followed by a weight loss of 6 5% between 350 -470 °C in the second stage of degradation and finally a weight loss of 3 % was accounted for in the third stage of degradation between 470 - 670 °C with the leftover of 17 % weight loss as non –decompose residue as shown in the **Appendix 15.2.** It is indicated from the DTA curves of the complexes that the compound decomposes without melting, this translated that under normal conditions complex **(9b)** compound does not have a melting point and all their stages of degradation follow exothermic decomposition.

d) Electrochemistry analysis of complex (9b) compound

The electrochemical analysis of manganese tyrosine-alanine dipeptide substituted phthalocyanine complex **(9b)** compound was performed by both Cyclic and square wave voltammetry. A glassy carbon electrode is used as the working electrode while platinum Pt as a counter electrode, tetrabutylammonium tetrafluoroborate as the electrolyte, and ferrocene /ferrocenium (Fc/Fc^{+}) as a pseudo-reference electrode in DMF. A wide potential range (-2.5 to +1.5 V versus Fc/Fc^{+}) was employed to explore the phthalocyanine complexes' electrochemical characteristics [119, 120]. The complex **(9b)** possesses a redox-inactive metal (manganese) center that undergoes two oxidations ($\mathbf{O_1}$ 0.24 volt and $\mathbf{O_2}$ 0.83 volt) which involve $\mathbf{[Pc^{(-2)}\,Mn^{(2)}]^{0}}$ / $\mathbf{[Pc^{(-1)}\,Mn^{(3)}]^{+2}}$and $\mathbf{[Pc^{(-1)}\,Mn^{(2)}]^{+}}$ / $\mathbf{[Pc^{(0)}\,Mn^{(3)}]^{+3}}$ for first $\mathbf{O_1}$ and second $\mathbf{O_2}$ oxidatıon electronic transitions related to the formation of cation radicals, three reductions ($\mathbf{R_4}$ -2.39 volt, $\mathbf{R_3}$ -1.89 volt, $\mathbf{R_2}$ -1.61 volt, and $\mathbf{R_1}$ -1.16 volt) these produce $\mathbf{[Pc^{(-5)}\,Mn^{(2)}]^{-3}}$ / $\mathbf{[Pc^{(-6)}\,Mn^{(2)}]^{-4}}$ for $\mathbf{R_4}$, $\mathbf{[Pc^{(-4)}\,Mn^{(2)}]^{-2}}$ / $\mathbf{[Pc^{(-5)}\,Mn^{(2)}]^{-3}}$ for $\mathbf{R_3}$, $\mathbf{[Pc^{(-3)}\,Mn^{(2)}]^{-1}}$ / $\mathbf{[Pc^{(-4)}\,Mn^{(2)}]^{-2}}$ for $\mathbf{R_2}$, and $\mathbf{[Pc^{(-2)}\,Mn^{(2)}]^{0}}$ / $\mathbf{[Pc^{(-3)}\,Mn^{(2)}]^{-1}}$ for $\mathbf{R_1}$ reduction transition related to the formation of anion radicals of the conjugated macrocycle Pc ring. The redox activity is directly connected with oxidation by removing electrons from the highest occupied molecular orbital (HOMO) and adding electrons to the lowest unoccupied molecular orbital (LUMO) of phthalocyanines macrocyclic. The voltammograms of square wave and cyclic voltammograms of complex **(9b)** compound are both shown in **Appendix 19.2a** and **19.2b** respectively.

4.3.2.3. Characterisation of FePc (9c) Complex

Characterization of phthalocyanine complex were performed by FT-IR spectra, UV-Visible spectra, thermal analysis (TGA and DTA) and electrochemistry techniques (CV and SWV)

a) FT-IR spectrum of complex (9c) compound

The FT-IR spectrum of iron tyrosine- alanine dipeptide substituted phthalocyanine complex **(9c)** shown in **Appendix 3.4** reported the absence of weak sharp nitrile C≡N peaks at 2232 cm^{-1} which affirmed the occurrence of cyclotetramerization of the compound (9) in the formation of the complex compound **(9c)**. Some of the most important peaks that occurred in the spectrum are the presence of a medium broad stretching peak of N-H bonds (Aliphatic amide) at 3309 cm^{-1}, a medium broad stretching peaks of C-H bond (methyl group) between 2982-2845 cm^{-1}, a weak broad bend vibration peak of C-H (Aromatic) overtone at 1764 cm^{-1}**,** a strong broad peak of carbonyl carbon C=O at 1701 cm^{-1} (ester C=O) and 1657 cm^{-1} for (amide C=O), a medium broad bending vibration signal of N-H (Amide) at 1593 cm^{-1}, a medium stretching peak of C-C (in-ring) aromatic at 1506 cm^{-1}, a medium broad bending vibration of C-H bond (methyl of protection group)

at 1394 cm^{-1}, a strong broad stretching peak signal of C-O-C (ether) at 1233 cm^{-1} and a medium broad stretching peak of C-N bond (aliphatic amines) at 1166 cm^{-1} and 1057 cm^{-1}.

b) UV-visible spectrum of complex (9c) compound

The UV-visible spectrum of iron tyrosine-alanine dipeptide substituted phthalocyanine complex **(9c)** dissolved in DMF is shown in **Appendix 11.3** The spectrum reported a single Q-band seen at 667 nm and B-band at 440 nm. A sharp shoulder is observed at 600 nm due to aggregation. Pc can form aggregates of cofacial structure (arrangement of molecules or materials in a way that their planes are parallel to each other (H-aggregates) within such supramolecular associates owing to π–π-stacking [123, 124, 125]. cofacial structures exhibit π-π stacking interactions, which can influence the material's electronic properties.

c) Thermal analysis of complex (9c) compound

It is reported in the TGA thermograms curve of the iron tyrosine-alanine dipeptide substituted phthalocyanine complex **(9c)** that the compound is thermally stable up to 180 °C and undergoes a 5% weight loss up to this temperature. This weight loss is thought to be due to the moisture absorbed and lost at the bagging of heating of the complex **(9c)**. The complex undergoes two stages of degradation with a weight loss of 42 % recorded between 180- 385 °C in the first stage of degradation followed by a weight reduction of 31 % occurring between 400-430 °C in the second stage of degradation with 17 % remaining material without decomposition left as residue as seen in the TGA thermogram curve in the **Appendix 15.3.** The DTA curves of the complex indicate that the compound decomposes without melting. Therefore, under normal conditions complex (**9c**) does not have a melting point and all their stages of degradation follow exothermic.

d) Electrochemistry analysis of complex (9c) compound

The electrochemical properties of iron tyrosine-alanine dipeptide substituted phthalocyanine complex **(9c)** were examined using cyclic and square wave voltammetry techniques. Similar to previous analyses, a glassy carbon electrode served as the working electrode while platinum was used as a counter electrode. The electrolyte comprised tetrabutylammonium tetrafluoroborate with ferrocene/ferrocenium (Fc/Fc^{+}) as a pseudo-reference electrode in DMF. The investigations were conducted over a potential range of -2.5 to +1.5 V versus Fc/Fc^{+}. The complex **(9c)** exhibited two Pc base oxidation process of $\mathbf{O_1}$ at 0.37 volt and $\mathbf{O_2}$ at 0.72 volt which involves $\mathbf{Pc^{(-2)}\,Fe^{(2)}}$ / $\mathbf{[Pc^{(-1)}Fe^{(3)}]^{+2}}$ and $\mathbf{[Pc^{(-1)}\,Fe^{(2)}]^{+}}$ / $\mathbf{[Pc^{(0)}\,Fe^{(3)}]^{+3}}$ for first $\mathbf{O_1}$ and second $\mathbf{O_2}$ oxidation transitions respectively related to the formation of cation radicals, along with four reduction processes ($\mathbf{R_4}$ at -2.35 volt, $\mathbf{R_3}$ at -1.98 volt, $\mathbf{R_2}$ at -1.77 volt, $\mathbf{R_1}$ at -1.12 volt) generated from $\mathbf{[Pc^{(-5)}\,Fe^{(2)}]^{-3}}$ / $\mathbf{[Pc^{(-6)}\,Fe^{(2)}]^{-4}}$ for $\mathbf{R_4}$, $\mathbf{[Pc^{(-4)}\,Fe^{(2)}]^{-2}}$ / $\mathbf{[Pc^{(-5)}\,Fe^{(2)}]^{-3}}$ for $\mathbf{R_3}$, $\mathbf{[Pc^{(-3)}\,Fe^{(2)}]^{-1}}$ / $\mathbf{[Pc^{(-4)}\,Fe^{(2)}]^{-2}}$ for $\mathbf{R_2}$, and $\mathbf{[Pc^{(-2)}\,Fe^{(2)}]^{0}}$ / $\mathbf{[Pc^{(-3)}\,Fe^{(2)}]^{-1}}$ for $\mathbf{R_1}$ reductıon electronic transfer related to the formation of

anion radicals. Iron metal is a redox-active metal that undergoes redox reaction to produce metal center reduction potential $\mathbf{M_R}$ -0.72 and oxidation potential value of $\mathbf{M_O}$ 0.15 involving electronic transition leading to the formation of anion and cation radicals as **[Pc $^{(-2)}$ Fe $^{(2)}$]^{0} / [Pc $^{(-2)}$ Fe $^{(1)}$]$^{-1}$** and **[Pc $^{(-2)}$ Fe $^{(2)}$]^{0} / [Pc $^{(-2)}$ Fe $^{(3)}$]$^{+1}$** respectively [126, 127].

The redox activity is connected to the transfer of electrons from the highest occupied molecular orbital (HOMO) and the lowest unoccupied molecular orbital (LUMO) of the phthalocyanine macrocycle. The voltammograms for the square wave and cyclic voltammetry of complex **(9c)** can be found in **Appendix 193a** and **19.3b**, respectively.

4.3.2.4. Characterisation of CoPc (9d) Complex

Characterization of phthalocyanine complex were performed by FT-IR spectra, UV-Visible spectra, thermal analysis (TGA and DTA) and electrochemistry techniques (CV and SWV)

a) FT-IR spectrum of complex (9d) compound

The FT-IR spectrum of cobalt tyrosine- alanine dipeptide substituted phthalocyanine complex **(9d)** shown in **Appendix 3.5** reported the absence of weak sharp nitrile C≡N peaks at 2232 cm^{-1} which affirmed the occurrence of cyclotetramerization of the compound **(9)** in the formation of the complex compound **(9d)**. Some of the most important peaks that occurred in the spectrum are the presence of a medium broad stretching peak of N-H bonds (Aliphatic amide) at 3317 cm^{-1}, a medium broad stretching peaks of C-H bond (methyl group) between 2978-2859 cm^{-1}, a weak broad bend vibration peak of C-H (Aromatic) overtone at 1766 cm^{-1}**,** a strong broad stretching peak signals of carbonyl carbon bond 1714 cm^{-1} (ester C=O) and 1658 cm^{-1} for (amide C=O), a medium broad bending vibration signal of N-H (Amide) at 1600 cm^{-1}, a medium stretching peak of C-C bond (in-ring) aromatic at 1506 cm^{-1} and 1476 cm^{-1}, a medium broad bending vibration of C-H bond (methyl of protection group) at 1365 cm^{-1}, a strong broad stretching peak signal of C-O-C bond (ether) at 1230 cm^{-1}, a medium broad stretching peak signals of C-N bond (aliphatic amines) at 1162 cm^{-1} and 1093 cm^{-1}.

b) UV-visible spectrum of complex (9d) compound

The UV-visible spectrum of cobalt tyrosine-alanine dipeptide substituted phthalocyanine complex **(9d)** dissolved in DMF is shown in **Appendix 11.4**. in the spectrum, a single Q-band is seen at 660 nm and a B-band at 432 nm. The small sharp shoulder at 600 nm is due to aggregation.

c) Thermal analysis of complex (9d) compound

The TGA thermograms curve reported in **Appendix 15.4** indicated that the cobalt tyrosine-alanine dipeptide substituted phthalocyanine complex **(9d)** compound is thermally stable up to 240 °C with only 5 % weight loss associated with moisture loss by the complex. The complex undergoes two stages of degradation with a weight loss of 5 0% recorded between 240- 440 °C in the first stage of degradation followed by a weight reduction of 25 % occurring between 440-530 °C in the second stage of degradation. 17 % remaining material was recorded as non-decomposition residue as seen in the TGA thermogram curve. The DTA curves of the complex indicate that the compound decomposes without melting. Therefore, under normal conditions complex (**9d**) does not have a melting point and all their stages of degradation follow exothermic decomposition.

d) Electrochemistry analysis of complex (9d) compound

The electrochemical properties of cobalt tyrosine-alanine dipeptide substituted phthalocyanine complex **(9d)** were examined using cyclic and square wave voltammetry techniques. Similar to previous analyses, a glassy carbon electrode served as the working electrode while platinum was used as a counter electrode. The electrolyte comprised tetrabutylammonium tetrafluoroborate with ferrocene/ferrocenium (Fc/Fc^{+}) as a pseudo-reference electrode in DMF. The investigations were conducted over a potential range of -2.5 to +1.5 V versus Fc/Fc^{+}. The complex **(9d)** exhibited two oxidation processes with potential values as $\mathbf{O_1}$ at 0.38 volt and $\mathbf{O_2}$ at 0.62 volt which involve $\mathbf{Pc^{(-2)}\,Co^{(2)}}$ / $\mathbf{[Pc^{(-1)}\,Co^{(3)}]^{+2}}$and $\mathbf{[Pc^{(-1)}\,Co^{(2)}]^{+}}$ / $\mathbf{[Pc^{(0)}\,Co^{(3)}]^{+3}}$ for first $\mathbf{O_1}$ and second $\mathbf{O_2}$ oxidatıons electronic transfer respectively for the formation of cation radicals. Four reduction processes were recorded as ($\mathbf{R_4}$ at -2.43 volt, $\mathbf{R_3}$ at -2.09 volt, $\mathbf{R_2}$ at -1.91 volt, $\mathbf{R_1}$ at -1.30 volt) result from $\mathbf{[Pc^{(-5)}\,Co^{(2)}]^{-3}}$ / $\mathbf{[Pc^{(-6)}\,Co^{(2)}]^{-4}}$ for $\mathbf{R_4}$, $\mathbf{[Pc^{(-4)}\,Co^{(2)}]^{-2}}$ / $\mathbf{[Pc^{(-5)}\,Co^{(2)}]^{-3}}$ for $\mathbf{R_3}$, $\mathbf{[Pc^{(-3)}\,Co^{(2)}]^{-1}}$ / $\mathbf{[Pc^{(-4)}\,Co^{(2)}]^{-2}}$ for $\mathbf{R_2}$, and $\mathbf{[Pc^{(-2)}\,Co^{(2)}]^{0}}$ / $\mathbf{[Pc^{(-3)}\,Co^{(2)}]^{-1}}$ for $\mathbf{R_1}$ reduction reaction from electrons transfer forming of anion radicals from Pc ring redox reaction. Cobalt metal is a redox-active metal that exhibits metal center redox reaction ($\mathbf{M_R}$ -0.89 and $\mathbf{M_O}$ 0.08) involves $\mathbf{[Pc^{(-2)}\,Co^{(2)}]^{0}}$ / $\mathbf{[Pc^{(-2)}\,Co^{(1)}]^{-1}}$ electronic transfer for metal base reduction $\mathbf{M_R}$, and $\mathbf{[Pc^{(-2)}\,Co^{(2)}]^{0}}$ / $\mathbf{[Pc^{(-2)}\,Co^{(3)}]^{+1}}$ for metal base oxidation $\mathbf{M_O}$ to formed anion and cation radicals respectively.

The redox activity is connected to the transfer of electrons from the highest occupied molecular orbital (HOMO) and the lowest unoccupied molecular orbital (LUMO) of the phthalocyanine macrocycle. The voltammograms for the square wave and cyclic voltammetry of complex **(9d)** can be found in **Appendix 19.4a** and **19.4b**, respectively.

4.3.2.5. Characterisation of NiPc (9e) Complex

Characterization of phthalocyanine complex were performed by FT-IR spectra, UV-Visible spectra, thermal analysis (TGA and DTA) and electrochemistry techniques (CV and SWV)

a) FT-IR spectrum of complex (9e) compound

The FT-IR spectrum of nickel tyrosine- alanine dipeptide substituted phthalocyanine complex **(9e)** shown in the **Appendix 3.6** recorded the absence of weak sharp nitrile C≡N peaks at 2232 cm^{-1} which confirmed the cyclotetramerization of the compound **(9)** in the formation of the complex **(9e)** compound. Among the most important peaks that appeared in the spectrum are the appearance of a medium broad stretching peak of N-H bonds (Aliphatic amide) at 3312 cm^{-1}, medium broad stretching peaks of C-H bond (methyl group) between 2977-2935 cm^{-1}, weak broad bend vibration peak of C-H (Aromatic) overtone at 1766 cm^{-1}, a medium broad peak of carbonyl carbon 1716 cm^{-1} (ester C=O) and 1657 cm^{-1} for (amide C=O), a medium broad bending vibration peak of N-H (Amides) at 1592 cm^{-1}**,** a medium broad stretching peak of C-C bond (in-ring) aromatic at 1506 cm^{-1} and 1475 cm^{-1}, a medium broad bending vibration of C-H bond (methyl of protection group) at 1391 cm^{-1} and 1365 cm^{-1}, a strong broad stretching peak of C-O-C bond (ethers) at 1233 and C-O bond (ester) 1162 cm^{-1} and a medium broad stretching peak of C-N bond (aliphatic amines) at 1094 cm^{-1}.

b) UV-visible spectrum of complex (9e) compound

The UV-visible spectrum of nickel tyrosine-alanine dipeptide substituted phthalocyanine complex **(9e)** dissolved in DMF is shown in **Appendix 11.5**. The spectrum indicated the presence of a single Q-band at 670 nm and a B-band at 430 nm. There is a cleared sharp shoulder appeared at 612 nm which is due to aggregation.

c) Thermal analysis of complex (9e) compound

TGA thermogram curve of the nickel tyrosine- alanine dipeptide substituted phthalocyanine complex **(9e)** compound as shown in **Appendix 15.5** reported the complex is thermally stable up to 120 °C with only 3% weight loss against the temperature due to the loss of moisture trapped in the complex. The complex recorded three stages of degradation with a weight loss of 19 % occurring between 120 °C - 210 °C in the first stage of degradation followed by a weight loss of 25 % observed between 210 ^{0}C - 500 °C in the second stage of degradation. Finally, a weight loss of 45 % was reported between 500 °C - 850 °C as the third stage with a leftover 9 % remaining as non-decompose residue which probably may consist of its metal oxide NiO as seen in the thermogram curve. Furthermore, the DTA curves reported that the complex decomposes without melting and this implies that under normal conditions, the complex does not possess melting point and undergoes decomposition exothermically.

d) Electrochemistry analysis of complex (9e) compound

The electrochemical analysis of nickel tyrosine-alanine dipeptide substituted phthalocyanine complex **(9e)** compound was performed by both Cyclic and square wave voltammetry. A glassy carbon electrode is used as the working electrode while platinum Pt as a counter electrode, tetrabutylammonium tetrafluoroborate as the electrolyte, and ferrocene /ferrocenium (Fc/Fc^{+}) as a pseudo-reference electrode in DMF. A wide potential range (-2.5 to +1.5 V versus Fc/Fc^{+}) was employed to explore the phthalocyanine complexes' electrochemical characteristics [119, 120]. The complex **(9e)** possesses a redox-inactive nickel metal center that undergoes two oxidations potential as $\mathbf{O_1}$ 0.29 volt from **[Pc $^{(-2)}$ Ni $^{(2)}$]^{0} / [Pc $^{(-1)}$ Ni $^{(2)}$] $^{+1}$** and $\mathbf{O_2}$ 0.67 volt from **[Pc $^{(-1)}$ Ni $^{(2)}$] $^{+1}$ / [Pc ^{0} Ni $^{(2)}$] $^{+2}$** electronic transition of the Pc macrocycle ring to formed cation. The redox reaction generates four reductions reaction $\mathbf{R_4}$ -2.38 volt**,** $\mathbf{R_3}$ -2.06 volt, $\mathbf{R_2}$ -1.84 volt, and $\mathbf{R_1}$ -1.42 volt involves electrons transition as **[Pc $^{(-5)}$ Ni $^{(2)}$]$^{-3}$ / [Pc $^{(-6)}$ Ni $^{(2)}$]$^{-4}$**, **[Pc $^{(-4)}$ Ni $^{(2)}$]$^{-2}$ / [Pc $^{(-5)}$ Ni $^{(2)}$]$^{-3}$**, **[Pc $^{(-3)}$ Ni $^{(2)}$]$^{-1}$ / [Pc $^{(-4)}$ Ni $^{(2)}$]$^{-2}$**, and **[Pc $^{(-2)}$ Ni $^{(2)}$]^{0} / [Pc $^{(-3)}$ Ni $^{(2)}$]$^{-1}$** respectively of the conjugated Pc macrocycle ring forming anionic radicals. The redox activity is directly connected with oxidation by removing electrons from the highest occupied molecular orbital (HOMO) and adding electrons to the lowest unoccupied molecular orbital (LUMO) of phthalocyanines macrocyclic [94, 121, 122]. The voltammograms of square wave and cyclic voltammograms of complex **(9e)** compound are both indicated in **Appendix 19.5a** and **19.5b** respectively.

4.3.2.6. Characterization of CuPc (9f) Complex

Characterization of phthalocyanine complex were performed by FT-IR spectra, UV-Visible spectra, thermal analysis (TGA and DTA) and electrochemistry techniques (CV and SWV)

a) FT-IR spectrum of complex (9f) compound

The FT-IR spectrum of copper tyrosine- alanine dipeptide substituted phthalocyanine complex **(9f)** shown in **Appendix 3.7** reported the absence of weak sharp nitrile C≡N peaks at 2232 cm^{-1} which testified the cyclotetramerization of the compound **(9)** in the formation of the complex **(9f)**. Some of the most important peaks that appeared in the spectrum are a medium broad stretching peaks of N-H bonds (Aliphatic amide) at 3238 cm^{-1}, a medium broad stretching peaks of C-H bond (methyl group) between 2936-2844 cm^{-1}, the medium broad peak of carbonyl carbon bond (ester C=O) and (amide C=O) between 1760 cm^{-1}- 1661 cm^{-1}, a medium broad bending vibration peak of N-H (Amines) at 1591 cm^{-1}**,** a medium stretching (in-ring) of C-C bond (Aromatic) at 1506 cm^{-1}, a medium broad bending vibration of C-H bond (methyl of protection group) at 1394 cm^{-1}, a strong broad stretching peak of C-O-C bond (ethers) at 1230 and C-O bond (ester) 1066 cm^{-1} and a medium broad stretching peak of C-N bond (aliphatic amine) at 1033 cm^{-1}.

b) UV-visible spectrum of complex (9f) compound

The UV-visible spectrum of copper tyrosine-alanine dipeptide substituted phthalocyanine complex **(9f)** dissolved in DMF is shown in **Appendix 11.6** The spectrum recorded a single Q-band signal at 670 nm and B-band at 490 nm. A small shoulder was observed at 612 nm which is due to aggregation.

c) Thermal analysis of complex (9f) compound

It is observed in the TGA thermograms curve of the copper tyrosine-alanine dipeptide substituted phthalocyanine complex **(9f)** that the compound is thermally stable up to 180 °C with 3% weight loss. This weight loss is thought to be due to the moisture absorbed and lost at the bagging of heating of the complex **(9f)**. The complex undergoes three stages of degradation with a weight loss of 5% recorded between 180 °C - 220 °C in the first stage of degradation followed by a weight reduction of 59 % occurs between 220 -501 °C in the second stage of degradation. The last degradation stage occurs between 501 – 660 °C with a weight loss of 6 % and a leftover of 27 % remaining material left as residue as seen in the TGA thermogram curve in **Appendix 15.6.** It is indicated from the DTA curves of the complex that the compound decomposes without melting. Therefore, under normal conditions complex (**9f**) does not have a melting point and all their stages of degradation follow exothermic decomposition.

d) Electrochemistry analysis of complex (9f) compound

The electrochemical analysis of copper tyrosine-alanine dipeptide substituted phthalocyanine complex **(9f)** compound was performed by both Cyclic and square wave voltammetry. A glassy carbon electrode is used as the working electrode while platinum Pt as a counter electrode, tetrabutylammonium tetrafluoroborate as the electrolyte, and ferrocene /ferrocenium (Fc/Fc^{+}) as a pseudo-reference electrode in DMF. A wide potential range (-2.5 to +1.5 V versus Fc/Fc^{+}) was employed to explore the phthalocyanine complexes' electrochemical characteristics. The complex **(9f)** possesses a redox-active copper metal center that undergoes two oxidation potentials of $\mathbf{O_1}$ 0.43 volt and $\mathbf{O_2}$ 0.86 volt from the electronic transition oxidation reaction of $\mathbf{[Pc^{(-2)}\,Cu^{(2)}]^{0}}$ / $\mathbf{[Pc^{(-1)}\,Cu^{(2)}]^{+1}}$ and $\mathbf{[Pc^{(-1)}\,Cu^{(2)}]^{+}}$ / $\mathbf{[Pc^{(0)}\,Cu^{(2)}]^{+2}}$ respectively and four reductions potentials as $\mathbf{R_4}$ -2.36 volt**,** $\mathbf{R_3}$ -2.05 volt, $\mathbf{R_2}$ -1.72 volt, and $\mathbf{R_1}$ -0.84 volt involves redox electrons transfer as $\mathbf{[Pc^{(-5)}\,Cu^{(2)}]^{-3}}$ / $\mathbf{[Pc^{(-6)}\,Cu^{(2)}]^{-4}}$, $\mathbf{[Pc^{(-4)}\,Cu^{(2)}]^{-2}}$ / $\mathbf{[Pc^{(-5)}\,Cu^{(2)}]^{-3}}$, $\mathbf{[Pc^{(-3)}\,Cu^{(2)}]^{-1}}$ / $\mathbf{[Pc^{(-4)}\,Cu^{(2)}]^{-2}}$, and $\mathbf{[Pc^{(-2)}\,Cu^{(2)}]^{0}}$ / $\mathbf{[Pc^{(-3)}\,Cu^{(2)}]^{-1}}$ respectively for the reduction reaction of the conjugated Pc macrocycle ring formed cation and anionic radicals.

The redox activity is directly connected with oxidation by removing electrons from the highest occupied molecular orbital (HOMO) and adding electrons to the lowest unoccupied molecular orbital (LUMO) of phthalocyanines macrocyclic. The voltammograms of square wave

and cyclic voltammograms of complex**(9f)** compound are both reported in **Appendix 19.6a** and **19.6b** respectively.

4.3.2.7. Characterisation of ZnPc (9g) Complex

Characterization of phthalocyanine complex were performed by FT-IR spectra, UV-Visible spectra, thermal analysis (TGA and DTA) and electrochemistry techniques (CV and SWV)

a) FT-IR spectrum of complex (9g) compound

The FT-IR spectrum of zinc tyrosine- alanine dipeptide substituted phthalocyanine complex **(9g)** shown in the **Appendix 3.8** shows the absence of weak sharp nitrile C≡N peaks at 2232 cm^{-1} which affirmed the occurrence of cyclotetramerization of the compound **(9)** in the formation of the complex compound **(9g)**. The most important peaks that occurred in the spectrum are a medium broad stretching peaks of N-H bonds (Aliphatic amide) at 3269 cm^{-1}, a medium broad stretching peaks of C-H bond (methyl group) between 2973 cm^{-1}-2866 cm^{-1}, a medium broad peak of carbonyl carbon 1711 cm^{-1} (ester C=O), a medium broad bending vibration signal of N-H (Amide) at 1650 cm^{-1} and 1650 cm^{-1}, a medium stretching peak of C=C (in-ring) aromatic at 1506 cm^{-1}, a medium stretching peak of C-C (in-ring) aromatic at 1475 cm^{-1} and 1447 cm^{-1}, a medium broad bending vibration of C-H bond (methyl of protection group) at 1393 cm^{-1}, a medium broad rocking vibration of C-H bond (methyl of protection group) at 1363 cm^{-1}, a strong broad peak signal of C-O-C (ether) at 1229 cm^{-1}, a strong broad peak signal of C-O (ester) at 1163 cm^{-1} and a medium broad stretching peak of C-N bond (aliphatic amines) at 1089 cm^{-1} and 1046 cm^{-1}.

b) UV-visible spectrum of complex (9g) compound

The UV-visible spectrum of zinc tyrosine-alanine dipeptide substituted phthalocyanine complex **(9g)** dissolved in DMF is shown in **Appendix-11.7.** The spectrum recorded a single Q-band signal at 660 nm and a B-band at 425 nm. A small shoulder was observed at 610 nm which is due to aggregation.

c) Thermal analysis of complex (9g) compound

The TGA thermograms curve observed in **Appendix-15.7** showed that the zinc tyrosine-alanine dipeptide substituted phthalocyanine complex **(9g)** is thermally stable up to 190 °C with only 5 % weight loss associated with moisture loss by the complex. The complex undergoes two stages of degradation with a weight loss of 10 % reported between 190 - 240 °C in the first stage of degradation followed by a weight reduction of 68 % occurring between 240 -525 °C in the second stage of degradation. A leftover of 17 % remaining material was recorded as residue as seen in the TGA thermogram curve. It is indicated from the DTA curves of the complex that the compound

decomposes without melting. Therefore, under normal conditions complex (**9d**) does not have a melting point and all their stages of degradation follow exothermic decomposition.

d) Electrochemistry analysis of complex (9g) compound

The electrochemical analysis of zinc tyrosine- alanine dipeptide substituted phthalocyanine complex **(9g)** compound was performed by both Cyclic and square wave voltammetry similar to those performed for the above complexes. The complex **(9g)** possesses a redox-inactive zinc metal center that undergoes Pc ring base electronic redox reactıon. The complex observed two oxidation potentials at $\mathbf{O_1}$ 0.29 volt and $\mathbf{O_2}$ 0.80 volt from the redox reactions of $\mathbf{[Pc^{(-2)}\,Zn^{(2)}]^{0}}$ / $\mathbf{[Pc^{(-1)}\,Zn^{(2)}]^{+1}}$ and $\mathbf{[Pc^{(-1)}\,Zn^{(2)}]^{+1}}$ / $\mathbf{[Pc^{(0)}\,Zn^{(2)}]^{+2}}$respectively and the four reductions reaction potentials of $\mathbf{R_4}$ -2.48 volt, $\mathbf{R_3}$ -2.15 volt, $\mathbf{R_2}$ -2.00 volt, and $\mathbf{R_1}$ -1.29 volt involves electrons transfer redox reaction as $\mathbf{[Pc^{(-5)}\,Zn^{(2)}]^{-3}}$ / $\mathbf{[Pc^{(-6)}\,Zn^{(2)}]^{-4}}$, $\mathbf{[Pc^{(-4)}\,Zn^{(2)}]^{-2}}$ / $\mathbf{[Pc^{(-5)}\,Zn^{(2)}]^{-3}}$, $\mathbf{[Pc^{(-3)}\,Zn^{(2)}]^{-1}}$ / $\mathbf{[Pc^{(-4)}\,Zn^{(2)}]^{-2}}$, and $\mathbf{[Pc^{(-2)}\,Zn^{(2)}]^{0}}$ / $\mathbf{[Pc^{(-3)}\,Zn^{(2)}]^{-1}}$ respectively from the conjugated Pc macrocycle ring formed cation and anion radicals. The redox activity is directly connected with oxidation by removing electrons from the highest occupied molecular orbital (HOMO) and adding electrons to the lowest unoccupied molecular orbital (LUMO) of phthalocyanines macrocyclic [94, 121, 122]. The voltammograms of square wave and cyclic voltammograms of complex **(9g)** compound are both indicated in **Appendix 19.7a** and **19.7b** respectively**.**

4.4. Characterisation of tyrosine- glycine dipeptide amino acids substituent and complexes

The dipeptide amino acid substituent methyl (tert-butoxycarbonyl)-*L*-tyrosyl glycinate **(Boc-Tyr-Gly-OCH_3) (10)** was characterized using FT-IR, ^{1}H-NMR, ^{13}C-NMR, mass spectroscopies, and elemental analysis while the ligand Methyl ((*S*)-2-((tert-butoxycarbonyl) amino)-3-(4-(3,4-dicyanophenoxy) phenyl) propanoyl) glycinate **(Boc-Tyr-Gly-OCH_3-O-PN) (11)** and complexes are characterized by FT-IR and UV-visible spectroscopies.

4.4.1. Characterisation of methyl (tert-butoxycarbonyl) -*L*-tyrosyl glycinate (Boc-Tyr-Gly-OCH_3) (10)

The FT-IR, ^{1}H-NMR, ^{13}C-NMR, and mass spectroscopies spectra of compound **(10)** are given in the **Appendix Section**. The carbons and hydrogens in compound **(10)** are numbered as in **Figure 4.8** below.

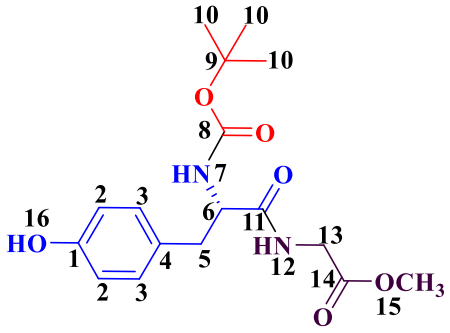

methyl (*tert*-butoxycarbonyl)-*L*-tyrosylglycinate

Boc-Tyr-Gly-OCH$_3$

Figure 4.8. Numbering of carbons and hydrogens in methyl (tert-butoxycarbonyl)-*L*-tyrosyl glycinate compound **(10)**

a) FT-IR spectrum of compound (10)

The FT-IR spectrum analysis of methyl (tert-butoxycarbonyl)-*L*-tyrosyl glycinate dipeptide indicated several significant peaks. Notably, medium broad stretching peaks for the N-H bond of the (amide group) were observed at 3366 cm^{-1} and 3333 cm^{-1}. A weak broad stretching peak for the O-H bond (aromatic) appeared at 2984 cm^{-1}, while a medium stretching peak for C-H bonds (aliphatic) was found at 2927 cm^{-1}. In addition, a strong broad stretching peak for the carbonyl C=O was detected at 1745 cm^{-1} (indicative of ester C=O) and 1689 cm^{-1} (secondary amide C=O). Other notable features included a medium sharp bending peak for the N-H bond (amide) at 1638 cm^{-1}, a medium broad bending peak for C-H bonds (methyl group) at 1440 cm^{-1}, and a medium broad bending vibration for O-H bonds (phenolic) at 1366 cm^{-1}.

Furthermore, there was a strong broad stretch for the C-O bond (C-O ether) at 1226 cm^{-1} and (C-O ester) at 1165 cm^{-1}. Lastly, the spectrum displayed medium broad stretching peaks for the C-N bond (amine) at 1048 cm^{-1} and 1027 cm^{-1}, as detailed in **Appendix 4.**

b) ^{1}H-NMR spectrum of compound (10)

The ^{1}H-NMR of methyl (*tert*-butoxycarbonyl)-*L*-tyrosyl glycinate dipeptide (10) taken in DMSO-d6, 298K**:** shown in **Appendix 8.1** revealed the presence of 1-proton singlet peak at 9.19 ppm belongs to proton H^{16} (-OH)**.** The triplet peaks signal of 1 proton observed at 8.38 ppm belongs to H^{12} (-NH)**.** The 2 protons produce double peak signals between 7.05 -7.07 ppm formed by H^{3} with coupling constant value of (distance between the two peaks) J= 8.4 Hz**.** The proton generated double peak signals between 6.89 - 6.91 ppm belong to H^{7} (-NH)**.** The double peak signals observed by 2 protons between 6.64 - 6.66 ppm occupy a distance of 8.8 Hz between the two peaks is belong to H^{2}**.** The quartet peak of 1-proton occurred between 4.09 and 4.12ppm belongs to proton H^{6}. The

multiple signals of 2- protons occurred between 3.85 - 3.90 ppm produced by proton H^{13}.The 2-protons split to produce double doublet peak signals between 2.61 -2.64 ppm and 2.85 -2.90 ppm belonging to proton H^5, the 9-protons given a singlet intense peak signal at 1.31 ppm belong to proton H^{10} and lastly, a peak at 3.36 ppm belongs to DMSO-d6 water and the peak at 2.51 ppm belongs to DMSO-d6.

c) ^{13}C-NMR spectrum of compound (10)

The ^{13}C-NMR spectrum of methyl (*tert*-butoxycarbonyl)-*L*-tyrosyl glycinate dipeptide **(10)** taken in DMSO-d6, 298K is shown in **Appendix 8.2.** The peak C^1 at 155.70 ppm is an aromatic carbon that is attached to the phenol functional group. The peak C^2 at 115.25 ppm is an aromatic carbon, the peak C^3at 130.57 ppm**,** 128.63 C^4, 037.06 C^6, 056.17 C^7, 156.19 C^9, 078.40 C^{10}, 028.63 C^{11}, 172.33 C^{12}, 047.99 C^{14}, 173.47 C^{15}.

d) Mass spectrum of compound (10)

The theoretically calculated molecular weight of the Boc-Tyr-Gly-OCH_3 compound is 352.39 g/mol. In the MALDI-TOF MS spectrum of compound (10) given in **Appendix 8.3**, the peak 352.306 [M] belongs to the compound. Above this, 374.373 [M+Na], 390.429 [M+K]. The peaks observed at the bottom of this peak indicate the compound resulting from the groups leaving the structure. According to calculations, the peak at 296.134 [M-$C(CH_3)_3$] corresponds to the breakage of the -$C(CH_3)_3$ group in the Boc protecting group.

4.4.2. Characterisation of methyl ((*S*)-2-((tert-butoxycarbonyl) amino)-3-(4-(3,4-dicyanophenoxy) phenyl) propanoyl) glycinate (Boc-Tyr-Gly-OCH_3-O-PN) (11)

The characterization of **(Boc-Tyr-Gly-OCH_3-O-PN) (11)** shown in **Figure 4.9** below was done by FT-IR, ^{1}H-NMR, and ^{13}C-NMR spectroscopies.

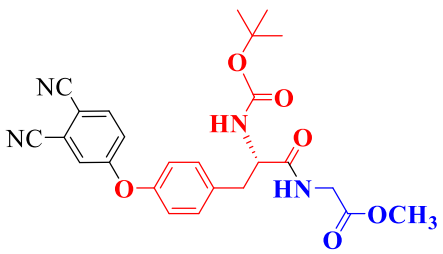

Figure 4.9. Methyl ((S)-2-((tert-butoxycarbonyl) amino)-3-(4-(3,4-dicyanophenoxy) phenyl) propanoyl) glycinate **(Boc-Tyr-Gly-OCH_3-O-PN) (11)**

a) FT-IR spectrum of compound (11)

The FT-IR (ATR, cm^{-1}) spectrum of methyl ((*S*)-2-((tert-butoxycarbonyl) amino)-3-(4-(3,4-dicyanophenoxy) phenyl) propanoyl) glycinate compound **(11)** obtained shown in **Appendix 4.1** demonstrated the presence of a weak sharp stretching peak signal of nitrile **C≡N** at 2233 cm^{-1} as one of the most important signals in the ligand compound**.** Some of the other important peaks in the spectrum are a medium broad stretching of N-H bond (amine) at 3331 cm^{-1}, and a -CH aliphatic bond signal presence at 2985 cm^{-1}**.** A presence of a strong broad stretching peak signal of the C=O (aliphatic ester) bond at 1711 cm^{-1}, a strong broad stretching peak signal of the C=O (secondary amide) bond at 1660 cm^{-1}, a medium stretching peak(in-ring) of C=C bond (Aromatics) at 1597 cm^{-1}, a medium broad stretching peak of C-C aromatic (in-ring) at 1486 cm^{-1}, a medium broad bending signal of C-H bond (methyl group) at 1438cm^{-1}, a medium broad rocking signal of C-H bond (methyl group) at 1368cm^{-1}**,** a strong broad peak at 1250 cm^{-1} is belong to C-O-C (ether), a medium broad stretching peak signal of C-N bond (aliphatic amines) at 1169 cm^{-1}.

4.4.2.1. Characterisation of CrPc (11a) Complex

Characterization of phthalocyanine complex were performed by FT-IR spectra, UV-Visible spectra, thermal analysis (TGA and DTA) and electrochemistry techniques (CV and SWV)

a) FT-IR spectrum of complex (11a) compound

The FT-IR spectrum of chromium tyrosine- glycine dipeptide substituted phthalocyanine complex **(11a)** shown in **Appendix 4.2** reported the absence of weak sharp nitrile C≡N peaks at 2232 cm^{-1} which indicated the occurrence of cyclotetramerization of the compound (11) in the formation of the complex compound (11a)**.** Furthermore, some of the most important peaks present are a medium broad stretching peaks of N-H bonds (Aliphatic amide) at 3260 cm^{-1}, a medium broad stretching peaks of C-H bond (methyl group) between 2934-2868 cm^{-1}, weak broad bend vibration peak of C-H (Aromatic) overtone at 1768 cm^{-1}**,** strong peaks of carbonyl carbon C=O at 1711 cm^{-1} (ester C=O) and 1657 cm^{-1} for (amide C=O)**,** a medium stretching peak(in-ring) of C=C bond (Aromatics) at 1593 cm^{-1}, a medium broad bending vibration of C-H bond (methyl of protection group) at 1386 cm^{-1}, a strong broad peak signal of C-O-C (ether) at 1232 cm^{-1} and a medium broad stretching peak of C-N bond (aliphatic amines) at 1069 cm^{-1}.

b) UV-visible spectrum of complex (11a) compound

The UV-visible spectrum of chromium tyrosine-glycine dipeptide substituted phthalocyanine complex (11a) dissolved in DMF is shown in **Appendix 12.1** reported the presence of a single Q-band spectrum at 680 nm and B-band at 375 nm. There is an appearance of a pronoun broad shoulder at 612 nm due to aggregation.

c) Thermal analysis of complex (11a) compound

TGA thermogram curve of the chromium tyrosine- glycine dipeptide substituted phthalocyanine complex **(11a)** compound as shown in **Appendix 16.1** presented the complex is thermally stable up to 200 ^{0}C with weight loss of 4 % against the temperature due to the loss of moisture trapped in the complex. The first degradation was observed between 200 - 295 °C with a weight loss of 9 %. The second stage of degradation is recorded between 295 and 500 °C with a weight loss of 71 %. The third stage of degradation occurred between 500 - 600 °C and accounted for a weight loss of only 3 % and leftover 13 % as residue provably of the metal oxide Cr_2O_3. Furthermore, the DTA thermogram curve revealed that the complex decomposes without melting and this implies that under normal conditions, the complex does not possess melting point and undergo decomposition exothermically.

d) Electrochemistry analysis of complex (11a) compound

The electrochemical analysis of chromium tyrosine- glycine dipeptide substituted phthalocyanine complex **(11a)** compound was performed by both cyclic and square wave voltammetry. A glassy carbon electrode is used as the working electrode while platinum Pt as a counter electrode, tetrabutylammonium tetrafluoroborate as the electrolyte, and ferrocene /ferrocenium (Fc/Fc^+) as a pseudo-reference electrode in DMF. A wide potential range (-2.5 to +1.5 V versus Fc/Fc^+) was employed to explore the phthalocyanine complexes' electrochemical characteristics [119, [120]. The complex **(11a)** possesses a redox-active metal (chromium) center observed two oxidation potentials of $\mathbf{O_1}$ 0.54 volt and $\mathbf{O_2}$ 0.85 volt from the redox reactions of **[Pc$^{(-2)}$ Cr$^{(2)}$]^0 / [Pc$^{(-1)}$Cr $^{(3)}$]$^{+2}$**and **[Pc $^{(-1)}$ Cr $^{(2)}$]$^+$ / [Pc $^{(0)}$ Cr $^{(3)}$]$^{+3}$** respectively forming cationic radicals and four reduction reactions observed with potential values of $\mathbf{R_4}$ -2.40 volt, $\mathbf{R_3}$ -2.10 volt, $\mathbf{R_2}$ -1.51 volt, and $\mathbf{R_1}$ -1.23volt obtained generated from redox reactions of **[Pc $^{(-5)}$ Cr $^{(2)}$]$^{-3}$ / [Pc $^{(-6)}$ Cr $^{(2)}$]$^{-4}$**, **[Pc $^{(-4)}$ Cr $^{(2)}$]$^{-2}$ / [Pc $^{(-5)}$ Cr $^{(2)}$]$^{-3}$**, **[Pc $^{(-3)}$ Cr $^{(2)}$]$^{-1}$ / [Pc $^{(-4)}$ Cr $^{(2)}$]$^{-2}$**, and **[Pc $^{(-2)}$ Cr $^{(2)}$]^0 / [Pc $^{(-3)}$ Cr $^{(2)}$]$^{-1}$** respectively forming anionic radicals from the redox reaction of the conjugated macrocycle Pc ring**.** The metal center redox reaction produced a metal reduction potential of $\mathbf{M_R}$ -1.12 volt and a metal oxidation potential value of $\mathbf{M_O}$ -0.23 volt from the redox reaction of **[Pc $^{(-2)}$ Cr $^{(2)}$]^0 / [Pc $^{(-2)}$ Cr $^{(1)}$]$^{-1}$** and **[Pc $^{(-2)}$ Cr $^{(2)}$]^0 / [Pc $^{(-2)}$ Cr $^{(3)}$] $^{+1}$** respectively forming anion and cation radicals. The result observed for metal base reduction $\mathbf{M_R}$ is similar to the value obtained from metal base reduction of **SI-L1 CrPc** complex.

The redox activity is directly connected with oxidation by removing electrons from the highest occupied molecular orbital (HOMO) and adding electrons to the lowest unoccupied molecular orbital (LUMO) of phthalocyanines macrocyclic. The voltammograms of square wave

and cyclic voltammograms of complex **(11a)** compound are both shown in **Appendix 20.1a** and **20.1b** respectively.

4.4.2.2. Characterization of MnPc (11b) Complex

Characterization of phthalocyanine complex were performed by FT-IR spectra, UV-Visible spectra, thermal analysis (TGA and DTA) and electrochemistry techniques (CV and SWV)

a) FT-IR spectrum of complex (11b) compound

FT-IR spectrum of manganese tyrosine- glycine dipeptide substituted phthalocyanine complex **(11b)** shown in **Appendix 4.3** reported the absence of a weak sharp nitrile C≡N bond peak signal at 2232 cm^{-1} which confirmed the formation of the complex through cyclotetramerization reaction of the compound **(11)**. Conversely, other most important peaks present in the spectrum are a medium broad stretching peaks of N-H bonds (Aliphatic amide) at 3261 cm^{-1}, a weak broad bend vibration peak of C-H (Aromatic) overtone at 1766 cm^{-1}, a medium peak of carbonyl carbon C=O at 1708 cm^{-1} (ester C=O) and at 1662 cm^{-1} for (amide C=O), a medium stretching peak(in-ring) of C=C bond (Aromatics) at 1595 cm^{-1}, a medium broad bending vibration of C-H bond (methyl of protection group) at 1389 cm^{-1}, a strong broad peak signal of C-O-C (ether) at 1233 cm^{-1} and a medium broad stretching peak of C-N bond (aliphatic amines) at 1163 cm^{-1} and 1075 cm^{-1}.

b) UV-visible spectrum of complex (11b) compound

Appendix 12.2 shows the UV-visible spectrum of a manganese tyrosine-glycine dipeptide substituted phthalocyanine complex (11b) dissolved in DMF. In the spectrum, a single Q-band is seen at 720 nm and a B-band at 412 nm. The broad shoulder at 670 nm is due to aggregation.

c) Thermal analysis of complex (11b) compound

It was observed from the TGA thermograms curve of the manganese tyrosine- glycine dipeptide substituted phthalocyanine complex **(11b)** that is thermally stable up to 160 ^{0}C with weight loss of 5 % which probably accounted for loss of moisture absorbed by the complex. The complex undergoes two stages of degradation. The first degradation indicated from the TGA thermogram curve of the complex is recorded between 160 - 520 °C with a weight loss of 63 %. The second degradation stage is recorded between 520 - 670 °C with a weight loss of 8 % and leftover of 24 % as residue as shown in **Appendix 16.2.** The DTA thermogram curves of the complex show that the degradation processes proceed exothermically and the complex decomposes without melting under normal conditions.

d) Electrochemistry analysis of complex (11b) compound

The electrochemical analysis of manganese tyrosine-glycine dipeptide substituted phthalocyanine complex **(11b)** compound was performed by both Cyclic and square wave voltammetry. A glassy carbon electrode is used as the working electrode while platinum Pt as a counter electrode, tetrabutylammonium tetrafluoroborate as the electrolyte, and ferrocene /ferrocenium (Fc/Fc^{+}) as a pseudo-reference electrode in DMF. A wide potential range (-2.5 to +1.5 V versus Fc/Fc^{+}) was employed to explore the phthalocyanine complexes' electrochemical characteristics [119, [120]. Manganese is known for its versatile role in redox reactions due to its multiple oxidation states. The complex **(11b)** possesses a redox-active manganese metal center that observed two Pc ring base oxidation potentials of $\mathbf{O_1}$ 0.46 volt and $\mathbf{O_2}$ 0.82 volt which obtained from redox reaction of **[Pc $^{(-2)}$ Mn $^{(2)}$]^{0} / [Pc $^{(-1)}$ Mn $^{(3)}$] $^{+2}$**and **[Pc $^{(-1)}$ Mn $^{(2)}$] $^{+}$ / [Pc $^{(0)}$ Mn $^{(3)}$] $^{+3}$** respectively for the formation of cation radicals. Alongside four reduction reactions were observed by the complex with potential values of $\mathbf{R_4}$ -2.39 volt, $\mathbf{R_3}$ -2.08 volt, $\mathbf{R_2}$ -1.65 volt, and $\mathbf{R_1}$ -1.27 volt produced from **[Pc $^{(-5)}$ Mn $^{(2)}$]$^{-3}$ / [Pc $^{(-6)}$ Mn $^{(2)}$]$^{-4}$, [Pc $^{(-4)}$ Mn $^{(2)}$]$^{-2}$ / [Pc $^{(-5)}$ Mn $^{(2)}$]$^{-3}$**, **[Pc $^{(-3)}$ Mn $^{(2)}$]$^{-1}$ / [Pc $^{(-4)}$ Mn $^{(2)}$]$^{-2}$**, and **[Pc $^{(-2)}$ Mn $^{(2)}$]^{0} / [Pc $^{(-3)}$ Mn $^{(2)}$]$^{-1}$** respectively obtain from Pc ring redox reactions. The Pc undergoes a metal base redox oxidation reaction to produce a positive potential value of $\mathbf{M_O}$ 0.25 from electronic transition of **[Pc $^{(-2)}$ Mn $^{(2)}$]^{0} / [Pc $^{(-2)}$ Mn $^{(3)}$] $^{+1}$** [126]. The voltammograms of square wave and cyclic voltammograms of complex **(11b)** compound are both shown in **Appendix 20.2a** and **20.2b** respectively.

4.4.2.3. Characterisation of FePc (11c) Complex

Characterization of phthalocyanine complex were performed by FT-IR spectra, UV-Visible spectra, thermal analysis (TGA and DTA) and electrochemistry techniques (CV and SWV)

a) FT-IR spectrum of complex (11c) compound

The FT-IR spectrum of iron tyrosine- glycine dipeptide substituted phthalocyanine complex **(11c)** shown in the **Appendix 4.4** revealed the absence of weak sharp nitrile C≡N peaks at 2232 cm^{-1} which confirmed the occurrence of cyclotetramerization of the compound **(11)** in the formation of the complex compound **(11c)**. Some of the most important peaks that occurred in the spectrum are the presence of a medium broad stretching peak of N-H bonds (Aliphatic amide) at 3260 cm^{-1}, a medium broad stretching peaks of C-H bond (methyl group) between 2941-2871 cm^{-1}**,** a weak broad bend vibration peak of C-H (Aromatic) overtone at 1768 cm^{-1}, a medium broad peak of carbonyl carbon C=O at 1710 cm^{-1} (ester C=O) and at 1658 cm^{-1} for (amide C=O), a medium stretching peak(in-ring) of C=C bond (Aromatics) at 1597 cm^{-1}, a medium broad bending vibration of C-H bond (methyl of protection group) at1431 cm^{-1} and 1381 cm^{-1}, a strong broad peak signal

of C-O-C (ether) at 1232 cm^{-1} and a medium broad stretching peak of C-N bond (aliphatic amines) at 1163 cm^{-1}.

b) UV-visible spectrum of complex (11c) compound

Appendix-12.3 show the UV-visible spectrum of iron tyrosine-glycine dipeptide substituted phthalocyanine complex (11c) dissolved in DMF. The spectrum indicated a single Q-band at 668 nm and a B-band at 420 nm. Due to aggregation, a sharp shoulder is observed at 605 nm.

c) Thermal analysis of complex (11c) compound

The TGA thermogram curve of the iron tyrosine-glycine dipeptide substituted phthalocyanine complex **(11c)** indicates the compound is thermally stable up to 160 °C with 5% weight loss due to loss of moisture trapped in the complex. The complex undergoes two stages of degradation, the first stage is recorded between 160- 420 °C with 40 % weight loss, while the second stage of degradation occurs between 420-640 °C with 42 % weight loss. A weight of 13 % remained as non-decomposition leftover residue which may probably be the metallic oxide FeO of the complex as seen in the TGA thermogram curve in **Appendix 16.3**. It is also indicated from the DTA curves of the complex that the compound decomposes exothermically without melting under normal conditions.

d) Electrochemistry analysis of complex (11c) compound

The electrochemical properties of iron tyrosine-glycine dipeptide substituted phthalocyanine complex **(11c)** were examined using cyclic and square wave voltammetry techniques. Similar to previous analyses, a glassy carbon electrode served as the working electrode while platinum was used as a counter electrode. The electrolyte comprised tetrabutylammonium tetrafluoroborate with ferrocene/ferrocenium (Fc/Fc^{+}) as a pseudo-reference electrode in DMF. The investigations were conducted over a potential range of -2.5 to +1.5 V versus Fc/Fc^{+}. The complex **(11c)** exhibited two Pc ring base oxidation processes potential values at 0.47 volt and 0.82 volt for $\mathbf{O_1}$ and $\mathbf{O_2}$ respectively which was obtained from redox reactions of $\mathbf{Pc^{(-2)}Fe^{(2)}}$ / $\mathbf{[Pc^{(-1)}Fe^{(3)}]^{+2}}$and $\mathbf{[Pc^{(-1)}Fe^{(2)}]^{+1}}$ / $\mathbf{[Pc^{(0)}Fe^{(3)}]^{+3}}$ for the formation of cationic radicals. The complex also generates four reduction processes with potential values of $\mathbf{R_4}$ at -2.42 volt, $\mathbf{R_3}$ at -2.16 volt, $\mathbf{R_2}$ at -1.93 volt, $\mathbf{R_1}$ at -1.30 volt from redox reaction of $\mathbf{[Pc^{(-5)}Fe^{(2)}]^{-3}}$ / $\mathbf{[Pc^{(-6)}Fe^{(2)}]^{-4}}$, $\mathbf{[Pc^{(-4)}Fe^{(2)}]^{-2}}$ / $\mathbf{[Pc^{(-5)}Fe^{(2)}]^{-3}}$, $\mathbf{[Pc^{(-3)}Fe^{(2)}]^{-1}}$ / $\mathbf{[Pc^{(-4)}Fe^{(2)}]^{-2}}$, and $\mathbf{[Pc^{(-2)}Fe^{(2)}]^{0}}$ / $\mathbf{[Pc^{(-3)}Fe^{(2)}]^{-1}}$ respectively for the formation of anionic radicals. Iron metal is a redox-active metal that undergoes a redox reaction to produce a metal center reduction potential value $\mathbf{M_R}$ -1.81 volt and oxidation potential value of $\mathbf{M_O}$ 0.38 volts involving electron transfer associated with the formation of anionic radical $\mathbf{[Pc^{(-2)}Fe^{(2)}]^{0}}$ / $\mathbf{[Pc^{(-2)}Fe^{(1)}]^{-1}}$ and $\mathbf{[Pc^{(-2)}Fe^{(2)}]^{0}}$ / $\mathbf{[Pc^{(-2)}Fe^{(3)}]^{+1}}$ respectively

The redox activity is connected to the transfer of electrons from the highest occupied molecular orbital (HOMO) and the lowest unoccupied molecular orbital (LUMO) of the phthalocyanine macrocycle. The voltammograms for the square wave and cyclic voltammetry of complex **(c)** can be found in **Appendix 20.3a** and **20.3b**, respectively.

4.4.2.4. Characterisation of CoPc (11d) Complex

Characterization of phthalocyanine complex were performed by FT-IR spectra, UV-Visible spectra, thermal analysis (TGA and DTA) and electrochemistry techniques (CV and SWV)

a) FT-IR spectrum of complex (11d) compound

The FT-IR spectrum of cobalt tyrosine- glycine dipeptide substituted phthalocyanine complex **(11d)** shown in **Appendix 4.5** observed the absence of a weak sharp nitrile C≡N peaks at 2232 cm^{-1} which confirmed the cyclotetramerization of the compound **(11)** in the formation of the complex **(11d)** compound. Some of the most important peaks that appeared in the spectrum are the presence of a medium broad stretching peak of N-H bonds (Aliphatic amide) at 3312 cm^{-1}, a weak broad bend vibration peak of C-H (Aromatic) overtone at 1769 cm^{-1}, a strong broad stretching carbonyl bond C=O at 1711 cm^{-1} and 1657 cm^{-1} (ester C=O), a medium stretching peak(in-ring) of C=C bond (Aromatics) at 1597 cm^{-1}, a medium stretching peak of C-C bond (Aromatic) at 1506 cm^{-1}, a medium broad bending vibration of C-H bond (methyl of protection groups) at 1473 cm^{-1} and 1390 cm^{-1}, a strong broad stretching peak of C-O-C bond at 1232 cm^{-1}, a medium broad stretching peak of C-N bond (aliphatic amines) at 1162 cm^{-1}, 1096 cm^{-1} and 1057 cm^{-1}.

b) UV-visible spectrum of complex (11d) compound

The UV-visible spectrum of cobalt tyrosine- glycine dipeptide substituted phthalocyanine complex **(11d)** dissolved in DMF as solvent shown in **Appendix 12.4** indicated the occurrence of a single Q-band spectrum seen at 670nm and B-band at 387 nm. A small shoulder was reported at 606 nm due to aggregation.

c) Thermal analysis of complex (11d) compound

TGA thermogram curve of the cobalt tyrosine- glycine dipeptide substituted phthalocyanine complex **(11d)** compound as shown in **Appendix 16.4** presented the complex is thermally stable up to 175 °C with weight loss of 3% against the temperature due to the loss of moisture trapped in the complex. The first degradation was observed between 175 - 220 °C with a weight loss of 12 %. The second stage of degradation is recorded between 220 and 475 °C with a weight loss of 20%. The third stage of degradation occurred between 475 - 650 °C, accounting for a weight loss of only 33 %. while the fourth stage of degradation was observed between 650 - and 800 °C reporting a weight loss of only 2 % and leftover 30 % as residue. Furthermore, the DTA thermogram curve

revealed that the complex decomposes without melting and this implies that under normal conditions, the complex does not possess melting point and undergo decomposition exothermically.

d) Electrochemistry analysis of complex (11d) compound

The electrochemical properties of cobalt tyrosine-glycine dipeptide substituted phthalocyanine complex **(11d)** were examined using cyclic and square wave voltammetry techniques. Similar to previous analyses, a glassy carbon electrode served as the working electrode while platinum was used as a counter electrode. The electrolyte comprised tetrabutylammonium tetrafluoroborate with ferrocene/ferrocenium (Fc/Fc^{+}) as a pseudo-reference electrode in DMF. The investigations were conducted over a potential range of -2.5 to +1.5 V versus Fc/Fc^{+}. The complex **(11d)** exhibited two oxidation reactions potential $\mathbf{O_1}$ at 0.43volt and $\mathbf{O_2}$ at 0.78 volt which were obtained from redox reactions of **Pc $^{(-2)}$ Co $^{(2)}$ / [Pc $^{(-1)}$ Co $^{(3)}$] $^{+2}$**and **[Pc $^{(-1)}$ Co $^{(2)}$] $^{+}$ / [Pc $^{(0)}$ Co $^{(3)}$] $^{+3}$** respectively for the formation of cationic radicals. Four reduction processes were recorded as ($\mathbf{R_4}$ at -2.44 volt, $\mathbf{R_3}$ at -2.12 volt, $\mathbf{R_2}$ at -1.49 volt, $\mathbf{R_1}$ at -1.12 volt) result from redox reactions of **[Pc $^{(-5)}$ Co $^{(2)}$]$^{-3}$ / [Pc $^{(-6)}$ Co $^{(2)}$]$^{-4}$**, **[Pc $^{(-4)}$ Co $^{(2)}$]$^{-2}$ / [Pc $^{(-5)}$ Co $^{(2)}$]$^{-3}$**, **[Pc $^{(-3)}$ Co $^{(2)}$]$^{-1}$ / [Pc $^{(-4)}$ Co $^{(2)}$]$^{-2}$**, and **[Pc $^{(-2)}$ Co $^{(2)}$]^{0} / [Pc $^{(-3)}$ Co $^{(2)}$]$^{-1}$** respectively for the formation of anion radicals generated from Pc ring redox reaction. CoPc complex possesses a redox-active metal center that exhibits redox reaction $\mathbf{M_R}$ -0.88 volt involves **[Pc $^{(-2)}$ Co $^{(2)}$]^{0} / [Pc $^{(-2)}$ Co $^{(1)}$]$^{-1}$** electronic transfer for metal base reduction $\mathbf{M_R}$ to formed anion and $\mathbf{M_O}$ 0.14 volt metal base oxidation involves as **[Pc $^{(-2)}$ Co $^{(2)}$]^{0} / [Pc $^{(-2)}$ Co $^{(3)}$] $^{+1}$** to formed cation radical. The voltammograms for the square wave and cyclic voltammetry of complex **(9d)** can be found in **Appendix 20.4a** and **20.4b** respectively.

4.4.2.5. Characterisation of NiPc (11e) Complex

Characterization of phthalocyanine complex were performed by FT-IR spectra, UV-Visible spectra, thermal analysis (TGA and DTA) and electrochemistry techniques (CV and SWV)

a) FT-IR spectrum of complex (11e) compound

The FT-IR spectrum of nickel tyrosine- glycine dipeptide substituted phthalocyanine complex **(11e)** shown in the **Appendix 4.6** revealed the absence of weak sharp nitrile C≡N peaks at 2232 cm^{-1} which confirmed the occurrence of cyclotetramerization of compound **(11)** in the formation of the complex **(11e)** compound. Among the most important peaks appeared in the spectrum are the presence of a medium broad stretching peak of N-H bonds (Aliphatic amide) at 3226 cm^{-1}, a weak broad bend vibration peak of C-H (Aromatic) overtone at 1768 cm^{-1}, a strong broad stretching carbonyl bond C=O at 1705 cm^{-1} (ester C=O) and 1661 cm^{-1}(amide C=O), a medium broad stretching peak of C=C bond (Aromatic) at 1602 cm^{-1}, a medium stretching peak (in-ring) of C=C bond (Aromatics) at 1597 cm^{-1}, a medium stretching peak (in ring) of C-C bond (Aromatic) at 1505 cm^{-1}, a medium broad bending vibration of C-H bond (methyl of protection

groups) at 1381 cm^{-1}, a strong broad stretching peak of C-O-C bond (ethers) at 1229 cm^{-1}, and medium broad stretching peaks of C-N bond (aliphatic amines) at 1165cm^{-1} and 1067cm^{-1}.

b) UV-visible spectrum of complex (11e) compound

The UV-visible spectrum of nickel tyrosine- glycine dipeptide substituted phthalocyanine complex **(11e)** dissolved in DMF as solvent shown in **Appendix 12.5** reported the appearance of a single Q-band spectrum at 678 nm and B-band at 460 nm. There is also the presence of a small shoulder at 653 nm due to aggregation.

c) Thermal analysis of complex (11e) compound

The TGA thermograms curve of the nickel tyrosine- glycine dipeptide substituted phthalocyanine complex **(11e)** compound is thermally stable up to 170 °C with only 3% weight loss as a result of moisture loss trapped in the complex. The complex undergoes thermal decomposition between 170 and 540 °C with 32% weight loss as first-stage degradation. Then, a weight loss of 10 % occurred between 540 - 890 °C in the second stage of degradation, and a weight of 51 % was left as residue shown in **Appendix 16.5**. However, the DTA thermogram curve of the complex revealed the compound undergoes exothermic decomposition without melting under normal conditions.

d) Electrochemistry analysis of complex (11e) compound

The electrochemical analysis of nickel tyrosine-glycine dipeptide substituted phthalocyanine complex **(11e)** compound was performed by both Cyclic and square wave voltammetry. A glassy carbon electrode is used as the working electrode while platinum Pt as a counter electrode, tetrabutylammonium tetrafluoroborate as the electrolyte, and ferrocene /ferrocenium (Fc/Fc^{+}) as a pseudo-reference electrode in DMF. A wide potential range (-2.5 to +1.5 V versus Fc/Fc^{+}) was employed to explore the phthalocyanine complexes' electrochemical characteristics [119, [120]. The complex **(11e)** possesses a redox-inactive nickel metal center that undergoes only a Pc ring redox reaction. The complex observed two oxidations potential of $\mathbf{O_1}$ 0.41 volt from $\mathbf{[Pc^{(-2)}\,Ni^{(2)}]^{0}}$ / $\mathbf{[Pc^{(-1)}\,Ni^{(2)}]^{+1}}$ and $\mathbf{O_2}$ 0.71 volt from $\mathbf{[Pc^{(-1)}\,Ni^{(2)}]^{+1}}$ / $\mathbf{[Pc^{0}\,Ni^{(2)}]^{+2}}$ redox reactions obtained from Pc macrocycle ring forming cationic radicals. The complex also undergoes redox reaction to generates four reduction reaction potentials of $\mathbf{R_4}$ -2.40 volt, $\mathbf{R_3}$ -2.11 volt, $\mathbf{R_2}$ -1.71 volt, and $\mathbf{R_1}$ -1.30 volt obtained from redox reactions $\mathbf{[Pc^{(-5)}\,Ni^{(2)}]^{-3}}$ / $\mathbf{[Pc^{(-6)}\,Ni^{(2)}]^{-4}}$, $\mathbf{[Pc^{(-4)}\,Ni^{(2)}]^{-2}}$ / $\mathbf{[Pc^{(-5)}\,Ni^{(2)}]^{-3}}$, $\mathbf{[Pc^{(-3)}\,Ni^{(2)}]^{-1}}$ / $\mathbf{[Pc^{(-4)}\,Ni^{(2)}]^{-2}}$, and $\mathbf{[Pc^{(-2)}\,Ni^{(2)}]^{0}}$ / $\mathbf{[Pc^{(-3)}\,Ni^{(2)}]^{-1}}$ respectively generated from conjugated Pc macrocycle ring forming anionic radicals. The redox activity is directly connected with oxidation by removing electrons from the highest occupied molecular orbital (HOMO) and adding electrons to the lowest unoccupied molecular orbital (LUMO) of phthalocyanines

macrocyclic [94, 121, 122]. The voltammograms of square wave and cyclic voltammograms of complex **(11e)** compound are both indicated in **Appendix 20.5a** and **20.5b** respectively.

4.4.2.6. Characterisation of CuPc (11f) Complex

Characterization of phthalocyanine complex were performed by FT-IR spectra, UV-Visible spectra, thermal analysis (TGA and DTA) and electrochemistry techniques (CV and SWV)

a) FT-IR spectrum of complex (11f) compound

The FT-IR spectrum of copper tyrosine- glycine dipeptide substituted phthalocyanine complex **(11f)** shown in the **Appendix 4.7** indicated the absence of weak sharp nitrile C≡N peaks at 2232 cm^{-1} which justified the occurrence of cyclotetramerization of compound **(11)** in the formation of the complex **(11f)**. The most important peaks appeared in the spectrum are a medium broad stretching peaks of N-H bond (Aliphatic amide) at 3306 cm^{-1}, a medium broad stretching peaks of C-H bond (methyl group) between 2941 $cm^{-1}$and 2846 cm^{-1}, a weak broad bend vibration peak of C-H (Aromatic) overtone at 1766 cm^{-1}, a medium broad peak of carbonyl carbon bond (ester C=O) and (amide C=O) at 1704 cm^{-1} and 1658 cm^{-1}, a medium stretching peak (in-ring) of C=C bond (Aromatic) at 1593 cm^{-1}**,** a medium stretching peak signal (in-ring) of C-C bond (Aromatic) at 1506 cm^{-1}, a medium broad bending vibration of C-H bond (methyl of protection group) at 1436 cm^{-1} and 1380 cm^{-1}, a strong broad stretching peak of C-O-C bond (ethers) at 1231 cm^{-1} and a medium broad stretching peaks of C-N bond (aliphatic amines) at 1143 cm^{-1}, 1067 cm^{-1} and 1032 cm^{-1}.

b) UV-visible spectrum of complex (11f) compound

The UV-visible spectrum of copper tyrosine-glycine dipeptide substituted phthalocyanine complex **(11f)** dissolved in DMF is shown in **Appendix 12.6** The spectrum recorded a single Q-band signal at 675 nm.

c) Thermal analysis of complex (11f) compound

It is observed in the TGA thermograms curve of the copper tyrosine-glycine dipeptide substituted phthalocyanine complex **(11f)** that the compound is thermally stable up to 190 °C with 5% weight loss. The weight loss occurred due to the loss of moisture absorbed by the complex **(11f)**. The complex undergoes two stages of degradation with a weight loss of 60 % recorded between 190 - 520 °C as the first stage of degradation followed by a weight reduction of 3 % occurring between 520 - 630 °C in the second stage of degradation. A leftover of 32% was recorded as remaining material lifted as residue as seen in the TGA thermogram curve in **Appendix 16.6.** It is indicated from the DTA curves of the complex that the compound decomposes exothermically without melting. Therefore, under normal conditions complex (**11f**) does not have a melting point.

d) Electrochemistry analysis of complex (11f) compound

The electrochemical analysis of copper tyrosine-glycine dipeptide substituted phthalocyanine complex **(11f)** compound was performed by both cyclic and square wave voltammetry. A glassy carbon electrode is used as the working electrode while platinum Pt as a counter electrode, tetrabutylammonium tetrafluoroborate as the electrolyte, and ferrocene /ferrocenium (Fc/Fc^{+}) as a pseudo-reference electrode in DMF. A wide potential range (-2.5 to +1.5 V versus Fc/Fc^{+}) was employed to explore the phthalocyanine complexes' electrochemical characteristics. The complex **(11f)** possesses a redox-active copper metal center that undergoes two oxidations $\mathbf{O_1}$ 0.36 volt and $\mathbf{O_2}$ 0.96 volt from the Pc ring conjugate with the electrons transition of the oxidation reaction $\mathbf{[Pc^{(-2)}\,Cu^{(2)}]^{0}}$ / $\mathbf{[Pc^{(-1)}\,Cu^{(2)}]^{+1}}$ and $\mathbf{[Pc^{(-1)}\,Cu^{(2)}]^{+}}$ / $\mathbf{[Pc^{(0)}\,Cu^{(2)}]^{+2}}$ respectively forming cation and three reductions reaction potential values $\mathbf{R_3}$ -2.48 volt, $\mathbf{R_2}$ -2.07 volt, and $\mathbf{R_1}$ -1.31 volt involve electrons transition as $\mathbf{[Pc^{(-4)}\,Cu^{(2)}]^{-2}}$ / $\mathbf{[Pc^{(-5)}\,Cu^{(2)}]^{-3}}$, $\mathbf{[Pc^{(-3)}\,Cu^{(2)}]^{-1}}$ / $\mathbf{[Pc^{(-4)}\,Cu^{(2)}]^{-2}}$, and $\mathbf{[Pc^{(-2)}\,Cu^{(2)}]^{0}}$ / $\mathbf{[Pc^{(-3)}\,Cu^{(2)}]^{-1}}$ respectively for the reduction reaction of the conjugated Pc macrocycle ring forming anionic radical. The redox activity is directly connected with oxidation by removing electrons from the highest occupied molecular orbital (HOMO) and adding electrons to the lowest unoccupied molecular orbital (LUMO) of phthalocyanines macrocyclic. The voltammograms of square wave and cyclic voltammograms of complex**(11f)** compound are both reported in **Appendix 20.6a** and **20.6b** respectively.

4.4.2.7. Characterization of ZnPc (11g) Complex

Characterization of phthalocyanine complex were performed by FT-IR spectra, UV-Visible spectra, thermal analysis (TGA and DTA) and electrochemistry techniques (CV and SWV)

a) FT-IR spectrum of complex (11g) compound

The zinc tyrosine- glycine dipeptide substituted phthalocyanine complex **(11g)** FT-IR spectrum shown in the **Appendix 4.8** indicated the absence of weak sharp nitrile C≡N peaks at 2232 cm^{-1} which affirmed the occurrence of the cyclotetramerization reaction of compound **(11)** with $Zn(CH_3COO)_2$ in the formation of the complex compound **(11g)**. Some of the most important peaks that appeared in the spectrum are the presence of medium broad stretching peaks of N-H bonds (Aliphatic amide) at 3284 cm^{-1}, a medium broad stretching peaks of C-H bond (methyl group) between 2978 - 2936 cm^{-1}, a weak broad bend vibration peak of C-H (Aromatic) overtone at 1769 cm^{-1}, a strong broad stretching carbonyl bond C=O at 1706 cm^{-1} (ester C=O), a medium stretching peak (in-ring) peak of C=C bond (Aromatic) at 1597 cm^{-1}, a medium stretching peak (in-ring) peak of C-C bond (Aromatic) at 1476 and 1393 cm^{-1}, a strong sharp stretching peak of C-O-C bond (Aryl ether) at 1231 cm^{-1}, a medium broad stretching peak of C-N bond (aliphatic amines) at 1164, 1088 and 1044 cm^{-1}.

b) UV-visible spectrum of complex (11g) compound

The UV-visible spectrum of zinc tyrosine- glycine dipeptide substituted phthalocyanine complex **(11g)** dissolved in DMF solvent is shown in **Appendix 12.7**. The spectrum reported a single Q-band at 676 nm and a B-band at 351 nm. The spectrum also consists of a sharp shoulder that appeared at 612 nm due to aggregation.

c) Thermal analysis of complex (11g) compound

TGA thermogram curve of the zinc tyrosine- glycine dipeptide substituted phthalocyanine complex **(11g)** compound as shown in **Appendix 16.7** reported the complex is thermally stable up to 190 °C with only 4 % weight loss against temperature due to the loss of moisture trapped in the complex. The complex undergoes a single stage of degradation with weight loss of 58 % recorded between 190 - 560 °C and a leftover of 38 % remained as non-decompose residue as seen in the thermogram curve. Furthermore, the DTA curves indicate that the complex decomposes without melting, under normal conditions, the complex does not possess a melting point and undergoes decomposition exothermically.

d) Electrochemistry analysis of complex (11g) compound

The electrochemical analysis of zinc tyrosine- glycine dipeptide substituted phthalocyanine complex **(11g)** compound was performed by both Cyclic and square wave voltammetry similar to those performed for the above complexes. The complex **(11g)** possesses a redox-inactive zinc metal center that undergoes Pc base electronic redox reactıon. The complex observed two oxidation at $\mathbf{O_1}$ 0.36 volt and $\mathbf{O_2}$ 0.65 volt from the electronic transition of $\mathbf{[Pc^{(-2)}\,Zn^{(2)}]^{0}\,/\,[Pc^{(-1)}\,Zn^{(2)}]^{+1}}$ and $\mathbf{[Pc^{(-1)}\,Zn^{(2)}]^{+1}\,/\,[Pc^{(0)}\,Zn^{(2)}]^{+2}}$, the four reductions reaction $\mathbf{R_4}$ -2.23 volt**,** $\mathbf{R_3}$ -1.97 volt, $\mathbf{R_2}$ -1.60 volt, and $\mathbf{R_1}$ -1.18 volt involves electrons transition as $\mathbf{[Pc^{(-5)}\,Zn^{(2)}]^{-3}\,/\,[Pc^{(-6)}\,Zn^{(2)}]^{-4}}$, $\mathbf{[Pc^{(-4)}\,Zn^{(2)}]^{-2}\,/\,[Pc^{(-5)}\,Zn^{(2)}]^{-3}}$, $\mathbf{[Pc^{(-3)}\,Zn^{(2)}]^{-1}\,/\,[Pc^{(-4)}\,Zn^{(2)}]^{-2}}$, and $\mathbf{[Pc^{(-2)}\,Zn^{(2)}]^{0}\,/\,[Pc^{(-3)}\,Zn^{(2)}]^{-1}}$ respectively for the conjugated Pc macrocycle ring formed cation and anion radicals. The redox activity is directly connected with oxidation by removing electrons from the highest occupied molecular orbital (HOMO) and adding electrons to the lowest unoccupied molecular orbital (LUMO) of phthalocyanines macrocyclic [94, 121, 122]. The voltammograms of square wave and cyclic voltammograms of complex **(11g)** compound are both indicated in **Appendix 20.7a** and **20.7b** respectively.

4.5. Characterization of tyrosine- valinate dipeptide amino acids substituent and complexes

The dipeptide amino acid substituent methyl (tert-butoxycarbonyl)-*L*-tyrosyl-*L*-valinate (Boc-Tyr-Val-OCH_3) **(12)** was characterized using FT-IR, ^{1}H-NMR, ^{13}C-NMR, mass spectroscopies and elemental analysis while the ligand Methyl ((*S*)-2-((tert-butoxycarbonyl) amino)-3-(4-(3,4-dicyanophenoxy) phenyl) propanoyl) valinate (Boc-Tyr-Val-OCH_3-O-PN) **(13)** and complexes are characterized by FT-IR and UV-visible spectroscopies.

4.5.1. Characterization of methyl (tert-butoxycarbonyl)-*L*- tyrosyl-*L*- valinate (Boc-Tyr-Val-OCH_3) (12)

The FT-IR, ^{1}H-NMR, ^{13}C-NMR, and mass spectroscopies spectra of compound **(12)** are given in the **Appendix Section**. The carbons and hydrogens in compound **(12)** are numbered as in **Figure 3.8** below.

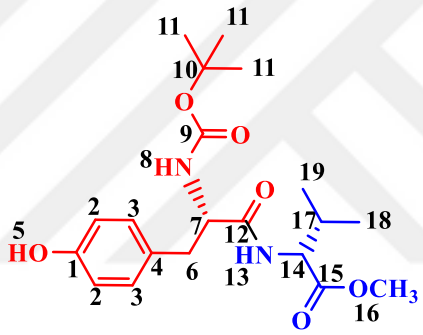

methyl (*tert*-butoxycarbonyl)-*L*-tyrosyl-*L*-valinate

(Boc-Tyr-Val-OCH $_3$) (12)

Figure 4.10. Numbering of carbons and hydrogens in methyl (tert-butoxycarbonyl)-*L*-tyrosyl valinate compound **(12)**

a) FT-IR spectrum of compound (12)

The FT-IR spectrum peaks of methyl (*tert*-butoxycarbonyl)-*L*-tyrosyl-*L*-valinate dipeptide compound **(12)** reported the presence of strong broad stretching peaks of O-H bond for (phenols) at 3313 cm^{-1}, a strong broad stretching peaks of N-H bond (amide) at 2967 cm^{-1}, a weak broad bend vibration peak of C-H (Aromatic) overtone at 1739 cm^{-1}, a strong broad stretching peak of carbonyl C=O at 1653 cm^{-1}(secondary amide C=O), a medium sharp bending peak of N-H bond (amide) at 1615 cm^{-1}, a strong broad stretching peak of C=C bond (aromatic) at 1516 cm^{-1}, a medium broad bending vibration peak of C-H bonds (methyl group) at 1439 cm^{-1}, a medium broad bending vibration of O-H bonds (phenol) at 1366 cm^{-1}, a medium broad stretching of C-N bond (amine) at

1224 cm^{-1} and finally a last important signal is a strong broad stretching peak of C-O bond (C-O ester) at 1165 cm^{-1} as it is shown in the **Appendix 5.**

b) ^{1}H-NMR spectrum of compound (12)

The ^{1}H-NMR of methyl (*tert*-butoxycarbonyl)-*L*-tyrosyl-*L*-valinate dipeptide **(12)** taken in DMSO-d_6, at 298 K: shown in **Appendix 9.1** indicated the presence of 1-proton singlet peak at 9.20 ppm belongs to H^5 (-OH). The doublet signals generated by 1-proton at 8.07 - 8.09 ppm belong to H^{13} (-NH). The 2 protons produce double signals belonging to H^3 occurring between 7.06 -7.08 ppm with coupling constant value of (distance between the two peaks) J= 8.4 Hz. The proton generated double peak signals at 6.89 - 6.91 ppm belong to H^8 (-NH). The double peaks signal of 2-protons at 6.65 - 6.67 ppm occupy a distance of 8.4 Hz between the two peaks is belong to H^2. The multiplet peaks signals produced by 2-proton at 4.17 - 4.24 ppm are generated by H^7 and H^{14}. The presence of 3 protons produces a singlet peak at 3.64 ppm is belongs to H^{16}. The 2-proton split to produce double doublet peak at 2.61 -2.65 ppm and 2.84 -2.83 ppm are possessed by proton H^6, the proton generated a multiplet peaks signals between 2.04 -2.06 ppm is produced by H^{17}. The 9-protons produce a singlet intense signal at 1.32 ppm is possessed by H^{11}, the 6-protons produce multiplet peak signals between 0.88 - 0.92 ppm are generated by H^{18} and H^{19} and lastly, a peak at 3.36 ppm belongs to DMSO-d6 water and the peak at 2.51 ppm belongs to DMSO-d6.

c) ^{13}C-NMR spectrum of compound (12)

The ^{13}C-NMR spectrum of methyl (*tert*-butoxycarbonyl)-*L*-tyrosyl-*L*-valinate dipeptide (10) recorded in DMSO-d6, 298K is presented in **Appendix 9.2**. The peak C^1 at 155.72 ppm is an aromatic carbon that is attached to the phenol functional group. The peak C^2 at 115.23 ppm is an aromatic carbon, the peak C^3 appears at 130.59 ppm, peak C^4 appears at 128.55 ppm, peak C^6 appears at 036.90 ppm, peak C^7 appears at 056.30 ppm, peak C^9 appears at 156.19 ppm, peak C^{10} appears at 078.45 ppm, 028.60 C^{11}, 172.76 C^{12}, 057.68 C^{14}, 172.38 C^{15}, 052.19 C^{16}, 030.61 C^{17}, 018.61 $C^{18,}$ and 019.36 C^{19}. This organized representation of the peaks should provide a clearer understanding of the chemical environment within the compound.

d) Mass spectrum of compound (12)

The theoretically calculated molecular weight of the Boc-Tyr-Val-OCH_3 compound is 394.47 g/mol. In the MALDI-TOF MS spectrum of compound **(12)** given in **Appendix 9.3,** the 394.512 [M] peak is produced by the compound. The peaks observed under this peak indicate the compound resulting from the groups leaving the structure. According to calculations, the peak at 338.361 corresponds to the rupture of the -$C(CH_3)_3$ group in the Boc protecting group, 338.361 [M-

$C(CH_3)_3$]. The peak at 294.149 corresponds to a second group separated from the structure. This corresponds to the complete rupture of the same Boc group 294.149 [M-Boc].

4.5.2. Characterisation of methyl ((*S*)-2-((tert-butoxycarbonyl) amino)-3-(4-(3,4-dicyanophenoxy) phenyl) propanoyl) valinate (Boc-Tyr-Val-OCH_3-O-PN) (13)

The characterization of (Boc-Tyr-Val-OCH_3-O-PN) **(13)** obtained shown in **Figure 3.9** below was done by FT-IR, ^{1}H-NMR, and ^{13}C-NMR spectroscopies.

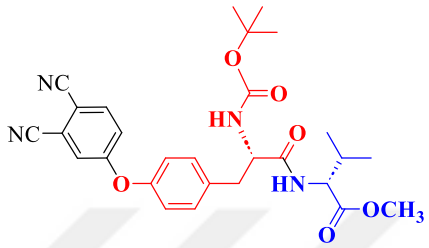

Figure 4.11. Methyl ((S)-2-((tert-butoxycarbonyl) amino)-3-(4-(3,4-dicyanophenoxy) phenyl) propanoyl) valinate **(Boc-Tyr-Val-OCH_3-O-PN) (13)**

a) FT-IR spectrum of compound (13)

The FT-IR (ATR, cm^{-1}) spectrum of compound (13) obtained is shown in **Appendix 5.1.** revealed the appearance of a weak sharp nitrile C≡N peaks at 2233 cm^{-1} as one of the most important signals in the ligand compound**.** Other important peaks in the spectrum are a medium broad stretching of N-H bond (amide) at 3353 and 3279 cm^{-1}, a medium broad stretching C-H aliphatic bond peak signal observed at 2966 $cm^{-1,}$ and a weak broad bend vibration peak signal of C-H (Aromatic) overtone at 1739 cm^{-1}**.** There is also the presence of strong broad stretching of the C=O (amide) bond at 1683 cm^{-1}, a medium broad bending peak signal of N-H (amine) at 1656 cm^{-1}, a medium broad stretching signal of C=C aromatic (in-ring) at 1592 cm^{-1}, then a medium broad stretching peak of C-C aromatic (in-ring) at 1486 cm^{-1}, a medium broad bending vibration signal of C-H bond (methyl group) at 1391cm^{-1}**,** a medium broad rocking signal of C-H bond (methyl group) at 1366 cm^{-1}, a strong broad peak at 1249, 1205 and 1168 cm^{-1} is belong to C-O-C (ether) or C-O (ester), a medium broad stretching peak signal of C-N bond (aliphatic amines) at 1018 cm^{-1}.

b) ^{1}H-NMR spectrum of compound (13)

The ^{1}H-NMR of methyl ((*S*)-2-((tert-butoxycarbonyl) amino)-3-(4-(3,4-dicyanophenoxy) phenyl) propanoyl) valinate **(13)** taken in DMSO-d6: shown in (**Appendix 9.4**) observed the presence of 1-proton doublet peak signal at 8.18 ppm with coupling constant value of (distance between the two peaks) J= 8.2 Hz, 1-proton split to produce double doublet peaks signal at 8.12 ppm with coupling constant value of J= 8.9 and J= 2.0 Hz, 1-proton doublet peak signal at 7.72

ppm with coupling constant value of J= 2.6 Hz, a multiplet peak signal of 2-proton observed between 7.48 - 7.40 ppm, 1-proton split to produce double doublet peaks signal at 7.37 ppm with coupling constant value of J= 8.8 and J= 2.6 Hz, 1-proton produce a multiplet peaks signals observed between 7.19 - 7.10 ppm, a multiplet peaks signals made by 1-proton is observed at 4.36 ppm- 4.26 ppm, 1-proton split to produce double doublet peaks at 4.23 ppm with coupling constant value of J= 8.3 and J= 6.2 Hz, 3-protons doublet with coupling constant value of J= 3.4 Hz appeared at 3.64 ppm, 1-proton split to produce double doublet peaks signal at 2.97 ppm with coupling constant value of J= 13.9 and J= 4.3 Hz, 1-proton produce a multiplet peaks signals observed between 2.83 ppm- 2.71 ppm, 1-proton produce a multiplet peaks signals observed between 2.12 - 1.99 ppm, 9-proton produce doublet peak signal at 1.32 ppm with coupling constant value of J= 2.7 Hz, 6-proton split to produce double doublet peaks signal at 0.91 ppm with coupling constant value of J= 9.7 and J= 6.7 Hz and lastly, a peak at 3.40 ppm belongs to DMSO-d_6 water and the peak at 2.51 ppm belongs to DMSO-d_6.

4.5.2.1. Characterisation of CrPc (13a) Complex

Characterization of phthalocyanine complex were performed by FT-IR spectra, UV-Visible spectra, thermal analysis (TGA and DTA) and electrochemistry techniques (CV and SWV)

a) FT-IR spectrum of complex (13a) compound

The FT-IR spectrum of chromium tyrosine- valine dipeptide substituted phthalocyanine complex **(13a)** shown in the **Appendix 5.2** revealed the absence of weak sharp nitrile C≡N peaks at 2232 cm^{-1} which confirmed the occurrence of cyclotetramerization of the compound **(13)** in the formation of the complex compound **(13a).** Furthermore, some of the most important peaks present are a medium broad stretching peaks of N-H bonds (Aliphatic amide) at 3281 cm^{-1}, a medium broad stretching peaks of C-H bond (methyl group) between 2971-2958 cm^{-1}, weak broad bend vibration peak of C-H (Aromatic) overtone at 1769 cm^{-1}**,** a strong peaks of carbonyl carbon C=O at 1713 cm^{-1} (ester C=O)**,** a medium stretching peak (in-ring) of C=C bond (Aromatics) at 1594 cm^{-1}, then a medium broad stretching peak of C-C aromatic (in-ring) at 1506 cm^{-1}, a medium broad bending vibration of C-H bond (methyl of protection group) at 1391 cm^{-1}, a strong broad peak signal of C-O-C (ether) at 1231 cm^{-1} and a medium broad stretching peak of C-N bond (aliphatic amines) at 1043 cm^{-1}.

b) UV-visible spectrum of complex (13a) compound

Appendix-13.1 show the UV-visible spectrum of chromium tyrosine-valine dipeptide substituted phthalocyanine complex **(13a)** dissolved in DMF. It indicates the existence of a single

Q-band spectrum at 680 nm and B-band at 360 nm. Due to aggregation, a cleared sharp shoulder appears at 612 nm.

c) Thermal analysis of complex (13a) compound

TGA thermogram curve of the chromium tyrosine- valine dipeptide substituted phthalocyanine complex **(13a)** compound as shown in **Appendix 17.1** reported that the complex is thermally stable up to 200 ^{0}C with weight loss of 5% due to the loss of moisture absorbed by the complex. The complex undergoes first-stage degradation between 200 °C - and 530 °C with a weight loss of 72 %. The second stage of degradation recorded only a 3 % weight loss between 530 - 860 °C, and a weight of 20 % was left over as residue. Furthermore, the DTA thermogram curve revealed that the complex decomposes without melting and this implies that under normal conditions, the complex does not possess a melting point and undergo decomposition exothermically.

d) Electrochemistry analysis of complex (13a) compound

The electrochemical analysis of chromium tyrosine- valine dipeptide substituted phthalocyanine complex **(13a)** compound was performed by both cyclic and square wave voltammetry. A glassy carbon electrode is used as the working electrode Pt, as a counter electrode, tetrabutylammonium tetrafluoroborate as the electrolyte, and ferrocene /ferrocenium (Fc/Fc^{+}) as a pseudo-reference electrode in DMF. A wide potential range (-2.5 to +1.5 V versus Fc/Fc^{+}) was employed to explore the phthalocyanine complexes' electrochemical characteristics [119, 120]. The complex **(13a)** possesses a redox-active metal (chromium) center that undergoes two oxidations ($\mathbf{O_1}$ 0.38 volt and $\mathbf{O_2}$ 0.70 volt) which involve $\mathbf{[Pc^{(-2)}\,Cr^{(2)}]^{0}}$ / $\mathbf{[Pc^{(-1)}Cr\,^{(3)}]^{+2}}$and $\mathbf{[Pc\,^{(-1)}\,Cr\,^{(2)}]^{+}}$ / $\mathbf{[Pc\,^{(0)}\,Cr\,^{(3)}]^{+3}}$ for first $\mathbf{O_1}$ and second $\mathbf{O_2}$ oxidation transitions related to the formation of cation radicals, four reductions redox reactions was observed ($\mathbf{R_4}$ -2.34 volt, $\mathbf{R_3}$ -2.97 volt, $\mathbf{R_2}$ -1.81 volt, and $\mathbf{R_1}$ -1.31volt) these obtain generated from $\mathbf{[Pc\,^{(-5)}\,Cr\,^{(2)}]^{-3}}$ / $\mathbf{[Pc\,^{(-6)}\,Cr\,^{(2)}]^{-4}}$ for $\mathbf{R_4}$, $\mathbf{[Pc\,^{(-4)}\,Cr\,^{(2)}]^{-2}}$ / $\mathbf{[Pc\,^{(-5)}\,Cr\,^{(2)}]^{-3}}$ for $\mathbf{R_3}$, $\mathbf{[Pc\,^{(-3)}\,Cr\,^{(2)}]^{-1}}$ / $\mathbf{[Pc\,^{(-4)}\,Cr\,^{(2)}]^{-2}}$ for $\mathbf{R_2}$, and $\mathbf{[Pc\,^{(-2)}\,Cr\,^{(2)}]^{0}}$ / $\mathbf{[Pc\,^{(-3)}\,Cr\,^{(2)}]^{-1}}$ for $\mathbf{R_1}$ electronic transition related to the formation of anion radicals from the redox reaction of the conjugated macrocycle Pc ring**.** The metal center redox reaction produced **(**$\mathbf{M_R}$ -1.09 and $\mathbf{M_O}$ - 0.18) involves $\mathbf{[Pc\,^{(-2)}\,Cr\,^{(2)}]^{0}}$ / $\mathbf{[Pc\,^{(-2)}\,Cr\,^{(1)}]^{-1}}$ for metal base reduction $\mathbf{M_R}$ and $\mathbf{[Pc\,^{(-2)}\,Cr\,^{(2)}]^{0}}$ / $\mathbf{[Pc\,^{(-2)}\,Cr\,^{(3)}]\,^{+1}}$ for metal base oxidation $\mathbf{M_O}$ to formed anion and cation radicals respectively. The redox activity is directly connected with oxidation by removing electrons from the highest occupied molecular orbital (HOMO) and adding electrons to the lowest unoccupied molecular orbital (LUMO) of phthalocyanines macrocyclic. The voltammograms of square wave and cyclic voltammograms of complex **(13a)** compound are both shown in **Appendix 21.1a** and **21.1b** respectively.

4.5.2.2. Characterization of MnPc (13b) Complex

Characterization of phthalocyanine complex were performed by FT-IR spectra, UV-Visible spectra, thermal analysis (TGA and DTA) and electrochemistry techniques (CV and SWV)

a) FT-IR spectrum of complex (13b) compound

FT-IR spectrum of manganese tyrosine- valine dipeptide substituted phthalocyanine complex **(13b)** shown in **Appendix 5.3** observed the absence of a weak sharp nitrile C≡N bond peak signal at 2232 cm^{-1} which indicated the formation of the complex through cyclotetramerization reaction of the compound **(13)**. Conversely, some of the presence of the most important peak in the spectrum is a medium broad stretching peak of N-H bonds (Aliphatic amide) at 3268 cm^{-1}, a medium broad stretching peak of C-H bond (methyl group) between 2966 - 2873 cm^{-1}, weak broad bend vibration peak of C-H (Aromatic) overtone at 1769 cm^{-1}, a medium peak of carbonyl carbon C=O at 1709 cm^{-1} (ester C=O), a medium stretching peak(in-ring) of C=C bond (Aromatics) at 1599 cm^{-1}, a medium broad bending vibration of C-H bond (methyl of protection group) at 1394 cm^{-1}, a strong broad peak signal of C-O-C (ether) at 1232 cm^{-1} and a medium broad stretching peak of C-N bond (aliphatic amines) at 1166 and 1076 cm^{-1}.

b) UV-visible spectrum of complex (13b) compound

The UV-visible spectrum of manganese tyrosine-valine dipeptide substituted phthalocyanine complex **(13b)** dissolved in DMF is shown in **Appendix 13.2** reported the appearance of a single Q-band peak signal at 710 nm and B-band at 487 nm. The clear pronouns shoulder at 650 nm are due to aggregation.

c) Thermal analysis of complex (13b) compound

The TGA thermograms curve of the manganese tyrosine- valine dipeptide substituted phthalocyanine complex **(13b)** revealed that the complex is thermally stable up to 170 °C with weight loss of 5 % which is provably accounted for loss of moisture absorbed by the complex. The complex undergoes two stages of degradation. The first degradation observed from the TGA thermogram curve of the complex is recorded between 170 - 490 °C with a weight loss of 84 %. The second degradation stage occurred between 490 - 860 °C with a weight loss of 5 % and leftover of 6 % as residue which is provable the metal oxide of the complex MnO as shown in **Appendix 17.2.** However, the DTA thermogram curves of the complex indicated that the degradation processes proceed exothermically and the complex decomposes without melting under normal conditions.

d) Electrochemistry analysis of complex (13b) compound

The electrochemical analysis of manganese tyrosine-valine dipeptide substituted phthalocyanine complex **(13b)** compound was performed by both Cyclic and square wave voltammetry. A glassy carbon electrode is used as the working electrode Pt, as a counter electrode, tetrabutylammonium tetrafluoroborate as the electrolyte, and ferrocene /ferrocenium (Fc/Fc^{+}) as a pseudo-reference electrode in DMF. A wide potential range (-2.5 to +1.5 V versus Fc/Fc^{+}) was employed to explore the phthalocyanine complexes' electrochemical characteristics [119, 120]. The complex **(13b)** possesses a redox-inactive metal (manganese) center that undergoes four Pc ring base redox reduction reactions generating the following redox potentials value as $\mathbf{R_4}$ -2.40 volt, $\mathbf{R_3}$ -1.90 volt, $\mathbf{R_2}$ -1.36 volt, and $\mathbf{R_1}$ -1.14 volt from these redox reactions **[Pc $^{(-5)}$ Mn $^{(2)}$]$^{-3}$ / [Pc $^{(-6)}$ Mn $^{(2)}$]$^{-4}$, [Pc $^{(-4)}$ Mn $^{(2)}$]$^{-2}$ / [Pc $^{(-5)}$ Mn $^{(2)}$]$^{-3}$, [Pc $^{(-3)}$ Mn $^{(2)}$]$^{-1}$ / [Pc $^{(-4)}$ Mn $^{(2)}$]$^{-2}$**, and **[Pc $^{(-2)}$ Mn $^{(2)}$]^{0} / [Pc $^{(-3)}$ Mn $^{(2)}$]$^{-1}$** for $\mathbf{R_4}$, $\mathbf{R_3}$, $\mathbf{R_2}$, and $\mathbf{R_1}$ respectively associated with the formation of anionic radicals. Two redox oxidations reactions were also reported which involve **[Pc $^{(-2)}$ Mn $^{(2)}$]^{0} / [Pc $^{(-1)}$ Mn $^{(3)}$] $^{+2}$**and **[Pc $^{(-1)}$ Mn $^{(2)}$] $^{+}$ / [Pc $^{(0)}$ Mn $^{(3)}$] $^{+3}$** that generate potential values of 0.54 volt and 0.88 volt for first $\mathbf{O_1}$ and second $\mathbf{O_2}$ **o**xidations potential respectively for the formation of cation radicals from the conjugated macrocycle Pc ring. The Pc undergoes a metal base redox oxidation reaction to produce a positive potential value of $\mathbf{M_O}$ 0.31 from the electronic transition of **[Pc $^{(-2)}$ Mn $^{(2)}$]^{0} / [Pc $^{(-2)}$ Mn $^{(3)}$] $^{+1}$** to formed cation.

The redox activity is directly connected with oxidation by removing electrons from the highest occupied molecular orbital (HOMO) and adding electrons to the lowest unoccupied molecular orbital (LUMO) of phthalocyanines macrocyclic. The voltammograms of square wave and cyclic voltammograms of complex **(13b)** compound are both shown in **Appendix 21.2a** and **21.2b** respectively.

4.5.2.3. Characterisation of FePc (13c) Complex

Characterization of phthalocyanine complex were performed by FT-IR spectra, UV-Visible spectra, thermal analysis (TGA and DTA) and electrochemistry techniques (CV and SWV)

a) FT-IR spectrum of complex (13c) compound

The FT-IR spectrum of iron tyrosine- valine dipeptide substituted phthalocyanine complex **(13c)** shown in **Appendix 5.4** reported the absence of a weak sharp nitrile C≡N peaks at 2232 cm^{-1} which confirmed the cyclotetramerization reaction of compound **(13)** in the formation of the complex compound **(13c)**. Other most important peaks occurred in the spectrum a medium broad stretching peaks of N-H bonds (Aliphatic amide) at 3251 cm^{-1}, medium broad stretching peaks of C-H bond (methyl group) between 2967 - 2871 cm^{-1}**,** a weak broad bend vibration peak of C-H

(Aromatic) overtone at 1768 cm^{-1}, a strong broad peak signal of carbonyl carbon C=O at 1713 cm^{-1} (ester C=O) and 1662 cm^{-1} for (amide C=O), a medium stretching peak(in-ring) of C=C bond (Aromatics) at 1599 cm^{-1}, a medium broad bending vibration of C-H bond (methyl of protection group) at1476 and 1365 cm^{-1}, a strong broad peak signal of C-O-C bond (ether) at 1232 cm^{-1} and a medium broad stretching peak of C-N bond (aliphatic amines) at 1163 cm^{-1}.

b) UV-visible spectrum of complex (13c) compound

The UV-visible spectrum of iron tyrosine-valine dipeptide substituted phthalocyanine complex **(13c)** dissolved in DMF is presented in **Appendix 13.3** The spectrum indicated a single Q-band at 685 nm and B-band at 420 nm and a shoulder is observed at 613 nm.

c) Thermal analysis of complex (13c) compound

The TGA thermograms curve of the iron tyrosine-valine dipeptide substituted phthalocyanine complex **(13c)** presented in **Appendix 17.3** indicates the compound is thermally stable up to180 °C with 3 % weight loss due to loss of moisture trapped in the complex. The complex undergoes three stages of degradation, the first stage is reported between 180 - 200 °C with only 5 % weight loss, while the second stage of degradation occurs between 200 -535 °C with 56 % weight loss. The final stage of degradation accounts for a weight loss of 6 % between 535 - 900 °C with 30 % remaining of the complex as a non-decompose leftover residue. It is also observed from the DTA curves of the complex that the compound does not have a melting point because it undergoes exothermic decomposition without melting under normal conditions.

d) Electrochemistry analysis of complex (13c) compound

The electrochemical properties of iron tyrosine-valine dipeptide substituted phthalocyanine complex **(13c)** were examined using cyclic and square wave voltammetry techniques. Similar to previous analyses, a glassy carbon electrode served as the working electrode while platinum was used as a counter electrode. The electrolyte comprised tetrabutylammonium tetrafluoroborate with ferrocene/ferrocenium (Fc/Fc^{+}) as a pseudo-reference electrode in DMF. The investigations were conducted over a potential range of -2.5 to +1.5 V versus Fc/Fc^{+}. The complex formed four redox reduction processes wıth potential values of $\mathbf{R_4}$ at -2.58 volt, $\mathbf{R_3}$ at -2.29 volt, $\mathbf{R_2}$ at -2.09 volt, $\mathbf{R_1}$ at -1.46 volt that are observed from the redox reactions $\mathbf{[Pc^{(-5)}\,Fe^{(2)}]^{-3}\,/\,[Pc^{(-6)}\,Fe^{(2)}]^{-4}}$, $\mathbf{[Pc^{(-4)}\,Fe^{(2)}]^{-2}\,/\,[Pc^{(-5)}\,Fe^{(2)}]^{-3}}$, $\mathbf{[Pc^{(-3)}\,Fe^{(2)}]^{-1}\,/\,[Pc^{(-4)}\,Fe^{(2)}]^{-2}}$, and $\mathbf{[Pc^{(-2)}\,Fe^{(2)}]^{0}\,/\,[Pc^{(-3)}\,Fe^{(2)}]^{-1}}$ for $\mathbf{R_4}$, $\mathbf{R_3}$, $\mathbf{R_2}$, and $\mathbf{R_1}$ reduction reaction respectively associated with electrons transfer for the formation of anionic radicals. The complex **(13c)** also exhibited two Pc base redox oxidation processes $\mathbf{O_1}$ and $\mathbf{O_2}$ with potential values of 0.38 volt and 0.74 volt respectively which involved the following redox reaction $\mathbf{Pc^{(-2)}\,Fe^{(2)}\,/\,[Pc^{(-1)}\,Fe^{(3)}]^{+2}}$and $\mathbf{[Pc^{(-1)}\,Fe^{(2)}]^{+1}/\,[Pc^{(0)}\,Fe^{(3)}]^{+3}}$ for first $\mathbf{O_1}$ and second $\mathbf{O_2}$

oxidatıon reaction observed for the formation of cation radical. Iron metal is a redox-active metal that undergoes metal base redox reaction to produce metal center oxidation $\mathbf{M_O}$ -0.24 with negative potential value [126, 127] generated from following redox reaction **[Pc $^{(-2)}$ Fe $^{(2)}$]^{0} / [Pc $^{(-2)}$ Fe $^{(3)}$]$^{+1}$** involving electronic transfer for the formation of cation radical and metal center reduction reaction $\mathbf{M_R}$ 0.76 potential value observed from redox reduction reaction **[Pc $^{(-2)}$ Fe $^{(2)}$]^{0} / [Pc $^{(-2)}$ Fe $^{(1)}$]$^{-1}$**for the formation of anionic radical. The reduction of the metal base center of the complex reported a different behavior from the other [128] as similarly indicated by Aktaş and co-workers [126] concerning Fe^2Pc giving reduction value (0.25 volt) at a more positive potential [129, [130].

The redox activity is connected to the transfer of electrons from the highest occupied molecular orbital (HOMO) and the lowest unoccupied molecular orbital (LUMO) of the phthalocyanine macrocycle. The voltammograms for the square wave and cyclic voltammetry of complex **(13c)** can be found in **Appendix 21.3a** and **21.3b**, respectively.

4.5.2.4. Characterization of CoPc (13d) Complex

Characterization of phthalocyanine complex were performed by FT-IR spectra, UV-Visible spectra, thermal analysis (TGA and DTA) and electrochemistry techniques (CV and SWV)

a) FT-IR spectrum of complex (13d) compound

The FT-IR spectrum of cobalt tyrosine- valine dipeptide substituted phthalocyanine complex **(13d)** revealed the absence of a weak sharp nitrile C≡N peaks at 2232 cm^{-1} which confirmed the formation of cyclotetramerization reaction of compound **(13)** to form the complex **(13d)** compound as reported in the **Appendix 5.5**. Some of the most important peaks appeared in the spectrum are medium broad stretching bond peaks of N-H bonds (Aliphatic amide) at 3313 cm^{-1}, a medium broad stretching peaks of C-H bond (methyl group) between 2967 - 2876 cm^{-1}**,** a weak broad bend vibration peak of C-H (Aromatic) overtone at 1771 cm^{-1}, a strong broad stretching carbonyl bond C=O at 1717 cm^{-1} (ester C=O) and 1661 cm^{-1} (amide C=O), a medium stretching peak(in-ring) of C=C bond (Aromatics) at 1597 cm^{-1}, a medium stretching peak of C-C bond (Aromatic) at 1506 cm^{-1}, a medium broad bending vibration of C-H bond (methyl of protection groups) at 1476 cm^{-1} and 1365 cm^{-1}, a strong broad stretching peak signals of C-O-C bond (ether) at 1232 cm^{-1} and O-C bond (ester) at 1164 cm^{-1}, a medium broad stretching peak of C-N bond (aliphatic amines) at 1091 and 1017 cm^{-1}.

b) UV-visible spectrum of complex (13d) compound

The UV-visible spectrum of cobalt tyrosine- valine dipeptide substituted phthalocyanine complex **(13d)** dissolved in DMF as solvent shown in **Appendix 13.4** revealed the appearance of

a single Q-band spectrum peak signal at 670nm and B-band at 400 nm and small shoulder appeared at 610 nm.

c) Thermal analysis of complex (13d) compound

The TGA and DTA thermogram curves of cobalt tyrosine- valine dipeptide substituted phthalocyanine complex **(13d)** compound presented in **Appendix 17.4** revealed that the complex was thermally stable up to 180 °C with only 1 % weight loss accounted as result of moisture loss absorbed by the complex. The complex undergoes three stages of degradation as seen on the TGA thermogram curve**.** The first decomposition is reported between 180 – 240 °C with a weight loss of 21 %. However, the second degradation was recorded between 240 – 460 °C giving a weight loss of 32 %. Furthermore, the final stage accounted for a 5% weight left of material as residue which may provably be the metal oxide CoO of the complex**.**

Conversely, the DTA thermogram curve of the complex shows that the complex decomposes without melting, this implies that under normal conditions the complex does not have a melting point and its degradation follows an exothermic pathway**.**

d) Electrochemistry analysis of complex (13d) compound

The electrochemical properties of cobalt tyrosine-valine dipeptide substituted phthalocyanine complex **(13c)** were examined using cyclic and square wave voltammetry techniques. Similar to previous analyses, a glassy carbon electrode served as the working electrode while platinum was used as a counter electrode. The electrolyte comprised tetrabutylammonium tetrafluoroborate with ferrocene/ferrocenium (Fc/Fc^{+}) as a pseudo-reference electrode in DMF. The investigations were conducted over a potential range of -2.5 to +1.5 V versus Fc/Fc^{+}. The complex formed four redox reduction processes wıth potential values of $\mathbf{R_4}$ at -2.41 volt, $\mathbf{R_3}$ at -2.15 volt, $\mathbf{R_2}$ at -1.91 volt, $\mathbf{R_1}$ at -1.30 volt that produce **[Pc $^{(-5)}$ Co $^{(2)}$]$^{-3}$ / [Pc $^{(-6)}$ Co $^{(2)}$]$^{-4}$**, **[Pc $^{(-4)}$ Co $^{(2)}$]$^{-2}$ / [Pc $^{(-5)}$ Co $^{(2)}$]$^{-3}$**, **[Pc $^{(-3)}$ Co $^{(2)}$]$^{-1}$ / [Pc $^{(-4)}$ Co $^{(2)}$]$^{-2}$**, and **[Pc $^{(-2)}$ Co $^{(2)}$]^{0} / [Pc $^{(-3)}$ Co $^{(2)}$]$^{-1}$** for $\mathbf{R_4}$, $\mathbf{R_3}$, $\mathbf{R_2}$, and $\mathbf{R_1}$ redox reductıon reaction respectively associated with electron transfer for the formation of anion radicals. The complex **(13c)** also exhibited two Pc base redox oxidation processes $\mathbf{O_1}$ and $\mathbf{O_2}$ with potential values of 0.50 volt and 0.92 volts respectively which involve [**Pc $^{(-2)}$ Co $^{(2)}$]^{0} / [Pc $^{(-1)}$ Co $^{(3)}$] $^{+2}$**and **[Pc $^{(-1)}$ Co $^{(2)}$] $^{+1}$ / [Pc $^{(0)}$ Co $^{(3)}$] $^{+3}$** redox reactions for first $\mathbf{O_1}$ and second $\mathbf{O_2}$ oxidatıon reaction observed for the formation of cation radical. Iron metal is a redox-active metal that undergoes metal base redox reaction to produce metal center oxidation $\mathbf{M_O}$ -0.24 volt with negative potential value involving electronic transition for the formation of cation radical **[Pc $^{(-2)}$ Co $^{(2)}$]^{0} / [Pc $^{(-2)}$ Co $^{(1)}$]$^{-1}$** [126, 127] and metal center reduction $\mathbf{M_R}$ 0.085 volt potential value observed from redox reaction **[Pc $^{(-2)}$ Co $^{(2)}$]^{0} / [Pc $^{(-2)}$ Co $^{(3)}$]$^{+1}$** for the formation of anionic radical.

The redox activity is connected to the transfer of electrons from the highest occupied molecular orbital (HOMO) and the lowest unoccupied molecular orbital (LUMO) of the phthalocyanine macrocycle. The voltammograms for the square wave and cyclic voltammetry of complex **(13c)** can be found in **Appendix 21.3a** and **21.3b**, respectively.

4.5.2.5. Characterisation of NiPc (13e) Complex

Characterization of phthalocyanine complex were performed by FT-IR spectra, UV-Visible spectra, thermal analysis (TGA and DTA) and electrochemistry techniques (CV and SWV)

a) FT-IR spectrum of complex (13e) compound

The FT-IR spectrum of nickel tyrosine- valine dipeptide substituted phthalocyanine complex **(13e)** presented in the **Appendix 5.6** indicated the absence of weak sharp nitrile C≡N peaks at 2232 cm^{-1} which confirmed the occurrence of cyclotetramerization of compound **(13)** in the formation of the complex **(13e)** compound. Among the most important peaks observed in the spectrum are the appearance of a medium broad stretching peak of N-H bonds (Aliphatic amide) at 3314 cm^{-1}, a medium broad stretching peak of C-H bond (methyl group) between 2967 - 2876 cm^{-1}**,** a weak broad bend vibration peak of C-H (Aromatic) overtone at 1770 cm^{-1}, a strong broad stretching carbonyl bond C=O at 1717 cm^{-1} (ester C=O) and 1658 cm^{-1}(amide C=O), a medium broad stretching peak (in-ring) of C=C bond (Aromatic) at 1592 cm^{-1}, a medium broad stretching peak (in ring) of C-C bond (Aromatic) at 1486 cm^{-1}, a medium broad bending vibration of C-H bond (methyl of protection groups) at 1381 cm^{-1}, a strong broad stretching peak of C-O-C bond (ethers) at 1229 cm^{-1}, and medium broad stretching peaks of C-N bond (aliphatic amines) at 1165cm^{-1} and 1067cm^{-1}.

b) UV-visible spectrum of complex (13e) compound

The UV-visible spectrum of a nickel tyrosine-valine dipeptide substituted phthalocyanine complex **(13e)** dissolved in DMF as a solvent, presented in **Appendix 13.5**, reported the appearance of a single Q-band spectrum at 675 nm and B-band at 375 nm and a broad shoulder is also present at 625 nm.

c) Thermal analysis of complex (13e) compound

The TGA thermogram curve of the nickel tyrosine- valine dipeptide substituted phthalocyanine complex **(13e)** compound is 190 °C thermally stable with only 1% weight loss as a result of moisture loss absorbed in the complex. The complex undergoes thermal decomposition between 190 - 238 °C with 17 % weight loss as first-stage degradation. Then by weight loss of 27 % occurred between 238 - 500 °C and 53 % between 500 - 630 °C in the second and third stages of degradation respectively. A weight of only 2 % was lifted as residue which could be probably

its metal oxide NiO as shown in **Appendix 17.5**. However, the DTA thermogram curve of the complex revealed the compound undergoes exothermic decomposition and degrades without melting under normal conditions.

d) Electrochemistry analysis of complex (13e) compound

The electrochemical analysis of nickel tyrosine-valine dipeptide substituted phthalocyanine complex **(13e)** compound was performed by both Cyclic and square wave voltammetry. A glassy carbon electrode is used as the working electrode while platinum Pt as a counter electrode, tetrabutylammonium tetrafluoroborate as the electrolyte, and ferrocene /ferrocenium (Fc/Fc^{+}) as a pseudo-reference electrode in DMF. A wide potential range (-2.5 to +1.5 V versus Fc/Fc^{+}) was employed to explore the phthalocyanine complexes' electrochemical characteristics [119, 120]. The complex **(13e)** possesses a redox-inactive nickel metal center that undergoes only a Pc ring redox reaction.

The complex exhibited two Pc ring base redox oxidations reactions with potential values of $\mathbf{O_1}$ 0.41 volt from **[Pc $^{(-2)}$ Ni $^{(2)}$]^{0} / [Pc $^{(-1)}$ Ni $^{(2)}$] $^{+1}$** and $\mathbf{O_2}$ 0.65 volt from **[Pc $^{(-1)}$ Ni $^{(2)}$] $^{+1}$ / [Pc ^{0} Ni $^{(2)}$] $^{+2}$** with the electronic transition to formed cation. The complex also undergoes reduction reaction to generates four redox potential values $\mathbf{R_4}$ -2.45 volt**,** $\mathbf{R_3}$ -2.06 volt, $\mathbf{R_2}$ -1.63 volt, and $\mathbf{R_1}$ -1.18 volt from redox reactions involves electrons transition as **[Pc $^{(-5)}$ Ni $^{(2)}$]$^{-3}$ / [Pc $^{(-6)}$ Ni $^{(2)}$]$^{-4}$**, **[Pc $^{(-4)}$ Ni $^{(2)}$]$^{-2}$ / [Pc $^{(-5)}$ Ni $^{(2)}$]$^{-3}$**, **[Pc $^{(-3)}$ Ni $^{(2)}$]$^{-1}$ / [Pc $^{(-4)}$ Ni $^{(2)}$]$^{-2}$**, and **[Pc $^{(-2)}$ Ni $^{(2)}$]^{0} / [Pc $^{(-3)}$ Ni $^{(2)}$]$^{-1}$** respectively forming anionic radicals. The redox activity is directly connected with oxidation by removing electrons from the highest occupied molecular orbital (HOMO) and adding electrons to the lowest unoccupied molecular orbital (LUMO) of phthalocyanines macrocyclic [94, 121, 122]. The voltammograms of square wave and cyclic voltammograms of complex **(13e)** compound are both indicated in **Appendix 21.5a** and **21.5b** respectively.

4.5.2.6. Characterization of CuPc (13f) Complex

Characterization of phthalocyanine complex were performed by FT-IR spectra, UV-Visible spectra, thermal analysis (TGA and DTA) and electrochemistry techniques (CV and SWV)

a) FT-IR spectrum of complex (13f) compound

The FT-IR spectrum of copper tyrosine- valine dipeptide substituted phthalocyanine complex **(13f)** shown in the **Appendix 5.7** indicated the absence of weak sharp nitrile C≡N peaks at 2232 cm^{-1} which justified the occurrence of cyclotetramerization reaction of compound **(13)** for the formation of the complex **(13f)**. Some of the most important peaks that appeared in the spectrum are a medium broad stretching peak of the N-H bond (Aliphatic amide) at 3313 cm^{-1}, a medium broad stretching peak of the C-H bond (methyl group) between 2966 - 2876 cm^{-1}, a weak broad bendıng vibration peak of C-H (Aromatic) overtone at 1770 cm^{-1}, a strong broad peak of carbonyl

carbon bond C=O of (ester C=O) and (amide C=O) at 1716 and 1661 cm^{-1} respectively, a medium stretching peak (in-ring) of C=C bond (Aromatics) at 1602 cm^{-1}**,** a medium stretching (in ring) of C-C bond (Aromatic) at 1506 cm^{-1}, a medium broad bending vibration of C-H bond (methyl of protection group) at 1476 and 1363 cm^{-1}, presence of a strong broad stretching peak of C-O-C bond (ether) at 1231 cm^{-1} and O-C bond (ester) at 1164 cm^{-1}, then a medium broad stretching peaks of C-N bond (aliphatic amines) at 1088 and 1041 cm^{-1}.

b) UV-visible spectrum of complex (13f) compound

The UV-visible spectrum of copper tyrosine-valine dipeptide substituted phthalocyanine complex **(13f)** dissolved in DMF is shown in **Appendix 13.6** The spectrum recorded a single Q-band signal at 675 nm and B-band at 425 nm. There is also the presence of a broad shoulder at 612 nm.

c) Thermal analysis of complex (13f) compound

It is recorded from the TGA thermograms curve of the copper tyrosine-valine dipeptide substituted phthalocyanine complex **(13f)** that the compound is thermally stable up to160 °C with only 2 % weight loss occurred due to loss of moisture absorbed by the complex **(13f)**. The complex undergoes four stages of degradation with weight loss of 15 % accounted between 160 - 200 °C as the first stage of degradation followed by a weight reduction of 9 % recorded between 200 - 300 °C in the second stage of degradation. The third stage reported a weight loss of 16 % between 300 - 460 °C and finally a weight loss of 50 % was observed between 460 - 640 °C. A leftover of 8 % was recorded as remaining material lifted as residue which is probably the metal oxide CuO as seen in the TGA thermogram curve in **Appendix 17.6.** It is indicated from the DTA curves of the complex that the compound decomposes exothermically without melting. Therefore, under normal conditions complex (**13f**) does not have a melting point.

d) Electrochemistry analysis of complex (13f) compound

The copper tyrosine-valine dipeptide substituted phthalocyanine complex **(13f)** compound electrochemical analysis was performed by both Cyclic and square wave voltammetry. A glassy carbon electrode is used as the working electrode while platinum Pt as a counter electrode, tetrabutylammonium tetrafluoroborate as the electrolyte, and ferrocene /ferrocenium (Fc/Fc^{+}) as a pseudo-reference electrode in DMF. A wide potential range (-2.5 to +1.5 V versus Fc/Fc^{+}) was employed to explore the phthalocyanine complexes' electrochemical characteristics. The complex **(13f)** possesses a redox-active copper metal center that undergoes two Pc ring base oxidation generating potential values of $\mathbf{O_1}$ -0.33 volt and $\mathbf{O_2}$ 0.51 volt from the redox oxidation reaction of $\mathbf{[Pc^{(-2)}\,Cu^{(2)}]^{0}}$ / $\mathbf{[Pc^{(-1)}\,Cu^{(2)}]^{+1}}$ and $\mathbf{[Pc^{(-1)}\,Cu^{(2)}]^{+}}$ / $\mathbf{[Pc^{(0)}\,Cu^{(2)}]^{+2}}$ respectively forming cation

and observed four reduction reactions potential values of **R_4** -2.59 volt**, R_3** -2.35 volt, **R_2** -2.16 volt, and **R_1** -1.65 volt produced from the following redox reactions **[Pc $^{(-5)}$ Cu $^{(2)}$]$^{-3}$ / [Pc $^{(-6)}$ Cu $^{(2)}$]$^{-4}$**, **[Pc $^{(-4)}$ Cu $^{(2)}$]$^{-2}$ / [Pc $^{(-5)}$ Cu $^{(2)}$]$^{-3}$**, **[Pc $^{(-3)}$ Cu $^{(2)}$]$^{-1}$ / [Pc $^{(-4)}$ Cu $^{(2)}$]$^{-2}$**, and **[Pc $^{(-2)}$ Cu $^{(2)}$]^{0} / [Pc $^{(-3)}$ Cu $^{(2)}$]$^{-1}$** respectively as a result of the reduction reaction of conjugated Pc macrocycle ring forming anionic radical. The redox activity is directly connected with oxidation by removing electrons from the highest occupied molecular orbital (HOMO) and adding electrons to the lowest unoccupied molecular orbital (LUMO) of phthalocyanines macrocyclic. The voltammograms of square wave and cyclic voltammograms of complex**(13f)** compound are both reported in **Appendix 21.6a** and **21.6b** respectively.

4.5.2.7. Characterisation of ZnPc (13g) Complex

Characterization of phthalocyanine complex were performed by FT-IR spectra, UV-Visible spectra, thermal analysis (TGA and DTA) and electrochemistry techniques (CV and SWV)

a) FT-IR spectrum of complex (13g) compound

The zinc tyrosine- valine dipeptide substituted phthalocyanine complex **(13g)** FT-IR spectrum shown in the **Appendix 5.8** indicated the absence of weak sharp nitrile C≡N peaks at 2232 cm^{-1} which affirmed the occurrence of the cyclotetramerization reaction of compound **(13)** in the formation of the complex compound **(13f)**. Other most important peaks that appeared in the spectrum are the presence of medium broad stretching peaks of N-H bonds (Aliphatic amide) at 3251 cm^{-1}, a medium broad stretching peaks of C-H bond (methyl group) between 2966 - 2876 cm^{-1}, a weak broad bend vibration peak of C-H (Aromatic) overtone at 1769 cm^{-1}, a strong broad stretching carbonyl bond C=O at 1713 cm^{-1} (ester C=O), a medium stretching (in-ring) peak of C=C bond (Aromatic) at 1602 cm^{-1}, a medium stretching (in ring) of C-C bond (Aromatic) at 1506 cm^{-1} and 1476 cm^{-1}, presence of a strong broad stretching peak of C-O-C bond (ether) at 1231 cm^{-1} and O-C bond (ester) at 1164 cm^{-1} a medium broad stretching peak of C-N bond (aliphatic amines) at 1089 and 1042 cm^{-1}.

b) UV-visible spectrum of complex (13f) compound

The UV-visible spectrum of zinc tyrosine- valine dipeptide substituted phthalocyanine complex **(13f)** dissolved in DMF solvent is shown in **Appendix 13.7**. The spectrum presented a single Q-band at 680 nm and a B-band at 375 nm. The spectrum also revealed a sharp clear shoulder appeared at 610 nm.

c) Thermal analysis of complex (13f) compound

The TGA thermogram curve of zinc tyrosine- valine dipeptide substituted phthalocyanine complex **(13f)** compound as shown in **Appendix 17.7** revealed the complex is thermally stable up

to 160 °C with only 3 % weight loss against temperature due to the loss of moisture trapped in the complex. The complex undergoes three stages of degradation with a weight loss of 13 % recorded between 160 - 200 °C for the first degradation, then 34 % weight loss was accounted for between 200 - 450 °C in the second stage while 48 % weight reduction is reported between 450 - 610 °C for the third stage. A leftover of 2 % remains as residue were recorded which is probably the metal oxide ZnO as seen in the thermogram curve. Furthermore, the DTA curves indicate that the complex decomposes without melting, under normal conditions, the complex does not possess a melting point and undergoes decomposition exothermically.

d) Electrochemistry analysis of complex (13f) compound

The electrochemical analysis of zinc tyrosine- valine dipeptide substituted phthalocyanine complex **(13g)** compound was performed by both Cyclic and square wave voltammetry similar to those performed for the above complexes. The complex **(13g)** possesses a redox-inactive zinc metal center that undergoes Pc base electronic redox reaction. The complex exhibits two oxidation potentials at $\mathbf{O_1}$ 0.50 volt and $\mathbf{O_2}$ 0.79 volt generated from the following redox oxidation reactions of $\mathbf{[Pc^{(-2)}\,Zn^{(2)}]^{0}}$ / $\mathbf{[Pc^{(-1)}\,Zn^{(2)}]^{+1}}$ and $\mathbf{[Pc^{(-1)}\,Zn^{(2)}]^{+1}}$ / $\mathbf{[Pc^{(0)}\,Zn^{(2)}]^{+2}}$ respectively to formed cationic radicals. The complex also observed four reductions reaction potentials as $\mathbf{R_4}$ -2.53 volt**,** $\mathbf{R_3}$ -1.92volt, $\mathbf{R_2}$ -1.40 volt, and $\mathbf{R_1}$ -1.15 volt obtained from redox reduction reaction involving electrons transition as $\mathbf{[Pc^{(-5)}\,Zn^{(2)}]^{-3}}$ / $\mathbf{[Pc^{(-6)}\,Zn^{(2)}]^{-4}}$, $\mathbf{[Pc^{(-4)}\,Zn^{(2)}]^{-2}}$ / $\mathbf{[Pc^{(-5)}\,Zn^{(2)}]^{-3}}$, $\mathbf{[Pc^{(-3)}\,Zn^{(2)}]^{-1}}$ / $\mathbf{[Pc^{(-4)}\,Zn^{(2)}]^{-2}}$, and $\mathbf{[Pc^{(-2)}\,Zn^{(2)}]^{0}}$ / $\mathbf{[Pc^{(-3)}\,Zn^{(2)}]^{-1}}$ respectively produce from the conjugated Pc macrocycle ring base forming anion radicals. The redox activity is directly connected with oxidation by removing electrons from the highest occupied molecular orbital (HOMO) and adding electrons to the lowest unoccupied molecular orbital (LUMO) of phthalocyanines macrocyclic [94, [121, [122]. The voltammograms of square wave and cyclic voltammograms of complex **(13g)** compound are both indicated in **Appendix 21.7a** and **21.7b** respectively

5. CONCLUSIONS

Pcs were synthesized by cyclotetramerization [21] of the previously prepared precursor methyl ((*S*)-2-((tert-butoxycarbonyl) amino)-3-(4-(3,4-dicyanophenoxy) phenyl) propanoyl)-*D*-phenylalaninate, methyl ((*S*)-2-((tert-butoxycarbonyl) amino)-3-(4-(3,4-dicyanophenoxy) phenyl) propanoyl)-*D*-alaninate, methyl ((*S*)-2-((tert-butoxycarbonyl) amino)-3-(4-(3,4-dicyanophenoxy) phenyl) propanoyl)glycinate and methyl ((*S*)-2-((tert-butoxycarbonyl) amino)-3-(4-(3,4-dicyanophenoxy) phenyl) propanoyl)-*L*-valinate ligands respectıvely with the presence of metal salts under argon atmosphere. The synthesized dipeptide-substituted phthalocyanines are subject to detailed characterization by modern analytical techniques. FT-IR and UV-visible spectroscopy are widely used to confirm the functional groups and electronic properties of the compounds. NMR (^{1}H and ^{13}C) spectroscopy examines the dipeptide groups with the phthalocyanine core.

The simplest and most basic method of showing the formation of phthalocyanine complex is to observe the formation of green or blue colour as characteristic of phthalocyanine compounds [39]. The fact that all of the obtained compounds are either blue or green indicates that phthalocyanine compounds are formed. In addition, the disappearance of the C≡N peaks at 2230 cm-^{1} absorption bond in the FT-IR spectra of the complexes indicates the formation of phthalocyanine compounds.

Examination of the FT-IR spectra of the phthalocyanine complexes of a particle set of ligands indicates that they are very similar to each other [126]. However, the FT-IR spectra of all the complexes reported the major important spectral peaks are wıthin the following ranges for specific functional groups of 1169 – 1020 cm^{-1} for C-N bond, 1597 – 1457 cm^{-1} for C = C bond (aromatic), 1250 – 1228 cm^{-1} for Ar–O–R bond (ether), 1719 – 1660 cm^{-1} for carbonyl carbon C = O (of ester and amide), 2985 – 2922 cm^{-1} for CH bond (aliphatic), 3073 – 3070 cm^{-1} for Ar–H (aromatic) and 3320– 3160 cm^{-1} for N-H (amide) were observed [21]

One of the simplest and most accurate methods for determining optoelectronic properties is UV-visible spectroscopy [111]. Through this beam, several characteristics can be found in this study. Bandgap energy is one of the most important properties in optoelectronics. The level of absorption of light is different for materials since each is different from the other. The electronic structure of Pcs and the position of optical absorption spectra are predicted to substantial influence on nonlinear optical activity [131]. The ground state optical absorptions in Pcs are overlooked by two large absorption bands matching the Q and B bands in the visible or near-infrared (IR) (670–1000 nm) and UV (325–370 nm) sections of the spectrum. When compared to the Q band, the B band is less strong and occurs at much higher energies about 350 nm [132]. Due to the π–π* transition from the highest occupied molecular orbital (HOMO) to the energy gap of the lowest unoccupied molecular orbital (LUMO) of the metal phthalocyanine (MPc) ring. The extensive π-

system provides pathways for electron delocalization, enhancing the electronic conductivity of phthalocyanine. The material can effectively transport electrons, making it useful in organic electronic devices, such as organic photovoltaics and photodetectors [133, 134, 135, 136, 137].

Furthermore, thermogravimetric analysis (TGA) and differential thermal analysis (DTA) demonstrate the thermal stability properties of the compounds**.** The complexes were characterized and evaluated result as a good material for both scientific and technological applications. The thermograph of the complexes shows that all the complexes have a thermal stability range between 120 - 240 °C as the case may be, beyond that, they begin to decompose without undergoing melting, which means under normal conditions the complexes do not have a melting point. The DTA graph shows their degradation is exothermic.

The electrochemical behavior of the complexes is examined by techniques such as cyclic voltammetry (CV) and square wave voltammetry (SWV)**.** In terms of electrochemical properties, dipeptide-substituted metallo-phthalocyanines exhibit novel and unique properties in addition to the known redox response of phthalocyanines. These compounds have been characterized in detail using cyclic voltammetry (CV) and electrochemical impedance spectroscopy (EIS) techniques. The presence of dipeptide groups leads to shifts in the redox potentials of phthalocyanines and improvements in electrochemical stability. Such properties increase the potential of these compounds for electrocatalytic applications, energy storage devices, and biosensor technologies [12, 138].

The thermal properties of dipeptide-substituted phthalocyanines depend on the type and position of the substitution. The addition of dipeptides to the phthalocyanine structure generally increases thermal stability and increases decomposition temperatures. Electrochemically, the presence of dipeptide groups can shift redox potentials and enhance electron transfer efficiency. These properties are particularly important for applications such as sensors, electrocatalysts, and energy storage devices.

In conclusion, novel tyrosine-based dipeptide-substituted metallo-phthalocyanine complexes have significant potential in electrochemistry research. The development of synthesis methods and the detailed study of their thermal and electrochemical properties reveal valuable insights to support the use of these compounds in different application fields. Future studies will take important steps toward unlocking the wider application potential of these compounds

RECOMMENDATIONS

These results might pave the way for further research into the synthesis of new peptide substituted phthalocyanine complexes and investigation of their photodynamic therapy, antibacterial and other biochemical properties.

REFERENCES

[1] Das P., Chakraborty K., Chakrabarty S., Ghosh S.and, Pal T., (2017), Reduced Graphene Oxide-Zinc Phthalocyanine Composites as Fascinating Material for Optoelectronic and Photocatalytic Applications, ChemistrySelect, 2 (11), 3297-3305,

[2] Ertem B., Sarkı G., Yalazan H., Bıyıklıoğlu Z.and, Kantekin H., (2017), The synthesis and electrochemical characterization of new metallophthalocyanines containing 4-aminoantipyrine moieties on peripherally positions, *Inorganica Chimica Acta*, **462**, 123-129,

[3] Demirol M., Sirka L., Çalışkan E., Biryan F., Koran K., Görgülü A. O.and, Yakuphanoğlu F., (2020), Synthesis and photodiode properties of chalcone substituted metallo-phthalocyanine, *Journal of Molecular Structure*, **1219**, 128571,

[4] Chen D., Song M., Huang J., Chen N., Xue J.and, Huang M., (2020), Photocyanine: A novel and effective phthalocyanine-based photosensitizer for cancer treatment, *Journal of Innovative Optical Health Sciences*, **13** (03), 2030009, 10.1142/s1793545820300098.

[5] Kurt Ö., Özçeşmeci İ., Koca A., Gül A.and, Koçak M. B., (2017), Synthesis, photophysical and electrochemical properties of novel hexadeca-substituted phthalocyanines bearing naphthoxy groups, *Dyes and Pigments*, **137**, 236-243,

[6] Ağırtaş M. S., Altındal A., Salih B., Saydam S.and, Bekaroğlu Ö., (2011), Synthesis, characterization, and electrochemical and electrical properties of novel mono and ball-type metallophthalocyanines with four 9, 9-bis (4-hydroxyphenyl) fluorene, *Dalton Transactions*, **40** (13), 3315-3324,

[7] Ceyhan T., Özdağ M. A., Salih B., Erbil M. K., Elmalı A., Özkaya A. R.and, Bekaroğlu Ö., (2008), Synthesis, Characterization, Nonlinear Absorption and Electrochromic Properties of Double-Decker Octakis (mercaptopropylisobutyl-POSS) phthalocyaninatolanthanide (III) Complexes, Wiley Online Library.

[8] Ahmedzade P., Demirelli K., Günay T., Biryan F.and, Alqudah O., (2015), Effects of Waste Polypropylene Additive on the Properties of Bituminous Binder, *Procedia Manufacturing*, **2**, 165-170, https://doi.org/10.1016/j.promfg.2015.07.029.

[9] Yang S., Yu Y., Gao X., Zhang Z.and, Wang F., (2021), Recent advances in electrocatalysis with phthalocyanines, *Chemical Society Reviews*, **50** (23), 12985-13011,

[10] Liu W., Jensen T. J., Fronczek F. R., Hammer R. P., Smith K. M.and, Vicente M. G. H., (2005), Synthesis and cellular studies of nonaggregated water-soluble phthalocyanines, *Journal of medicinal chemistry*, **48** (4), 1033-1041,

[11] Wang J., Khanamiryan A. K.and, Leznoff C. C., (2004), Multisubstituted phthalonitriles for phthalocyanine synthesis, *Journal of Porphyrins and Phthalocyanines*, **8** (11), 1293-1299,

[12] Koran K., Çalışkan E., Öztürk D. A., Çapan İ., Tekin S., Sandal S.and, Görgülü A. O., (2023), The first peptide derivatives of dioxybiphenyl-bridged spiro cyclotriphosphazenes: In vitro cytotoxicity activities and DNA damage studies, *Bioorganic Chemistry*, **132**, 106338,

[13] Tataroglu A., Koran K., Çaliskan E., Al-Sehemi A. G., Görgülü A. O., Al-Ghamdi A.and, Yakuphanoglu F., (2019), Metallo-Phthalocyanines Based Photocapacitors, *Silicon*, **11**, 1275-1286,

[14] Jia N., He C., Wang S., Song W., Chen Z., Zu Y., Gao Y.and, Dong Y., (2018), Effect of central metals and peripheral substituents on the third-order nonlinear optical properties of tetra-benzimidazole and benzothiazole substituted phthalocyanines, *Optical Materials*, **76**, 81-89,

[15] Kakı E., Gögsu N., Altındal A., Salih B.and, Bekaroğlu Ö., (2019), Synthesis, characterization and VOCs adsorption kinetics of diethylstilbestrol-substituted metallophthalocyanines, *Journal of Porphyrins and Phthalocyanines*, **23** (01n02), 166-174,

[16] Farajzadeh N., Özdemir S., Tollu G., Bayır Z. A.and, Koçak M. B., (2022), Biological properties of hexadeca-substituted metal phthalocyanines bearing different functional groups, *Journal of Inorganic Biochemistry*, **234**, 111888,

[17] Pontón I.and, Sánchez-García D., (2021), Preparation of porphyrin and phthalocyanine conjugates for biomedical applications, *Journal of Porphyrins and Phthalocyanines*, **25** (10n12), 917-929,

[18] Dognini P., Coxon C. R., Alves W. A.and, Giuntini F., (2021), Peptide-Tetrapyrrole Supramolecular Self-Assemblies: State of the Art, *Molecules*, **26** (3), 693,

[19] Ke M. R., Yeung S. L., Fong W. P., Ng D. K.and, Lo P. C., (2012), A phthalocyanine–peptide conjugate with high in vitro photodynamic activity and enhanced in vivo tumor-retention property, *Chemistry–A European Journal*, **18** (14), 4225-4233,

[20] Shah A., Adhikari B., Martic S., Munir A., Shahzad S., Ahmad K.and, Kraatz H.-B., (2015), Electron transfer in peptides, *Chemical Society Reviews*, **44** (4), 1015-1027,

[21] Şenoğlu S., Güleç M., Dokgöz E. Y., Öztürk A. B., İzbudak B., Salih B., Olgun A.and, Ceyhan T., (2023), Synthesis, characterization, in vitro cytotoxicity of novel metallo phthalocyanines with four methylpropiophenonyl clusters and their effects on Caenorhabditis elegans thermotolerance, *Chemical Papers*, **77** (3), 1561-1572,

[22] Göksel M., Durmuş M.and, Atilla D., (2016), Peptide-substituted phthalocyanine photosensitizers: design, synthesis, photophysicochemical and photobiological studies, *Photochemical & Photobiological Sciences*, **15**, 1318-1329,

[23] Nesterova I. V., Verdree V. T., Pakhomov S., Strickler K. L., Allen M. W., Hammer R. P.and, Soper S. A., (2007), Metallo-phthalocyanine near-IR fluorophores: Oligonucleotide conjugates and their applications in PCR assays, *Bioconjugate chemistry*, **18** (6), 2159-2168,

[24] Mudyiwa M., Ndinguri M. W., Soper S. A.and, Hammer R. P., (2010), Microwave assisted solid-phase synthesis of substituted tetraazaporphyrins and a phthalocyanine-peptide conjugate, *Journal of Porphyrins and Phthalocyanines*, **14** (10), 891-903,

[25] Erdem S. S., Nesterova I. V., Soper S. A.and, Hammer R. P., (2009), Mono-amine functionalized phthalocyanines: microwave-assisted solid-phase synthesis and bioconjugation strategies, *The Journal of organic chemistry*, **74** (24), 9280-9286,

[26] Erdem S. S., Nesterova I. V., Soper S. A.and, Hammer R. P., (2008), Solid-phase synthesis of asymmetrically substituted "AB3-type" phthalocyanines, *The Journal of organic chemistry*, **73** (13), 5003-5007,

[27] Nemykin V. N.and, Lukyanets E. A., (2010), Synthesis of substituted phthalocyanines, *ARKIVOC: Online Journal of Organic Chemistry*,

[28] Kobayashi N.and, Fukuda T., (2006), Recent progress in phthalocyanine chemistry: Synthesis and characterization, *Functional dyes*, 1-45,

[29] Isago H., (2015), Optical spectra of phthalocyanines and related compounds, *NIMS Monographs*,

[30] Hamam K. J.and, Alomari M. I., (2017), A study of the optical band gap of zinc phthalocyanine nanoparticles using UV–Vis spectroscopy and DFT function, *Applied Nanoscience*, **7** (5), 261-268,

[31] El-Nahass M., Abd-El-Rahman K.and, Darwish A., (2005), Fourier-transform infrared and UV–vis spectroscopes of nickel phthalocyanine thin films, *Materials Chemistry and Physics*, **92** (1), 185-189,

[32] Albeiicio F., Chinchilla R., Dodsworth D. J.and, Najera C., (2001), New trends in peptide coupling reagents, *Organic Preparations and Procedures International*, **33** (3), 203-303,

[33] Montalbetti C. A.and, Falque V., (2005), Amide bond formation and peptide coupling, *Tetrahedron*, **61** (46), 10827-10852,

[34] Sibrian-Vazquez M., Ortiz J., Nesterova I. V., Fernández-Lázaro F., Sastre-Santos A., Soper S. A.and, Vicente M. G. H., (2007), Synthesis and properties of cell-targeted Zn (II)− phthalocyanine− peptide conjugates, *Bioconjugate chemistry*, **18** (2), 410-420,

[35] Liu Q., Pang M., Tan S., Wang J., Chen Q., Wang K., Wu W.and, Hong Z., (2018), Potent peptide-conjugated silicon phthalocyanines for tumor photodynamic therapy, *Journal of Cancer*, **9** (2), 310,

[36] Linstead R., (1934), 212. Phthalocyanines. Part I. A new type of synthetic colouring matters, *Journal of the Chemical Society (Resumed)*, 1016-1017,

[37] Linstead R.and, Lowe A., (1934), 214. Phthalocyanines. Part III. Preliminary experiments on the preparation of phthalocyanines from phthalonitrile, *Journal of the Chemical Society (Resumed)*, 1022-1027,

[38] McKeown N. B., (1998), *Phthalocyanine materials: synthesis, structure and function*, Cambridge university press 0521496233.

[39] Engel M. K.and, Hokoku K. R. K., (1997), Single-crystal and solid-state molecular structures of phthalocyanine complexes, *Kawamura Rikagaku Kenkyusho Hokoku*, **8**, 11-54,

[40] Özil M., Ağar E., Şaşmaz S., Kahveci B., Akdemir N.and, Gümrükçüoğlu İ. E., (2007), Microwave-assisted synthesis and characterization of the monomeric phthalocyanines containing naphthalene-amide group moieties and the polymeric phthalocyanines containing oxa-aza bridge, *Dyes and Pigments*, **75** (3), 732-740,

[41] Akkoç B., Samsunlu T., Işık Ş., Özçeşmeci M., Atmaca G. Y., Erdoğmuş A., Serhatlı M.and, Hamuryudan E., (2022), Pegylated metal-free and zinc(ii) phthalocyanines: synthesis, photophysicochemical properties and in vitro photodynamic activities against head, neck and colon cancer cell lines, *Dalton Transactions*, **51** (26), 10136-10147, 10.1039/D2DT00704E.

[42] Szwajca A.and, Pankiewicz R., (2024), Quantum Chemical Stability Analysis of Phthalocyanine Metal One-Dimensional Polymers with Bidentate Ligands, *Molecules*, **29** (17), 4111,

[43] Hussein N. A., (1990), Semiconducting properties of some u-bridged phthalocyanines, University of Nottingham.

[44] Moser F. H.and, Thomas A. L., (1964), Phthalocyanine compounds, *Journal of Chemical Education*, **41** (5), 245,

[45] Hamad O. A., Kareem R. O.and, Omer P. K., (2024), Properties, Characterization, and Application of Phthalocyanine and Metal Phthalocyanine, *Journal of Chemical Reviews*, **6** (1),

[46] Leznoff C. C., D'Ascanio A. M.and, Yildiz S. Z., (2000), Phthalocyanine formation using metals in primary alcohols at room temperature, *Journal of Porphyrins and Phthalocyanines*, **4** (1), 103-111,

[47] Brinkmann M., Wittmann J., Chaumont C.and, Andre J., (1997), Effects of solvent on the morphology and crystalline structure of lithium phthalocyanine thin films and powders, *Thin Solid Films*, **292** (1-2), 192-203,

[48] D'Ascanio A. M., (1999), A study of solvent and metal effects on the formation of phthalocyanines at room temperature, York University Ontario.

[49] Iwatsu F., Kobayashi T.and, Uyeda N., (1980), Solvent effects on crystal growth and transformation of zinc phthalocyanine, *The journal of physical chemistry*, **84** (24), 3223-3230,

[50] Suito E.and, Uyeda N., (1963), Transformation and growth of copper-phthalocyanine crystal in organic suspension, *Kolloid-Zeitschrift und Zeitschrift für Polymere*, **193**, 97-111,

[51] Hoshino A., Takenaka Y.and, Miyaji H., (2003), Redetermination of the crystal structure of α-copper phthalocyanine grown on KCl, *Acta Crystallographica Section B: Structural Science*, **59** (3), 393-403,

[52] Lozzi L., Santucci S., La Rosa S., Delley B.and, Picozzi S., (2004), Electronic structure of crystalline copper phthalocyanine, *The Journal of chemical physics*, **121** (4), 1883-1889,

[53] Cruickshank A. C., Dotzler C. J., Din S., Heutz S., Toney M. F.and, Ryan M. P., (2012), The crystalline structure of copper phthalocyanine films on ZnO (1100), *Journal of the American Chemical Society*, **134** (35), 14302-14305,

[54] Basova T., Semyannikov P., Plyashkevich V., Hassan A.and, Igumenov I., (2009), Volatile phthalocyanines: vapor pressure and thermodynamics, *Critical reviews in solid state and materials sciences*, **34** (3-4), 180-189,

[55] Thomas A. L., (2024), *Phthalocyanine research and applications*, CRC Press 104028146X.

[56] Lawton E. A., (1958), The thermal stability of copper phthalocyanine, *The journal of physical chemistry*, **62** (3), 384-384,

[57] Yılmaz E., (2015), Yeni bis-ftalosiyanin bileşiklerinin sentezi, karakterizasyonu ve termal özelliklerinin araştırılması/syenthesis and characterization of new bis-phthalocyanine compounds and investigation of thermal properties.

[58] Leznoff C.and, Lever A., (1989), Properties and Applications, *VCH New York*,

[59] de Keijzer M., (2014), The delight of modern organic pigment creations, *Issues in contemporary oil paint*, 45-73,

[60] Li F., Gentemann S., Kalsbeck W. A., Seth J., Lindsey J. S., Holten D.and, Bocian D. F., (1997), Effects of central metal ion (Mg, Zn) and solvent on singletexcited-state energy flow in porphyrin-based nanostructures, *Journal of Materials Chemistry*, **7** (7), 1245-1262,

[61] Leznoff C. C., (1989), Phthalocyanines, *Properties and Applications*,

[62] Bekaroğlu Ö., (1996), Phthalocyanines containing macrocycles, *Applied organometallic chemistry*, **10** (8), 605-622,

[63] Christie R., (2014), *Colour chemistry*, Royal Society of Chemistry 1849733287.

[64] Brown S. B., Brown E. A.and, Walker I., (2004), The present and future role of photodynamic therapy in cancer treatment, *The lancet oncology*, **5** (8), 497-508,

[65] Yano S., Hirohara S., Obata M., Hagiya Y., Ogura S.-i., Ikeda A., Kataoka H., Tanaka M.and, Joh T., (2011), Current states and future views in photodynamic therapy, *Journal of Photochemistry and Photobiology C: Photochemistry Reviews*, **12** (1), 46-67,

[66] Allison R. R.and, Sibata C. H., (2010), Oncologic photodynamic therapy photosensitizers: a clinical review, *Photodiagnosis and photodynamic therapy*, **7** (2), 61-75,

[67] Dolmans D. E., Fukumura D.and, Jain R. K., (2003), Photodynamic therapy for cancer, *Nature reviews cancer*, **3** (5), 380-387,

[68] Jiang Z., Shao J., Yang T., Wang J.and, Jia L., (2014), Pharmaceutical development, composition and quantitative analysis of phthalocyanine as the photosensitizer for cancer photodynamic therapy, *Journal of pharmaceutical and biomedical analysis*, **87**, 98-104,

[69] Allison R., Mota H.and, Sibata C., (2004), Clinical PD/PDT in North America: an historical review, *Photodiagnosis and photodynamic therapy*, **1** (4), 263-277,

[70] Emmelius M., Pawlowski G.and, Vollmann H. W., (1989), Materials for optical data storage, *Angewandte Chemie International Edition in English*, **28** (11), 1445-1471,

[71] Bouvet M.and, Pauly A., (2006), Molecular semiconductor-based gas sensors, American Scientific Publishers Los Angeles, CA, USA, pp. 227-270.

[72] Britannica I. E., (1957), *Encyclopædia britannica*, Encyclopaedia Britannica, Incorporated

[73] Zhou R., Josse F., Göpel W., Öztürk Z.and, Bekaroğlu Ö., (1996), Phthalocyanines as sensitive materials for chemical sensors, *Applied organometallic chemistry*, **10** (8), 557-577,

[74] Spadavecchia J., Ciccarella G.and, Rella R., (2005), Optical characterization and analysis of the gas/surface adsorption phenomena on phthalocyanines thin films for gas sensing application, *Sensors and Actuators B: Chemical*, **106** (1), 212-220,

[75] Ho K.-C.and, Tsou Y.-H., (2001), Chemiresistor-type NO gas sensor based on nickel phthalocyanine thin films, *Sensors and Actuators B: Chemical*, **77** (1-2), 253-259,

[76] Capone S., Mongelli S., Rella R., Siciliano P.and, Valli L., (1999), Gas sensitivity measurements on NO2 sensors based on copper (II) tetrakis (n-butylaminocarbonyl) phthalocyanine LB films, *Langmuir*, **15** (5), 1748-1753,

[77] Gounden D., Nombona N.and, Van Zyl W. E., (2020), Recent advances in phthalocyanines for chemical sensor, non-linear optics (NLO) and energy storage applications, *Coordination Chemistry Reviews*, **420**, 213359,

[78] Wring S. A., Hart J. P., Bracey L.and, Birch B. J., (1990), Development of screen-printed carbon electrodes, chemically modified with cobalt phthalocyanine, for electrochemical sensor applications, *Analytica chimica acta*, **231**, 203-212,

[79] Demir E., Silah H.and, Uslu B., (2022), Phthalocyanine modified electrodes in electrochemical analysis, *Critical Reviews in Analytical Chemistry*, **52** (2), 425-461,

[80] Güngör S., Taşaltın C., Gürol İ., Baytemir G., Karakuş S.and, Taşaltın N., (2022), Copper phthalocyanine-borophene nanocomposite-based non-enzymatic electrochemical urea biosensor, *Applied Physics A*, **128** (1), 89,

[81] Mashazi P. N., Ozoemena K. I.and, Nyokong T., (2006), Tetracarboxylic acid cobalt phthalocyanine SAM on gold: Potential applications as amperometric sensor for H2O2 and fabrication of glucose biosensor, *Electrochimica Acta*, **52** (1), 177-186,

[82] Wang K., Xu J.-J.and, Chen H.-Y., (2005), A novel glucose biosensor based on the nanoscaled cobalt phthalocyanine–glucose oxidase biocomposite, *Biosensors and Bioelectronics*, **20** (7), 1388-1396,

[83] Brogdon P., Cheema H.and, Delcamp J. H., (2018), Near-infrared-absorbing metal-free organic, porphyrin, and phthalocyanine sensitizers for panchromatic dye-sensitized solar cells, *ChemSusChem*, **11** (1), 86-103,

[84] Gao D., Wong R. C., Wang Y., Guo X., Yang Z.and, Lo P.-C., (2020), Shifting the absorption to the near-infrared region and inducing a strong photothermal effect by encapsulating zinc (II) phthalocyanine in poly (lactic-co-glycolic acid)-hyaluronic acid nanoparticles, *Acta Biomaterialia*, **116**, 329-343,

[85] Fabian J., Nakazumi H.and, Matsuoka M., (1992), Near-infrared absorbing dyes, *Chemical Reviews*, **92** (6), 1197-1226,

[86] Henari F., Davey A., Blau W., Haisch P.and, Hanack M., (1999), The electronic and non-linear optical properties of oxo-titanium phthalocyanines, *Journal of Porphyrins and Phthalocyanines*, **3** (5), 331-338,

[87] Safian N. A. M., Anuar A., Omar A.-Z., Bawazeer T. M., Alsenany N., Alsoufi M. S., Supangat A.and, Roslan N. A., (2021), Enhanced sensitivity of zinc phthalocyanine-based microporous humidity sensors by varying size of electrode gaps, *Sensors and Actuators B: Chemical*, **343**, 130158,

[88] CP K. P., Aralekallu S.and, Koodlur Sannegowda L., (2024), Efficacy of Phthalocyanine-Based Catalysts in Electrochemical Sensors: A Comprehensive Review, *Advanced Sensor Research*, **3** (12), 2400088,

[89] Kerdcharoen T.and, Kladsomboon S., (2013), Optical chemical sensor and electronic nose based on porphyrin and phthalocyanine, *Applications of Nanomaterials in Sensors and Diagnostics*, 237-255,

[90] Kim S., Brady J., Al-Badani F., Yu S., Hart J., Jung S., Tran T.-T.and, Myung N. V., (2021), Nanoengineering approaches toward artificial nose, *Frontiers in Chemistry*, **9**, 629329,

[91] Li Y., Wang Z., Zhao T., Li H., Jiang J.and, Ye J., (2024), Electronic nose for the detection and discrimination of volatile organic compounds: Application, challenges, and perspectives, *TrAC Trends in Analytical Chemistry*, 117958,

[92] Rollmann L. D.and, Iwamoto R. T., (1968), Electrochemistry, electron paramagnetic resonance, and visible spectra of cobalt, nickel, copper, and metal-free phthalocyanines in dimethyl sulfoxide, *Journal of the American Chemical Society*, **90** (6), 1455-1463,

[93] Geiger D. K., Ferraudi G., Madden K., Granifo J.and, Rillema D. P., (1985), Redox reactivity of transition-metal phthalocyanines: ligand radical formation vs. metal center oxidation, *The journal of physical chemistry*, **89** (18), 3890-3894, 10.1021/j100264a025.

[94] Kumar A., Zhang G., Liu W.and, Sun X., (2022), Electrocatalysis and activity descriptors with metal phthalocyanines for energy conversion reactions, *Journal of Electroanalytical Chemistry*, **922**, 116799,

[95] Huang S., Chen K.and, Li T.-T., (2022), Porphyrin and phthalocyanine based covalent organic frameworks for electrocatalysis, *Coordination Chemistry Reviews*, **464**, 214563,

[96] Aralekallu S., Sannegowda L. K.and, Singh V., (2023), Developments in electrocatalysts for electrocatalytic hydrogen evolution reaction with reference to bio-inspired phthalocyanines, *International Journal of Hydrogen Energy*, **48** (44), 16569-16592,

[97] Monama G. R., Modibane K. D., Ramohlola K. E., Molapo K. M., Hato M. J., Makhafola M. D., Mashao G., Mdluli S. B.and, Iwuoha E. I., (2019), Copper (II) phthalocyanine/metal organic framework electrocatalyst for hydrogen evolution reaction application, *International Journal of Hydrogen Energy*, **44** (34), 18891-18902,

[98] Chen L., Sagar R. U. R., Chen J., Liu J., Aslam S., Nosheen F., Anwar T., Hussain N., Hou X.and, Liang T., (2021), Cobalt phthalocyanine as an efficient catalyst for hydrogen evolution reaction, *International Journal of Hydrogen Energy*, **46** (37), 19338-19346,

[99] Nikoloudakis E., López-Duarte I., Charalambidis G., Ladomenou K., Ince M.and, Coutsolelos A. G., (2022), Porphyrins and phthalocyanines as biomimetic tools for photocatalytic H 2 production and CO 2 reduction, *Chemical Society Reviews*, **51** (16), 6965-7045,

[100] Zhao Y.-Y., Zhang L., Chen Z., Zheng B.-Y., Ke M., Li X.and, Huang J.-D., (2021), Nanostructured phthalocyanine assemblies with efficient synergistic effect of type I photoreaction and photothermal action to overcome tumor hypoxia in photodynamic therapy, *Journal of the American Chemical Society*, **143** (34), 13980-13989,

[101] Nabid M., Sedghi R., Jamaat P., Safari N.and, Entezami A., (2007), Catalytic oxidative polymerization of aniline by using transition-metal tetrasulfonated phthalocyanine, *Applied Catalysis A: General*, **328** (1), 52-57,

[102] Stiven A., (2022), Synthesis and characterisation of novel phthalocyanine-based porous materials,

[103] Rajagopal G., Kim S.-S.and, Kwak J.-M., (2006), Aluminium phthalocyanine: an active and simple catalyst for cyanosilylation of ketones, *Bulletin of the Korean Chemical Society*, **27** (11), 1907-1909,

[104] Singhal S., Jain S. L.and, Sain B., (2010), Heterogeneously Catalyzed Oxidative Cyanation of Tertiary Amines with Sodium Cyanide/Hydrogen Peroxide using Polymer-Supported Iron (II) Phthalocyanines as Catalyst, *Advanced Synthesis & Catalysis*, **352** (8), 1338-1344,

[105] Martynov A. G., Birin K. P., Gorbunova Y. G.and, Tsivadzea A. Y., (2013), Modern synthetic approaches to phthalonitriles with special emphasis on transition-metal catalyzed cyanation reactions, *Macroheterocycles*, **6**, 23-32,

[106] Gamelas S. R., Tomé J. P., Tomé A. C.and, Lourenço L. M., (2023), Advances in photocatalytic degradation of organic pollutants in wastewaters: harnessing the power of phthalocyanines and phthalocyanine-containing materials, *RSC advances*, **13** (48), 33957-33993,

[107] Meunier B.and, Sorokin A., (1997), Oxidation of pollutants catalyzed by metallophthalocyanines, *Accounts of Chemical Research*, **30** (11), 470-476,

[108] Kluson P., Drobek M., Zsigmond A., Baranyi J., Bata P., Zarubova S.and, Kalaji A., (2009), Environmentally friendly phthalocyanine catalysts for water decontamination—Non-photocatalytic systems, *Applied Catalysis B: Environmental*, **91** (3-4), 605-609,

[109] Mahmiani Y., Sevim A. M.and, Gül A., (2016), Photocatalytic degradation of persistent organic pollutants under visible irradiation by TiO2 catalysts sensitized with Zn (II) and Co (II) tetracarboxy-phthalocyanines, *Journal of Porphyrins and Phthalocyanines*, **20** (08n11), 1190-1199,

[110] Nevin W., (1983), *Photovoltaic properties of some tetraphenylporphyrins*, Nottingham Trent University (United Kingdom) 1369326882.

[111] Mamand D., Anwer T. K., Qadr H.and, Mussa C. H., (2022), Investigation of spectroscopic and optoelectronic properties of phthalocyanine molecules, *Russian Journal of General Chemistry*, **92** (9), 1827-1838,

[112] Moussavi M., De Cian A., Fischer J.and, Weiss R., (1988), Synthesis, structure and spectroscopic properties of the reduced and reduced protonated forms of lutetium diphthalocyanine, *Inorganic Chemistry*, **27** (7), 1287-1291,

[113] Basova T., Gürek A. G., Ahsen V.and, Ray A., (2013), Electrochromic lutetium phthalocyanine films for in situ detection of NADH, *Optical Materials*, **35** (3), 634-637,

[114] Karadağ S., Bozoğlu C., Şener M. K.and, Koca A., (2014), Synthesis and electrochemical properties of a double-decker lutetium (III) phthalocyanine bearing electropolymerizable substituents on non-peripheral positions, *Dyes and Pigments*, **100**, 168-176,

[115] Gregory P., (2012), Industrial applications of phthalocyanines, *Journal of Porphyrins and Phthalocyanines*,

[116] Sharman W. M. and, Van Lier J. E., (2000), Synthesis of Phthalocyanine 97, The Porphyrin Handbook: Phthalocyanines: Spectroscopic and Electrochemical Characterization, **16**, 1,

[117] Özdemir Ü. Ö., Aktan E., Ilbiz F., Gündüzalp A. B., Özbek N., Sarı M., Çelik Ö.and, Saydam S., (2014), Characterization, antibacterial, anticarbonic anhydrase II isoenzyme, anticancer,

electrochemical and computational studies of sulfonic acid hydrazide derivative and its Cu (II) complex, *Inorganica Chimica Acta*, **423**, 194-203,

[118] Armarego W. L., (2022), Purification of laboratory chemicals: Part 2 inorganic chemicals, catalysts, biochemicals, physiologically active chemicals, nanomaterials, Butterworth-Heinemann 0323958281.

[119] Shago R. F., (2010), Syntheses, electrochemistry and spectroscopic studies of metallocene-containing porphyrin complexes with biomedical applications, University of the Free State.

[120] Rebis T., Lijewski S., Nowicka J., Popenda L., Sobotta L., Jurga S., Mielcarek J., Milczarek G.and, Goslinski T., (2015), Electrochemical properties of metallated porphyrazines possessing isophthaloxybutylsulfanyl substituents: Application in the electrocatalytic oxidation of hydrazine, *Electrochimica Acta*, **168**, 216-224,

[121] Masa J., Ozoemena K. I., Schuhmann W.and, Zagal J. H., (2013), Fundamental studies on the electrocatalytic properties of metal macrocyclics and other complexes for the electroreduction of O2, Electrocatalysis in Fuel Cells: A Non-and Low-Platinum Approach, Springer, pp. 157-212,

[122] Koifman O. I., Ageeva T. A., Beletskaya I. P., Averin A. D., Yakushev A. A., Tomilova L. G., Dubinina T. V., Tsivadze A. Y., Gorbunova Y. G.and, Martynov A. G., (2020), Macroheterocyclic compounds a key building block in new functional materials and molecular devices, *Макрогетероциклы*, **13** (4), 311-467,

[123] Perevalov V., Vinokurov E., Zuev K., Vasilenko E.and, Tsivadze A. Y., (2017), Modification and application of metal phthalocyanines in heterogeneous systems, *Protection of Metals and Physical Chemistry of Surfaces*, **53**, 199-214,

[124] Gorbunova Y. G., Martynov A., Tsivadze A. Y., Kadish K., Smith K.and, Guilard R., (2012), Handbook of Porphyrin Science, Kad ish, KM, Smith, KM, and Guilard, R., Eds., Sin gapore: World Scientific.

[125] Gorbunova Y. G., Lapkina L. A.and, Tsivadze A. Y., (2003), Supramolecular systems constructed from crownphthalocyaninates, *J. Coord. Chem.*, **56** (14), 1223-1232,

[126] Aktaş Kamiloğlu A., Akyüz D., Koca A.and, Acar İ., (2018), Synthesis and investigation of spectroelectrochemical properties of peripherally tetra-substituted phthalocyanine bearing 3-(4-{[3-(trifluoromethyl) benzyl] oxy} phenyl) propan-1-ol and its metallo compounds, *Journal of Inclusion Phenomena and Macrocyclic Chemistry*, **92**, 223-235,

[127] Cui L., Liu Y.and, He X., (2014), Iron (II) tetraaminophthalocyanine functionalized graphene: synthesis, characterization and their application in direct methanol fuel cell, *Journal of Electroanalytical Chemistry*, **727**, 91-98,

[128] Jin Z., Nolan K., McArthur C., Lever A.and, Leznoff C., (1994), Synthesis, electrochemical and spectroelectrochemical studies of metal-free 2, 9, 16, 23-tetraferrocenylphthalocyanine, *Journal of organometallic chemistry*, **468** (1-2), 205-212,

[129] Matemadombo F., David Maree M., Ozoemena K. I., Westbroek P.and, Nyokong T., (2005), Synthesis, electrochemical and spectroelectrochemical studies of octaphenylthio-substituted phthalocyanines, *Journal of Porphyrins and Phthalocyanines*, **9** (07), 484-490,

[130] Nevin W., Liu W., Melnik M.and, Lever A., (1986), Spectro-electrochemistry of cobalt and iron tetrasulphonated phthalocyanines, *Journal of electroanalytical chemistry and interfacial electrochemistry*, **213** (2), 217-234,

[131] Drechsel J., Männig B., Kozlowski F., Pfeiffer M., Leo K.and, Hoppe H., (2005), Efficient organic solar cells based on a double pin architecture using doped wide-gap transport layers, *Applied Physics Letters*, **86** (24),

[132] Mamand D. M.and, Qadr H. M., (2023), Optoelectronic properties of benzimidazobenzophenanthroline thin film, *Russian Microelectronics*, **52** (4), 325-336,

[133] Chen C.-Y., Tan G.-H., Hsu H.-L., Chen C.-P.and, Lin H.-W., (2020), Recent progress on advanced optical structures for emerging photovoltaics and photodetectors, *Advanced Energy and Sustainability Research*, **1** (1), 2000035,

[134] Lin C.-F., Zhang M., Liu S.-W., Chiu T.-L.and, Lee J.-H., (2011), High photoelectric conversion efficiency of metal phthalocyanine/fullerene heterojunction photovoltaic device, *International journal of molecular sciences*, **12** (1), 476-505,

[135] Islam Z. U., Tahir M., Syed W. A., Aziz F., Wahab F., Said S. M., R. Sarker M., Md Ali S. H.and, Sabri M. F. M., (2020), Fabrication and Photovoltaic Properties of Organic Solar Cell Based on Zinc Phthalocyanine, *Energies*, **13** (4), 962,

[136] Yoon S. M., Lou S. J., Loser S., Smith J., Chen L. X., Facchetti A.and, Marks T., (2012), Fluorinated Copper Phthalocyanine Nanowires for Enhancing Interfacial Electron Transport in Organic Solar Cells, *Nano Letters*, **12** (12), 6315-6321, 10.1021/nl303419n.

[137] Kaur N., Singh M., Pathak D., Wagner T. and, Nunzi J., (2014), Organic materials for photovoltaic applications: Review and mechanism, *Synthetic Metals*, **190**, 20-26,

[138] Idris S., Çalışkan E. and, Saydam S., (2024), Synthesis, Thermal and Electrochemical Properties of Dipeptide Substituted Metallo-Phthalocyanine Complexes, *MW Journal of Science*, **1** (3), 25-40,

APPENDICES

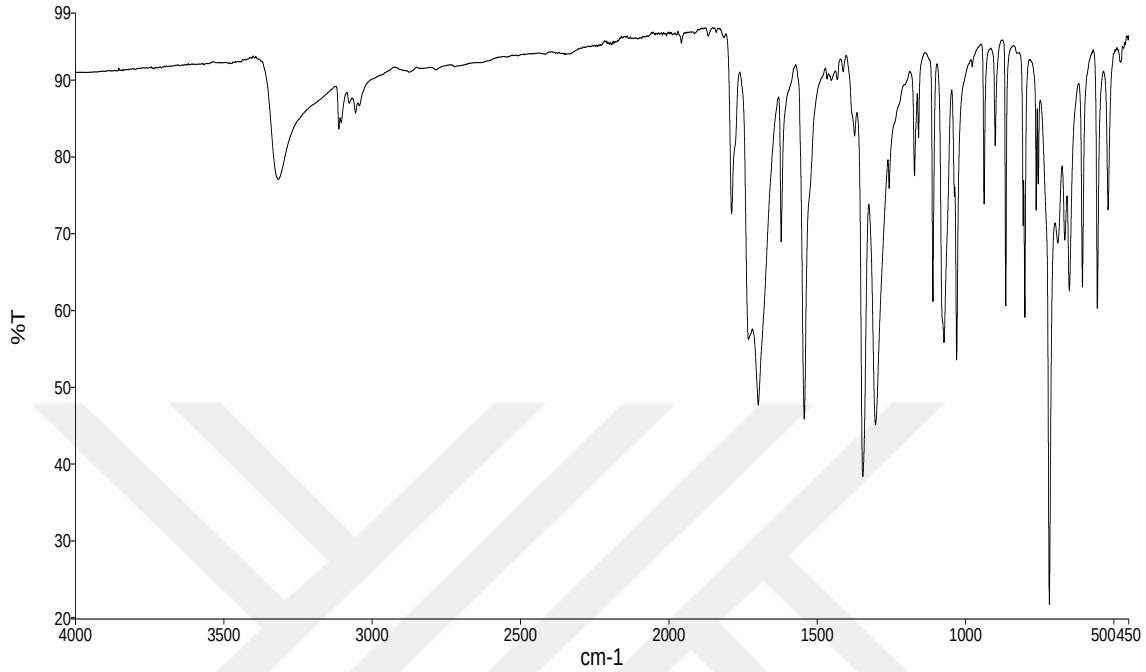

Appendix-1.1: FT-IR spectrum of 4-nitrophthalimide **(2)**

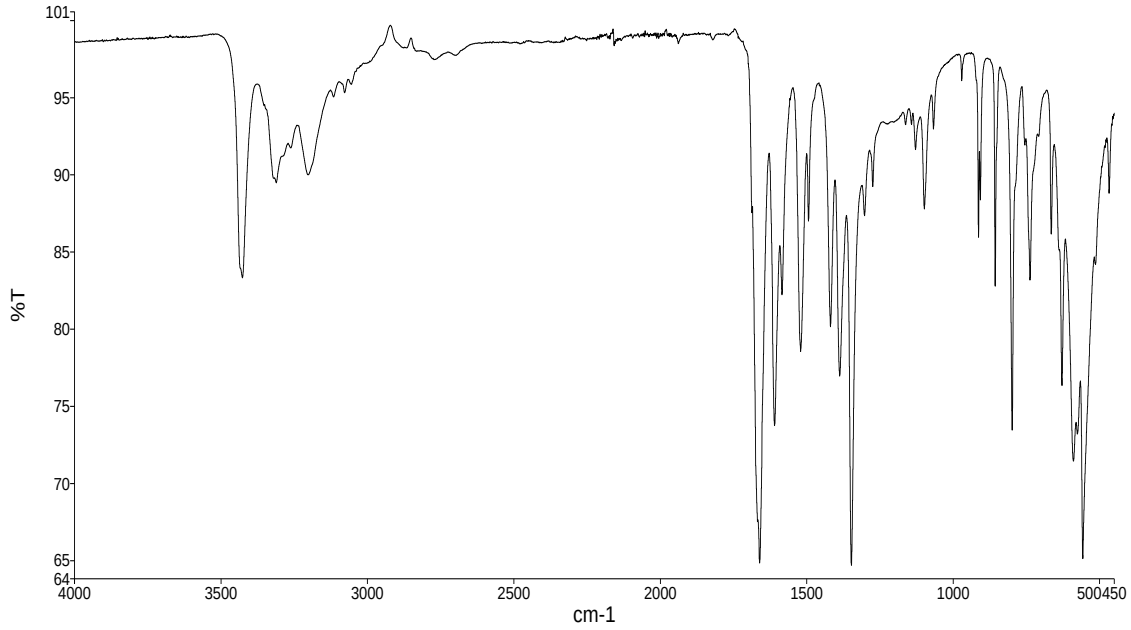

Appendix-1.2: FT-IR spectrum of 4-nitrophthalamide **(3)**

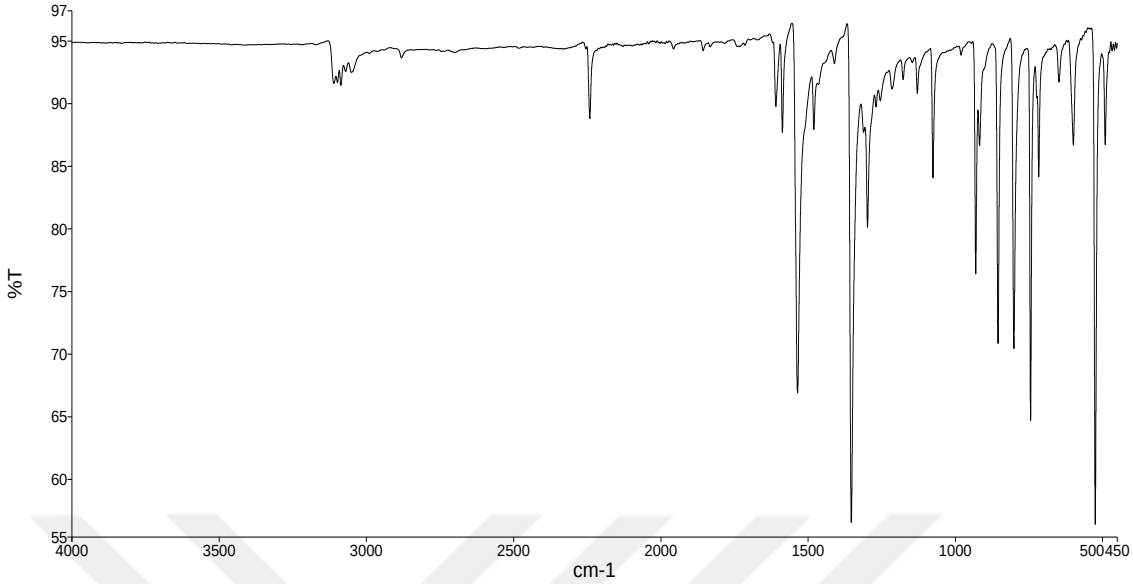

Appendix-1.3: FT-IR spectrum of 4-nitrophthalonitrile (4)

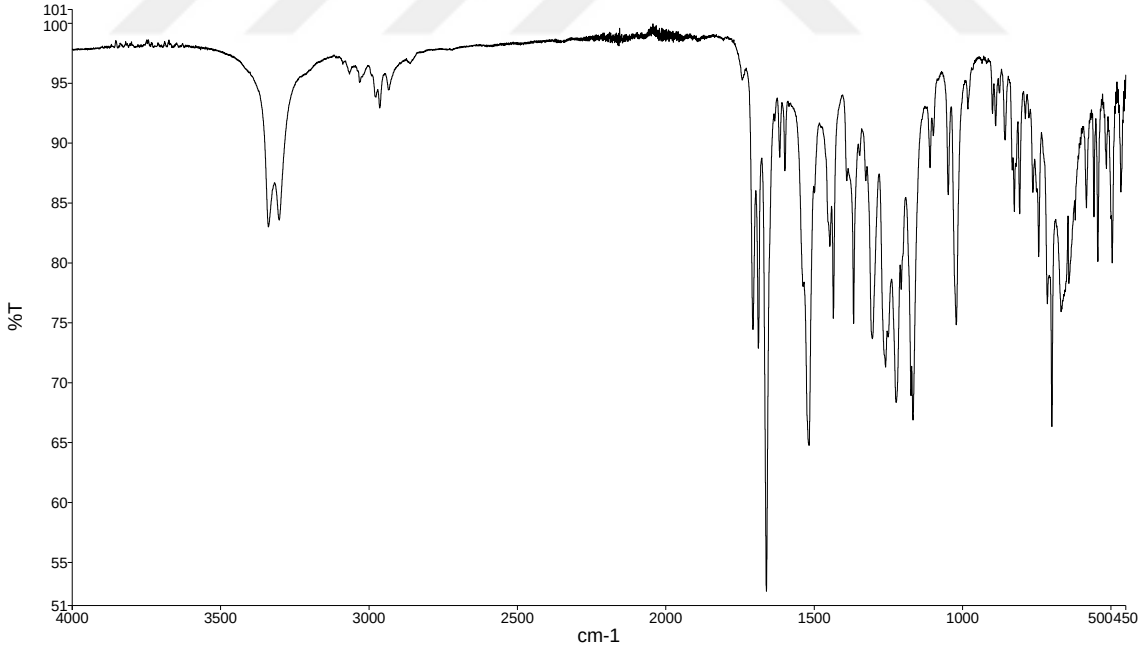

Appendix-2: FT-IR spectrum of methyl (tert-butoxycarbonyl)-L-tyrosyl-D-phenylalaninate dipeptide **(6)**

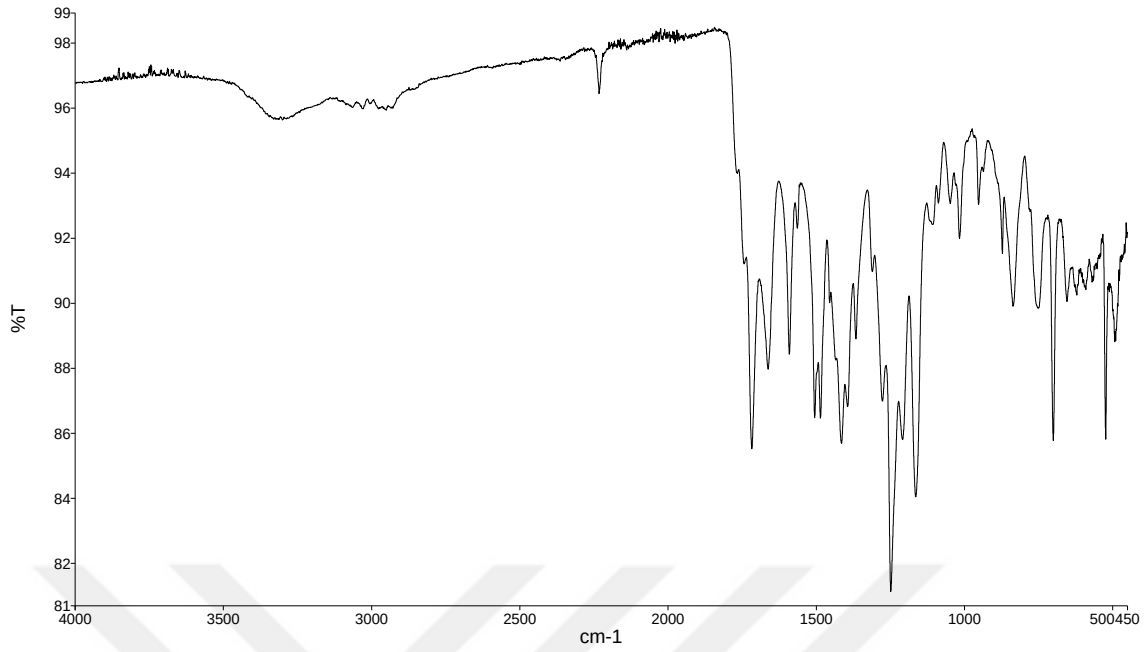

Appendix-2.1: FT-IR spectrum of Boc-Tyr-Phe-OCH_3-O-PN compound **(7)**

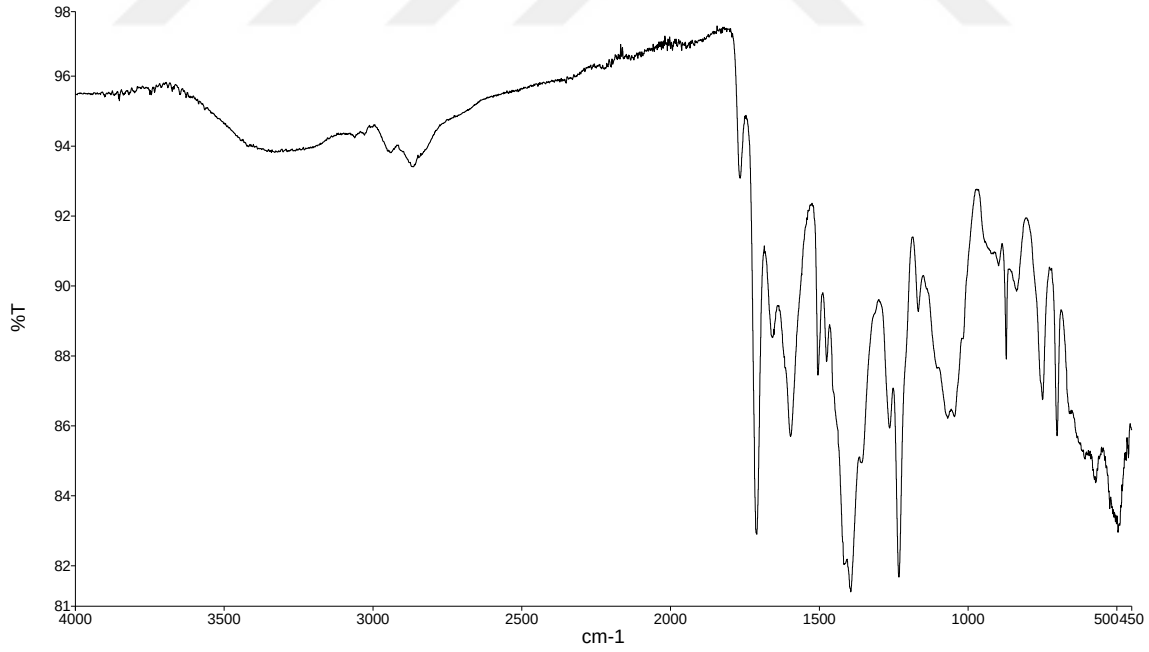

Appendix-2.2: FT-IR of tyrosine- phenylalanine dipeptide substituted phthalocyanine (CrPc) complex **(7a)**

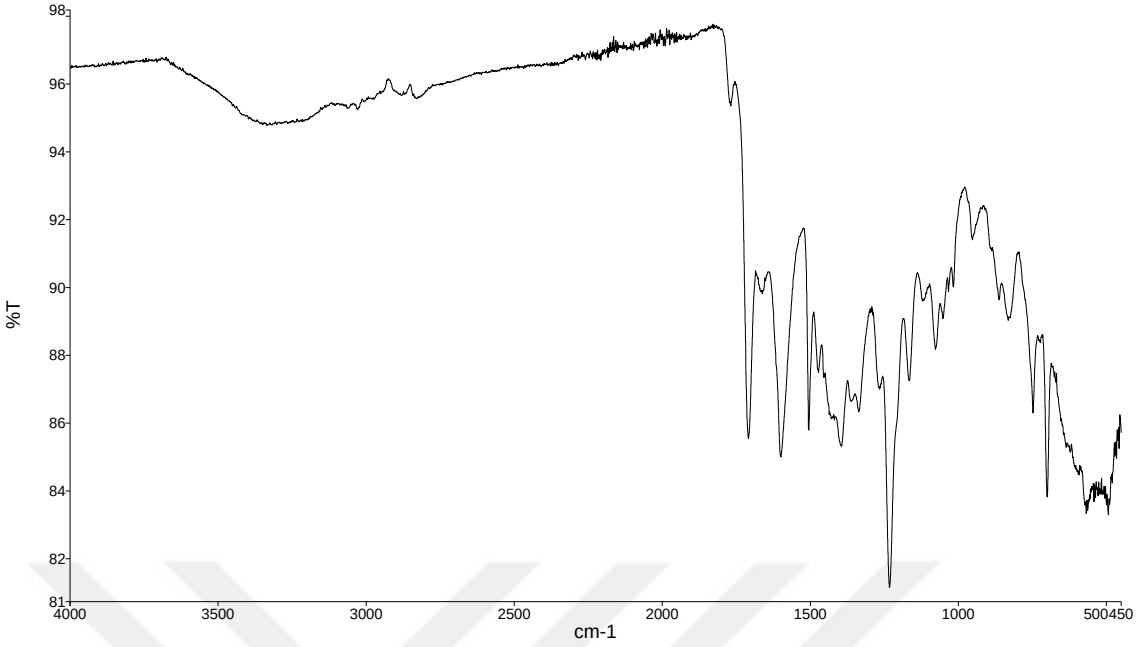

Appendix-2.3: FT-IR of tyrosine- phenylalanine dipeptide substituted phthalocyanine (MnPc) complex **(7b)**

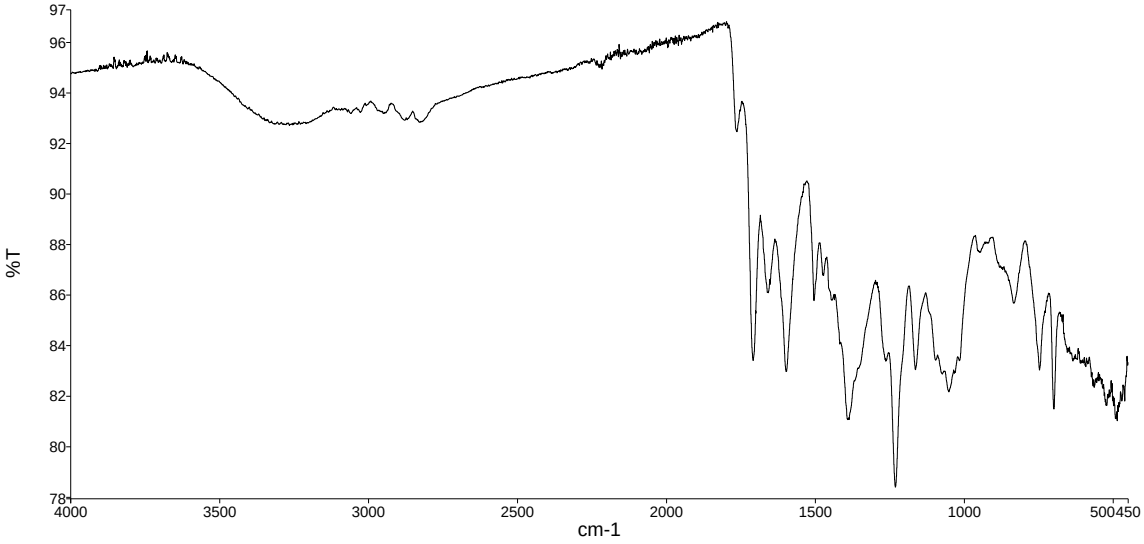

Appendix-2.4: FT-IR of tyrosine- phenylalanine dipeptide substituted phthalocyanine (FePc) Complex **(7c)**

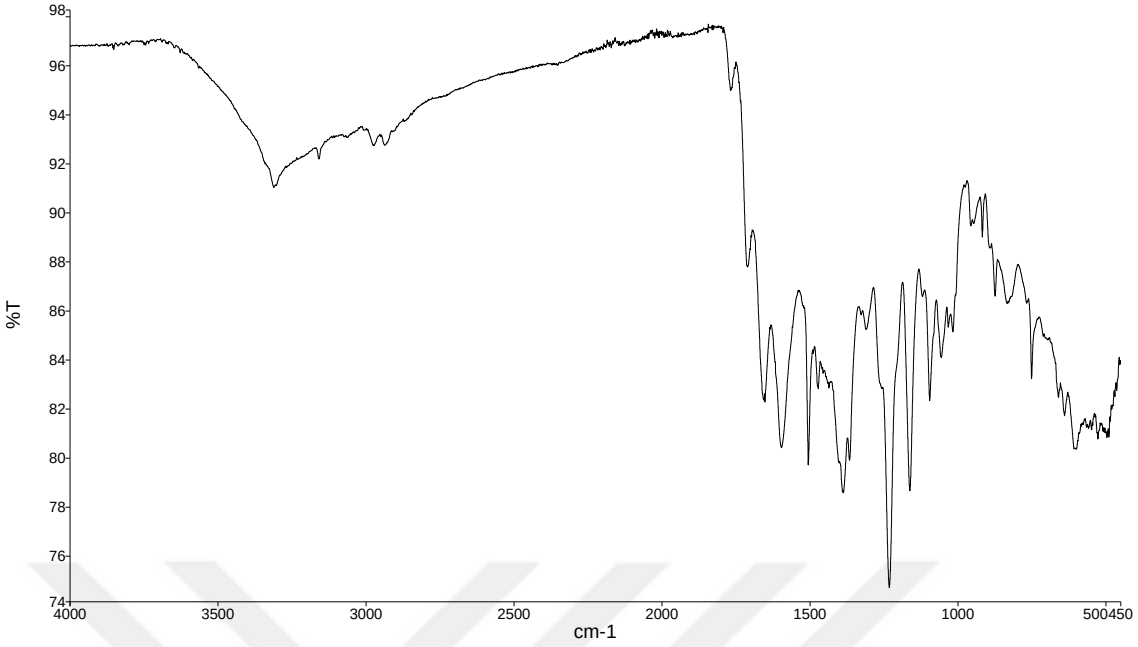

Appendix-2.5: FT-IR of tyrosine- phenylalanine dipeptide substituted phthalocyanine (CoPc) Complex **(7d)**

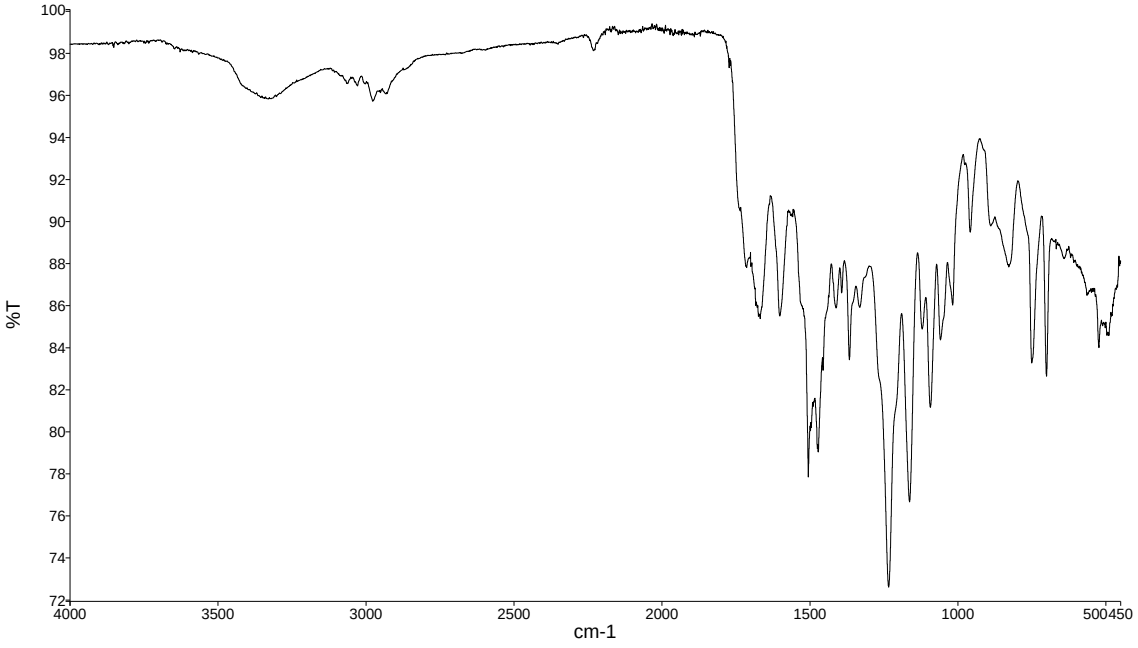

Appendix-2.6: FT-IR of tyrosine- phenylalanine dipeptide substituted phthalocyanine (NiPc) Complex **(7e)**

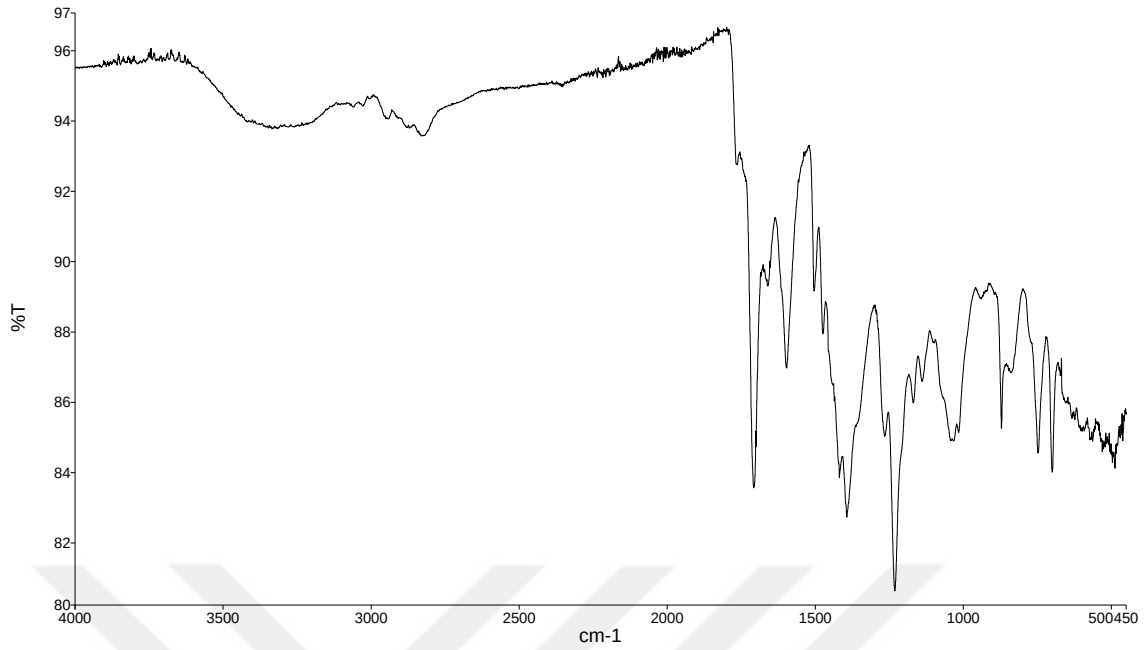

Appendix-2.7: FT-IR of tyrosine- phenylalanine dipeptide substituted phthalocyanine (CuPc) Complex **(7f)**

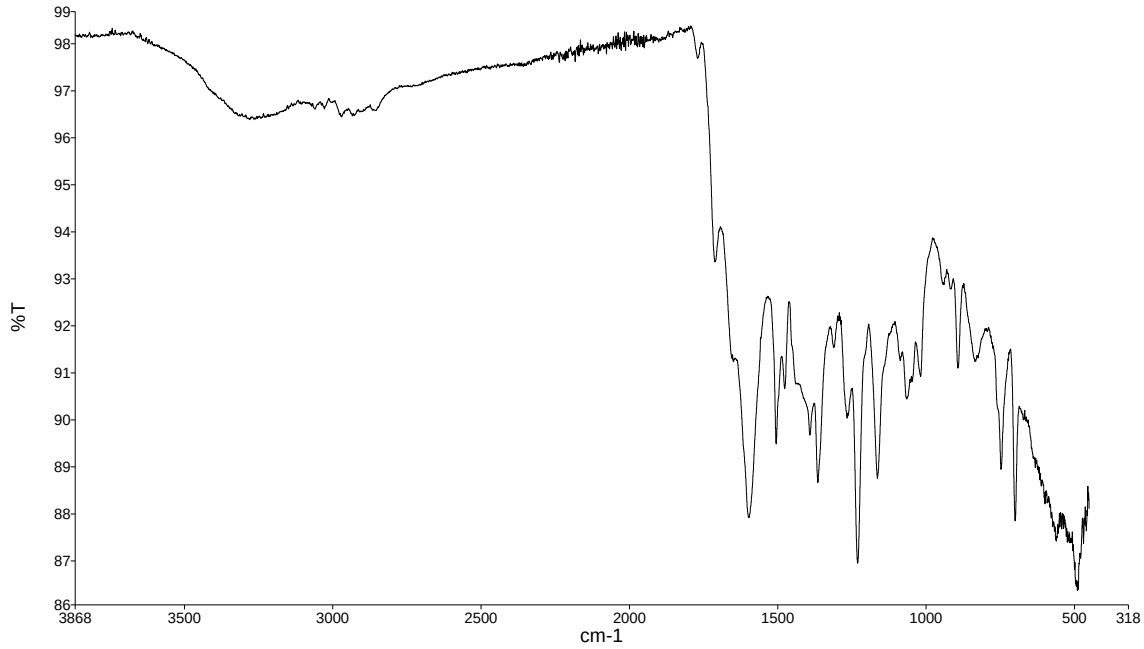

Appendix-2.8: FT-IR of tyrosine- phenylalanine dipeptide substituted phthalocyanine (ZnPc) Complex **(7g)**

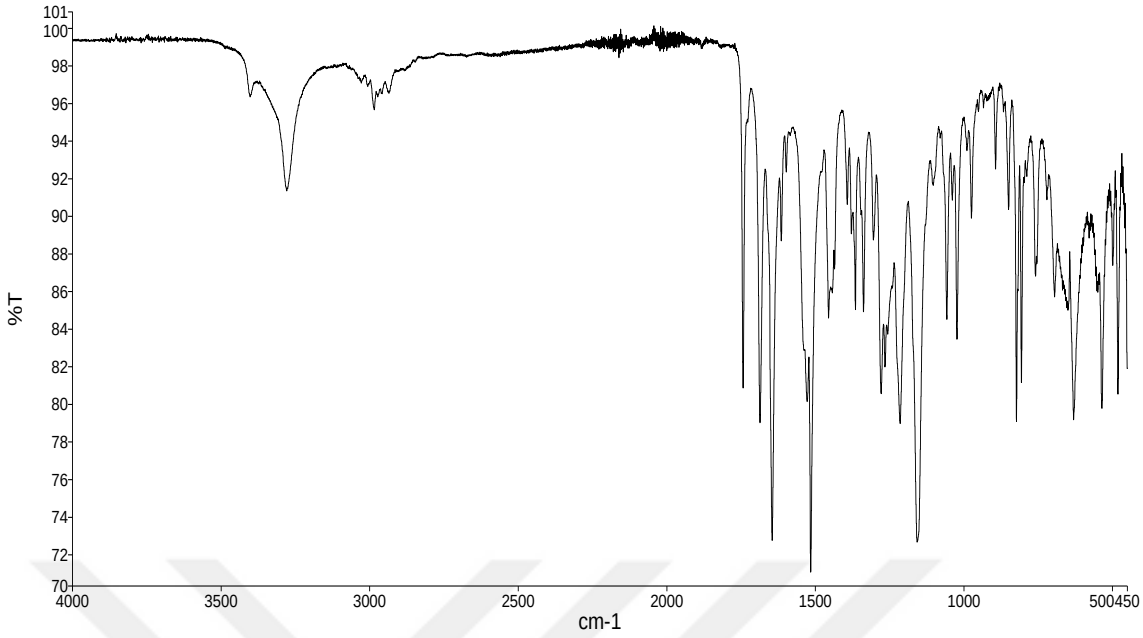

Appendix-3: FT-IR spectrum of methyl (*tert*-butoxycarbonyl)-*L*-tyrosyl-*D*-alaninate dipeptide **(8)**

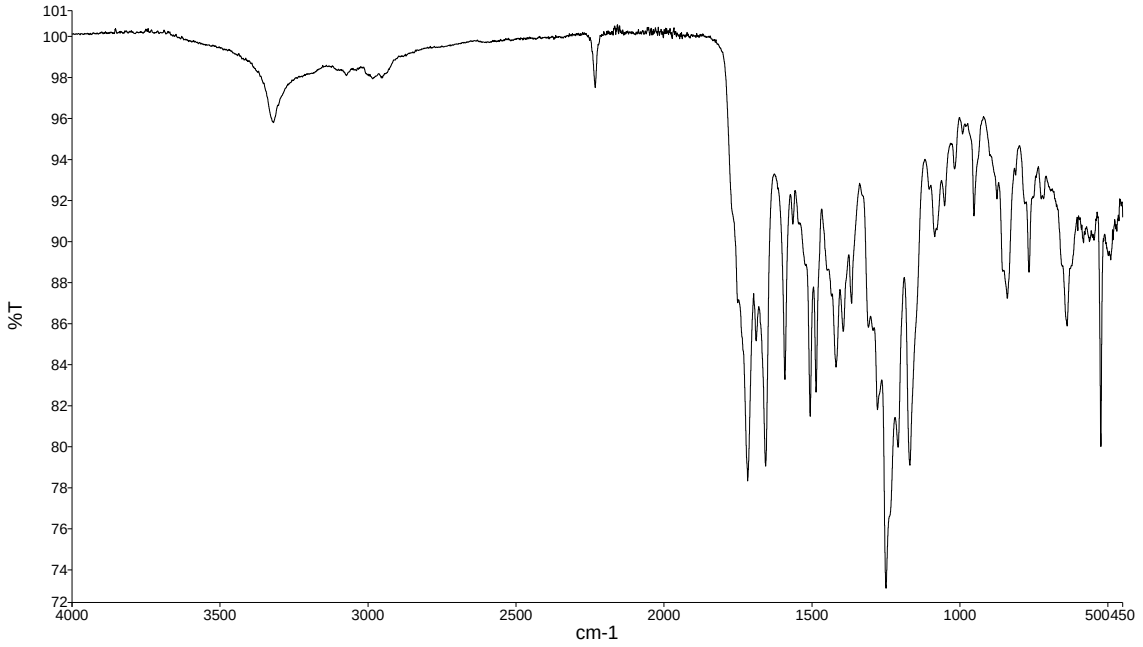

Appendix-3.1: FT-IR spectrum of Boc-Tyr-Ala-OCH_3-O-PN compound **(9)**

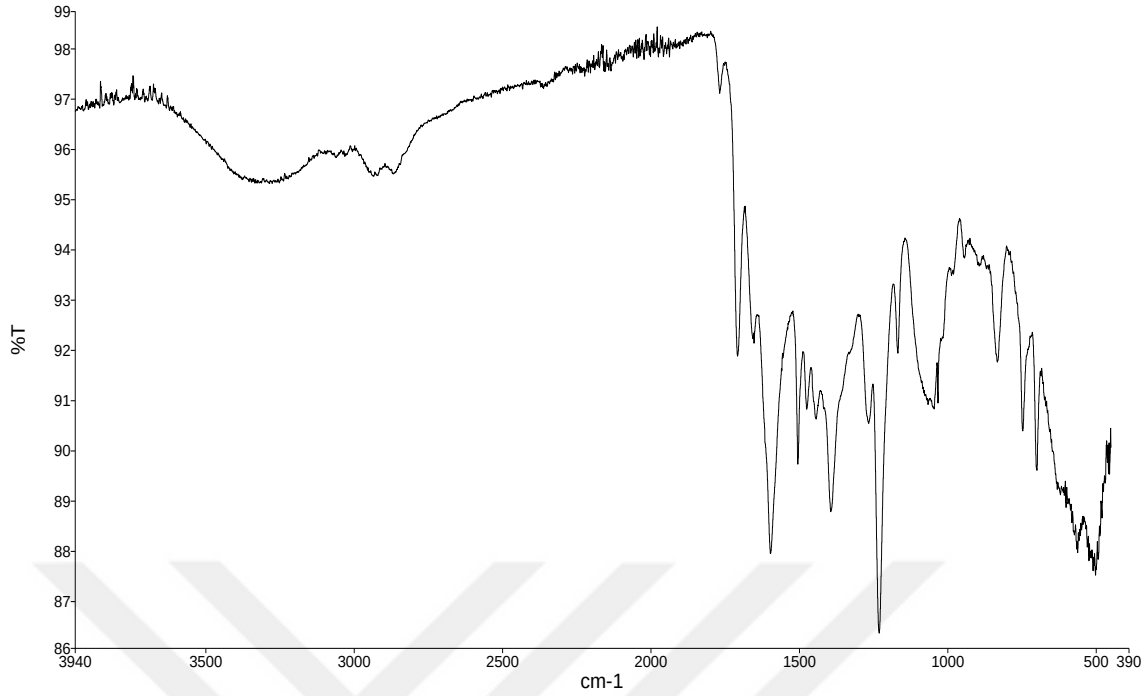

Appendix-3.2: FT-IR of tyrosine- alanine dipeptide substituted phthalocyanine (CrPc) Complex **(9a)**

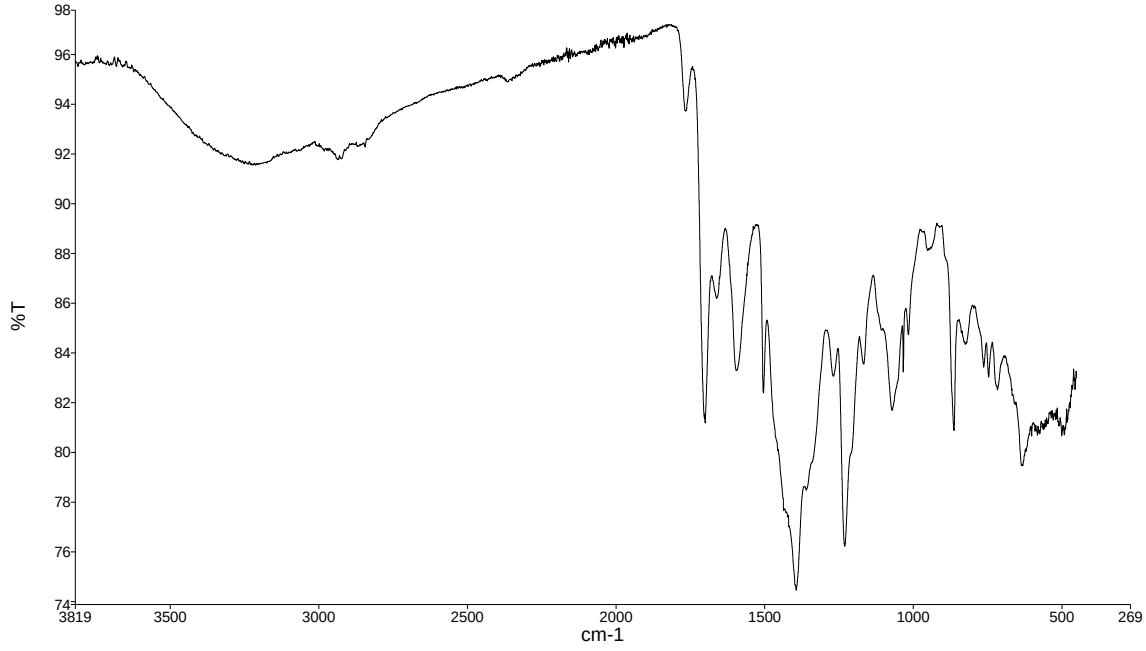

Appendix-3.3: FT-IR of tyrosine- alanine dipeptide substituted phthalocyanine (MnPc) Complex **(9b)**

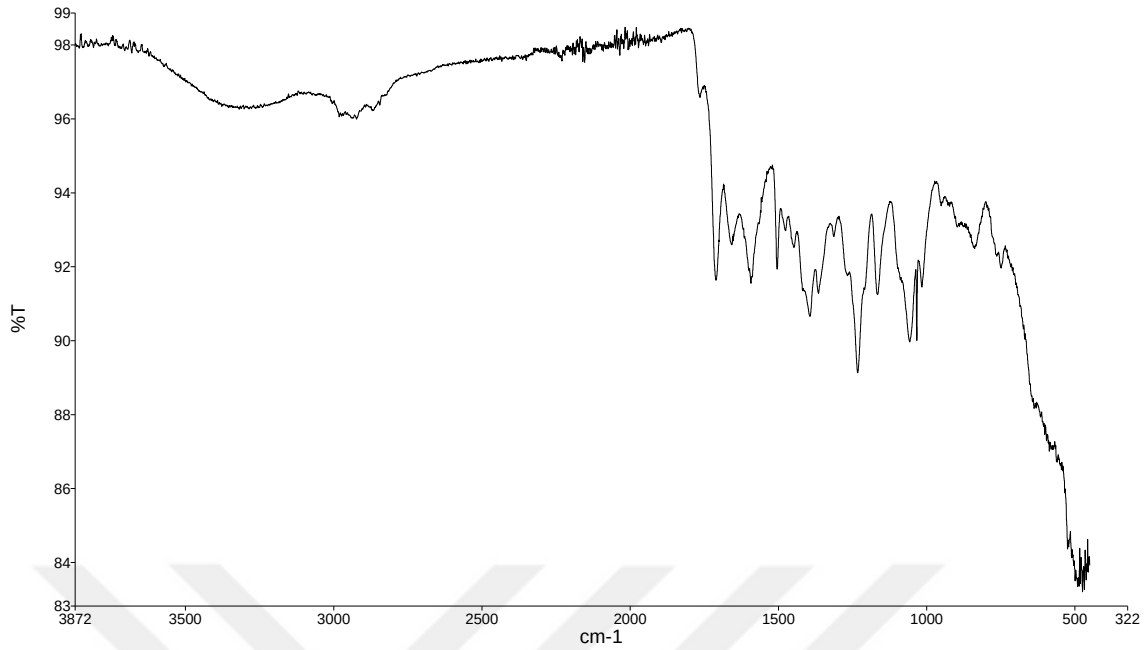

Appendix-3.4: FT-IR of tyrosine- alanine dipeptide substituted phthalocyanine (FePc) Complex **(9c)**

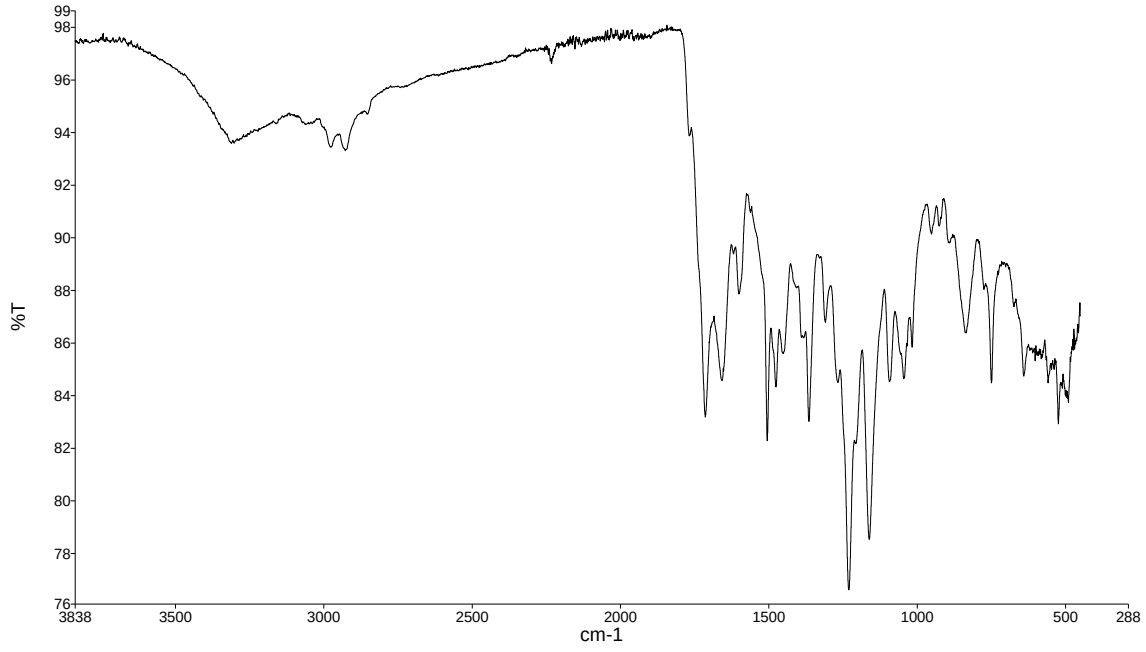

Appendix-3.5: FT-IR of tyrosine- alanine dipeptide substituted phthalocyanine (CoPc) Complex **(9d)**

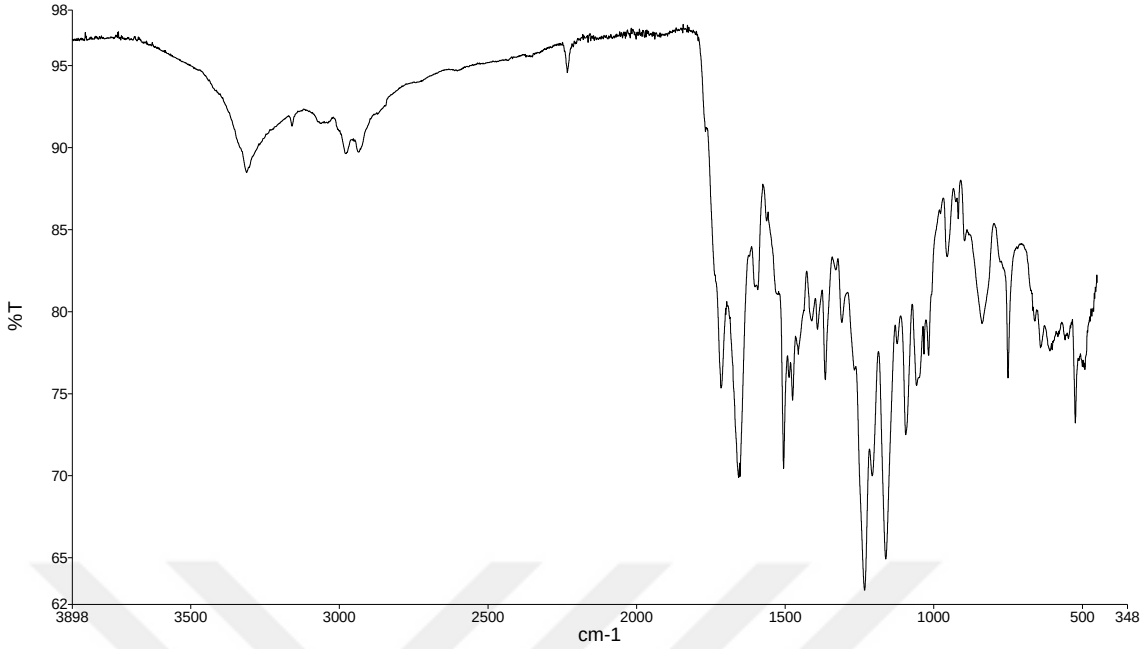

Appendix-3.6: FT-IR of tyrosine- alanine dipeptide substituted phthalocyanine (NiPc) Complex **(9e)**

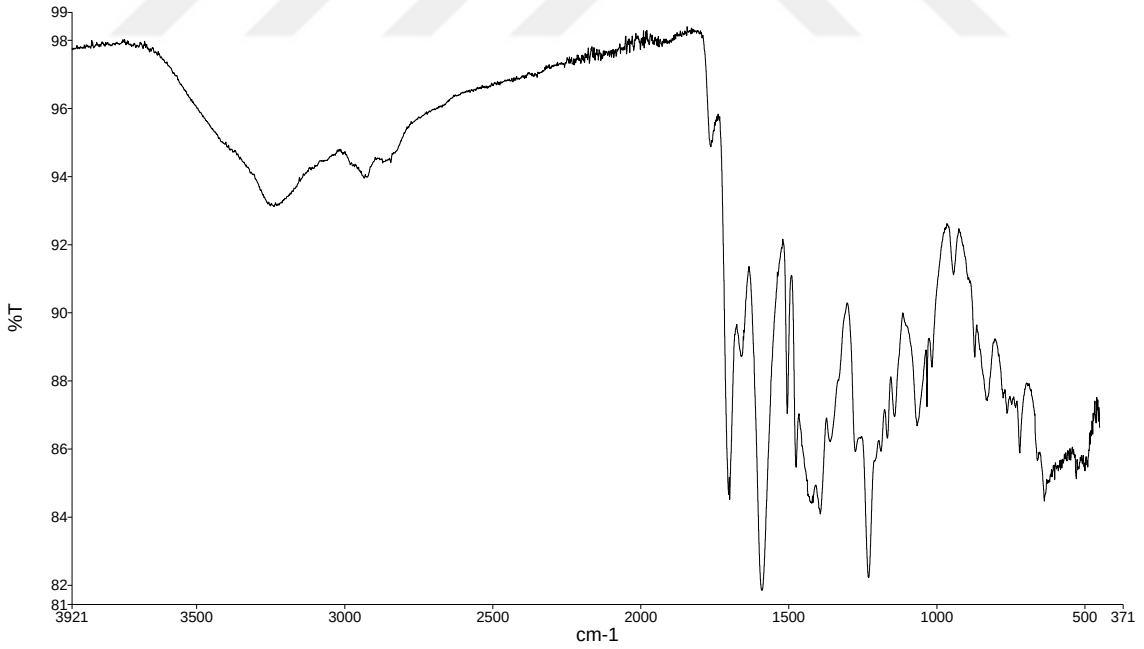

Appendix-3.7: FT-IR of tyrosine- alanine dipeptide substituted phthalocyanine (CuPc) Complex **(9f)**

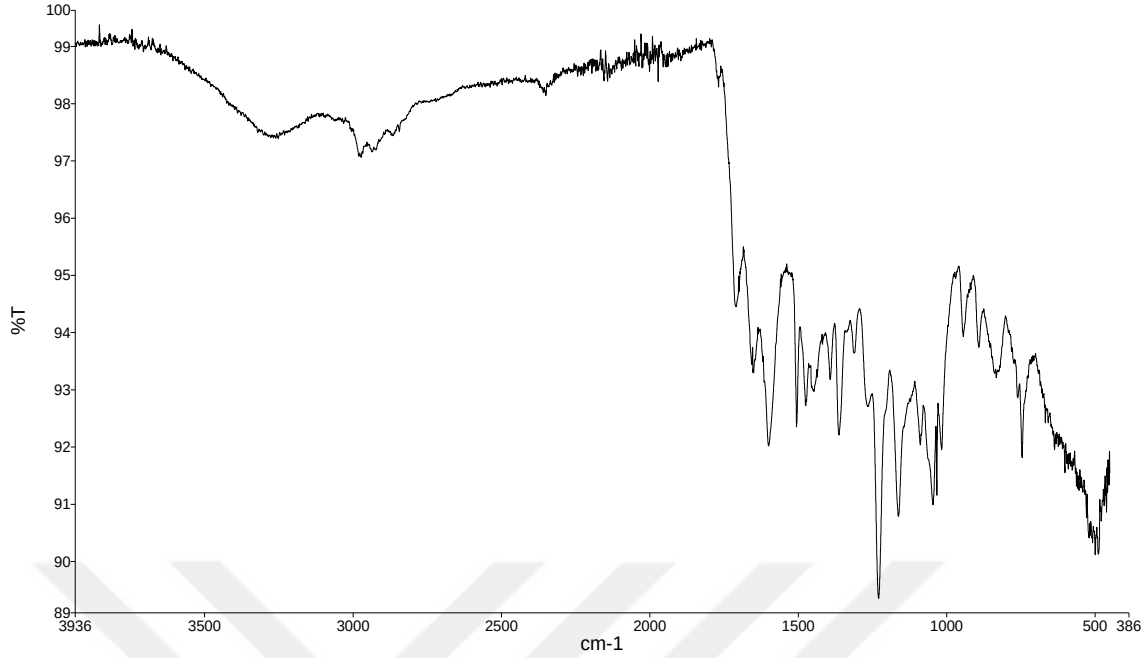

Appendix-3.8: FT-IR of tyrosine- alanine dipeptide substituted phthalocyanine (ZnPc) Complex **(9g)**

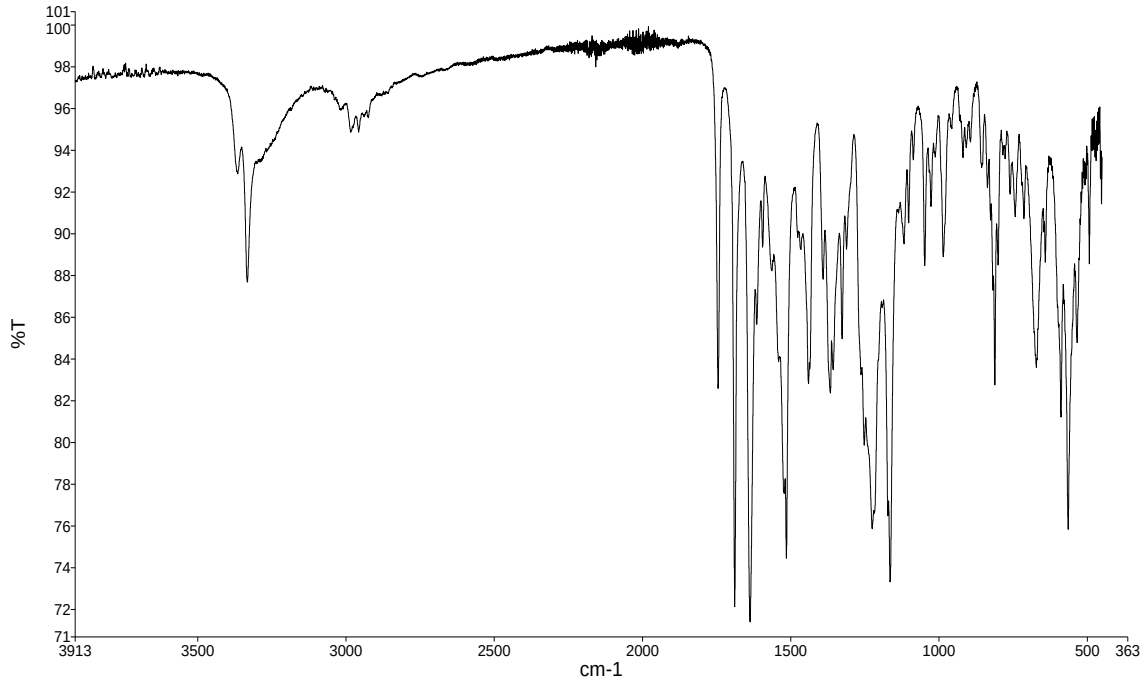

Appendix-4: FT-IR spectrum of methyl (*tert*-butoxycarbonyl)-*L*-tyrosyl glycinate dipeptide **(10)**

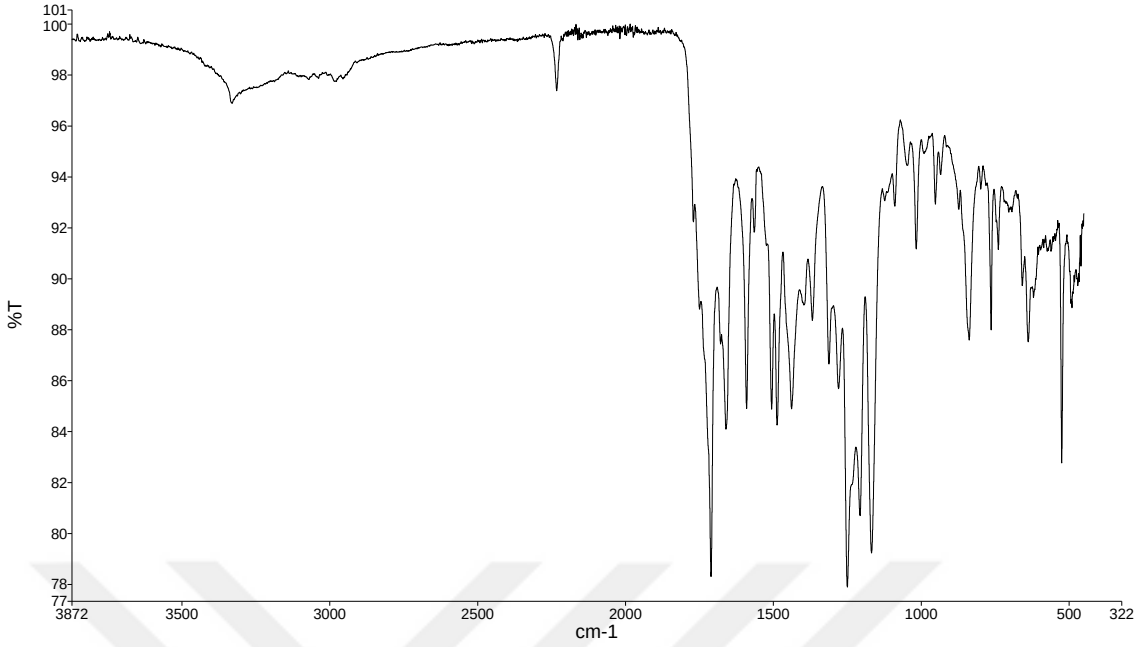

Appendix-4.1: FT-IR spectrum of Boc-Tyr-Gly-OCH_3-O-PN compound **(11)**

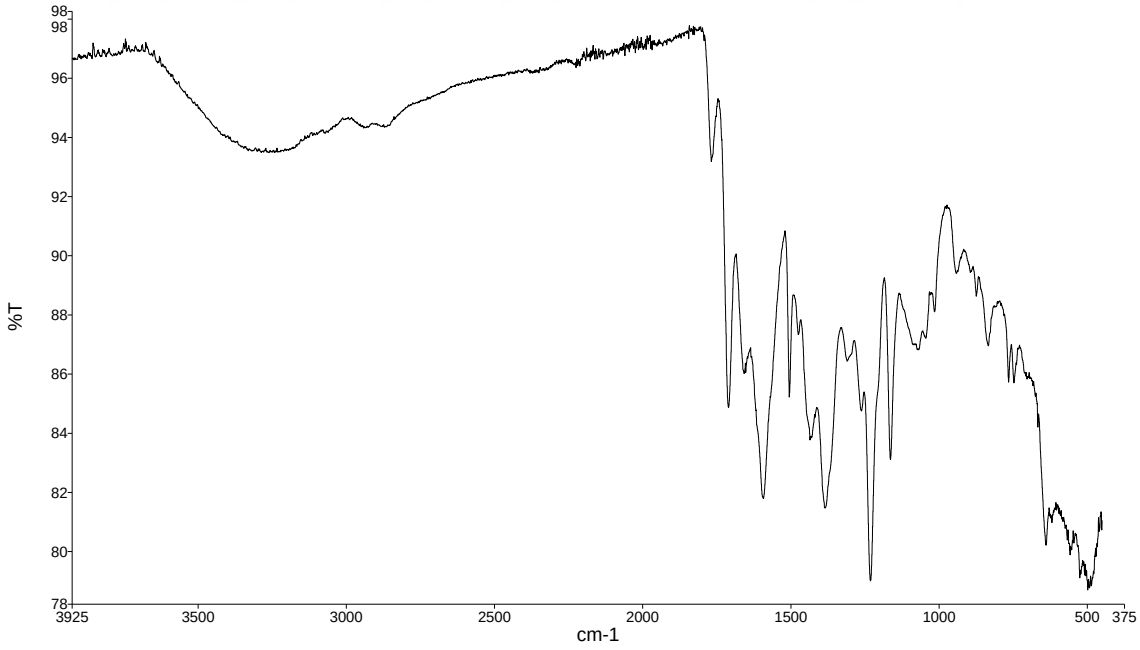

Appendix-4.2: FT-IR of tyrosine- glycine dipeptide substituted phthalocyanine (CrPc) Complex **(11a)**

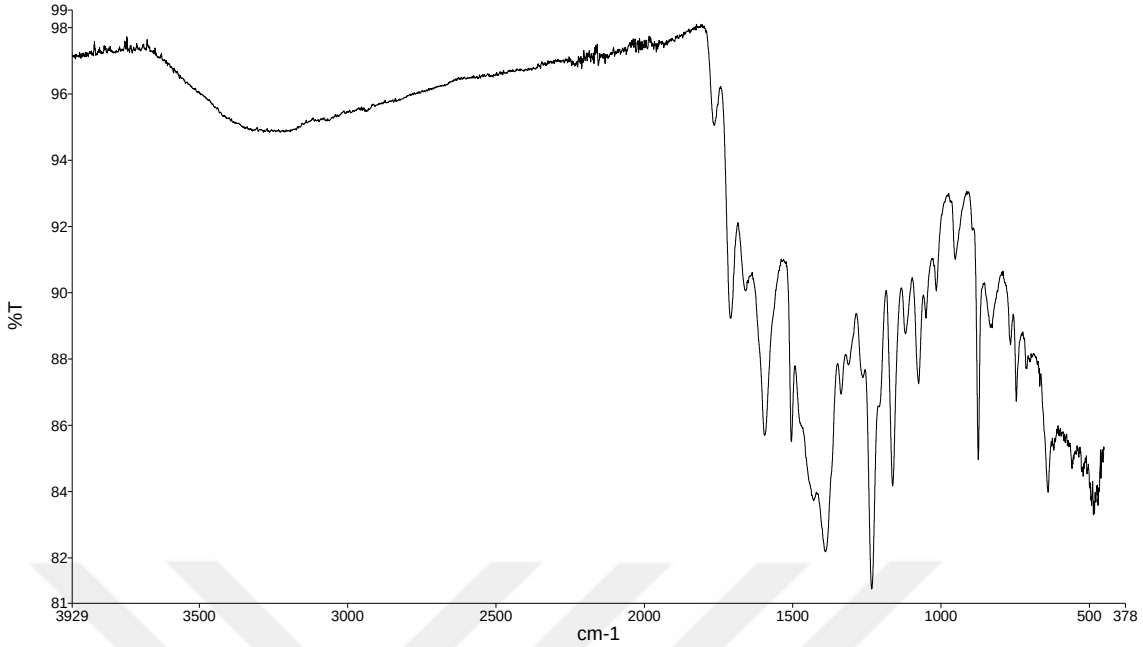

Appendix-4.3: FT-IR of tyrosine- glycine dipeptide substituted phthalocyanine (MnPc) Complex **(11b)**

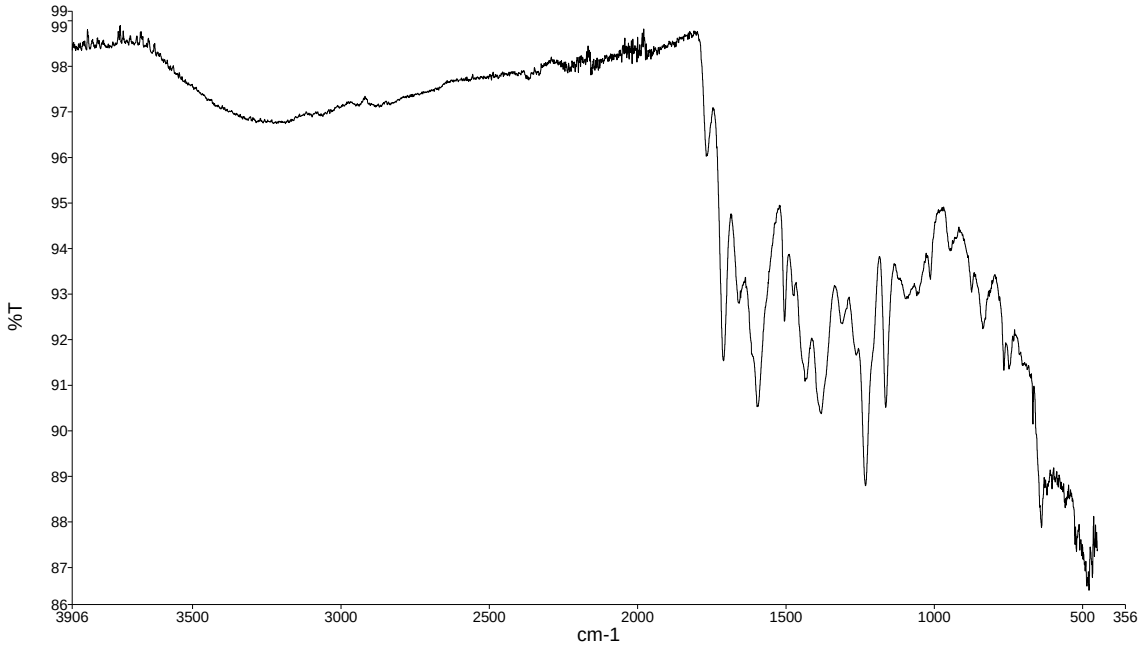

Appendix-4.4: FT-IR of tyrosine- glycine dipeptide substituted phthalocyanine (FePc) Complex **(11c)**

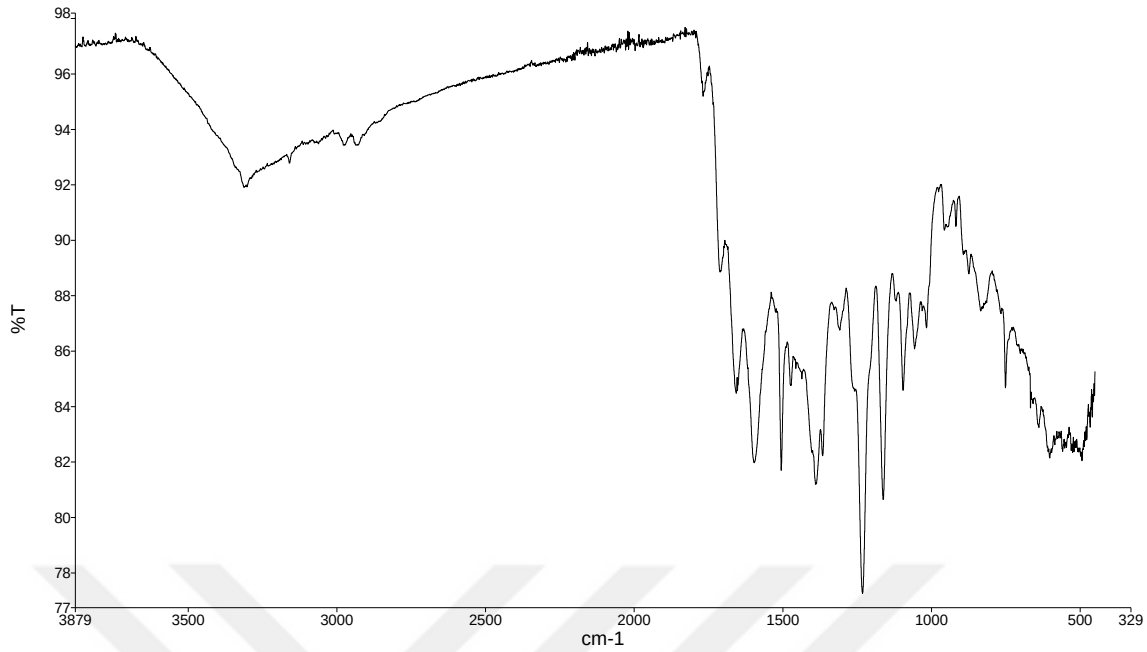

Appendix-4.5: FT-IR of tyrosine- glycine dipeptide substituted phthalocyanine (CoPc) Complex **(11d)**

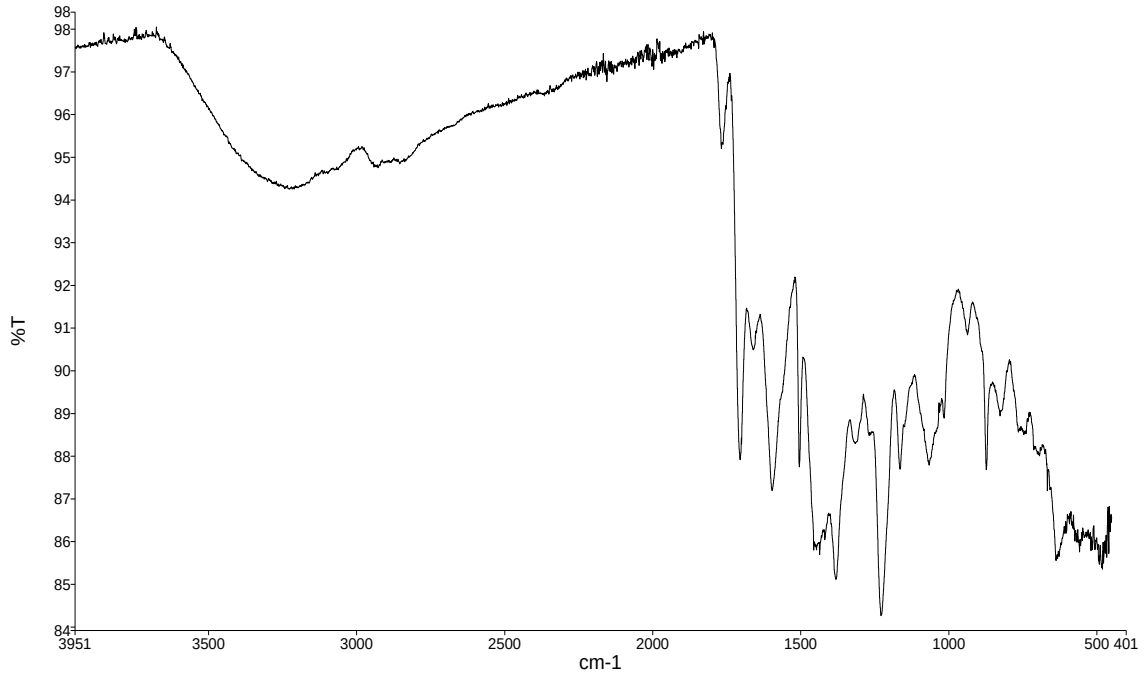

Appendix-4.6: FT-IR of tyrosine- glycine dipeptide substituted phthalocyanine (NiPc) Complex **(11e)**

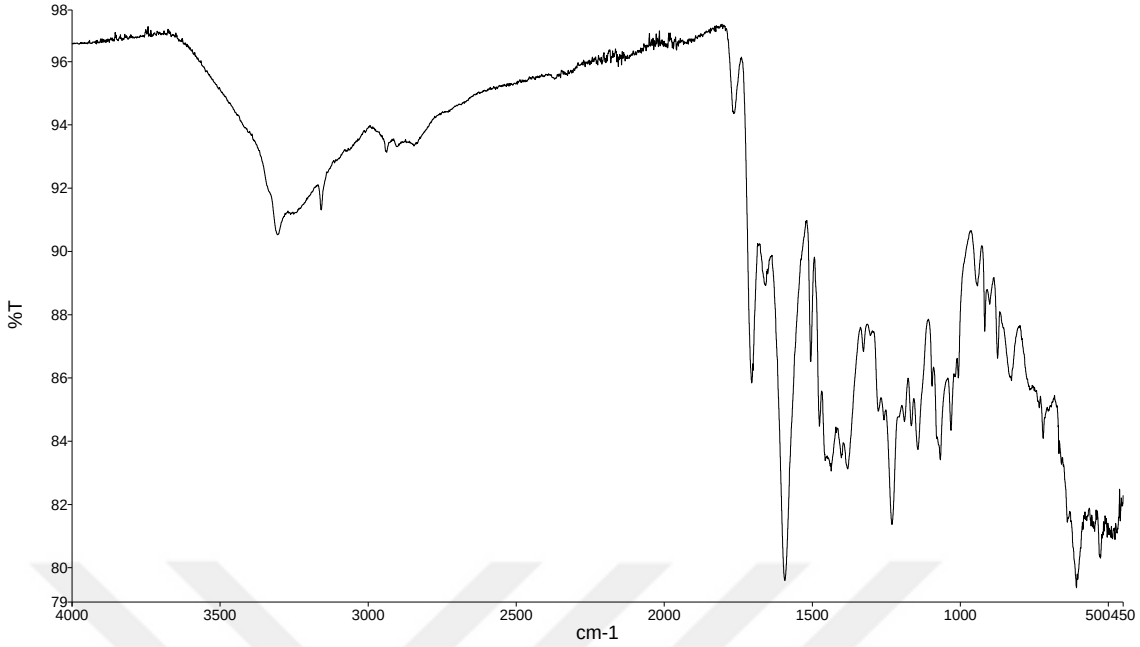

Appendix-4.7: FT-IR of tyrosine- glycine dipeptide substituted phthalocyanine (CuPc) Complex **(11f)**

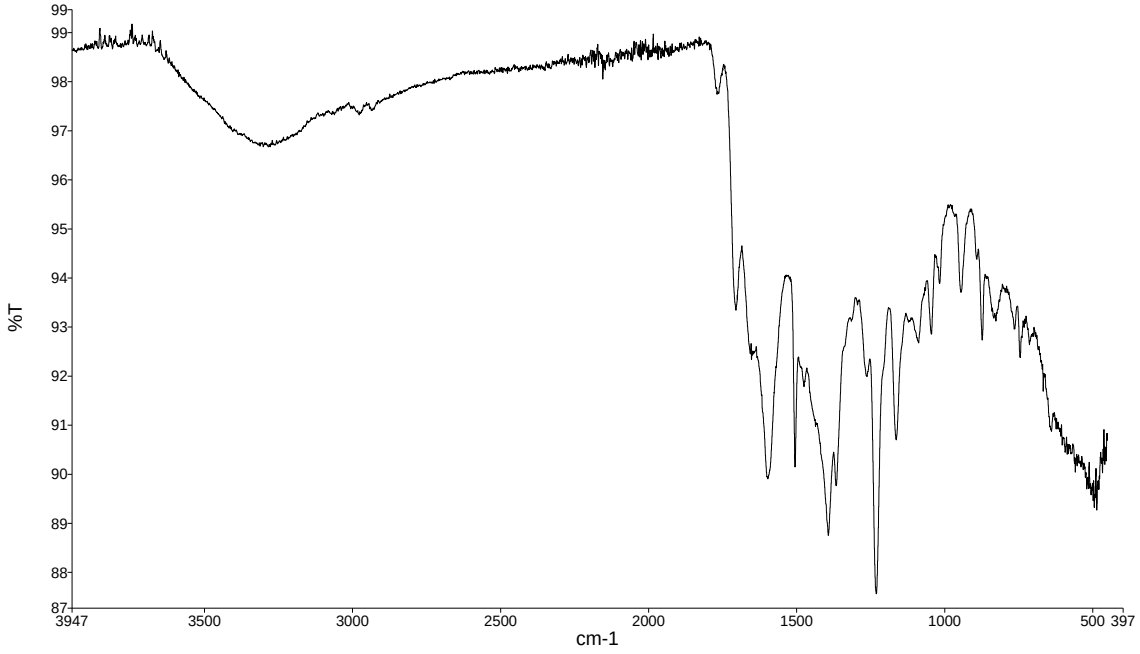

Appendix-4.8: FT-IR of tyrosine- glycine dipeptide substituted phthalocyanine (ZnPc) Complex **(11g)**

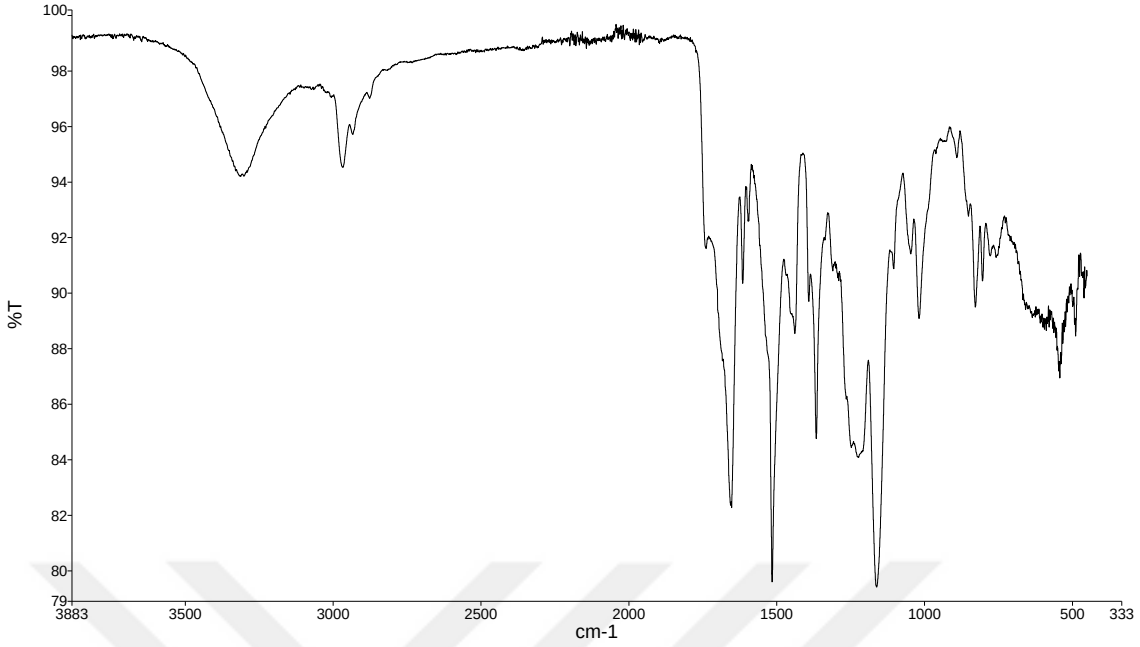

Appendix-5: FT-IR spectrum of methyl (*tert*-butoxycarbonyl)-*L*-tyrosyl-*L*-valinate dipeptide **(12)**

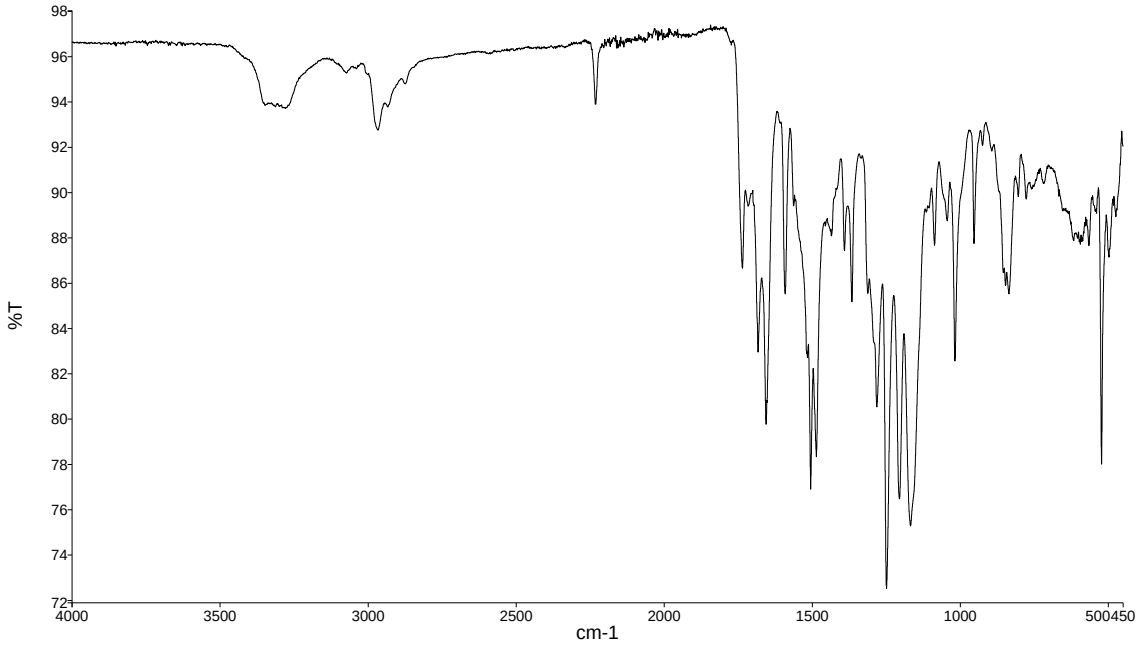

Appendix-5.1: FT-IR spectrum of Boc-Tyr-Val-OCH_3-O-PN compound **(13)**

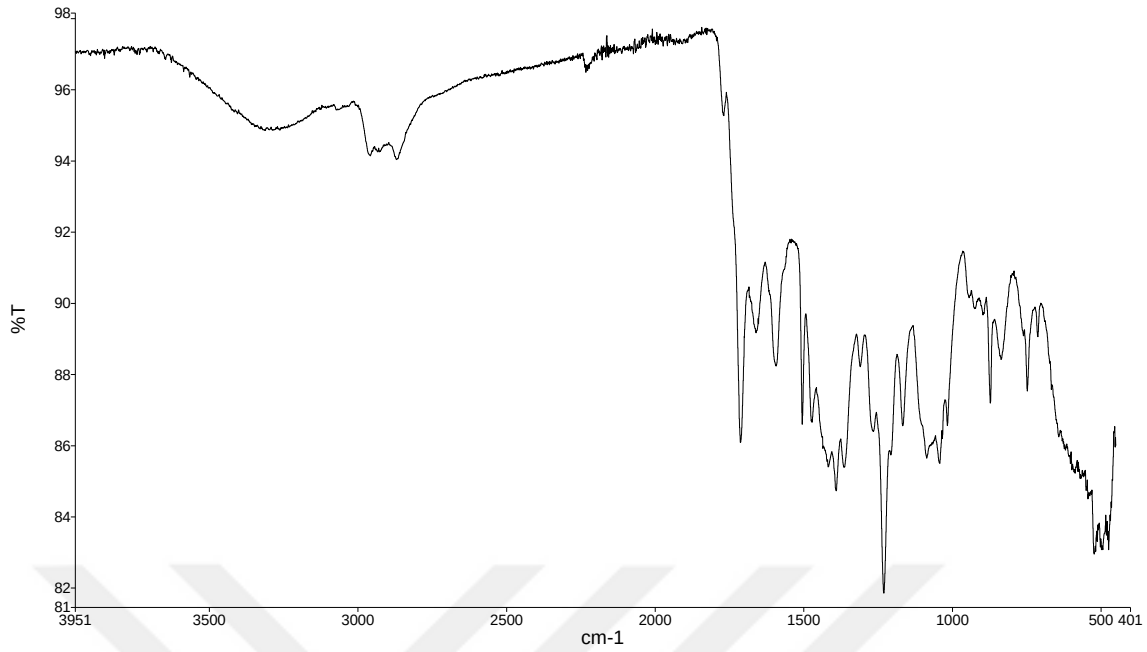

Appendix-5.2: FT-IR of tyrosine- valine dipeptide substituted phthalocyanine (CrPc) Complex **(13a)**

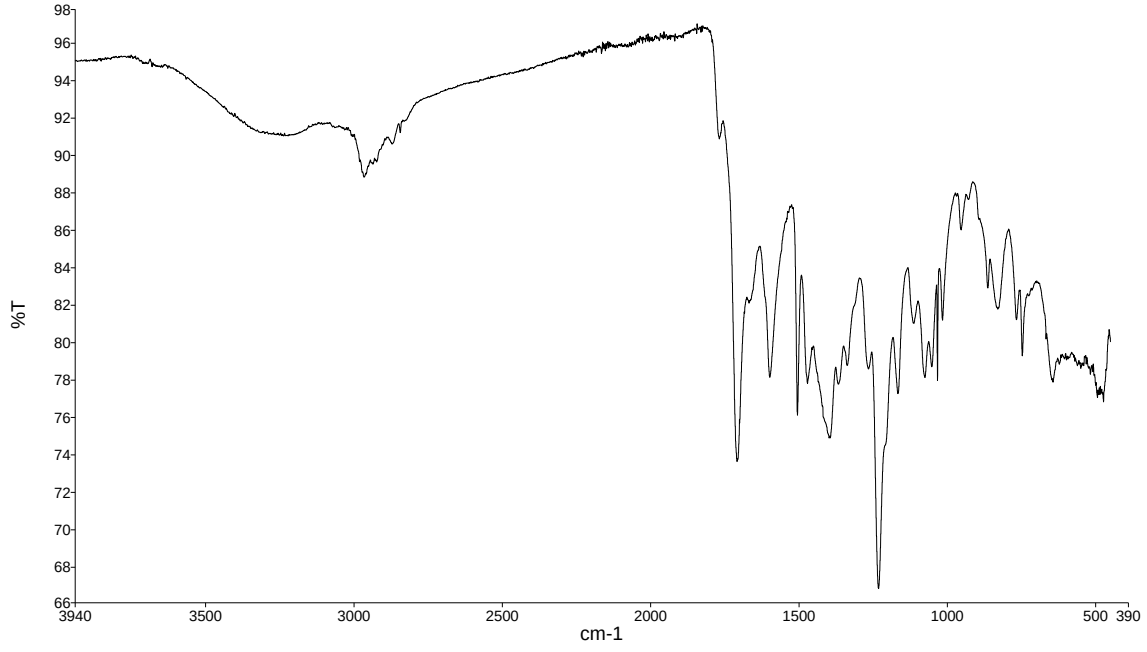

Appendix-5.3: FT-IR of tyrosine- valine dipeptide substituted phthalocyanine (MnPc) Complex **(13b)**

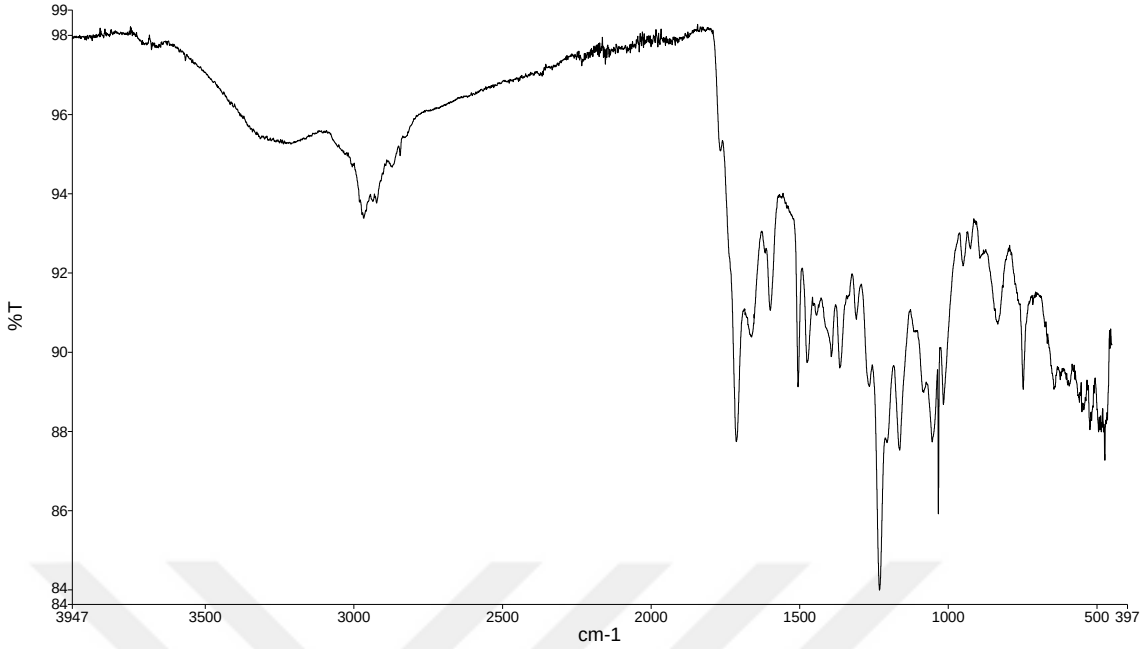

Appendix-5.4: FT-IR of tyrosine- valine dipeptide substituted phthalocyanine (FePc) Complex **(13c)**

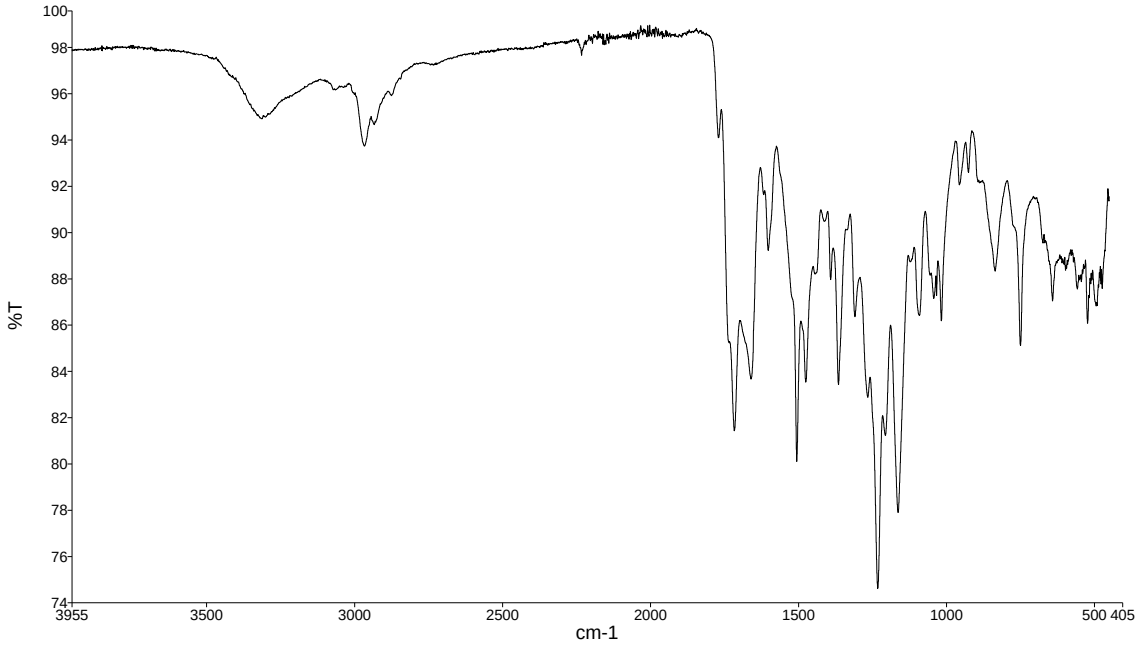

Appendix-5.5: FT-IR of tyrosine- valine dipeptide substituted phthalocyanine (CoPc) Complex **(13d)**

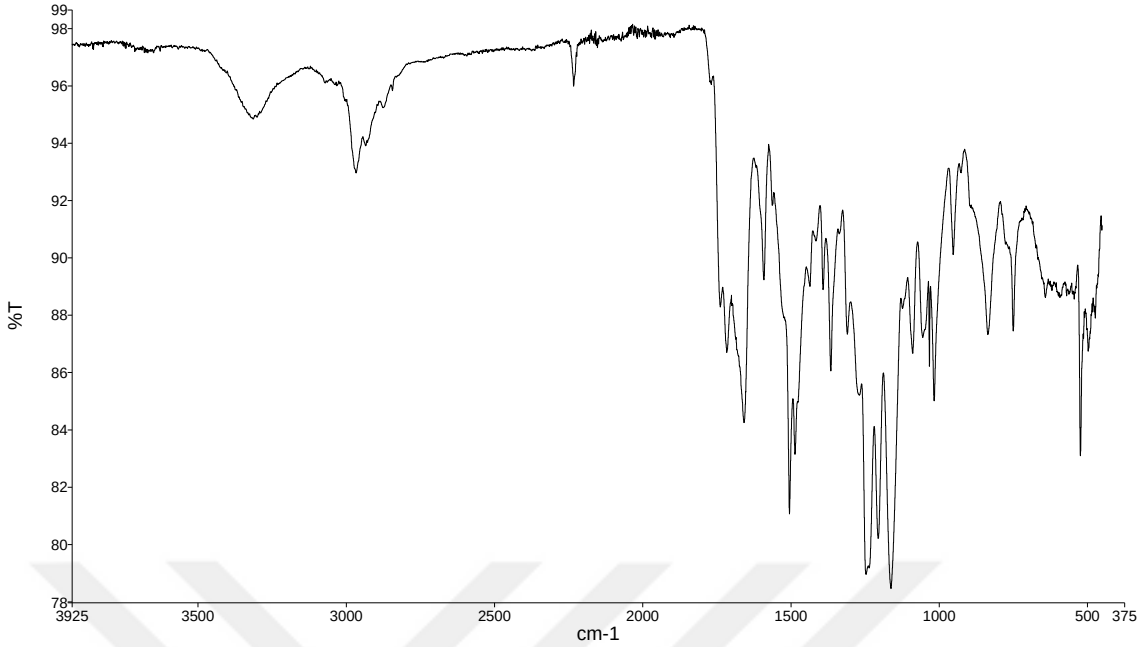

Appendix-5.6: FT-IR of tyrosine- valine dipeptide substituted phthalocyanine (NiPc) Complex **(13e)**

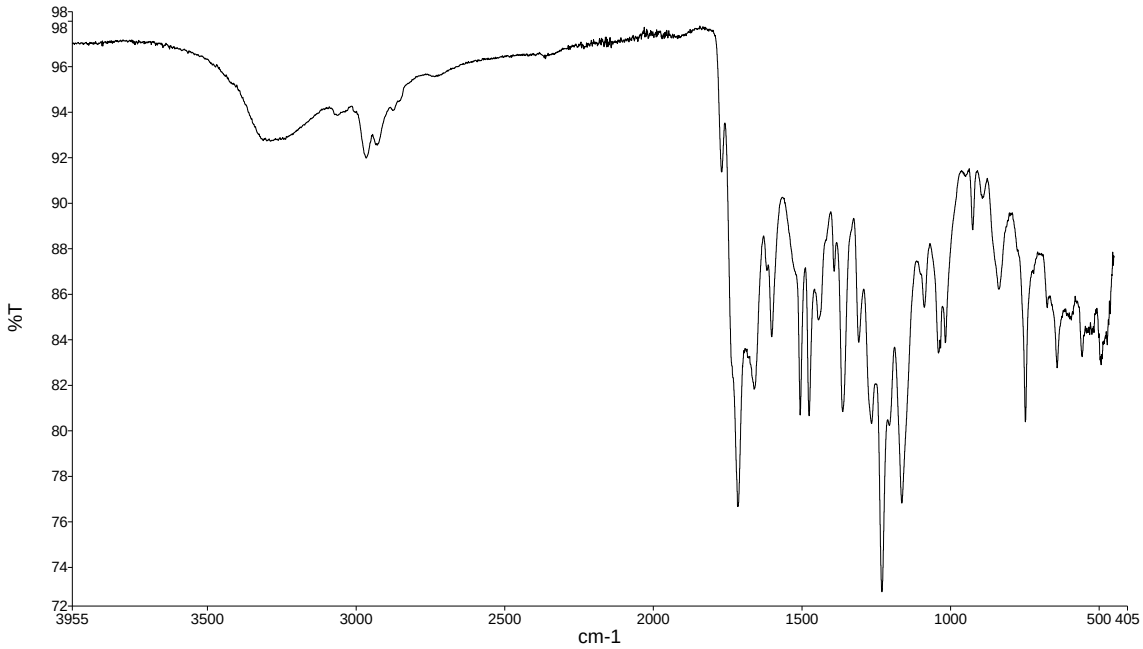

Appendix-5.7: FT-IR of tyrosine- valine dipeptide substituted phthalocyanine (CuPc) Complex **(13f)**

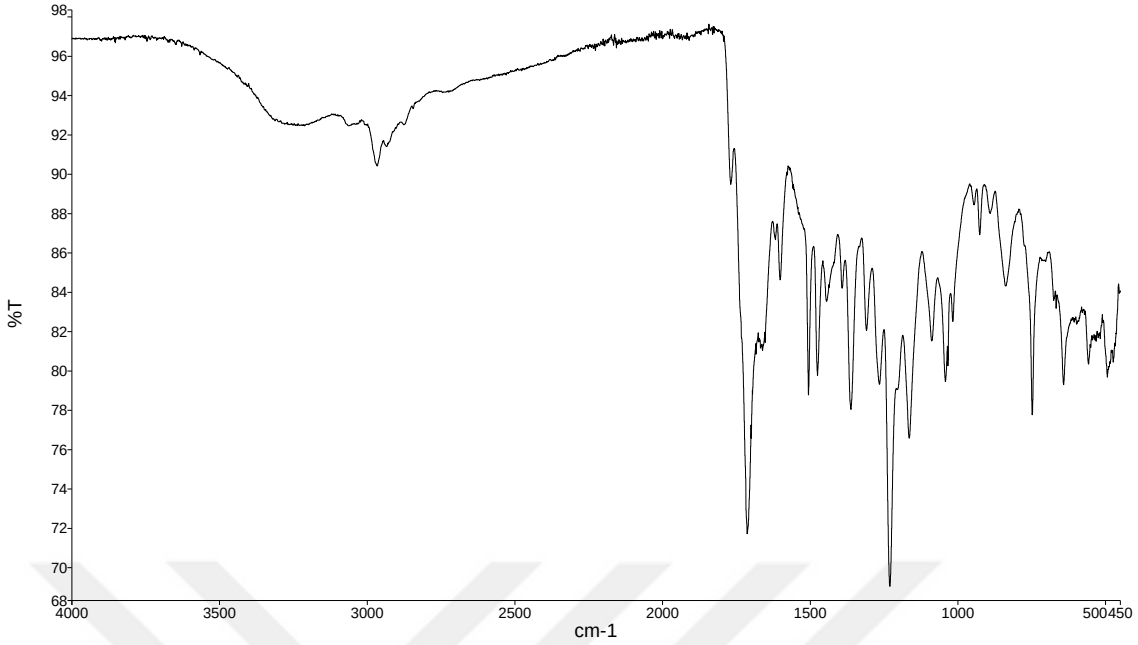

Appendix-5.8: FT-IR of tyrosine- valine dipeptide substituted phthalocyanine (ZnPc) Complex **(13g)**

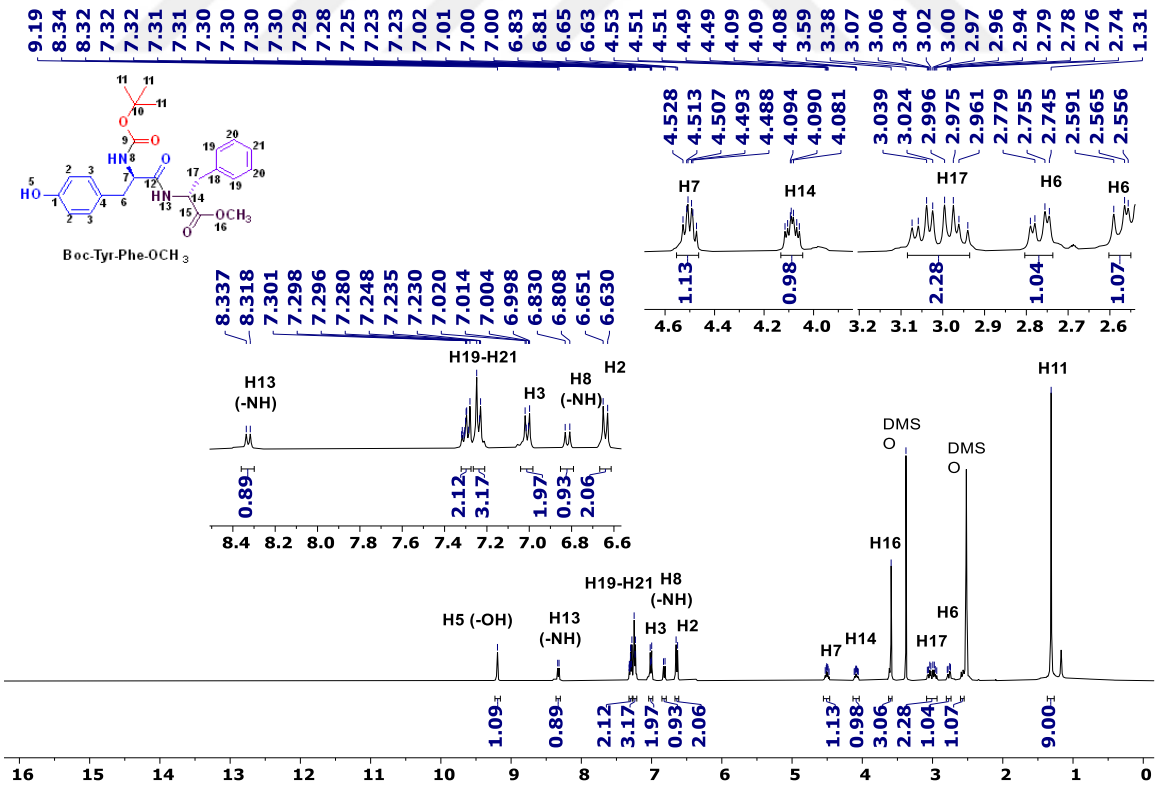

Appendix-6.1: ^{1}H-NMR spectrum of **Boc-Tyr-Phe-OCH$_3$** compound **(6)** in (DMSO-d6)

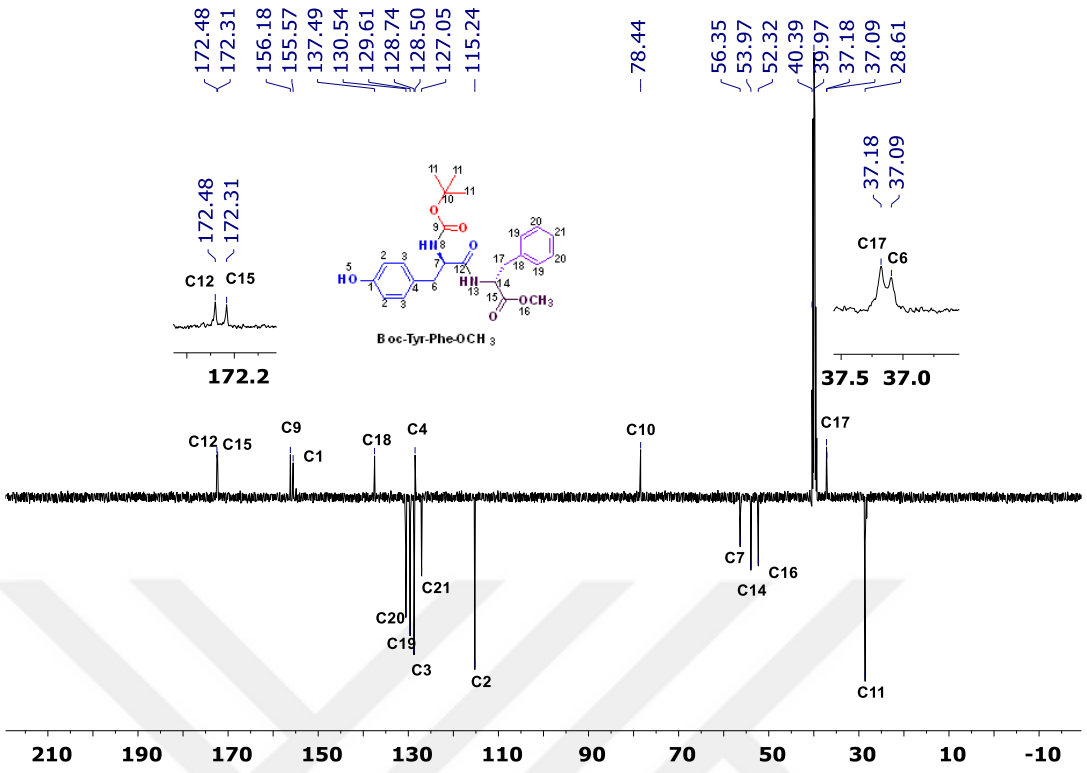

Appendix-6.2: ^{13}C-APT NMR spectrum of **Boc-Tyr-Phe-OCH$_3$** compound **(6)** in (DMSO-d6)

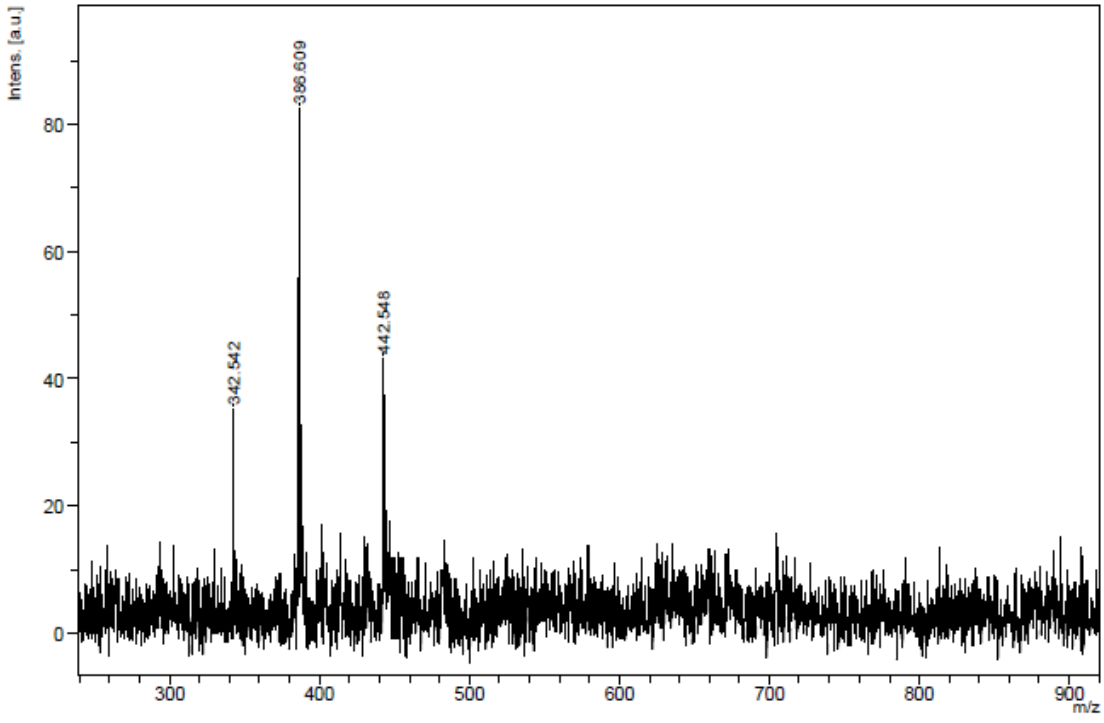

Appendix-6.3: MALDI-TOF MS spectrum of Boc-Tyr-Phe-OCH$_3$ compound (6)

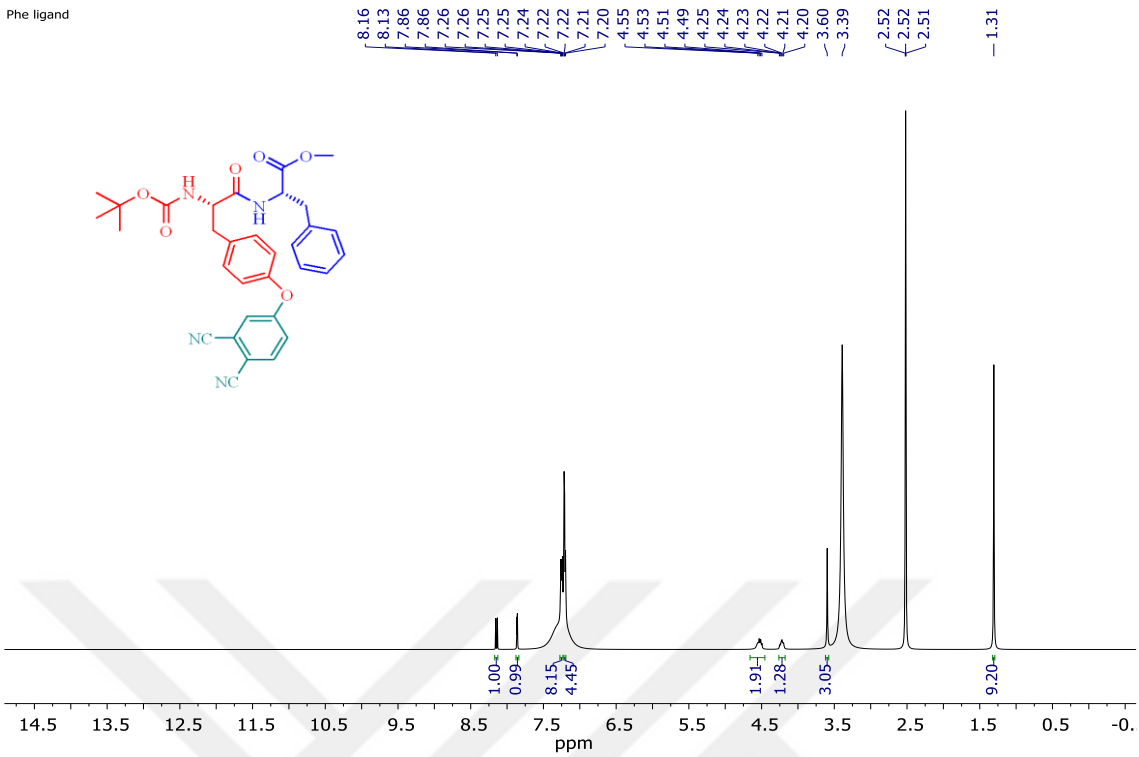

Appendix-6.4: ^{1}H-NMR spectrum of methyl((S)-2-((tert-butoxycarbonyl) amino)-3-(4-(3,4-dicyanophenoxy) phenyl) propanoyl)-*D*- phenylalaninate **(Boc-Tyr-Phe-OCH$_3$-O-**PN**) (7)** in (DMSO-d6)

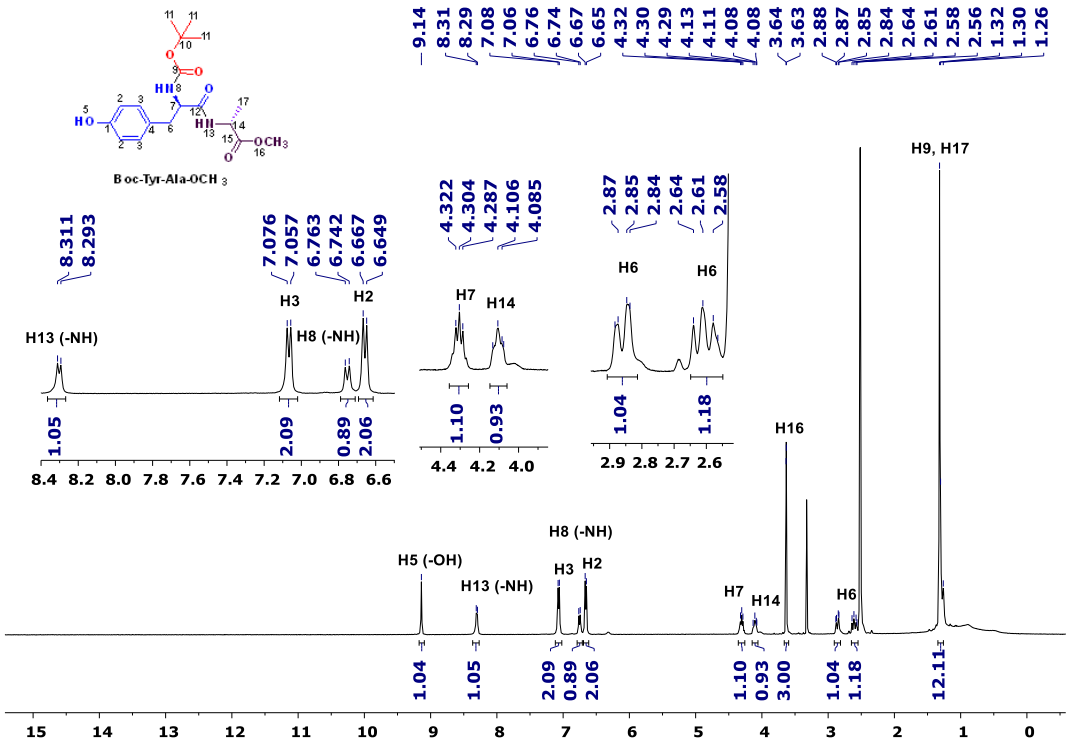

Appendix-7.1: ^{1}H-NMR spectrum of **Boc-Tyr-Ala-OCH$_3$** compound **(8)** in (DMSO-d6)

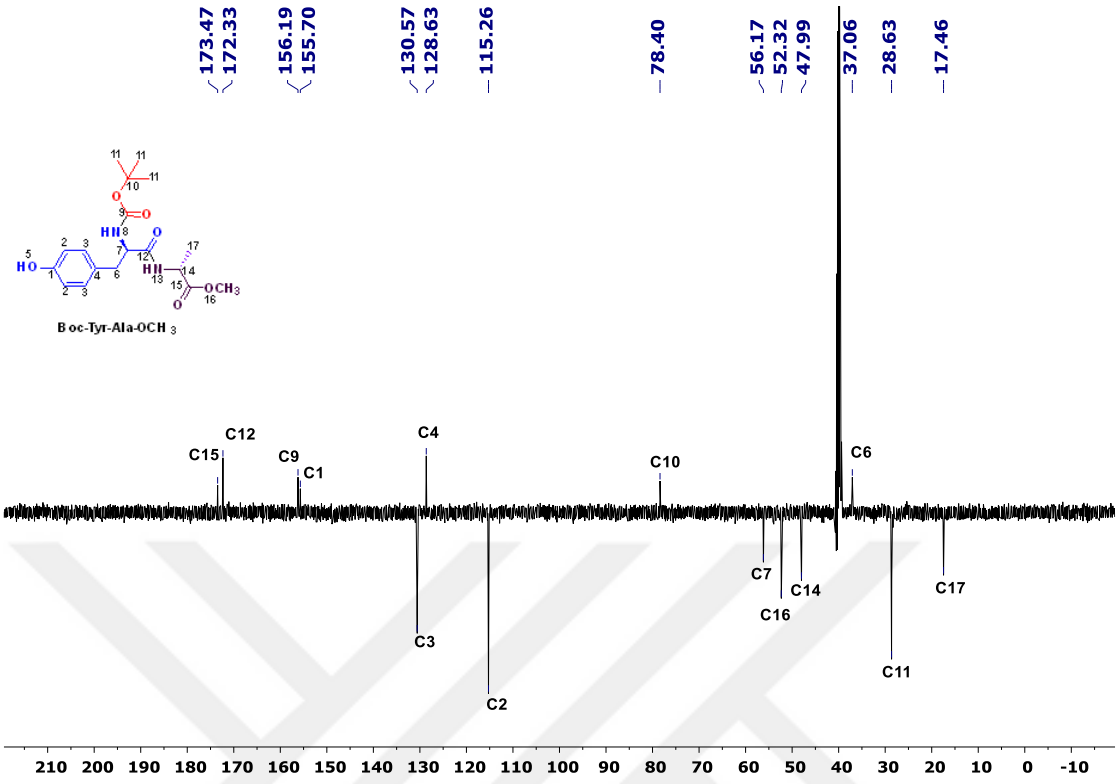

Appendix-7.2: ^{13}C-APT NMR spectrum of **Boc-Tyr-Ala-OCH$_3$** compound **(8)** in (DMSO-d6)

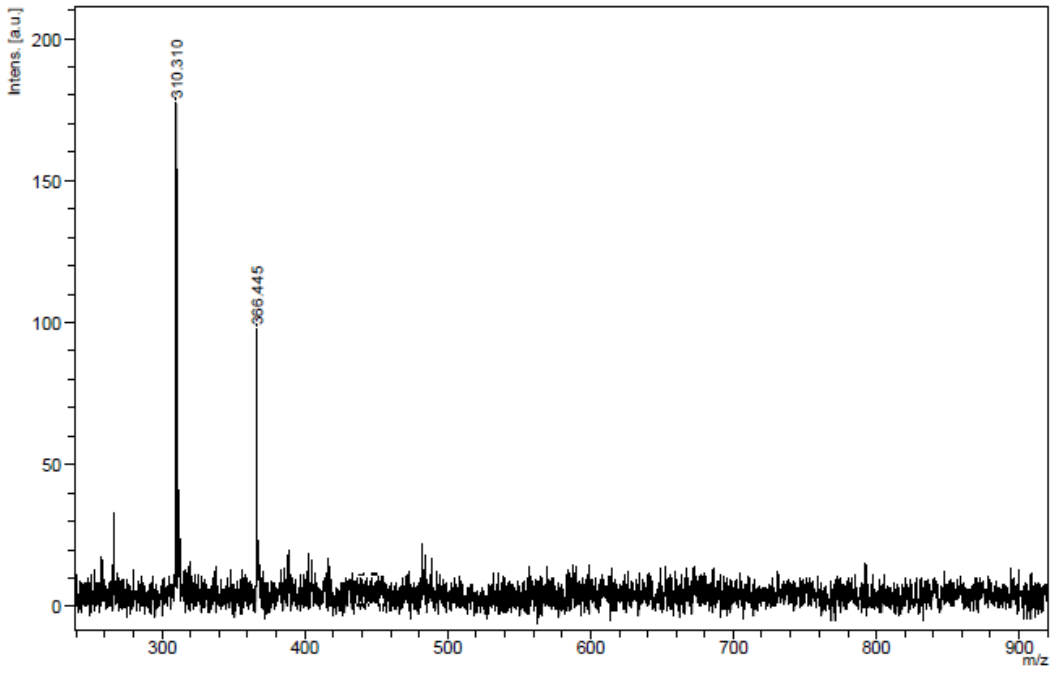

Appendix-7.3: MALDI-TOF MS spectrum of **Boc-Tyr-Ala-OCH$_3$** compound **(8)**

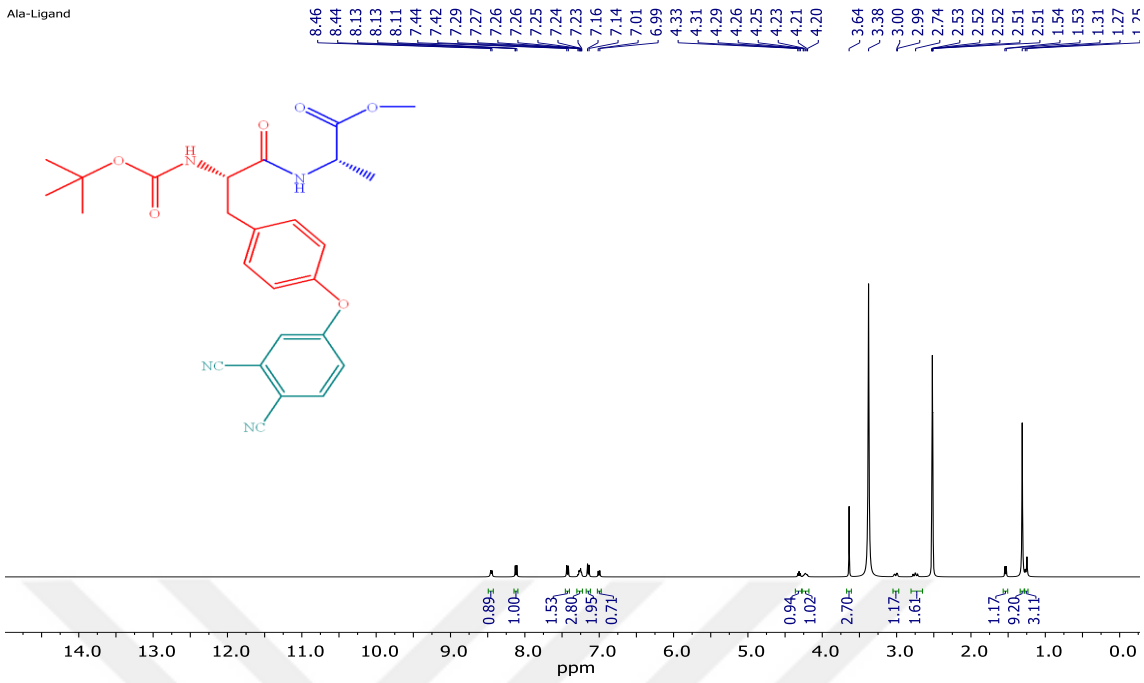

Appendix-7.4: ^{1}H-NMR spectrum of methyl((S)-2-((tert-butoxycarbonyl) amino)-3-(4-(3,4-dicyanophenoxy) phenyl) propanoyl)-*D*-alaninate **(Boc-Tyr-Ala-OCH$_3$-O-PN) (9)** in (DMSO-d6)

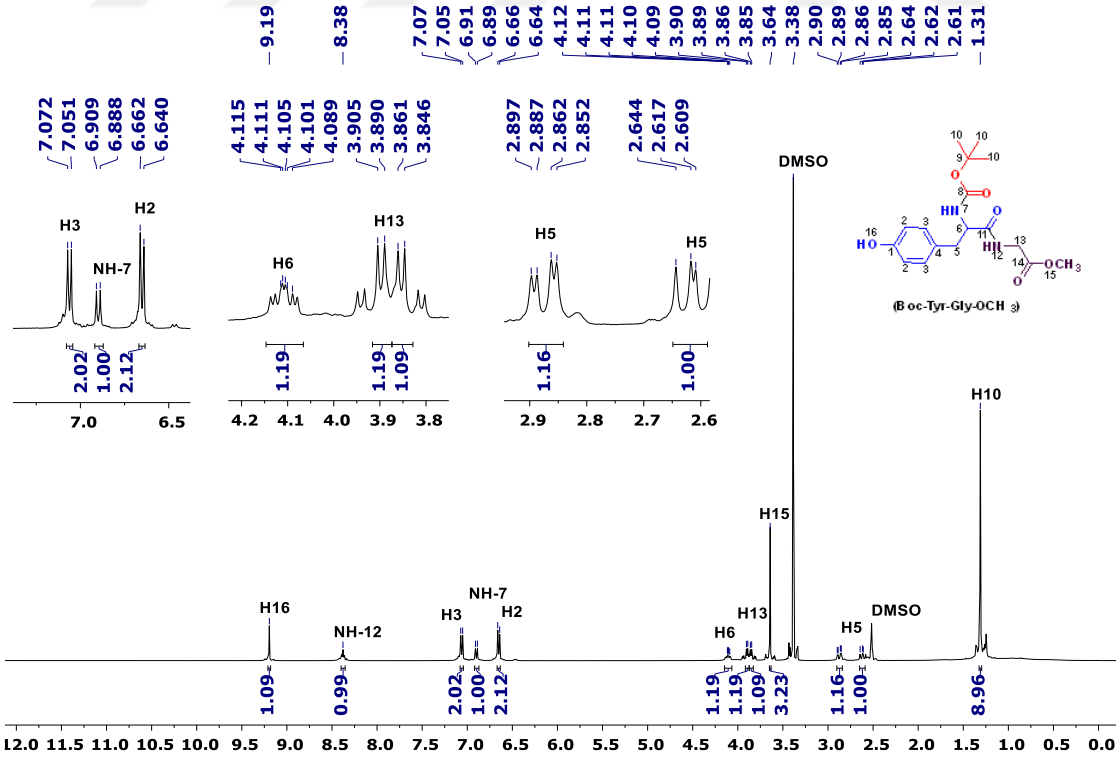

Appendix-8.1: ^{1}H-NMR spectrum of **Boc-Tyr-Gly-OCH$_3$** compound **(10)** in (DMSO-d6)

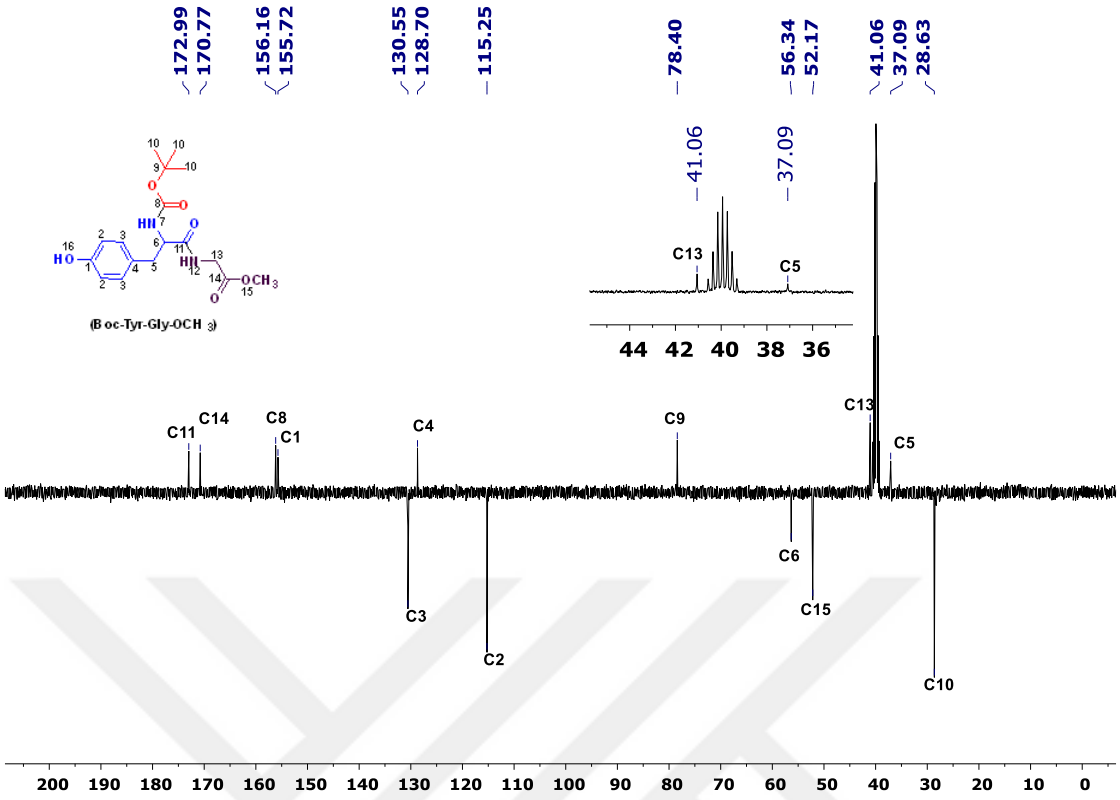

Appendix-8.2: ^{13}C-APT NMR spectrum of **Boc-Tyr-Gly-OCH$_3$** compound **(10)** in (DMSO-d6)

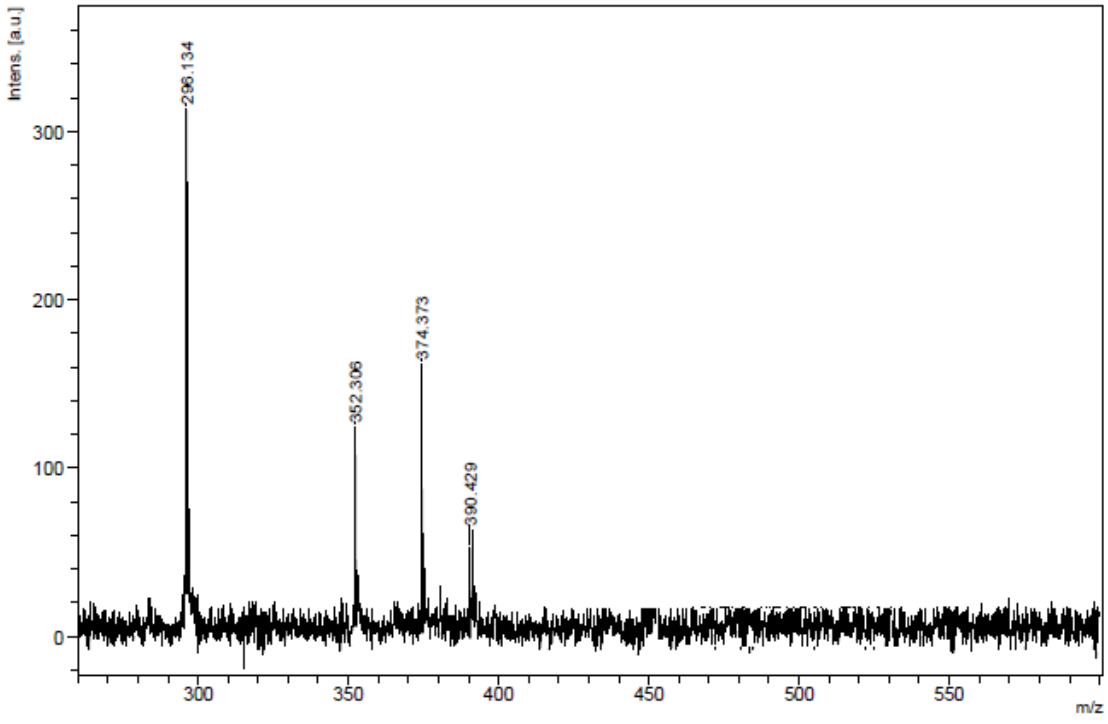

Appendix-8.3: MALDI-TOF MS spectrum of Boc-Tyr-Gly-OCH$_3$ compound (10)

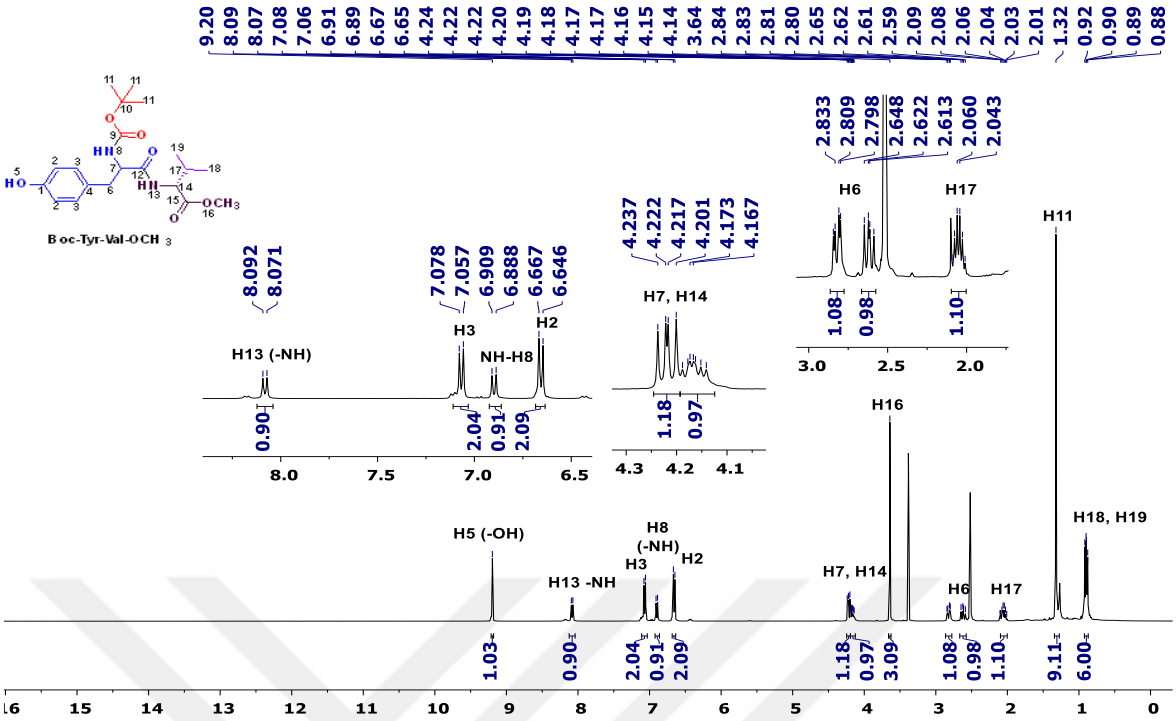

Appendix-9.1: ^{1}H-NMR spectrum of **Boc-Tyr-Val-OCH$_3$** compound **(12)** in (DMSO-d6)

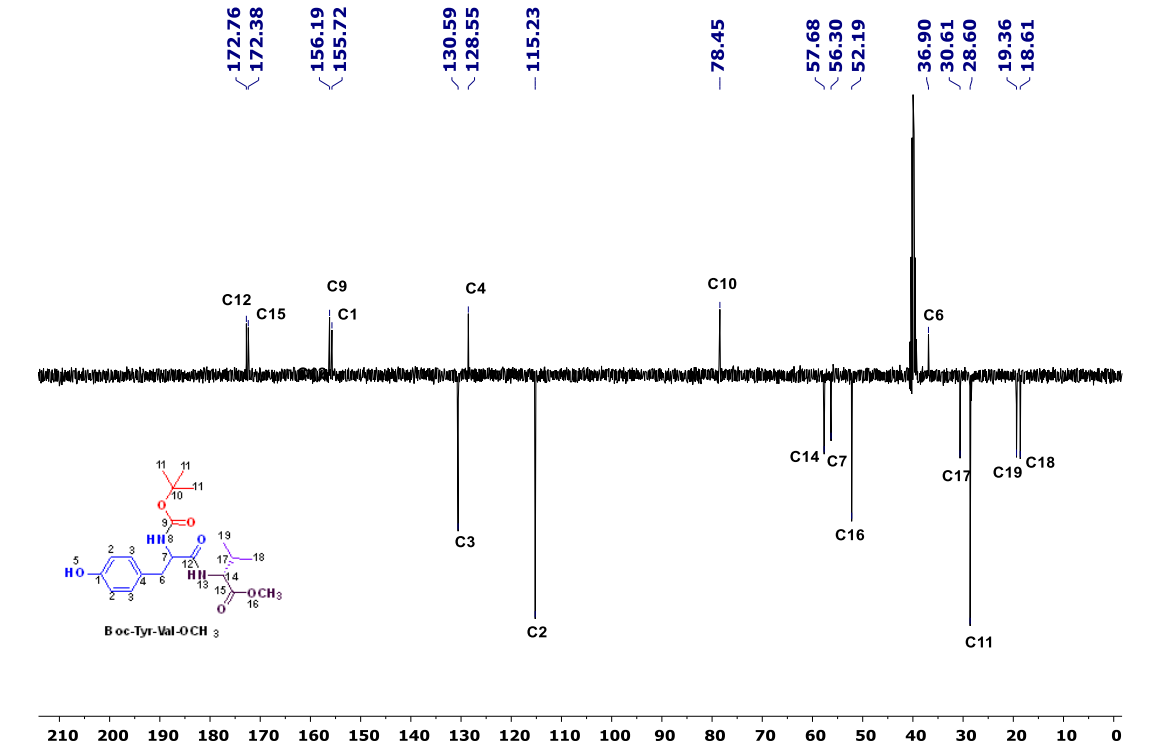

Appendix-9.2: ^{13}C-APT NMR spectrum **of Boc-Tyr-Val-OCH$_3$** compound **(12)** in (DMSO-d6)

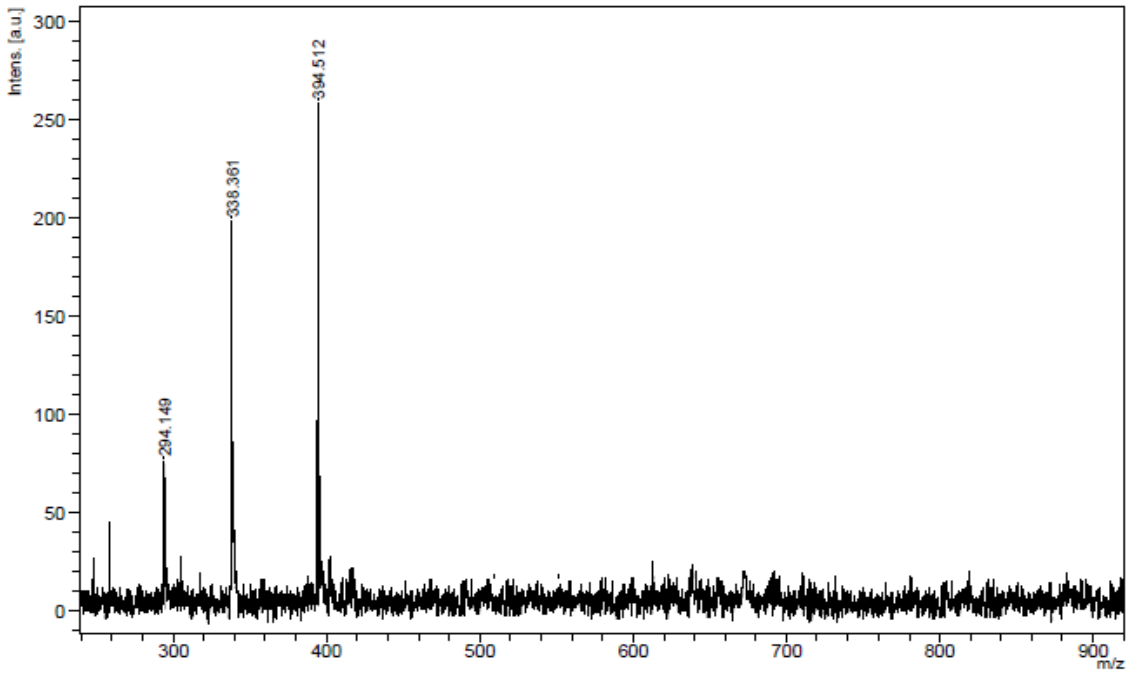

Appendix-9.3: MALDI-TOF MS spectrum of (Boc-Tyr-Val-OCH_3) compound (12)

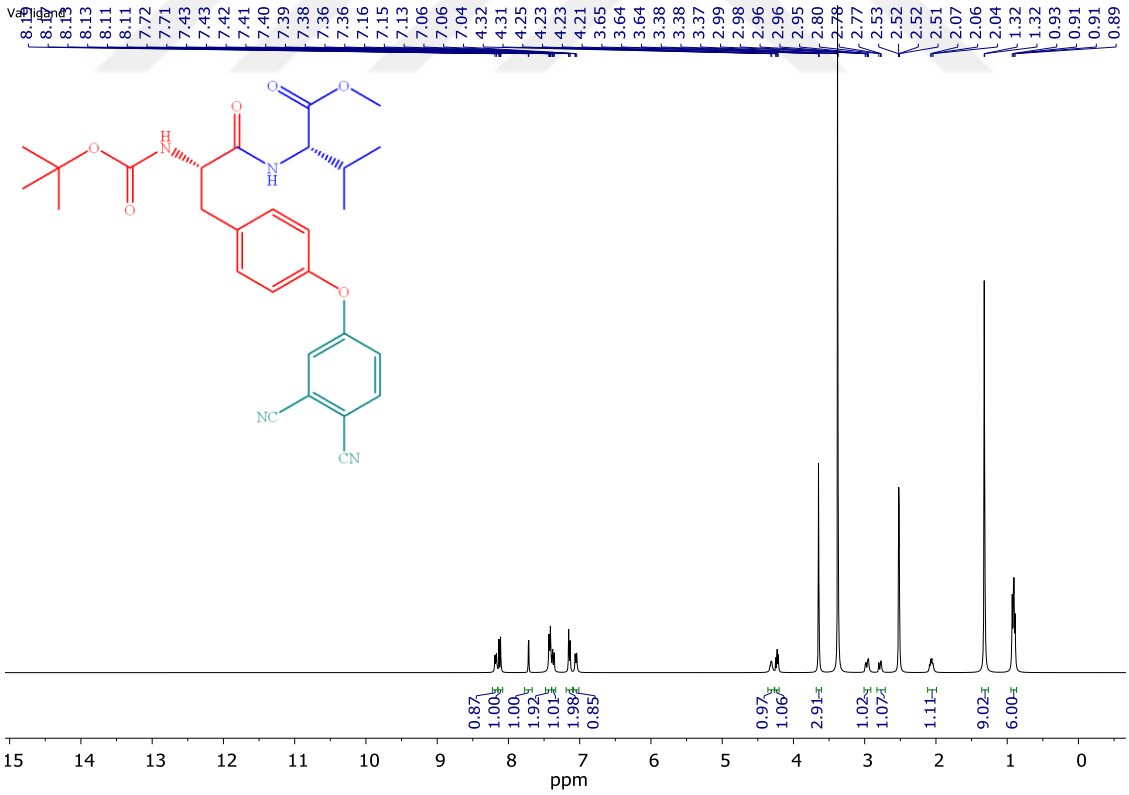

Appendix-9.4: ^{1}H-NMR spectrum of methyl ((S)-2-((tert-butoxycarbonyl) amino)-3-(4-(3,4-dicyanophenoxy) phenyl) propanoyl) valinate **(Boc- Tyr-Val-OCH_3-O-PN) (13)** in (DMSO-d6)

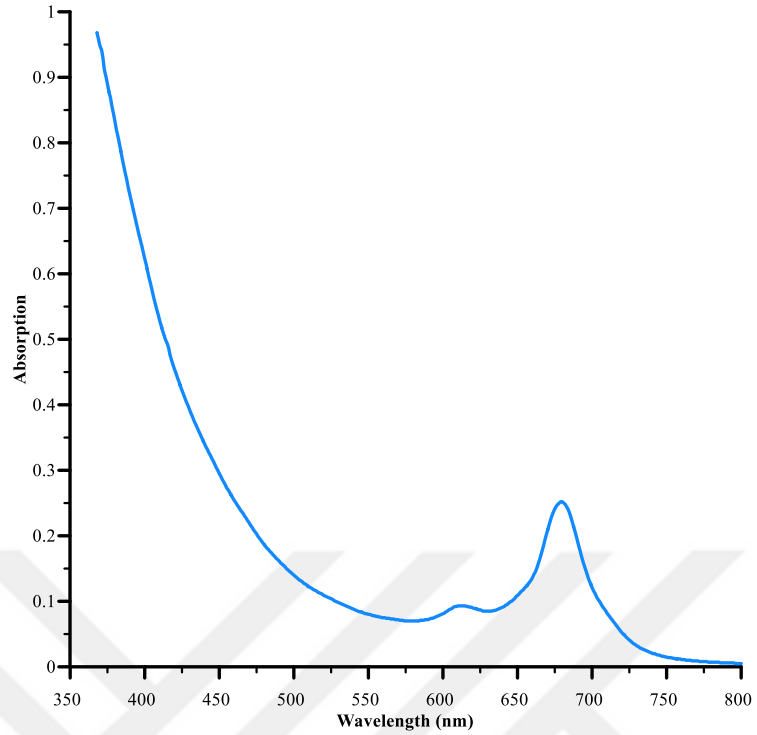

Appendix-10.1: UV-visible absorption spectrum of CrPc tyrosine – phenylalanine dipeptide substituted phthalocyanine complex **(7a)** compound

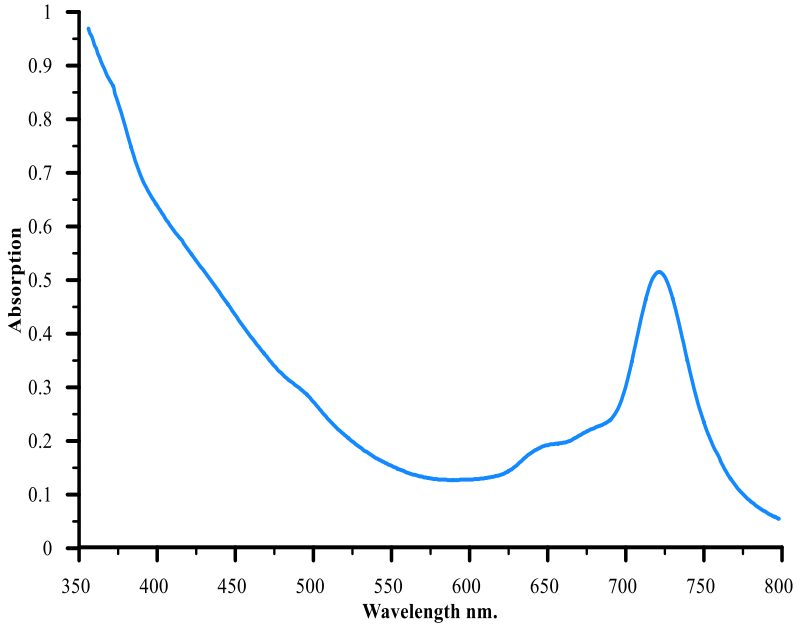

Appendix-10.2: UV-visible absorption spectrum of MnPc tyrosine – phenylalanine dipeptide substituted phthalocyanine complex **(7b)** compound

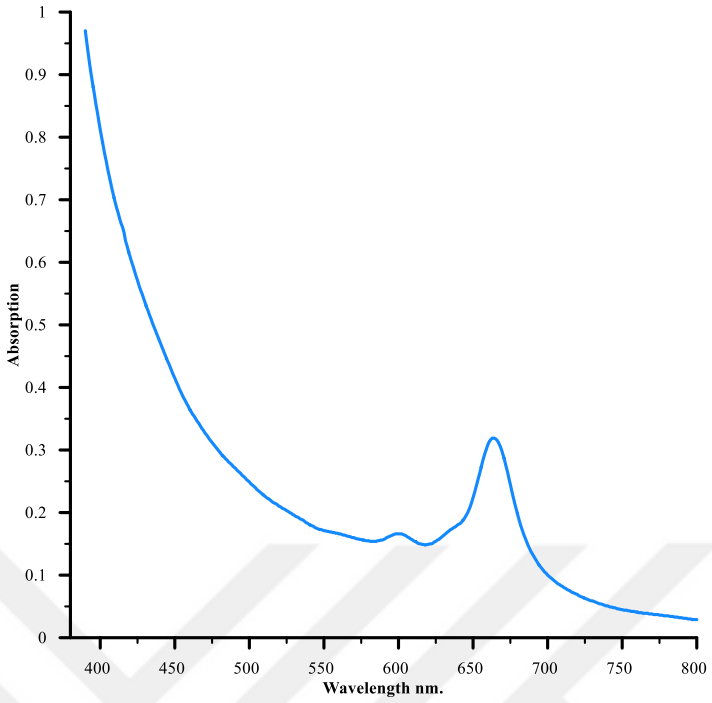

Appendix-10.3: UV-visible absorption spectrum of FePc tyrosine – phenylalanine dipeptide substituted phthalocyanine complex **(7c)** compound.

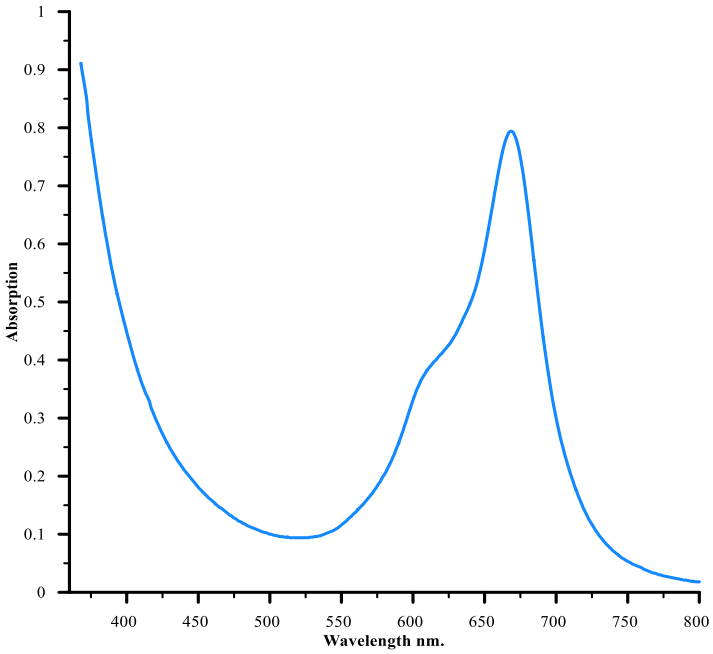

Appendix-10.4: UV-visible absorption spectrum of CoPc tyrosine – phenylalanine dipeptide substituted phthalocyanine complex **(7d)** compound.

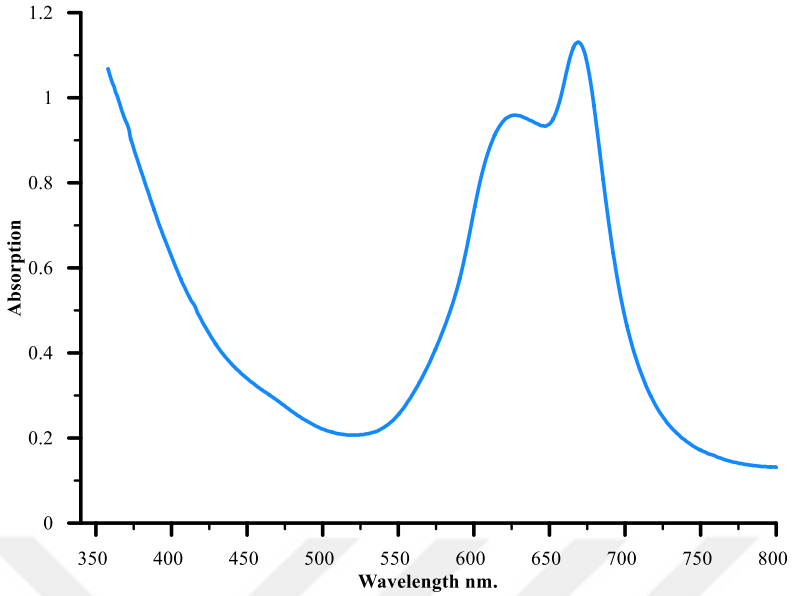

Appendix-10.5: UV-visible absorption spectrum of NiPc tyrosine – phenylalanine dipeptide substituted phthalocyanine complex **(7e)** compound.

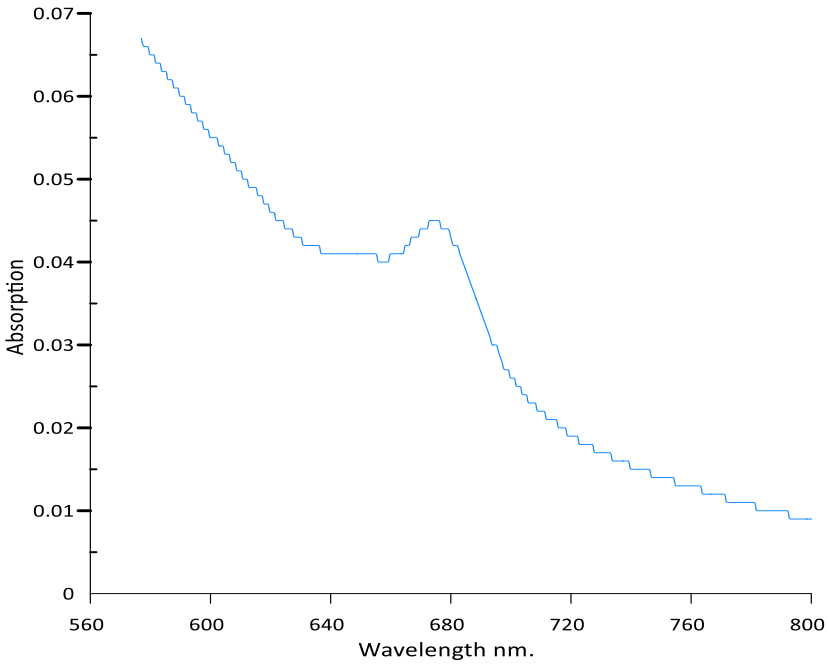

Appendix-10.6: UV-visible absorption spectrum of CuPc tyrosine – phenylalanine dipeptide substituted phthalocyanine complex **(7f)** compound.

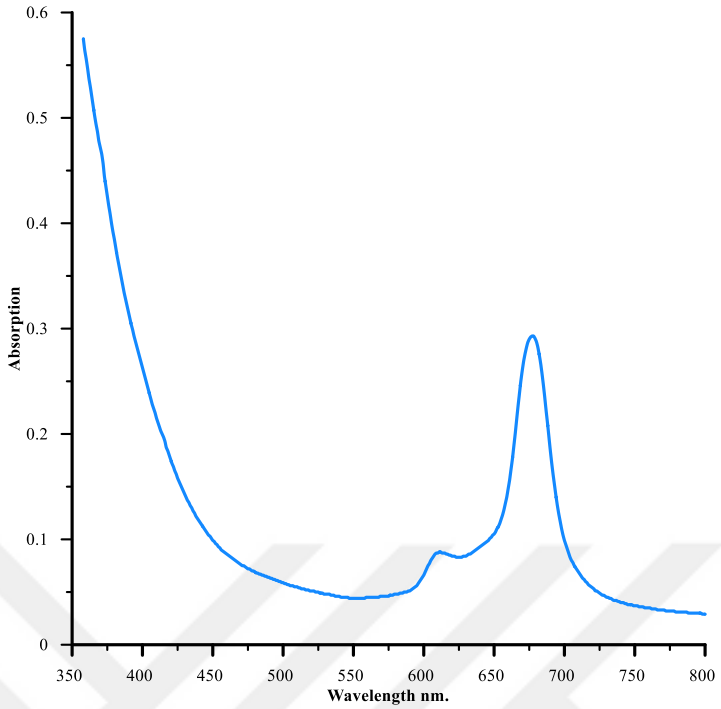

Appendix-10.7: UV-visible absorption spectrum of ZnPc tyrosine – phenylalanine dipeptide substituted phthalocyanine complex **(7g)** compound.

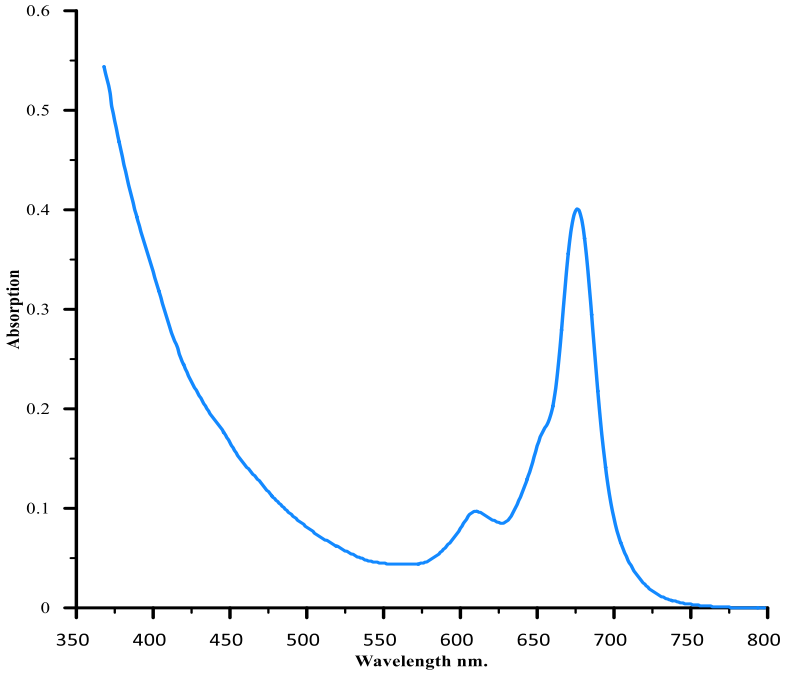

Appendix-11.1: UV-visible absorption spectrum of CrPc tyrosine – alanine dipeptide substituted phthalocyanine complex **(9a)** compound.

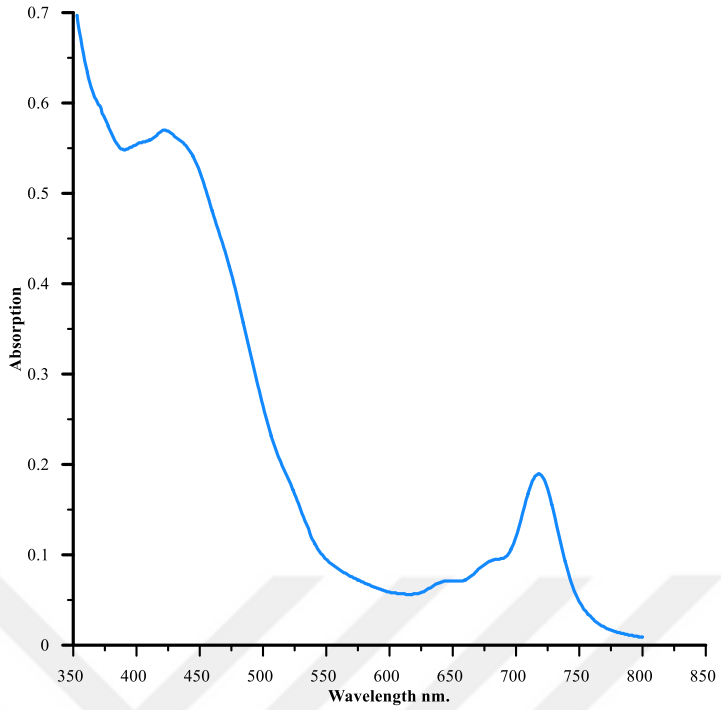

Appendix-11.2: UV-visible absorption spectrum of MnPc tyrosine – alanine dipeptide substituted phthalocyanine complex **(9b)** compound.

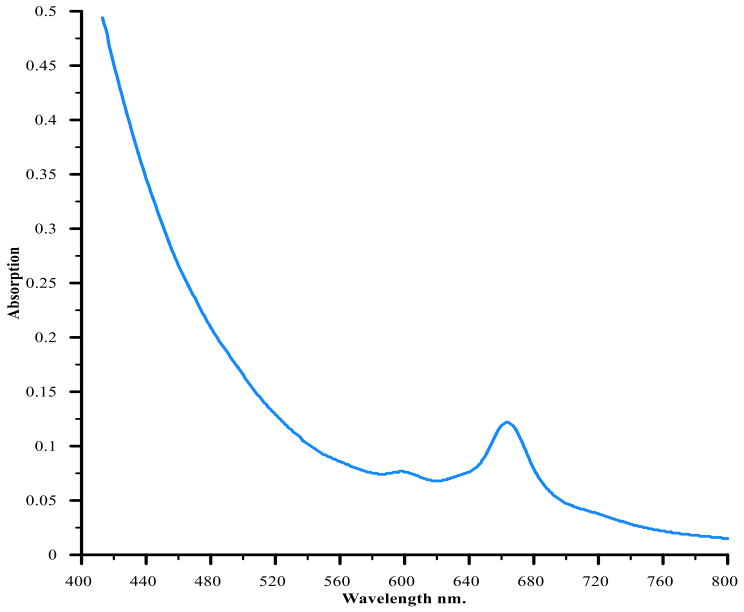

Appendix-11.3: UV-visible absorption spectrum of FePc tyrosine – alanine dipeptide substituted phthalocyanine complex **(9c)** compound.

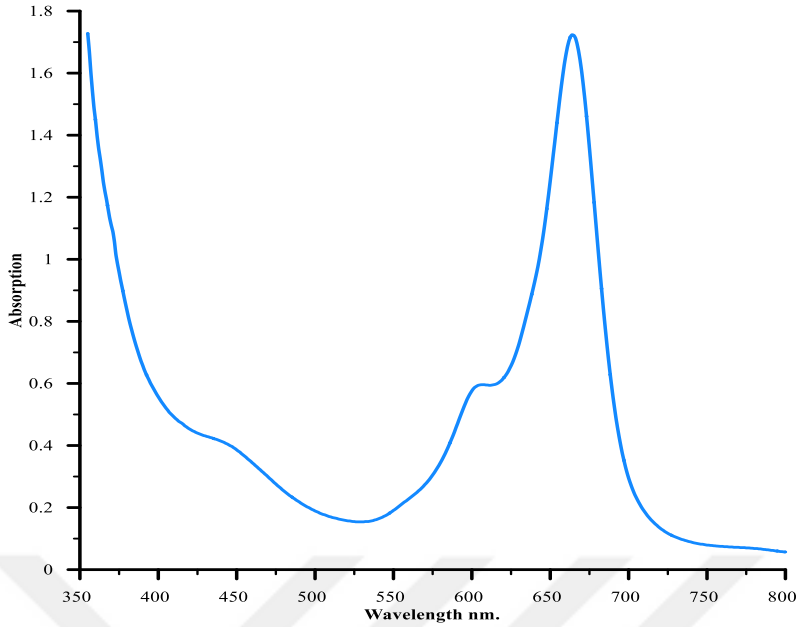

Appendix-11.4: UV-visible absorption spectrum of CoPc tyrosine – alanine dipeptide substituted phthalocyanine complex **(9d)** compound.

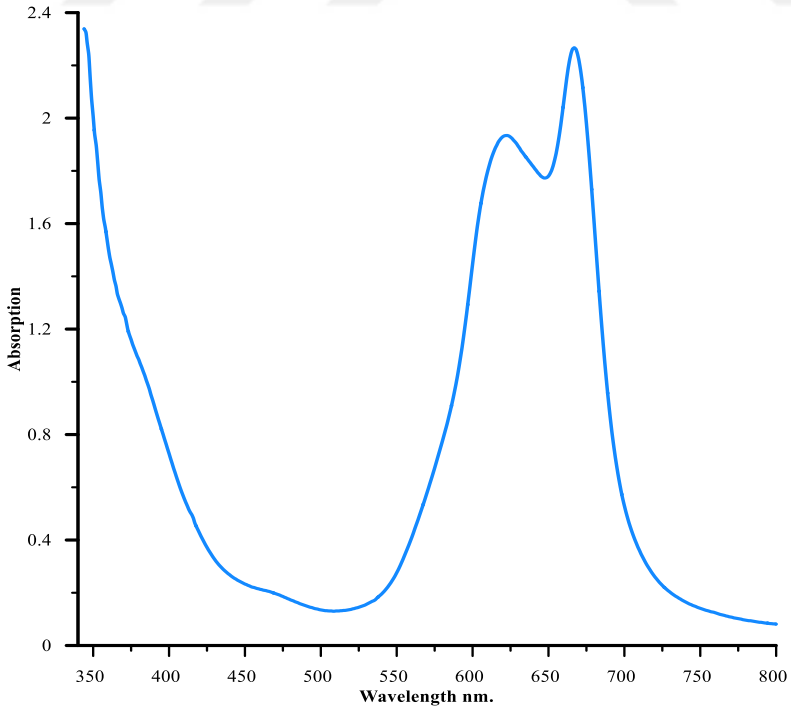

Appendix-11.5: UV-visible absorption spectrum of NiPc tyrosine – alanine dipeptide substituted phthalocyanine complex **(9e)** compound.

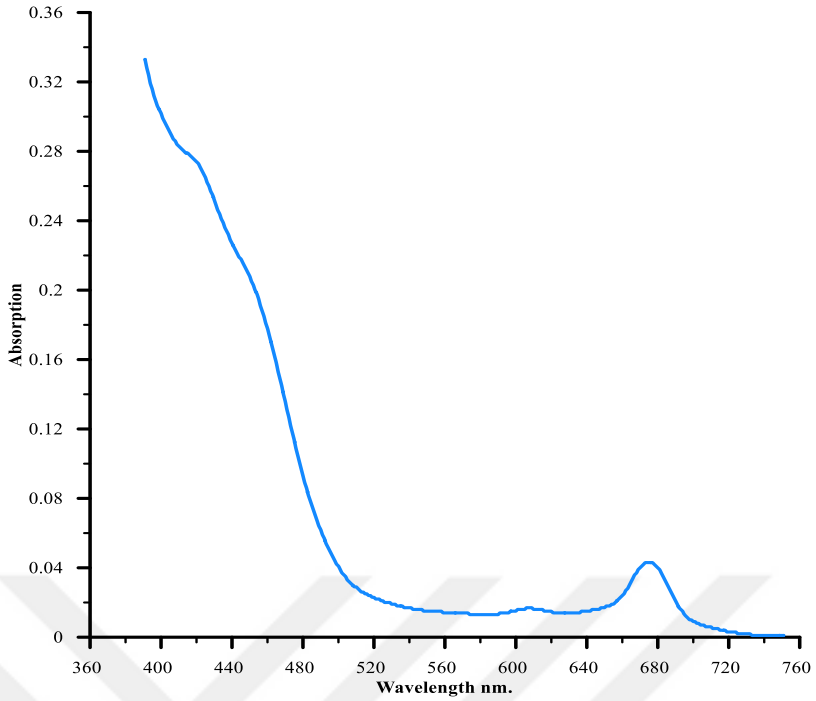

Appendix-11.6: UV-visible absorption spectrum of CuPc tyrosine – alanine dipeptide substituted phthalocyanine complex **(9f)** compound.

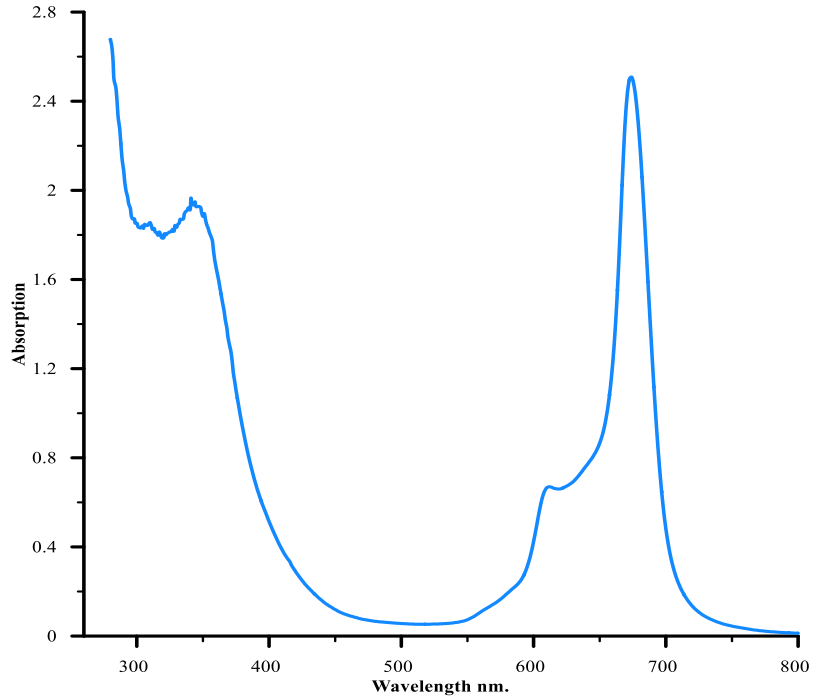

Appendix-11.7: UV-visible absorption spectrum of ZnPc tyrosine – alanine dipeptide substituted phthalocyanine complex **(9g)** compound.

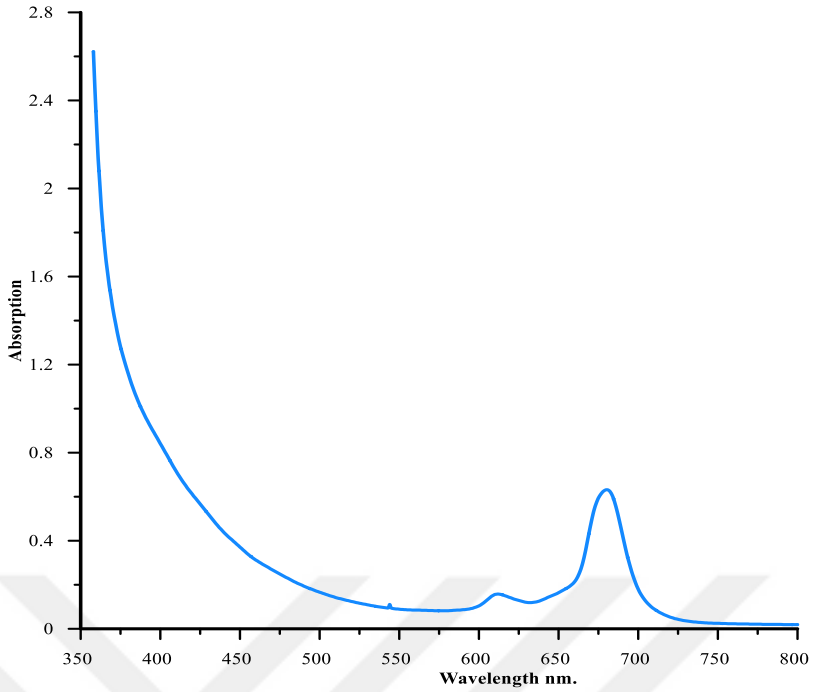

Appendix-12.1: UV-visible absorption spectrum of CrPc tyrosine – glycine dipeptide substituted phthalocyanine complex **(11a)** compound.

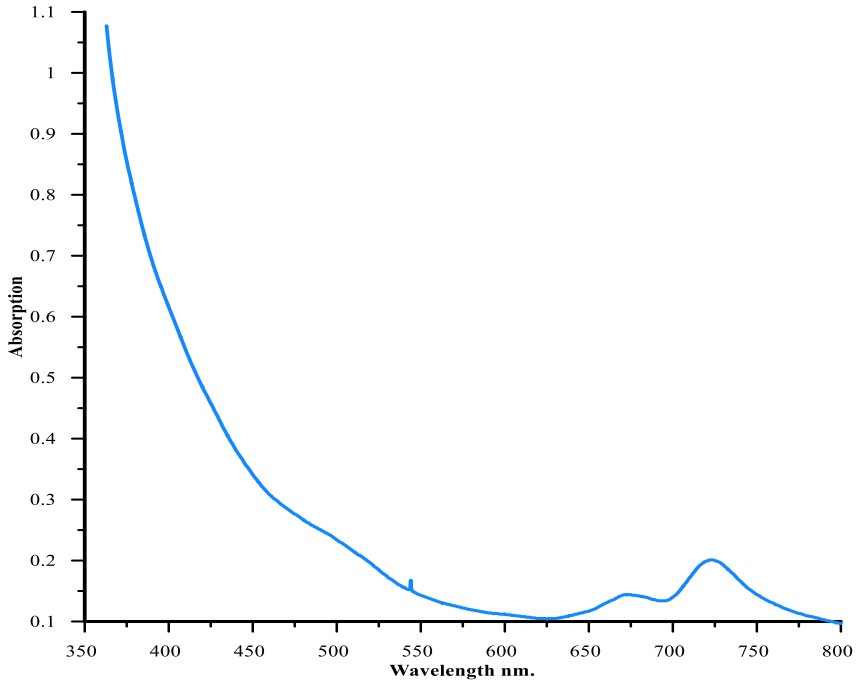

Appendix-12.2: UV-visible absorption spectrum of MnPc tyrosine – glycine dipeptide substituted phthalocyanine complex **(11b)** compound.

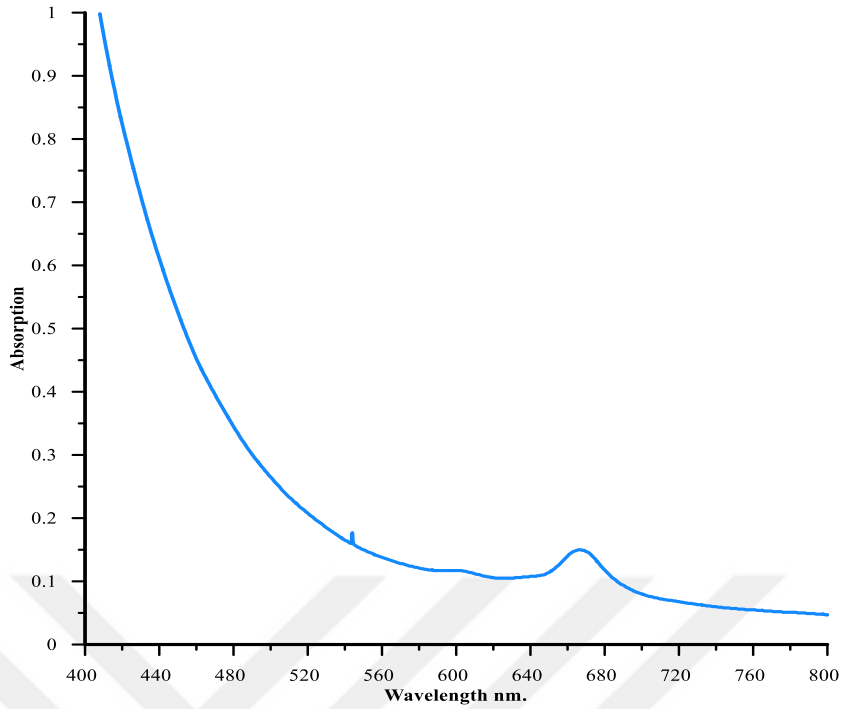

Appendix-12.3: UV-visible absorption spectrum of FePc tyrosine – glycine dipeptide substituted phthalocyanine complex **(11c)** compound.

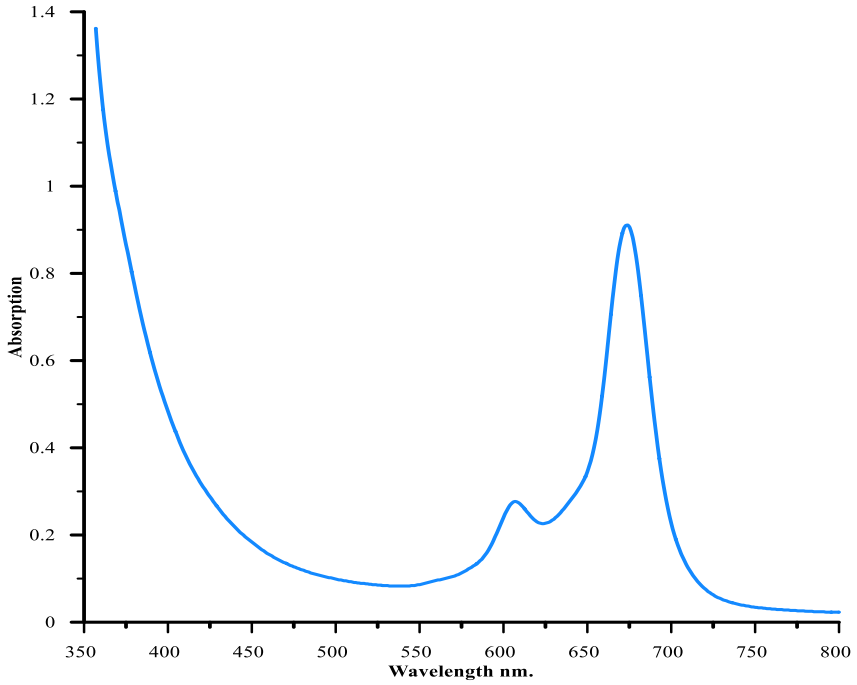

Appendix-12.4: UV-visible absorption spectrum of CoPc tyrosine – glycine dipeptide substituted phthalocyanine complex **(11d)** compound.

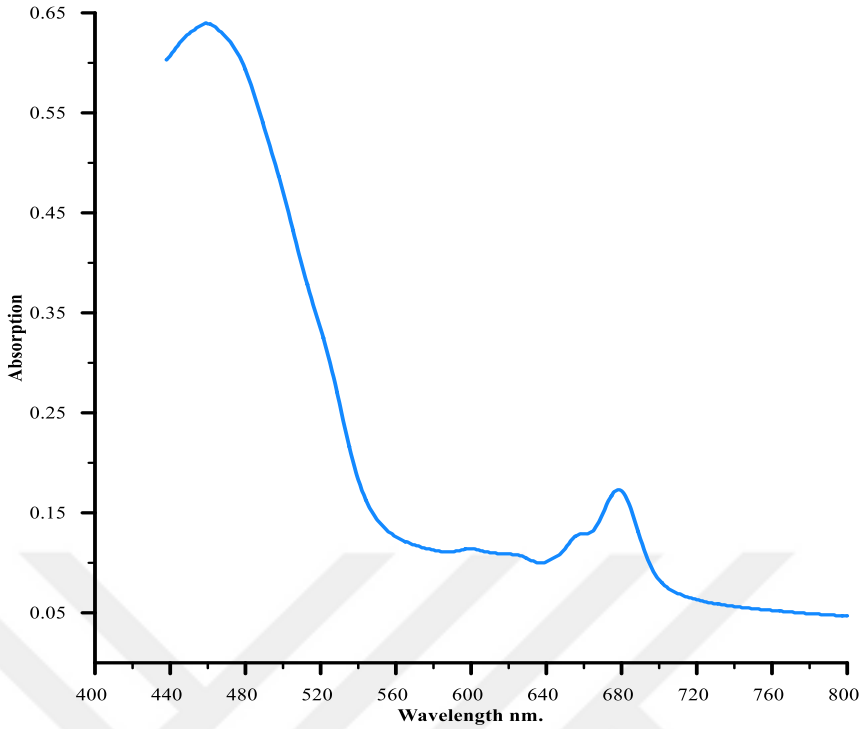

Appendix-12.5: UV-visible absorption spectrum of NiPc tyrosine – glycine dipeptide substituted phthalocyanine complex **(11e)** compound.

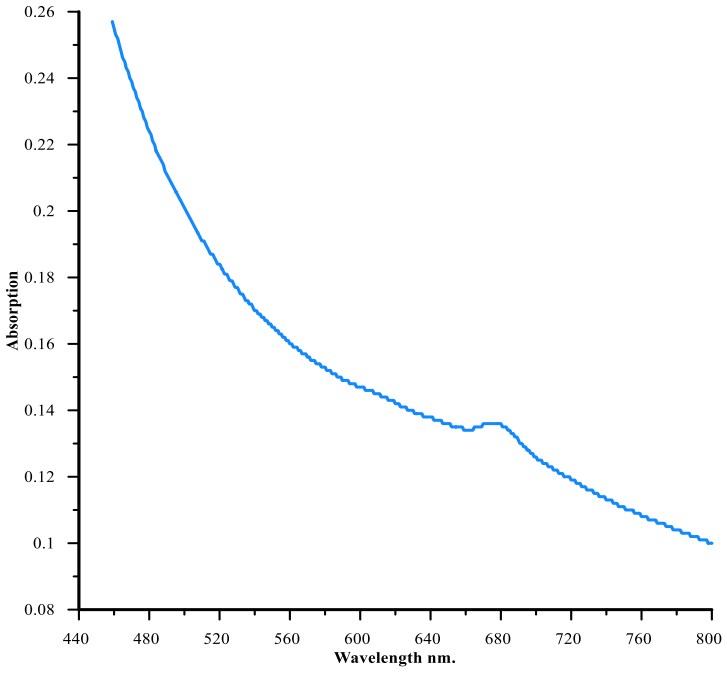

Appendix-12.6: UV-visible absorption spectrum of CuPc tyrosine – glycine dipeptide substituted phthalocyanine complex **(11f)** compound.

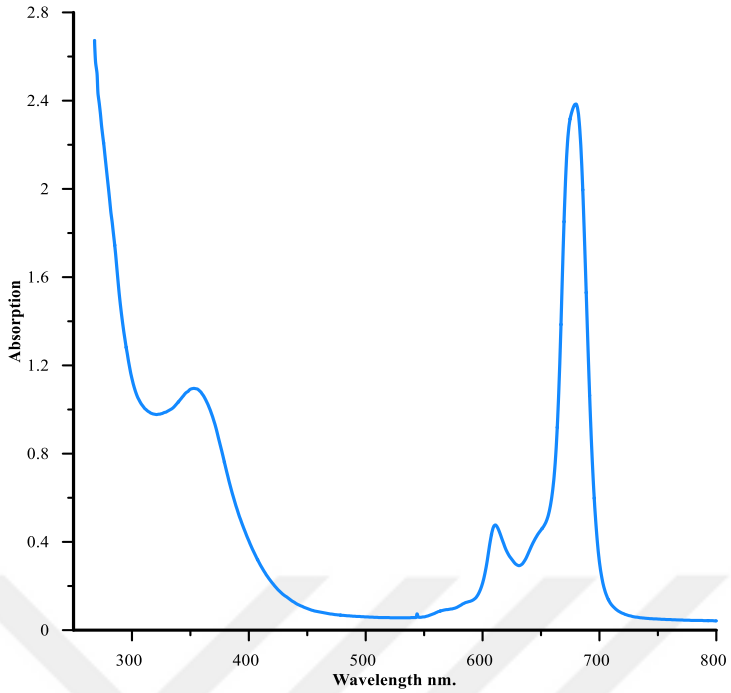

Appendix-12.7: UV-visible absorption spectrum of ZnPc tyrosine – glycine dipeptide substituted phthalocyanine complex **(11g)** compound.

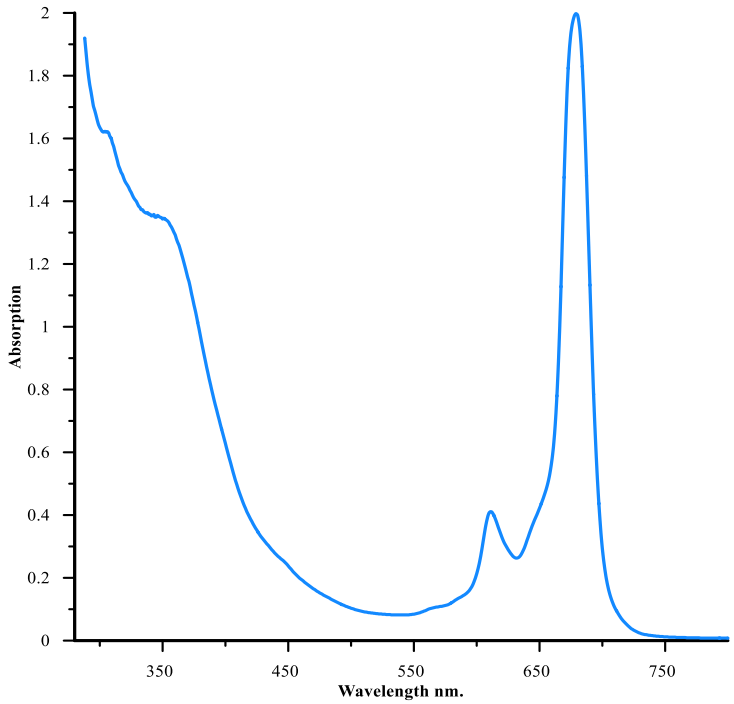

Appendix-13.1: UV-visible absorption spectrum of CrPc tyrosine – valine dipeptide substituted phthalocyanine complex **(13a)** compound.

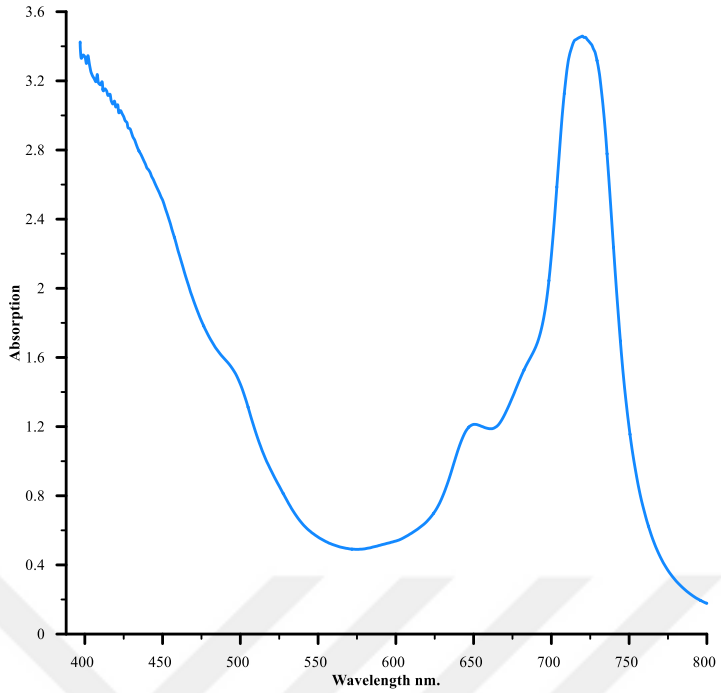

Appendix-13.2: UV-visible absorption spectrum of MnPc tyrosine – valine dipeptide substituted phthalocyanine complex **(13b)** compound

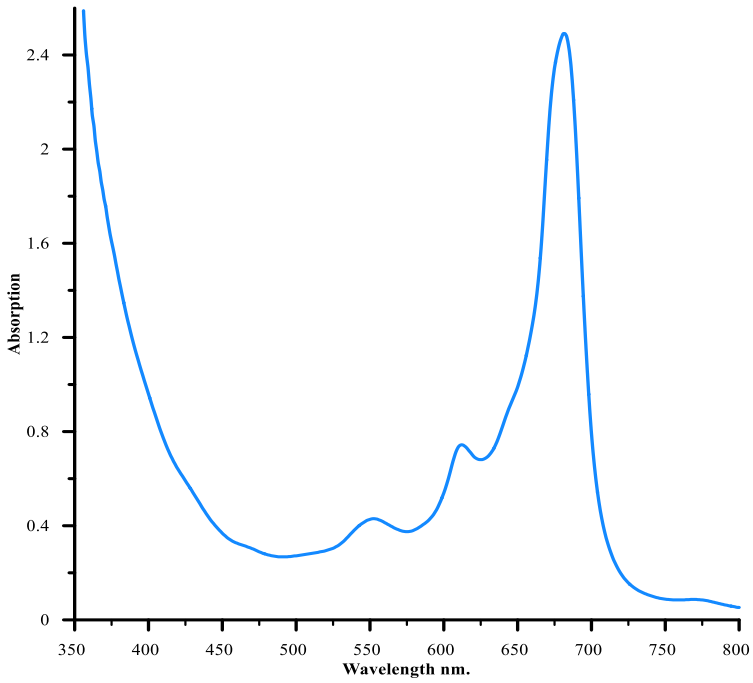

Appendix-13.3: UV-visible absorption spectrum of FePc tyrosine – valine dipeptide substituted phthalocyanine complex **(13c)** compound.

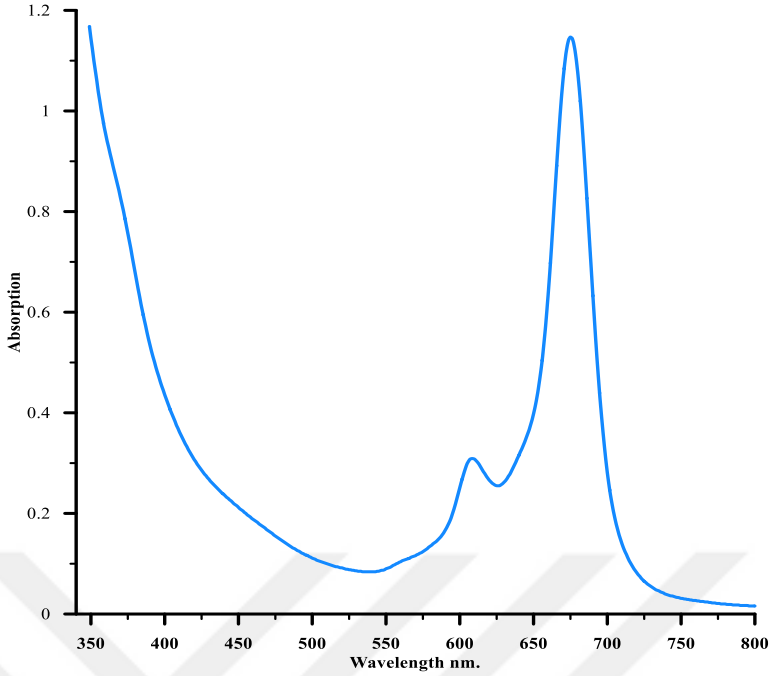

Appendix-13.4: UV-visible absorption spectrum of CoPc tyrosine – valine dipeptide substituted phthalocyanine complex **(13d)** compound.

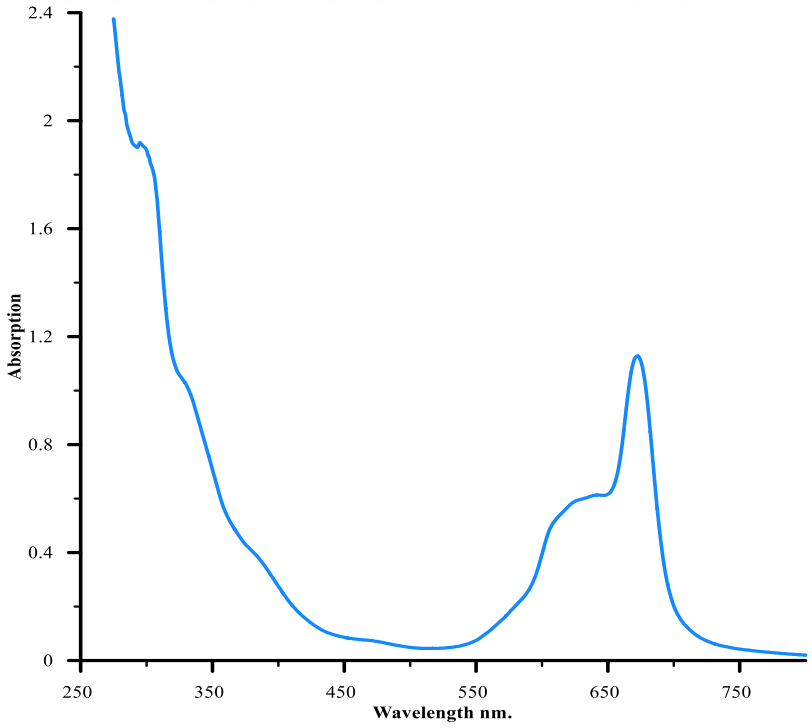

Appendix-13.5: UV-visible absorption spectrum of NiPc tyrosine – valine dipeptide substituted phthalocyanine complex **(13e)** compound.

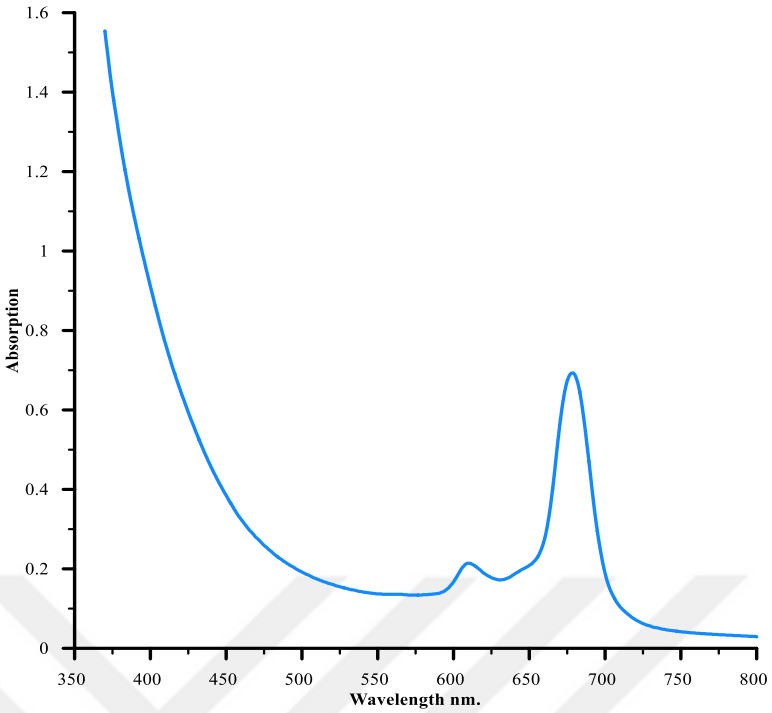

Appendix-13.6: UV-visible absorption spectrum of CuPc tyrosine – valine dipeptide substituted phthalocyanine complex **(13f)** compound.

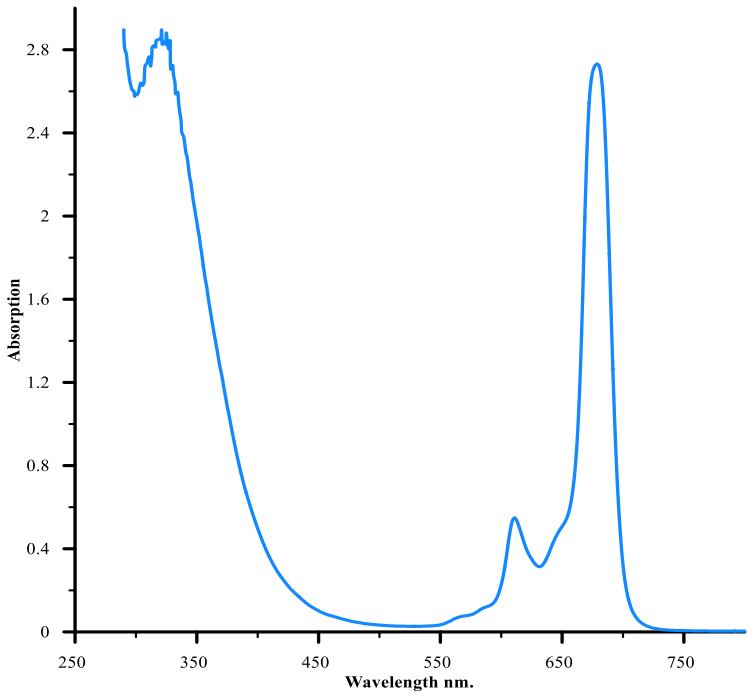

Appendix-13.7: UV-visible absorption spectrum of ZnPc tyrosine – valine dipeptide substituted phthalocyanine complex **(13g)** compound**.**

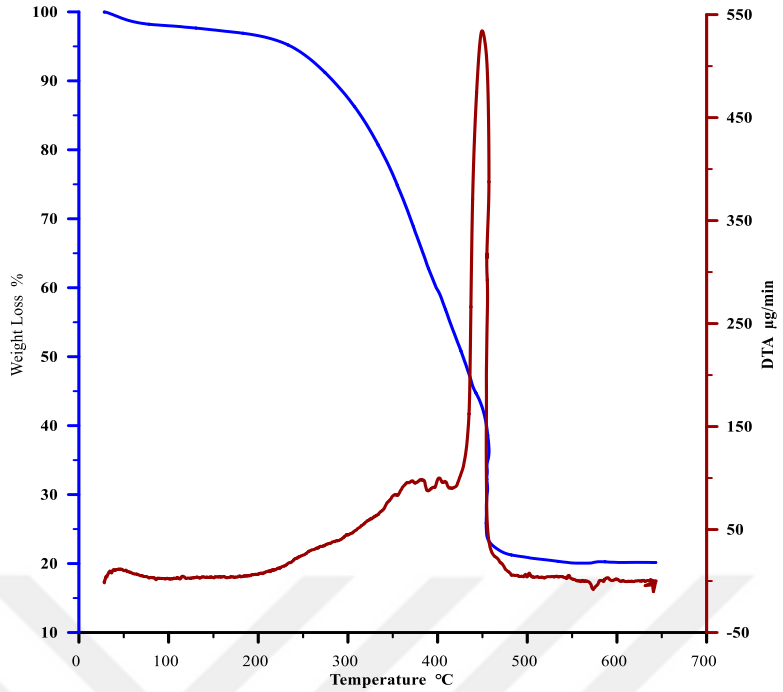

Appendix-14.1: TGA (blue) and DTA (red) thermograms chromium tyrosine - phenylalanine dipeptide substituted phthalocyanine complex **(7a)** compound.

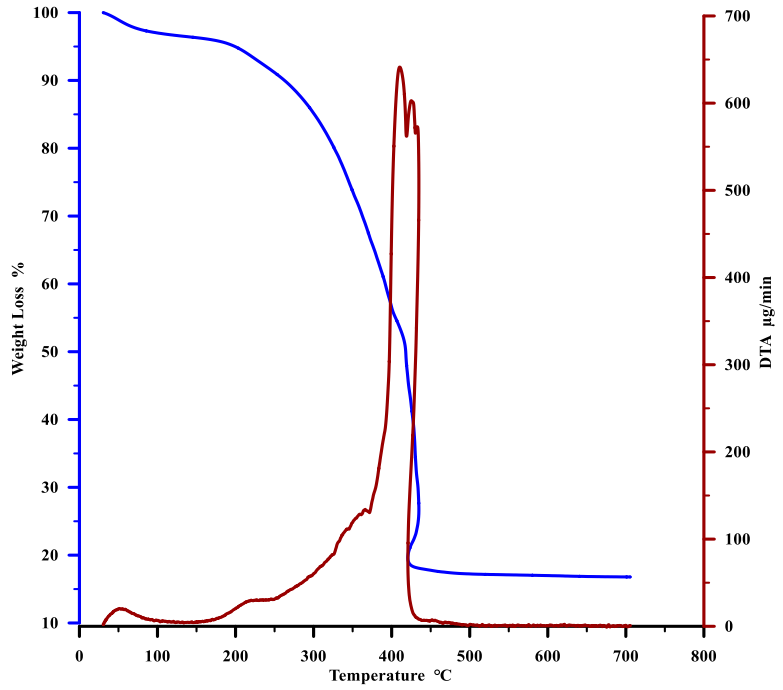

Appendix-14.2: TGA (blue) and DTA (red) thermograms manganese tyrosine - phenylalanine dipeptide substituted phthalocyanine complex **(7b)** compound.

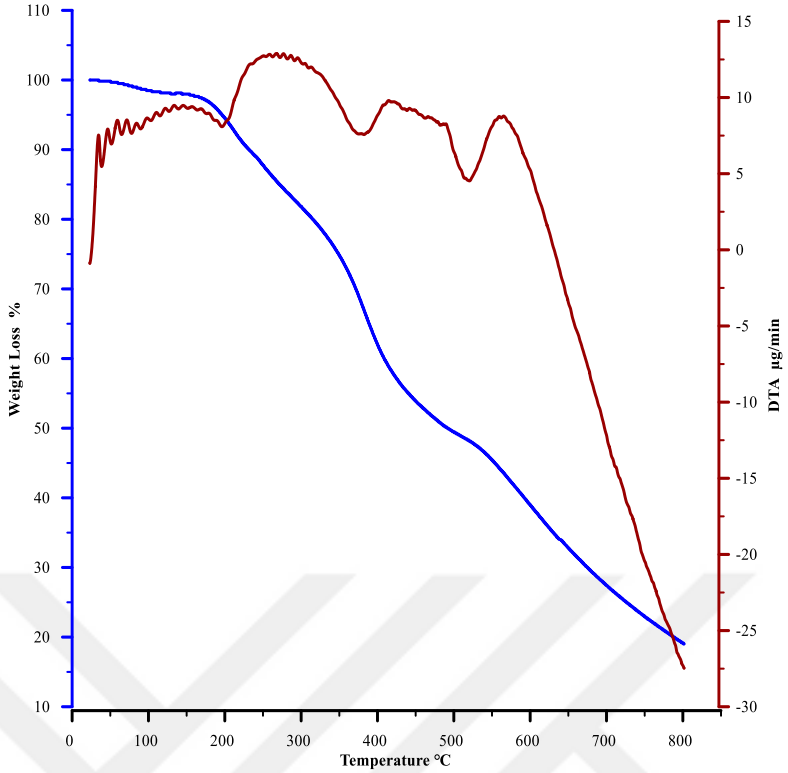

Appendix-14.3: TGA (blue) and DTA (red) thermograms iron tyrosine - phenylalanine dipeptide substituted phthalocyanine complex **(7c)** compound.

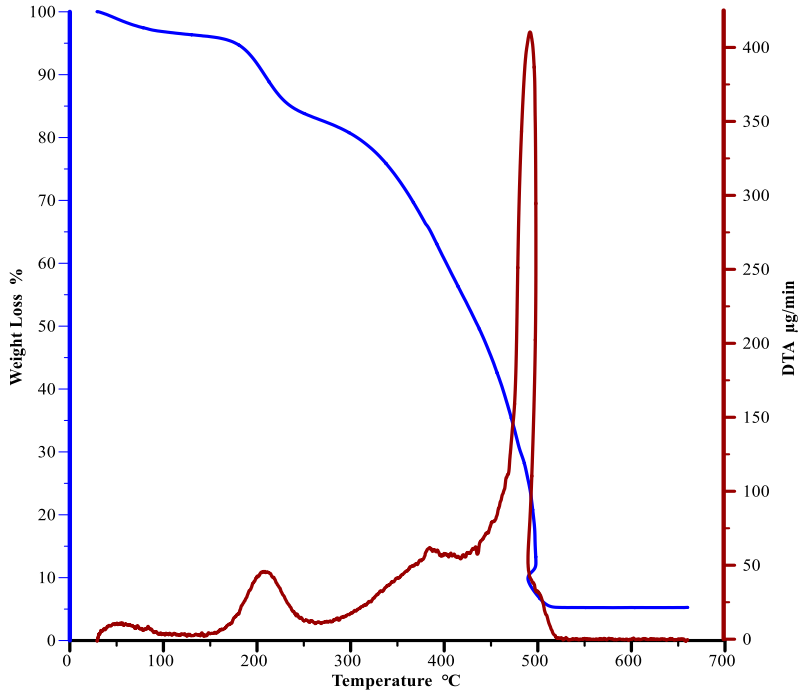

Appendix-14.4: TGA (blue) and DTA (red) thermograms cobalt tyrosine - phenylalanine dipeptide substituted phthalocyanine complex **(7d)** compound.

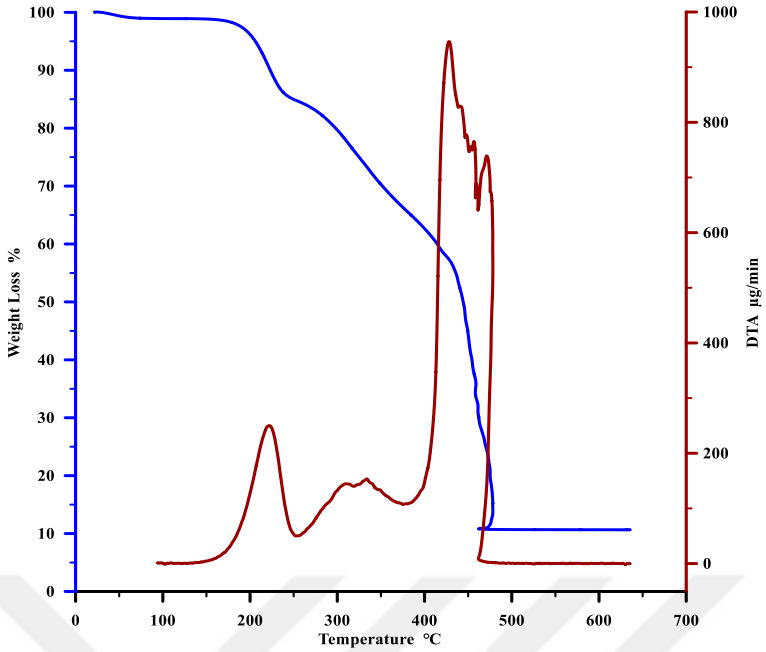

Appendix-14.5: TGA (blue) and DTA (red) thermograms nickel tyrosine - phenylalanine dipeptide substituted phthalocyanine complex **(7e)** compound.

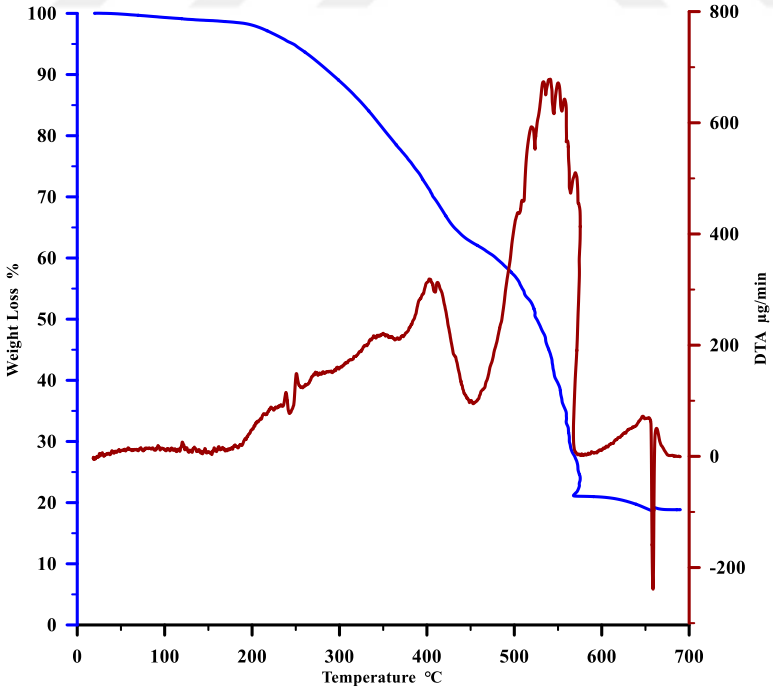

Appendix-14.6: TGA (blue) and DTA (red) thermograms copper tyrosine - phenylalanine dipeptide substituted phthalocyanine complex **(7f)** compound.

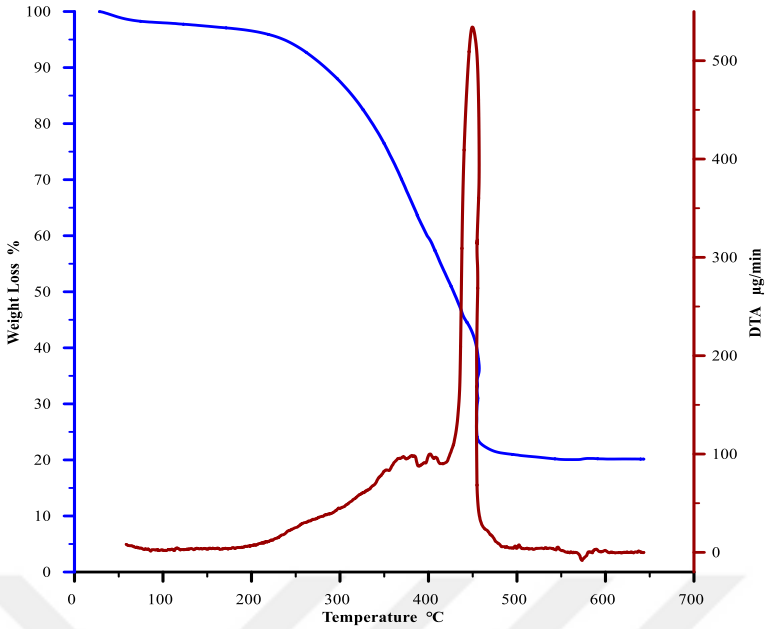

Appendix-14.7: TGA (blue) and DTA (red) thermograms zinc tyrosine - phenylalanine dipeptide substituted phthalocyanine complex **(7g)** compound.

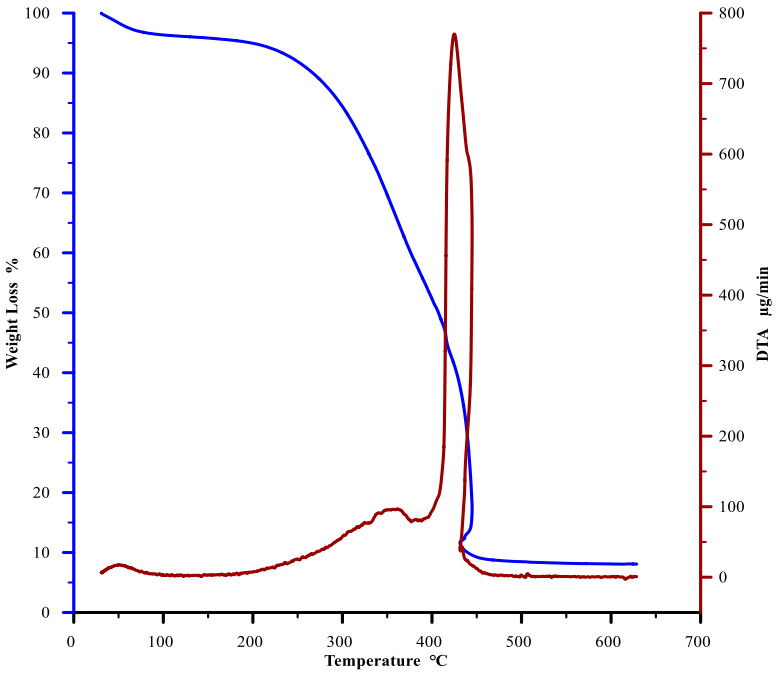

Appendix-15.1: TGA (blue) and DTA (red) thermograms chromium tyrosine - alanine dipeptide substituted phthalocyanine complex **(9a)** compound.

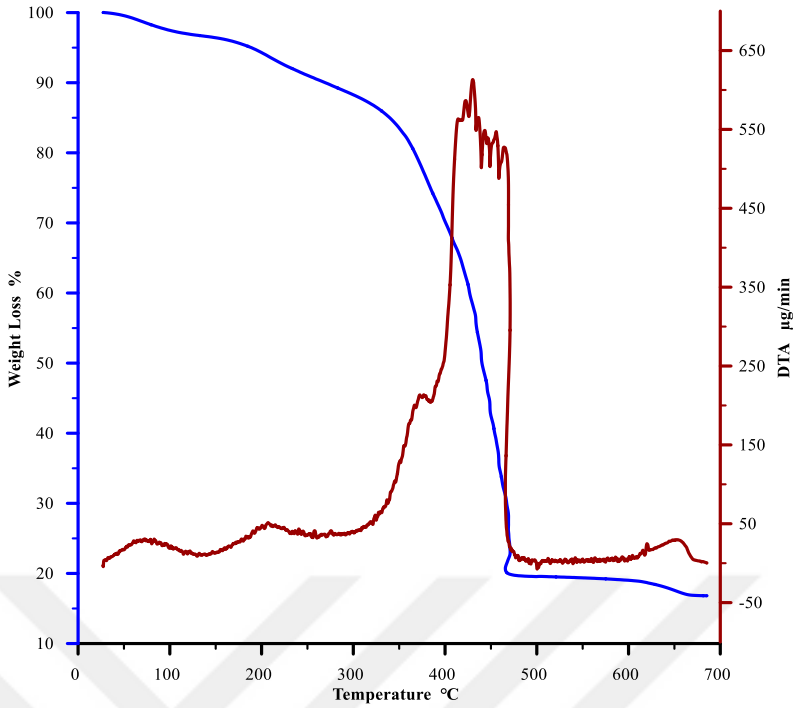

Appendix-15.2: TGA (blue) and DTA (red) thermograms manganese tyrosine - alanine dipeptide substituted phthalocyanine complex **(9b)** compound.

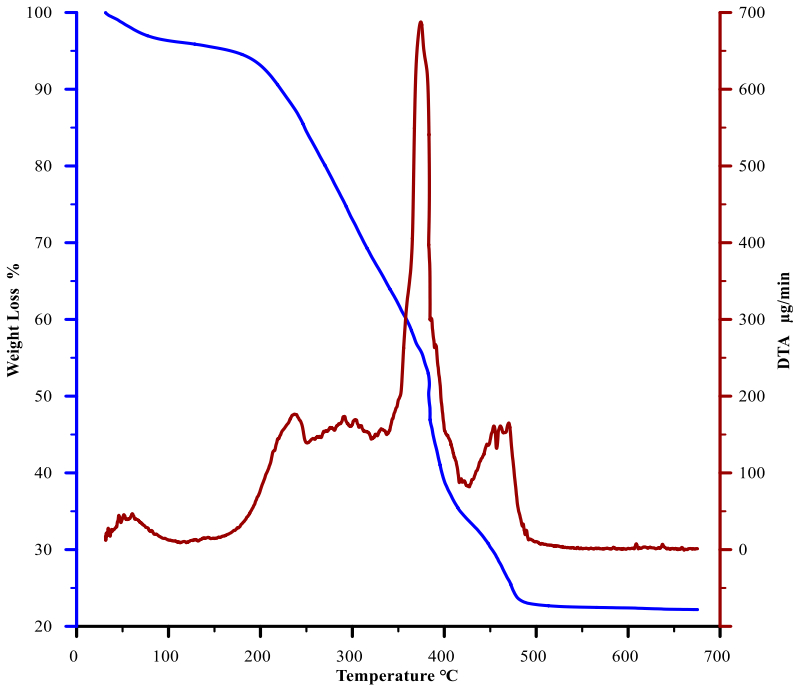

Appendix-15.3: TGA (blue) and DTA (red) thermograms iron tyrosine - alanine dipeptide substituted phthalocyanine complex **(9c)** compound.

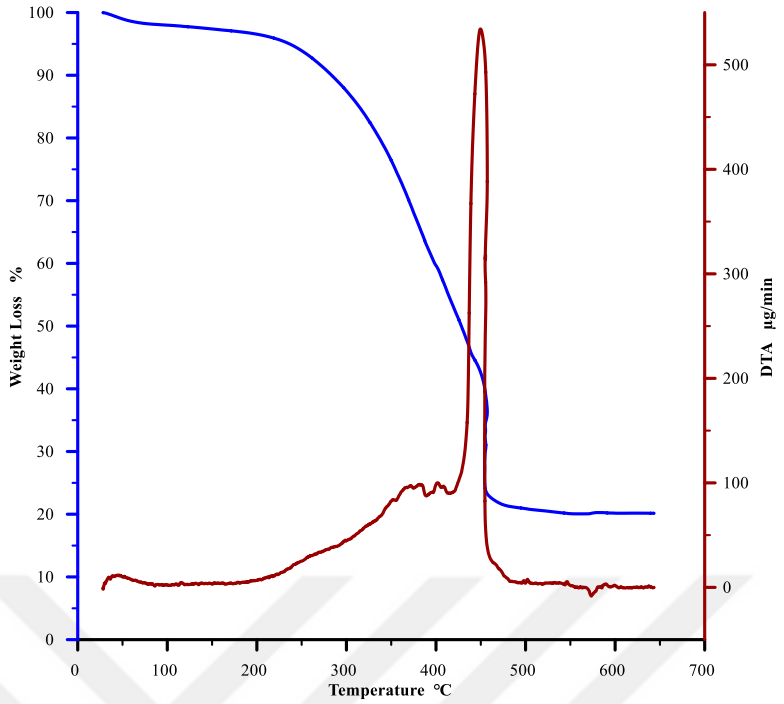

Appendix-15.4: TGA (blue) and DTA (red) thermograms cobalt tyrosine - alanine dipeptide substituted phthalocyanine complex **(9d)** compound.

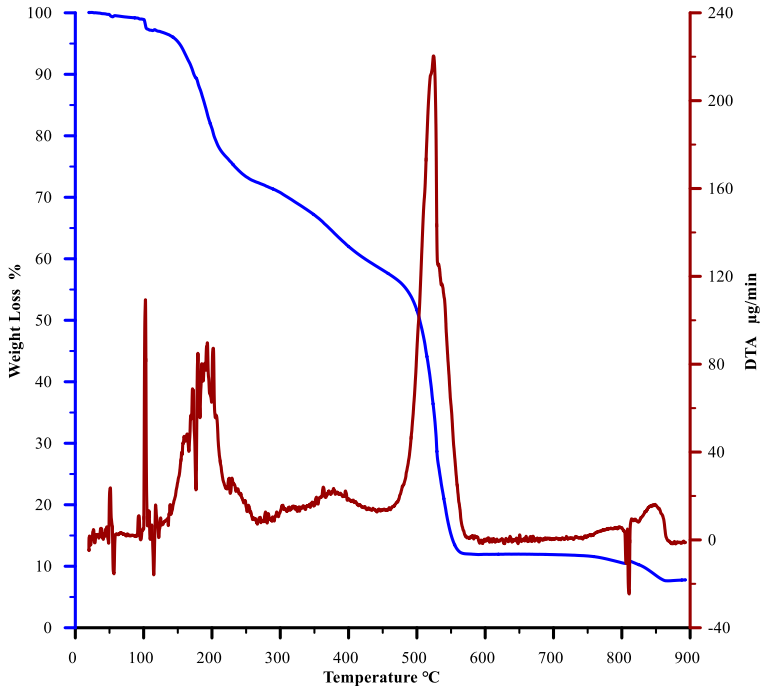

Appendix-15.5: TGA (blue) and DTA (red) thermograms nickel tyrosine - alanine dipeptide substituted phthalocyanine complex **(9e)** compound.

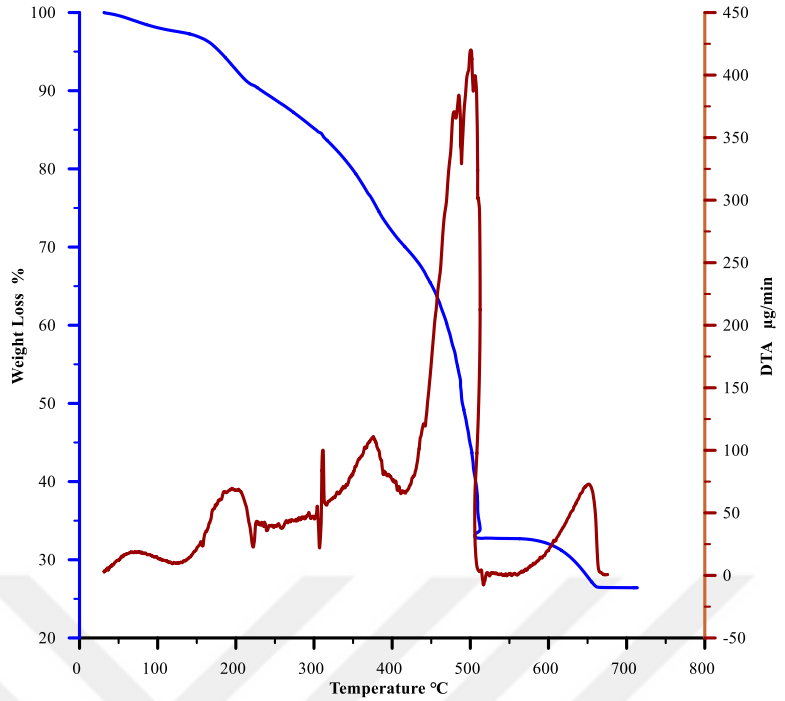

Appendix-15.6: TGA (blue) and DTA (red) thermograms copper tyrosine - alanine dipeptide substituted phthalocyanine complex **(9f)** compound.

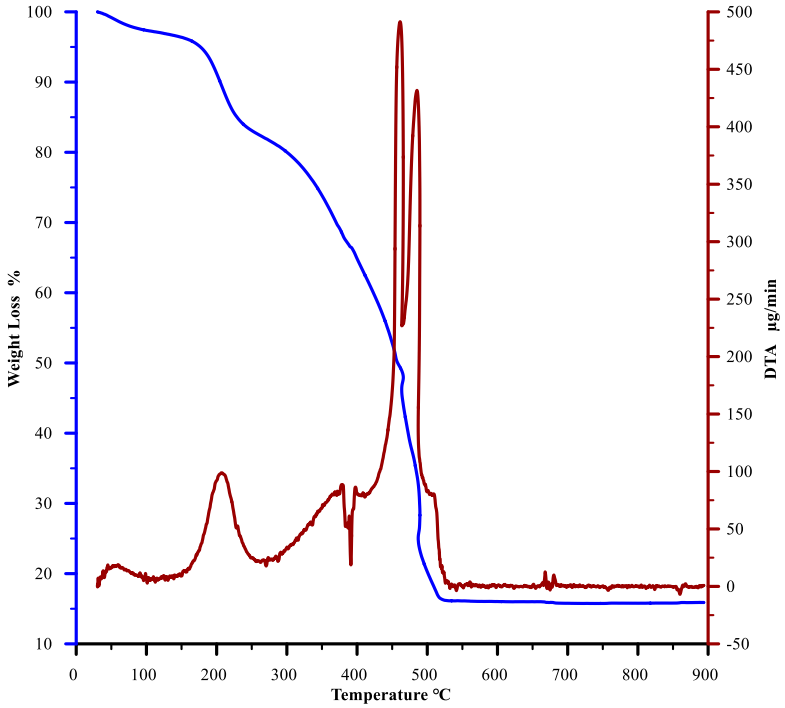

Appendix-15.7: TGA (blue) and DTA (red) thermograms of zinc tyrosine - alanine dipeptide substituted phthalocyanine complex **(9g)** compound.

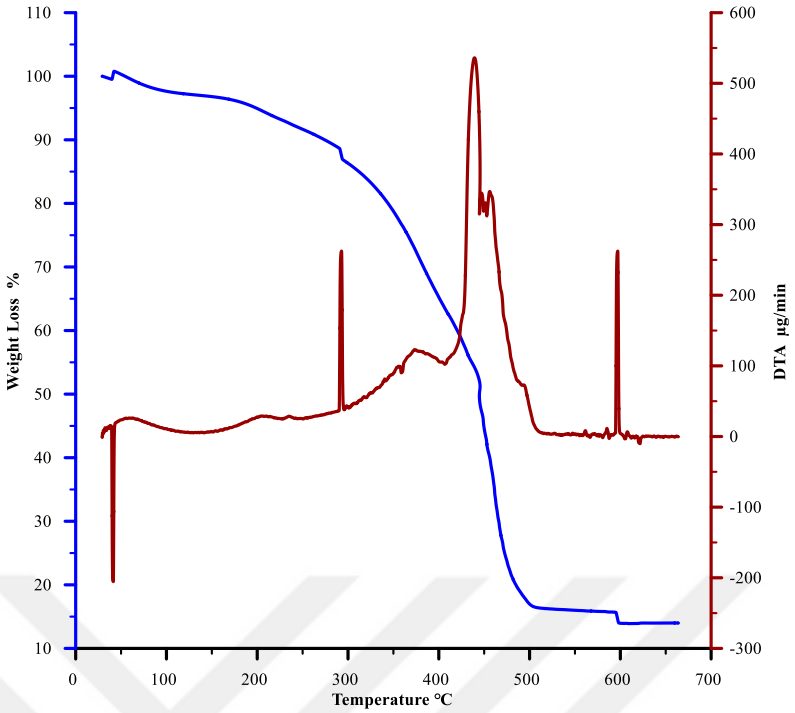

Appendix-16.1: TGA (blue) and DTA (red) thermograms chromium tyrosine - glycine dipeptide substituted phthalocyanine complex **(11a)** compound.

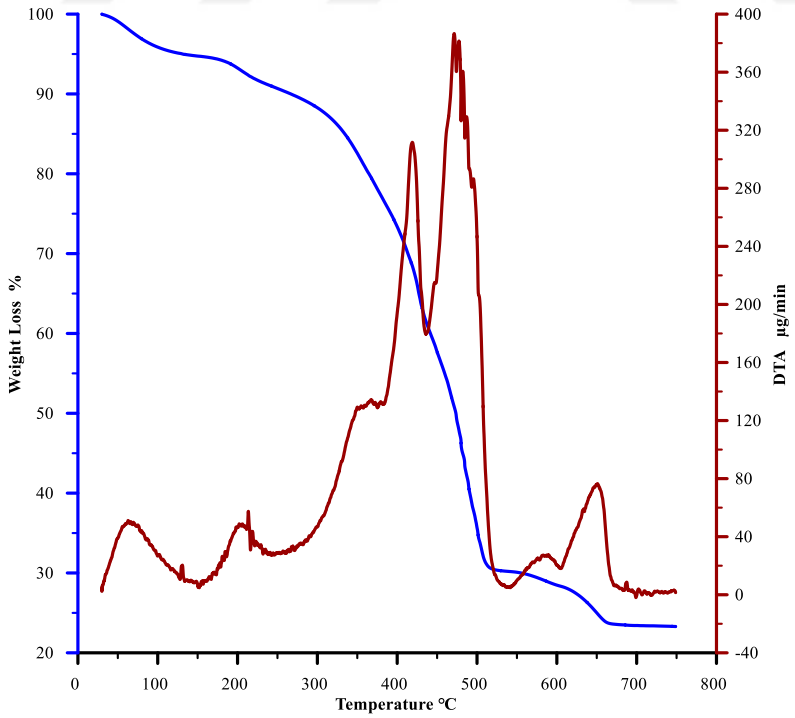

Appendix-16.2: TGA (blue) and DTA (red) thermograms manganese tyrosine - glycine dipeptide substituted phthalocyanine complex **(11b)** compound.

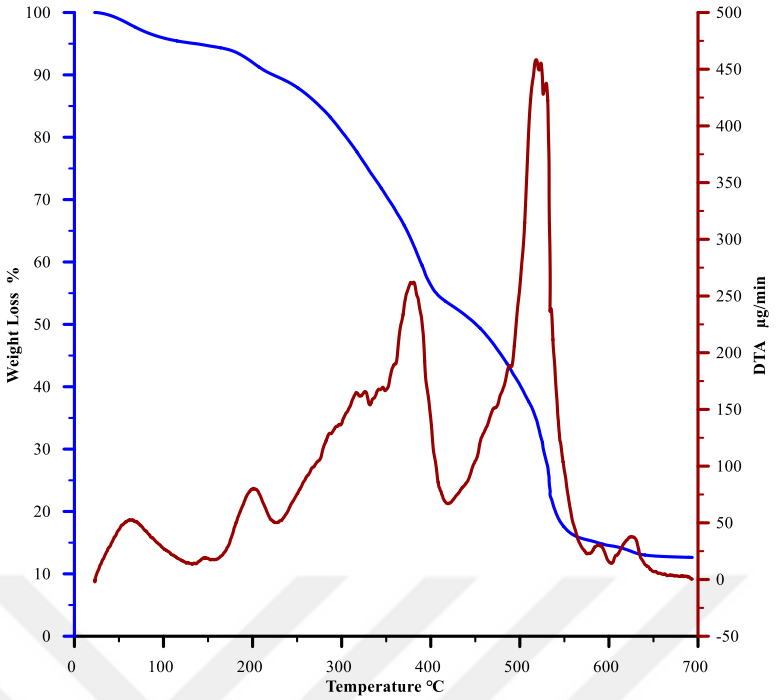

Appendix-16.3: TGA (blue) and DTA (red) thermograms iron tyrosine - glycine dipeptide substituted phthalocyanine complex **(11c)** compound.

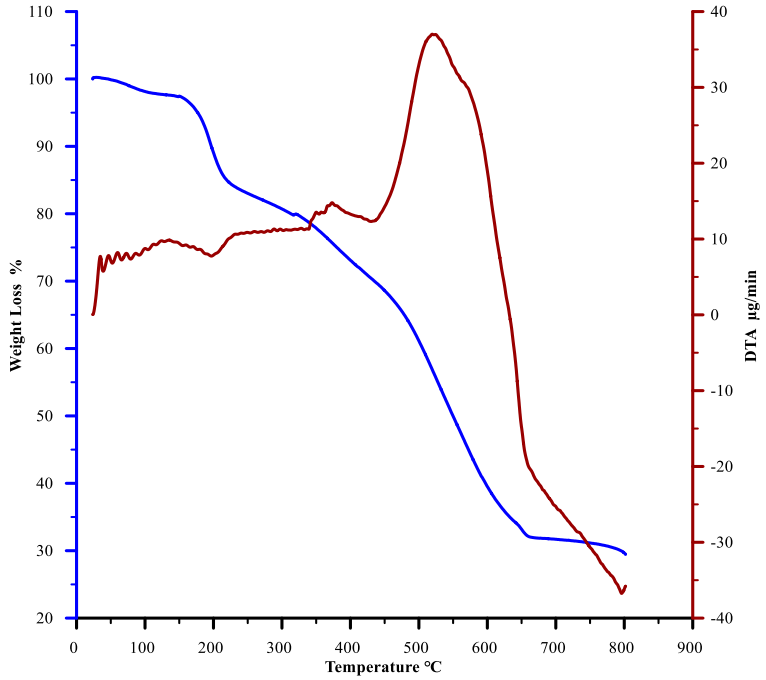

Appendix-16.4: TGA (blue) and DTA (red) thermograms cobalt tyrosine - glycine dipeptide substituted phthalocyanine complex **(11d)** compound.

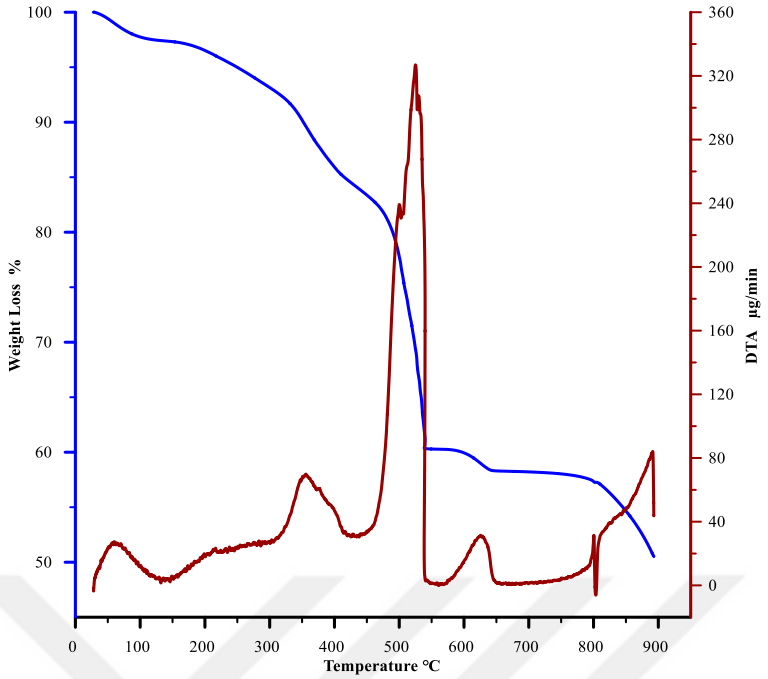

Appendix-16.5: TGA (blue) and DTA (red) thermograms nickel tyrosine - glycine dipeptide substituted phthalocyanine complex **(11e)** compound.

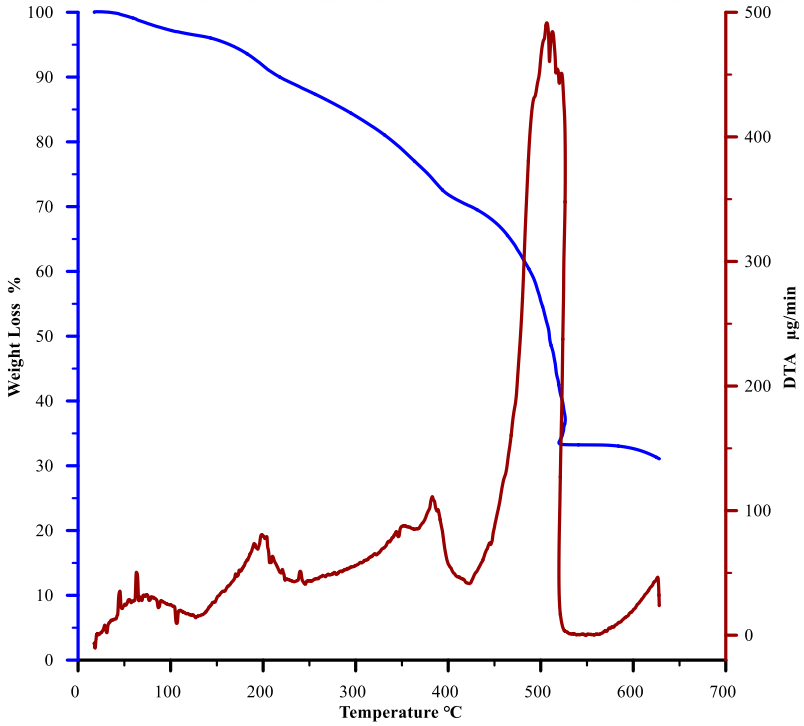

Appendix-16.6: TGA (blue) and DTA (red) thermograms copper tyrosine - glycine dipeptide substituted phthalocyanine complex **(11f)** compound.

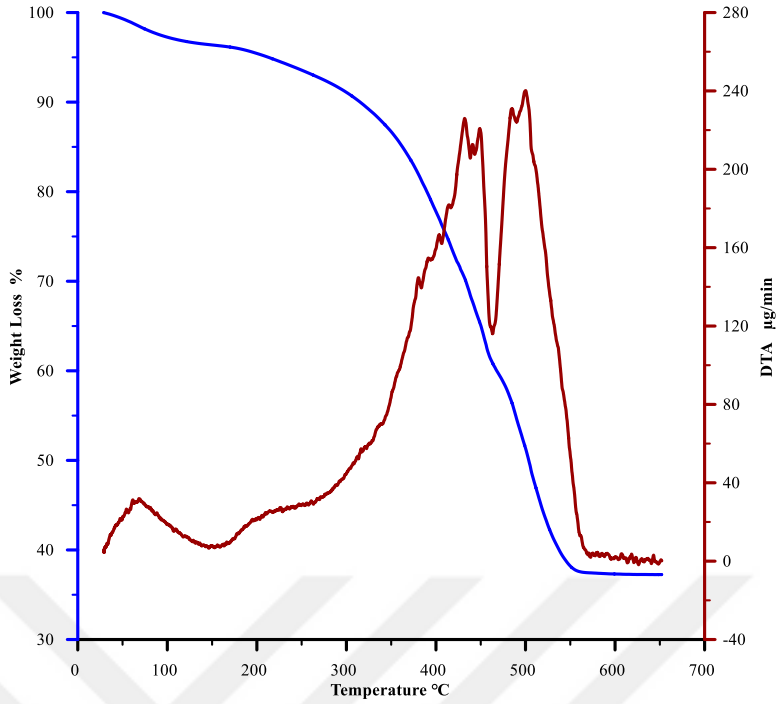

Appendix-16.7: TGA (blue) and DTA (red) thermograms zinc tyrosine - glycine dipeptide substituted phthalocyanine complex **(11g)** compound.

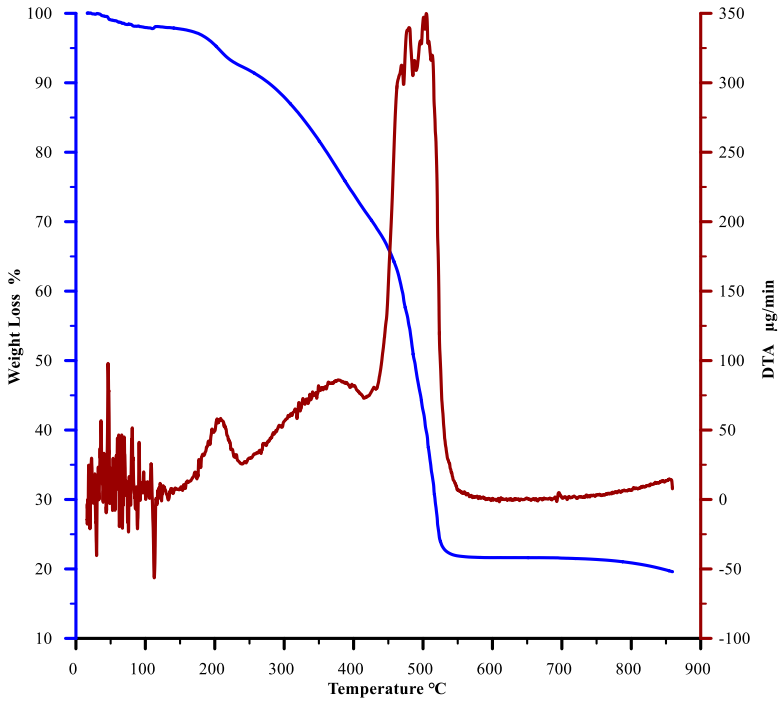

Appendix-17.1: TGA (blue) and DTA (red) thermograms chromium tyrosine - valine dipeptide substituted phthalocyanine complex **(13a)** compound.

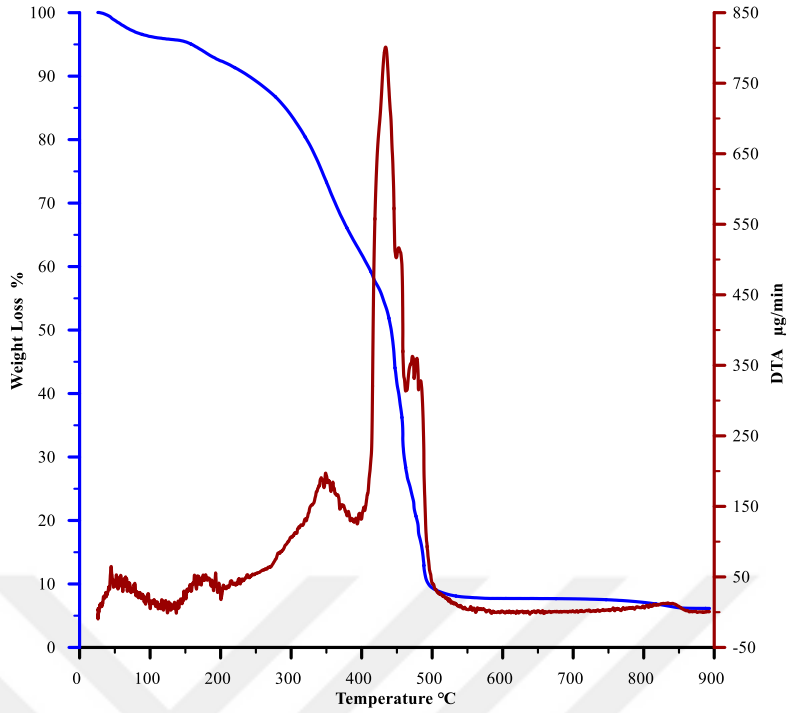

Appendix-17.2: TGA (blue) and DTA (red) thermograms manganese tyrosine - valine dipeptide substituted phthalocyanine complex **(13b)** compound.

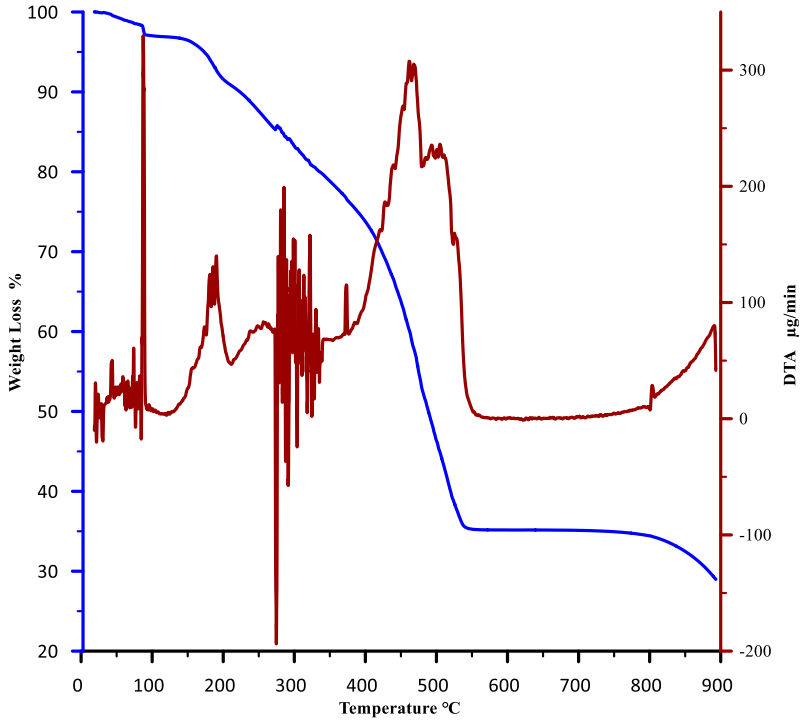

Appendix-17.3: TGA (blue) and DTA (red) thermograms iron tyrosine - valine dipeptide substituted phthalocyanine complex **(13c)** compound.

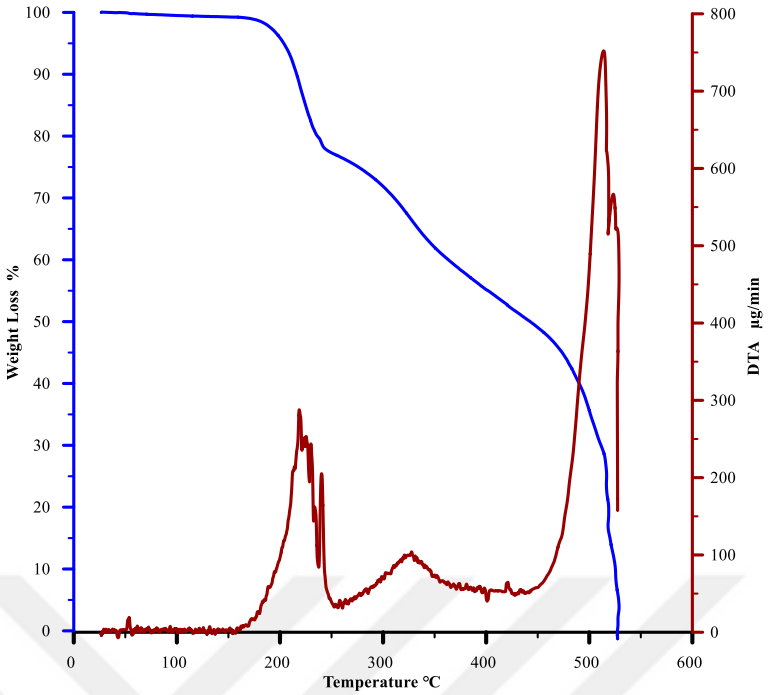

Appendix-17.4: TGA (blue) and DTA (red) thermograms cobalt tyrosine - valine dipeptide substituted phthalocyanine complex **(13d)** compound.

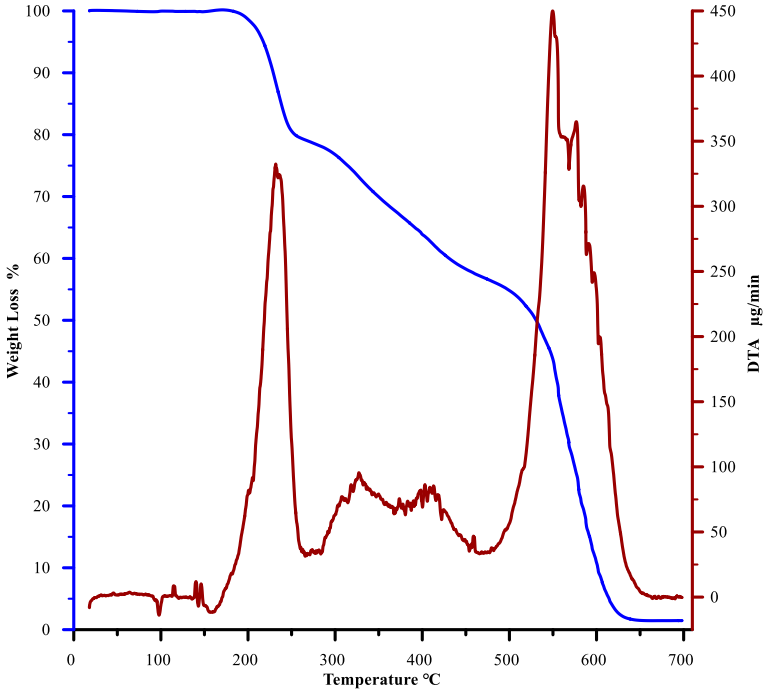

Appendix-17.5: TGA (blue) and DTA (red) thermograms nickel tyrosine - valine dipeptide substituted phthalocyanine complex **(13e)** compound.

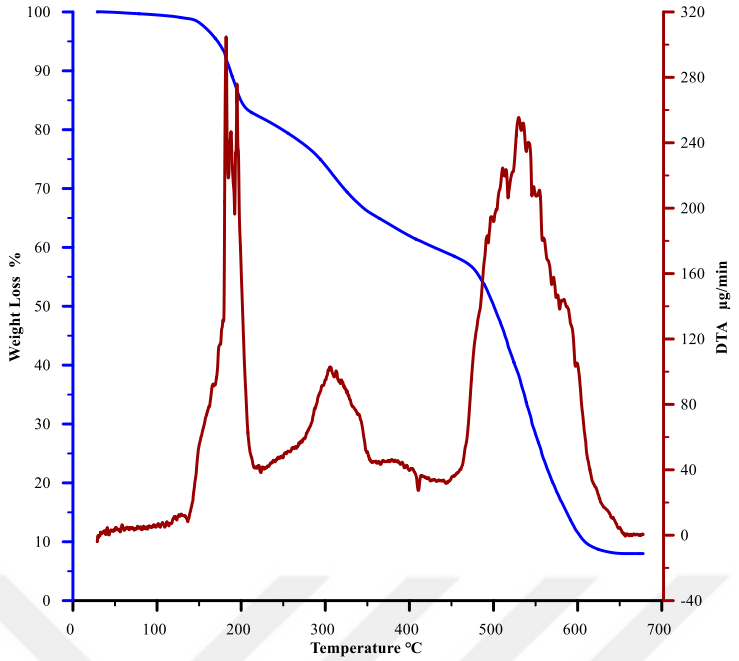

Appendix-17.6: TGA (blue) and DTA (red) thermograms copper tyrosine - valine dipeptide substituted phthalocyanine complex **(13f)** compound.

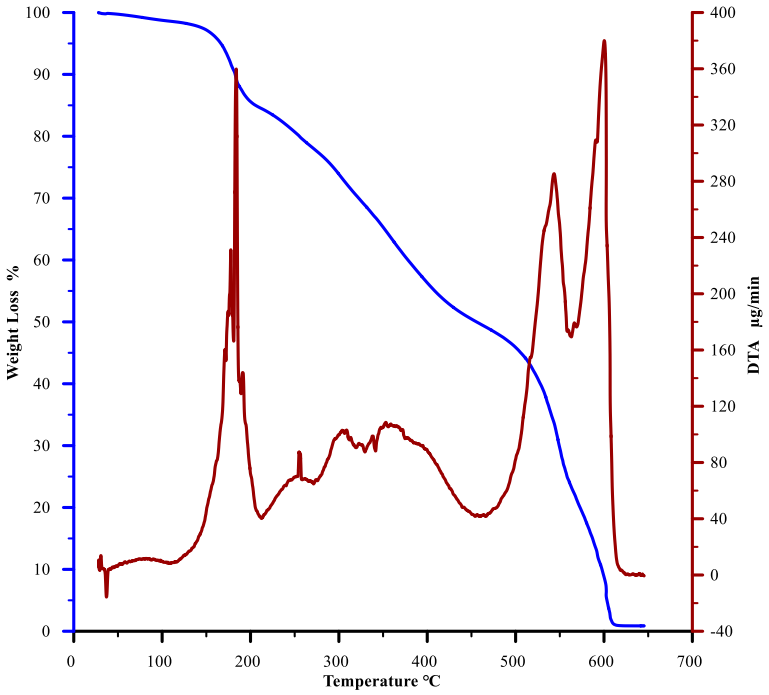

Appendix-17.7: TGA (blue) and DTA (red) thermograms zinc tyrosine - valine dipeptide substituted phthalocyanine complex **(13g)** compound.

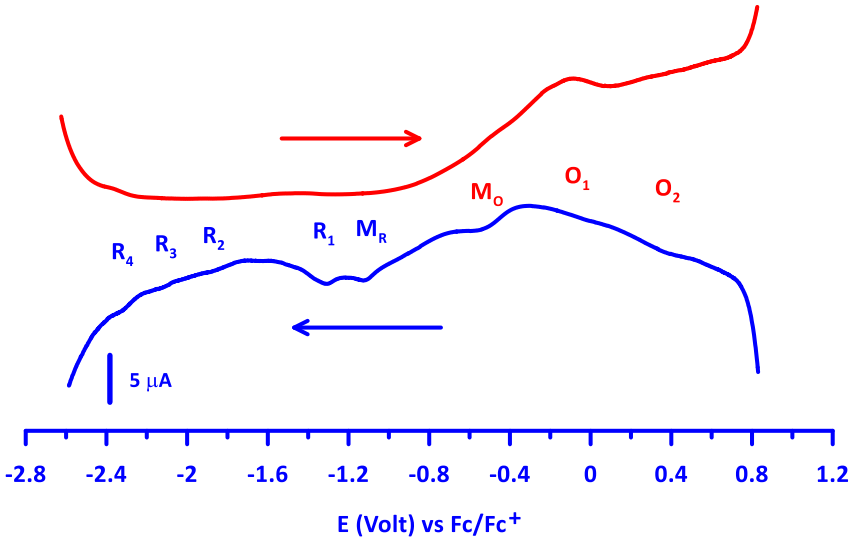

Appendix-18.1a: Square wave voltammograms of CrPc **(7a)**, 10 Hz, pulse size 25 mV, scan directions shown by arrow.

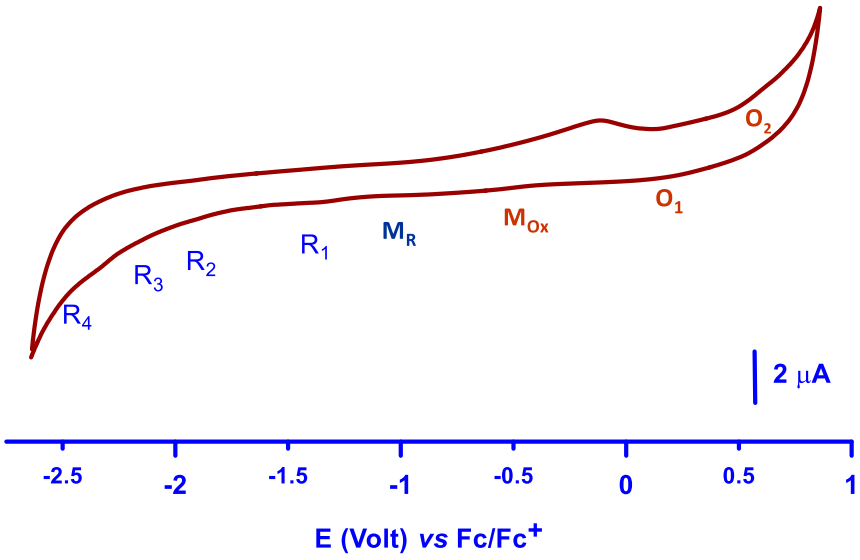

Appendix-18.1b: Cyclic voltammograms of CrPc **(7a)** in DMF, scan rate 50 mV s^{-1}.

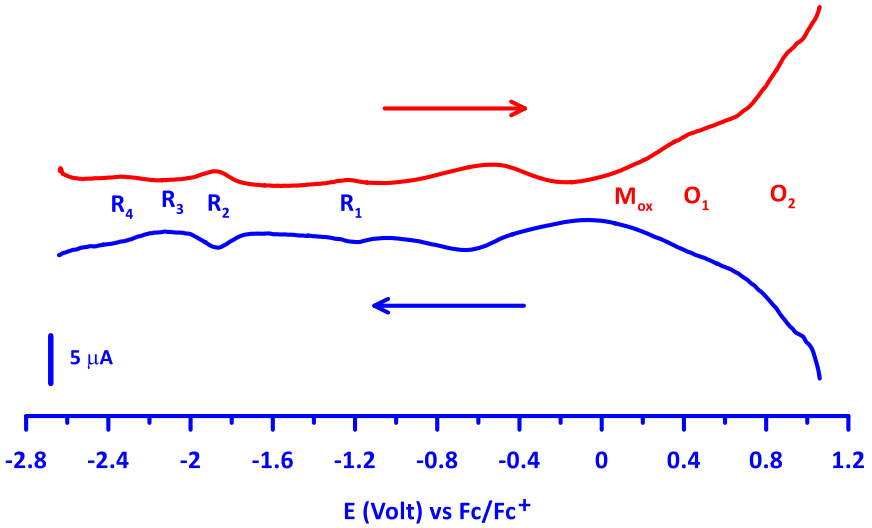

Appendix-18.2a: Square wave voltammograms of MnPc **(7b)**,10 Hz, pulse size 25 mV, scan directions shown by arrow.

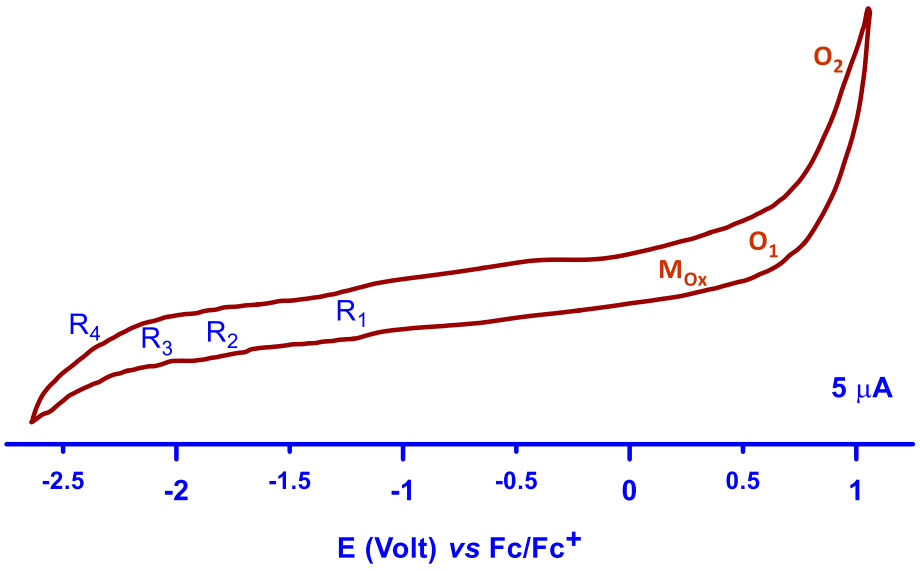

Appendix-18.2b: Cyclic voltammograms of MnPc **(7b)** in DMF, scan rate 100 mV s^{-1}.

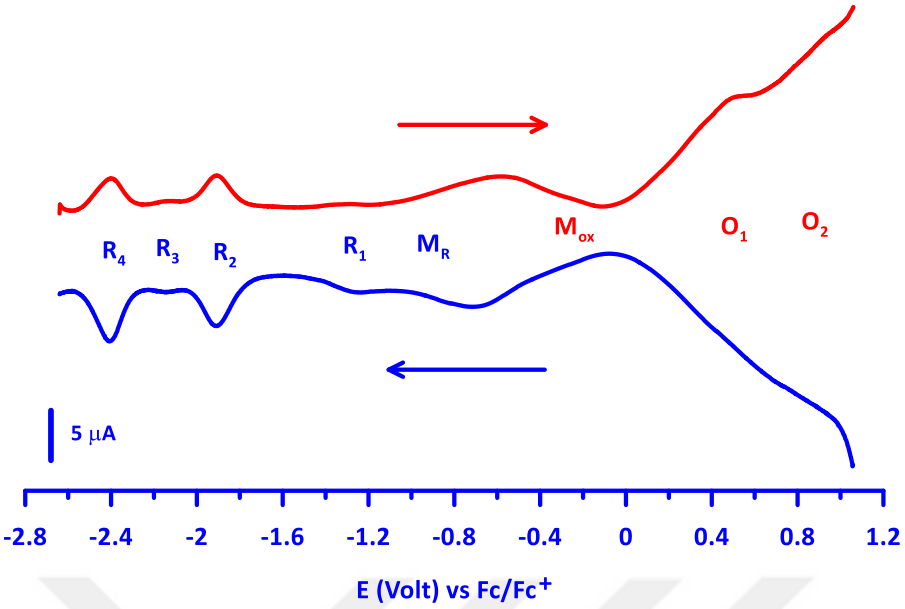

Appendix-18.3a: Square wave voltammograms of FePc **(7c)**,10 Hz, pulse size 25 mV, scan directions shown by arrow.

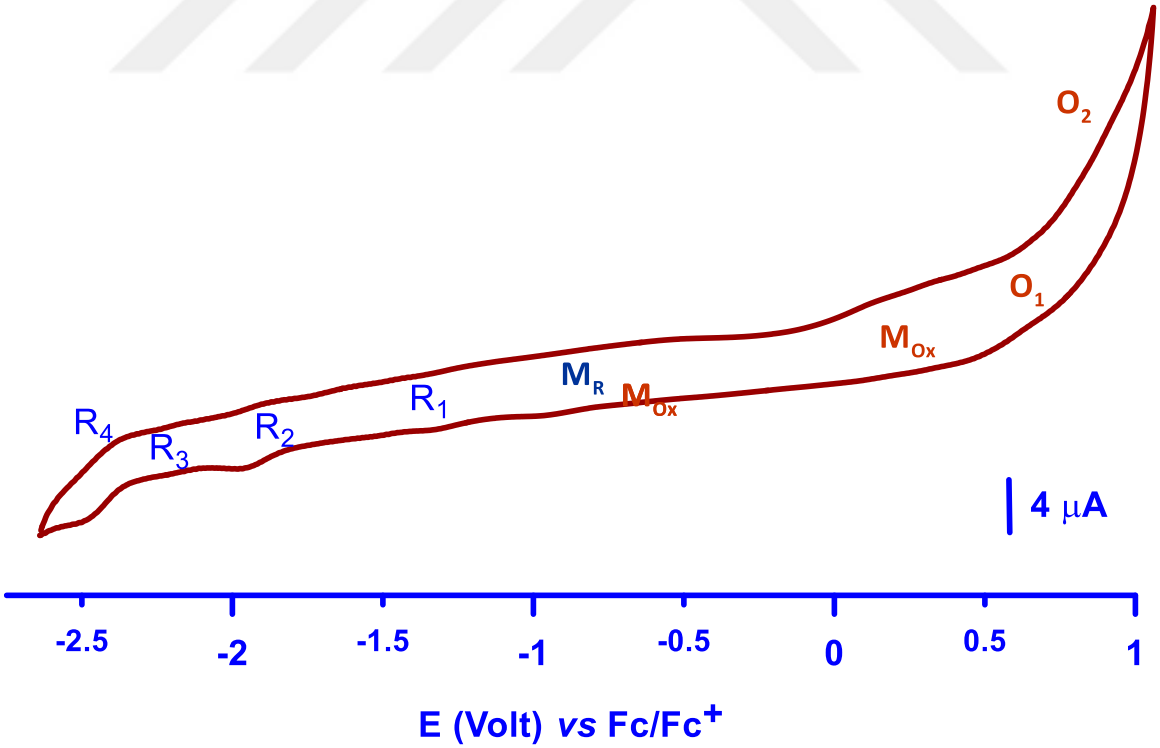

Appendix-18.3b: Cyclic voltammograms of FePc **(7c)** in DMF, scan rate 100 mV s^{-1}

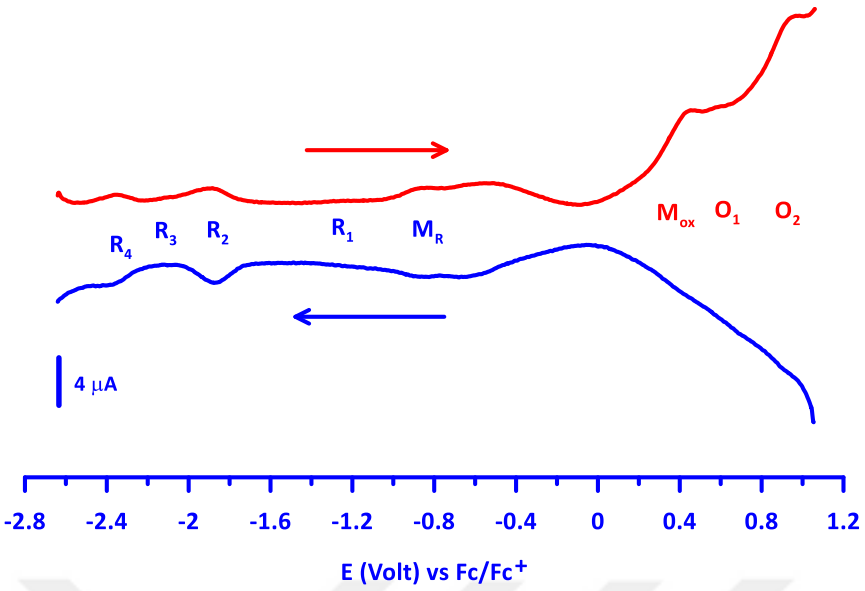

Appendix-18.4a: Square wave voltammograms of CoPc **(7d)**,10 Hz, pulse size 25 mV, scan directions shown by arrow.

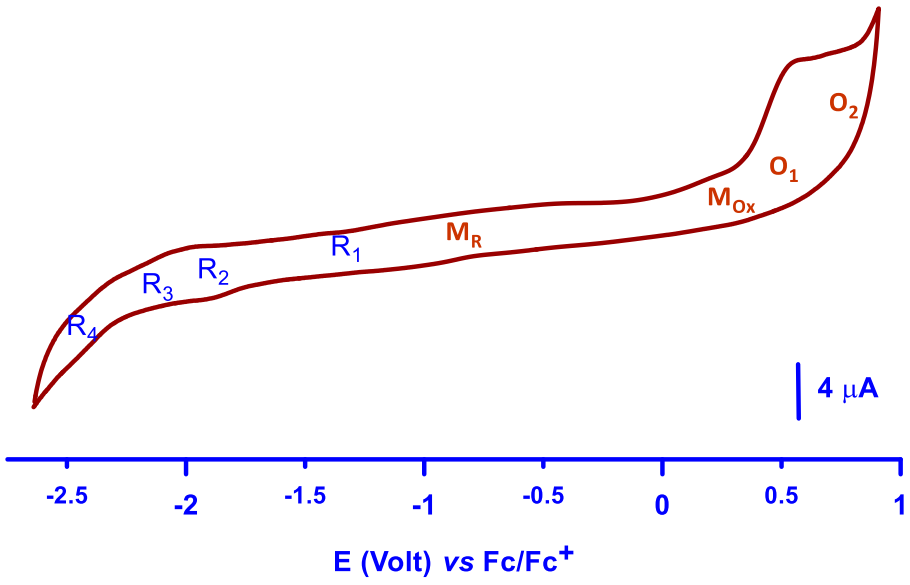

Appendix-18.4b: Cyclic voltammograms of CoPc **(7d)** in DMF, scan rate 100 mV s^{-1}

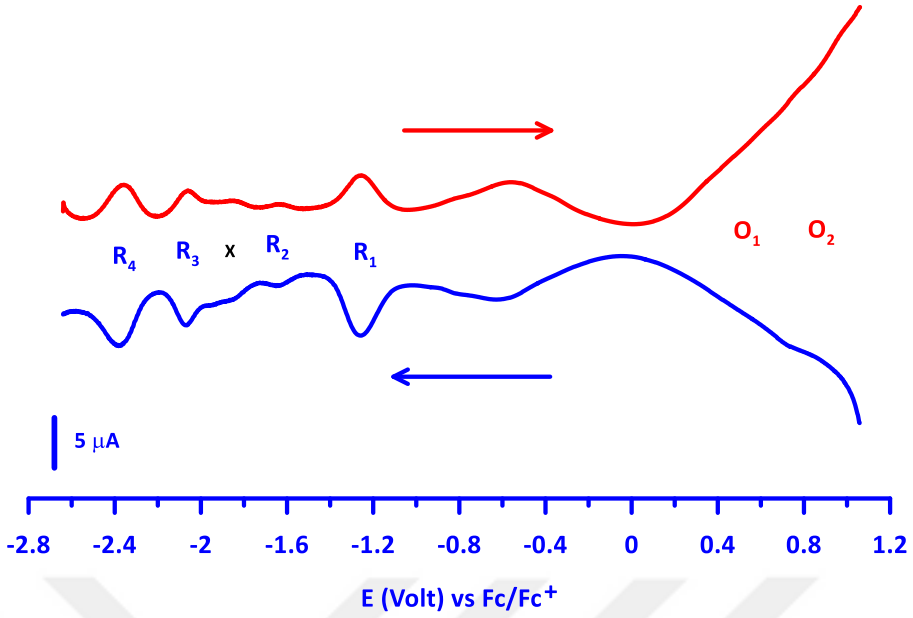

Appendix-18.5a: Square wave voltammograms of NiPc **(7e)**,10 Hz, pulse size 25 mV, scan directions shown by arrow.

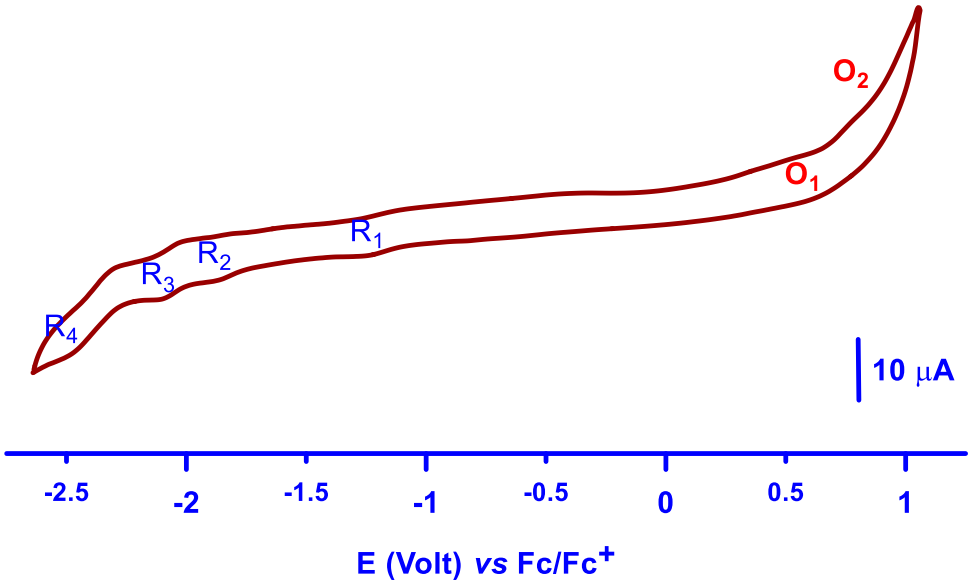

Appendix-18.5b: Cyclic voltammograms of NiPc **(7e)** in DMF, scan rate 100 mV s^{-1}

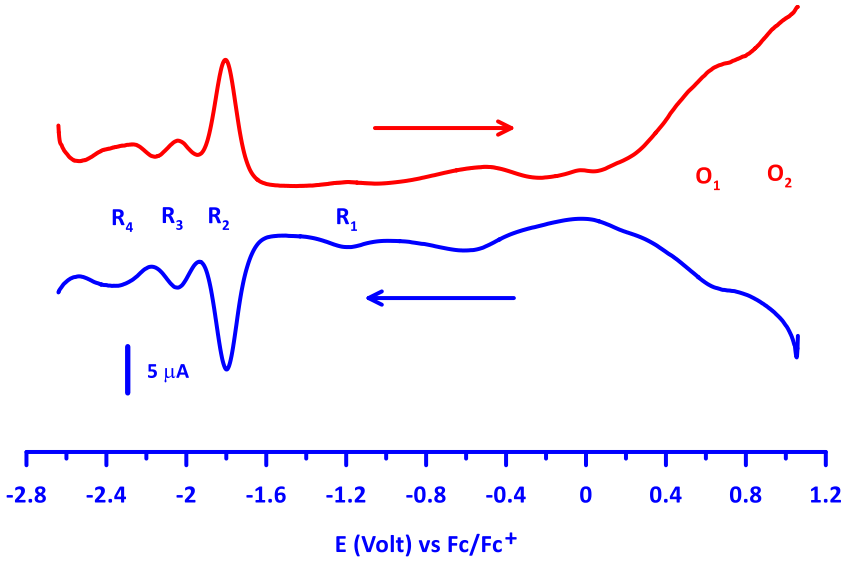

Appendix-18.6a: Square wave voltammograms of CuPc **(7f)**,10 Hz, pulse size 25 mV, scan directions shown by arrow.

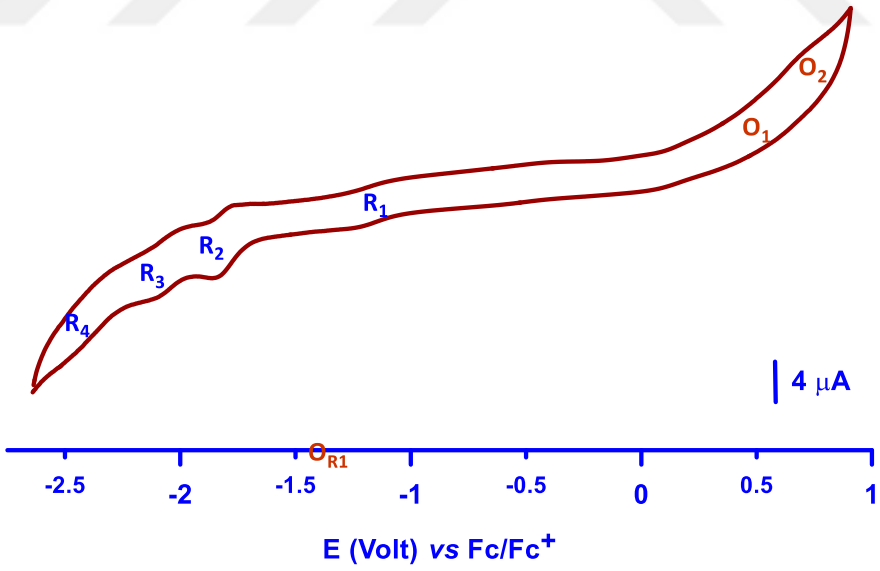

Appendix-18.6b: Cyclic voltammograms of CuPc **(7f)** in DMF, scan rate 100 mV s^{-1}

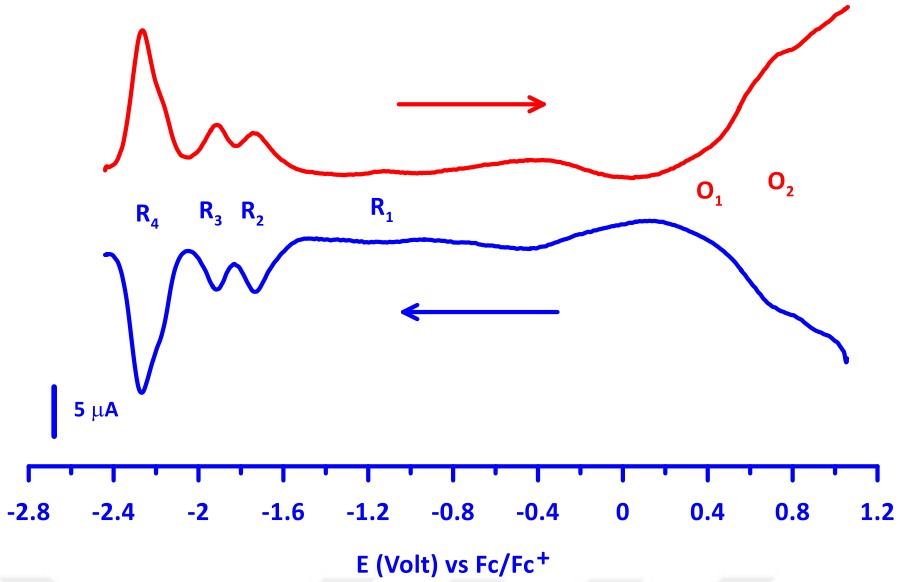

Appendix-18.7a: Square wave voltammograms of ZnPc **(7g)**,10 Hz, pulse size 25 mV, scan directions shown by arrow.

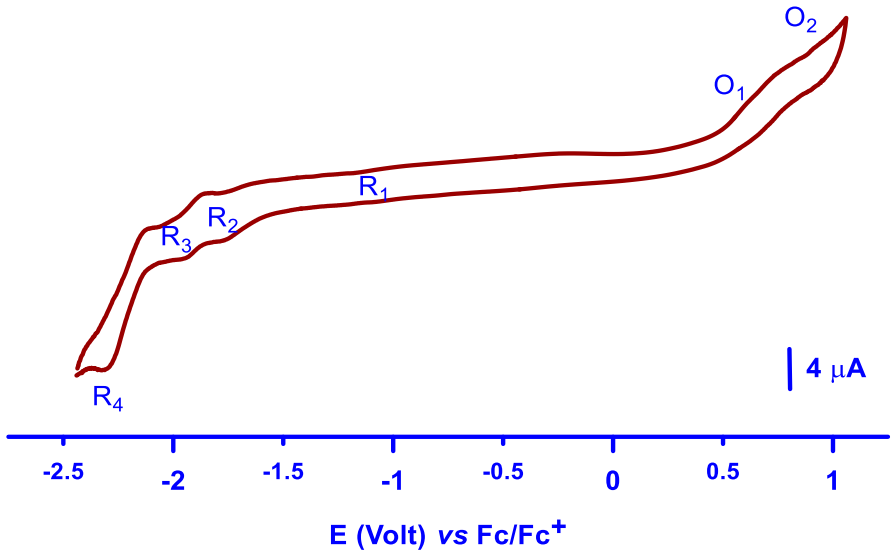

Appendix-18.7b: Cyclic voltammograms of ZnPc **(7g)** in DMF, scan rate 100 mV s^{-1}.

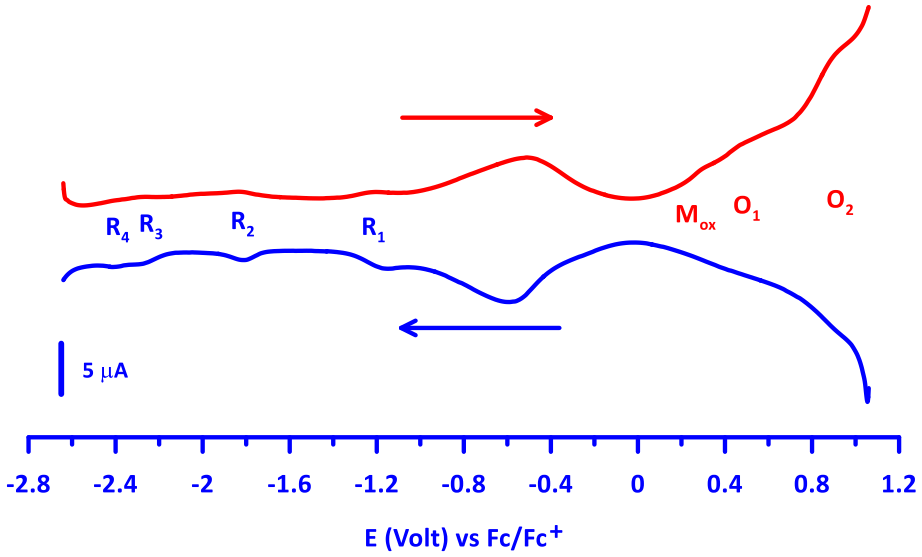

Appendix-19.1a: Square wave voltammograms of CrPc **(9a)**,10 Hz, pulse size 25 mV, scan directions shown by arrow.

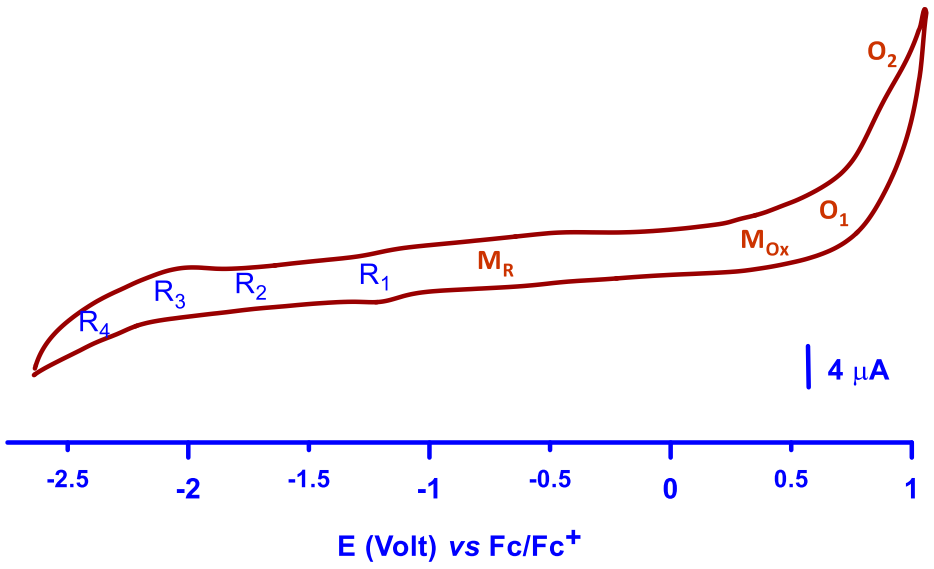

Appendix-19.1b: Cyclic voltammograms of CrPc **(9a)** in DMF, scan rate 100 mV s^{-1}.

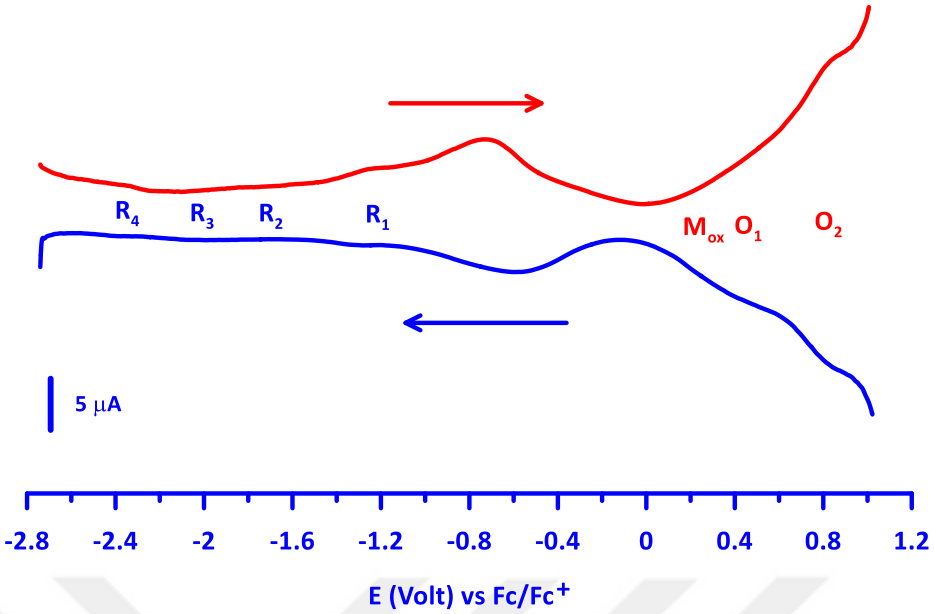

Appendix-19.2a: Square wave voltammograms of MnPc **(9b)**,10 Hz, pulse size 25 mV, scan directions shown by arrow.

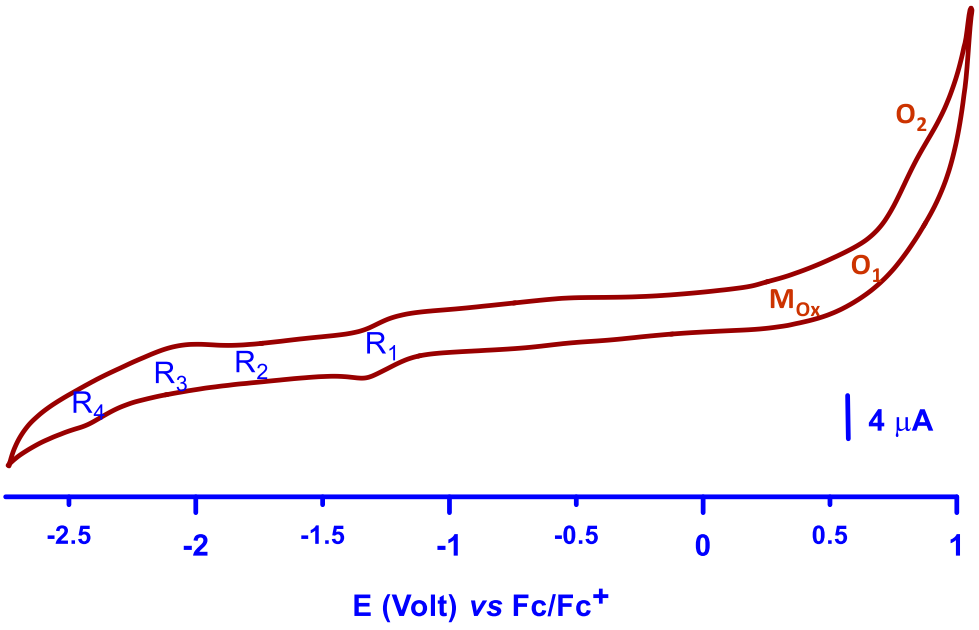

Appendix-19.2b: Cyclic voltammograms of MnPc **(9b)** in DMF, scan rate 100 mV s^{-1}

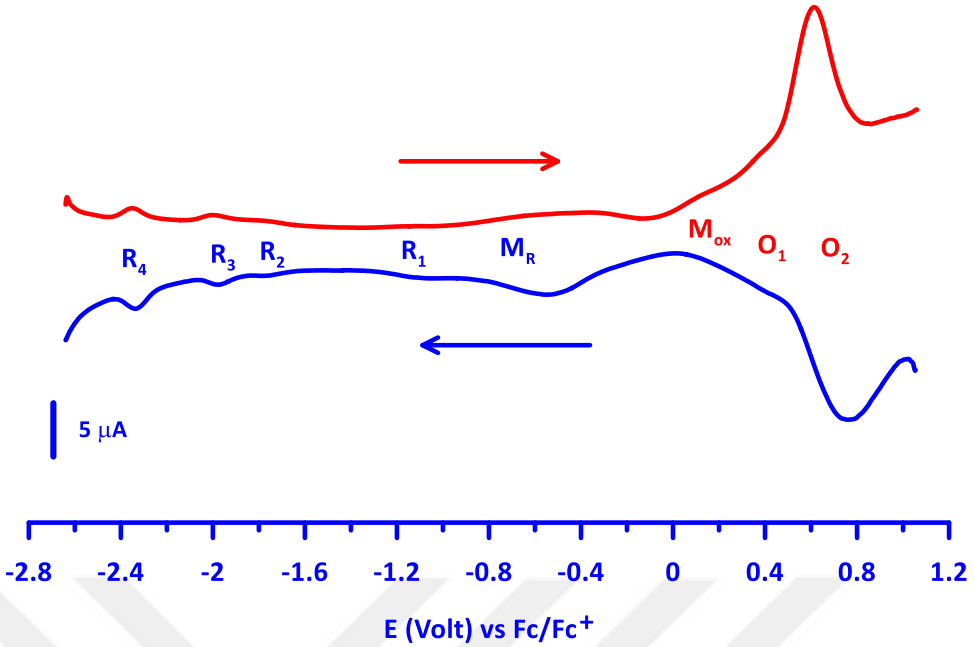

Appendix-19.3a: Square wave voltammograms of FePc **(9c)**,10 Hz, pulse size 25 mV, scan directions shown by arrow.

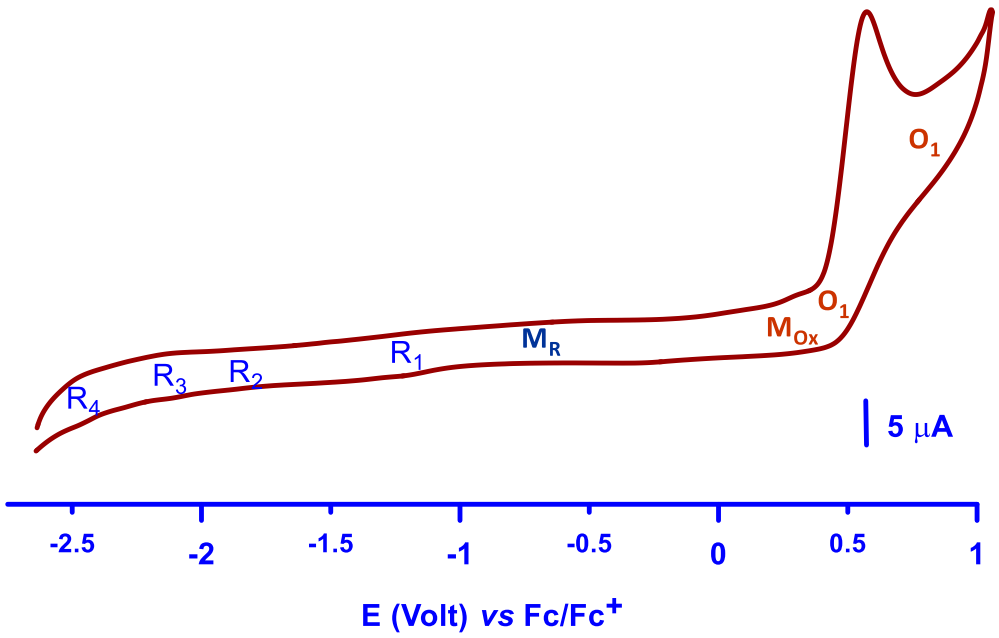

Appendix-19.3b: Cyclic voltammograms of FePc **(9c)** in DMF, scan rate 100 mV s^{-1}

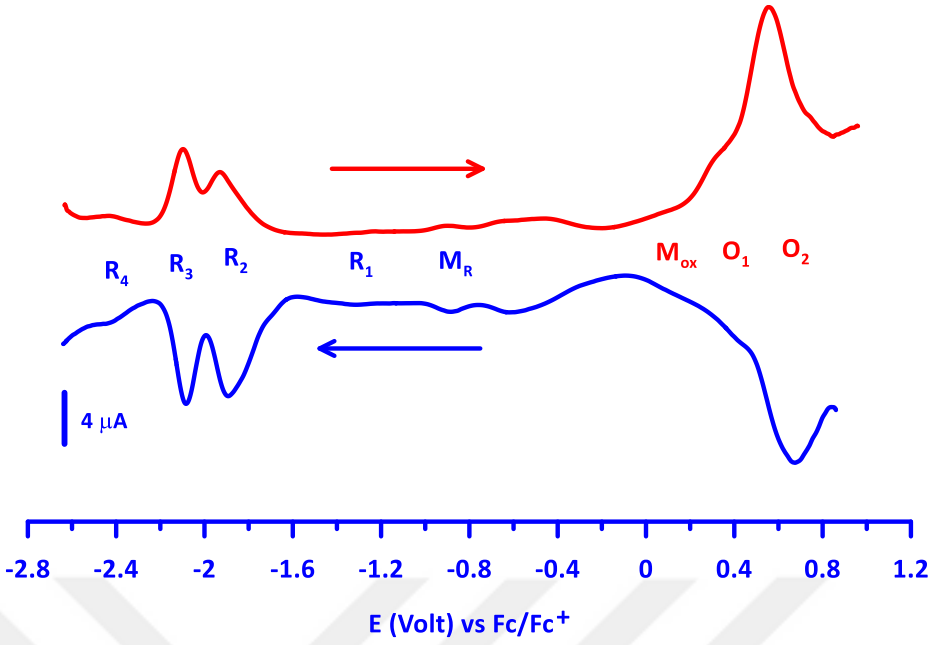

Appendix-19.4a: Square wave voltammograms of CoPc **(9d)**,10 Hz, pulse size 25 mV, scan directions shown by arrow.

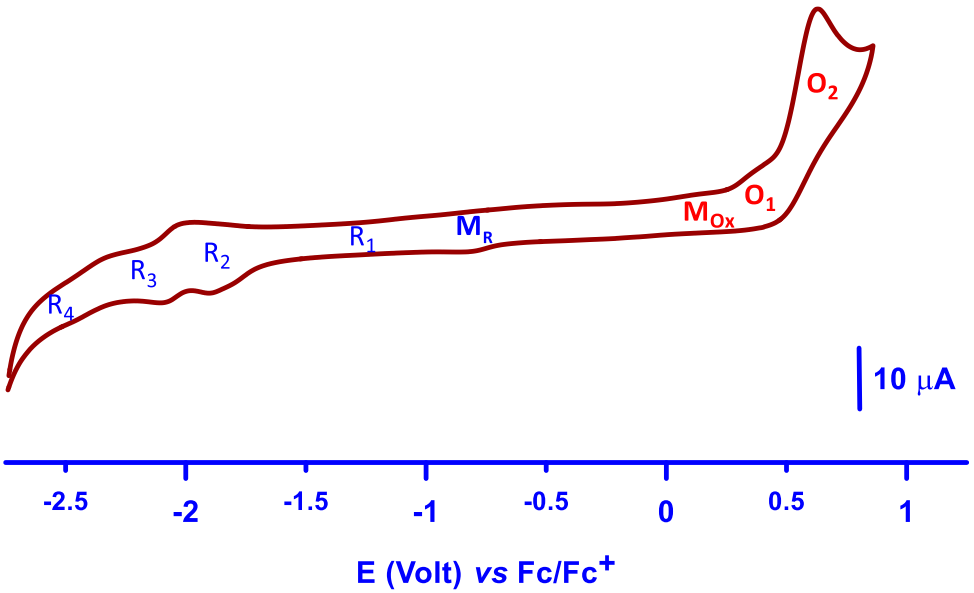

Appendix-19.4b: Cyclic voltammograms of CoPc **(9d)** in DMF, scan rate 100 mV s^{-1}.

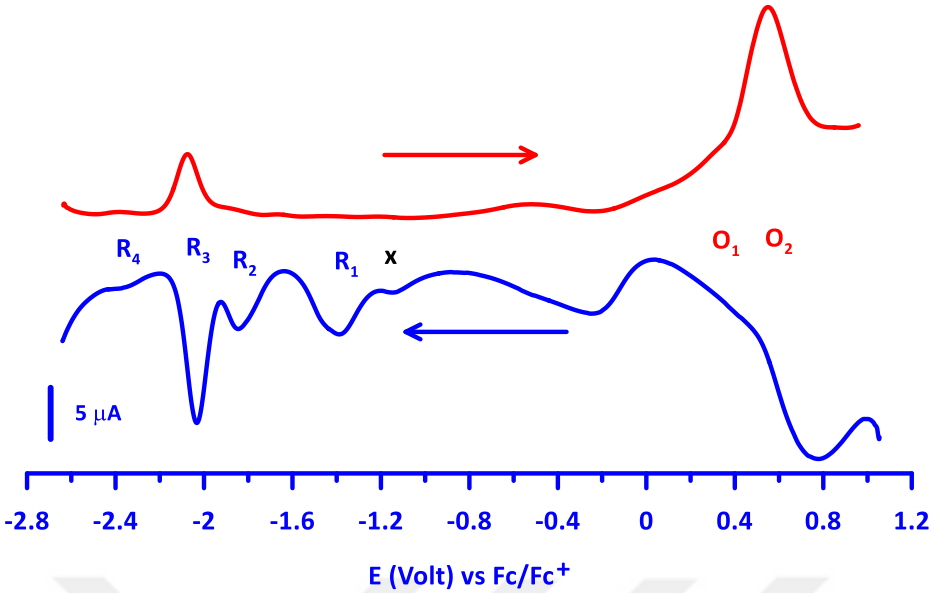

Appendix-19.5a: Square wave voltammograms of NiPc **(9e)**,10 Hz, pulse size 25 mV, scan directions shown by arrow.

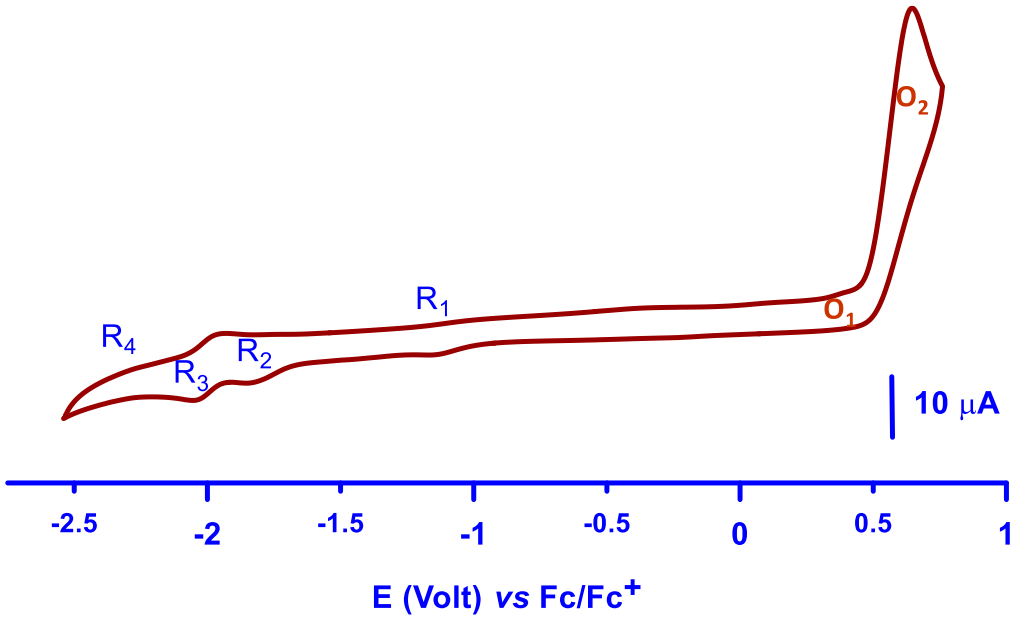

Appendix-19.5b: Cyclic voltammograms of NiPc **(9e)** in DMF, scan rate 100 mV s^{-1}

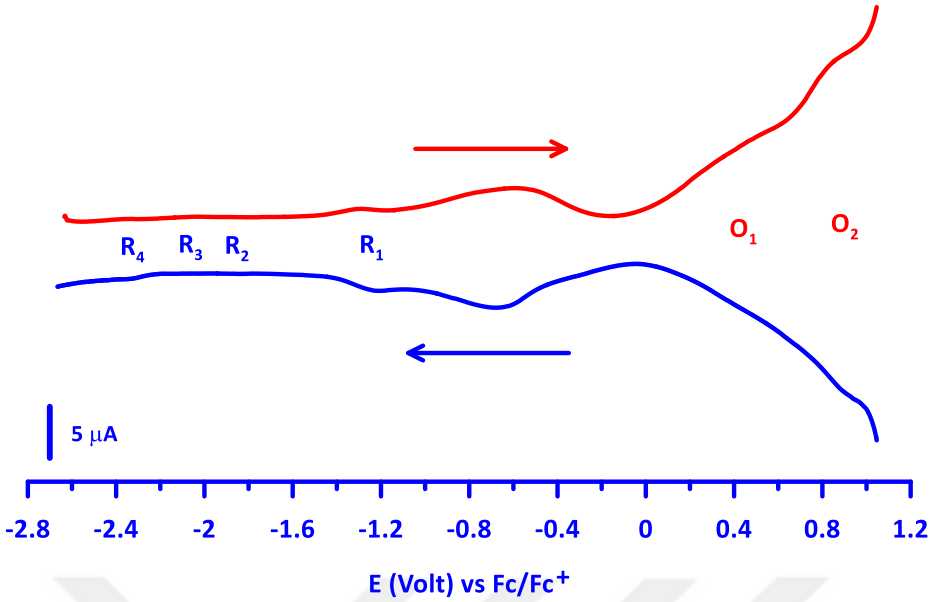

Appendix-19.6a: Square wave voltammograms of CuPc **(9f)**,10 Hz, pulse size 25 mV, scan directions shown by arrow.

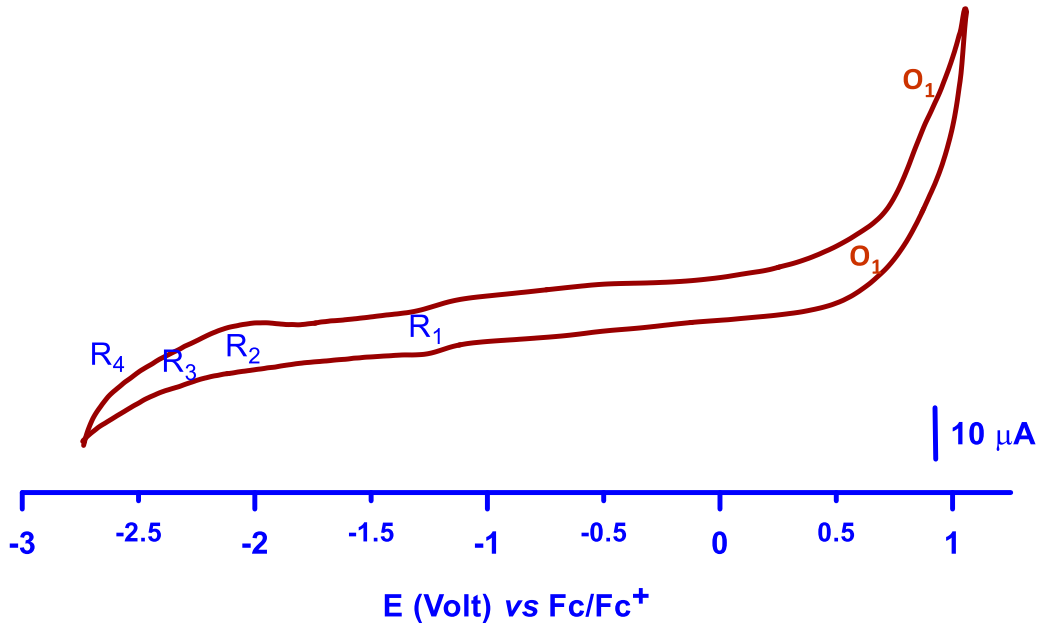

Appendix-19.6b: Cyclic voltammograms of CuPc **(9f)** in DMF, scan rate 100 mV s^{-1}

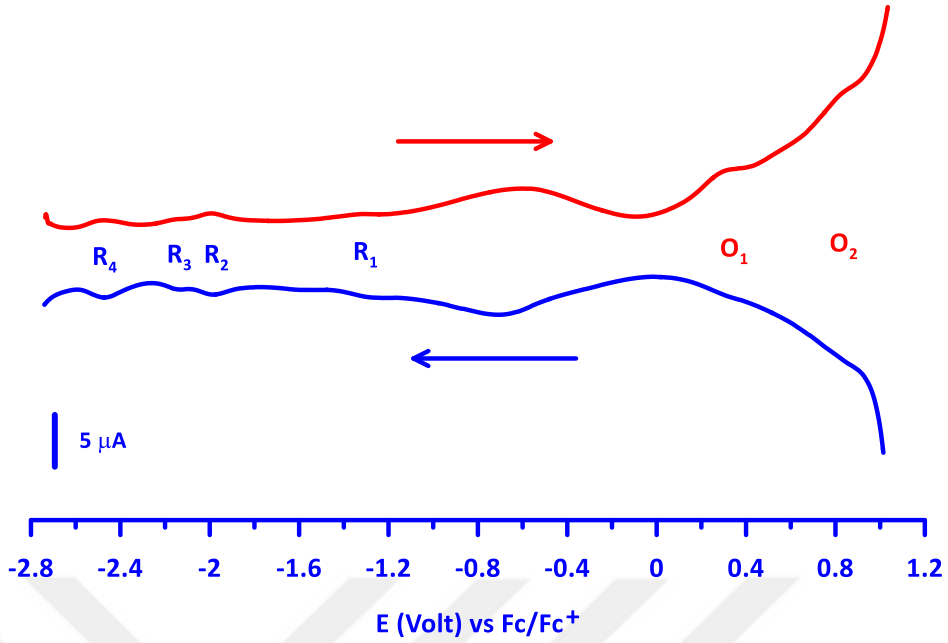

Appendix-19.7a: Square wave voltammograms of ZnPc **(9g)**,10 Hz, pulse size 25 mV, scan directions shown by arrow.

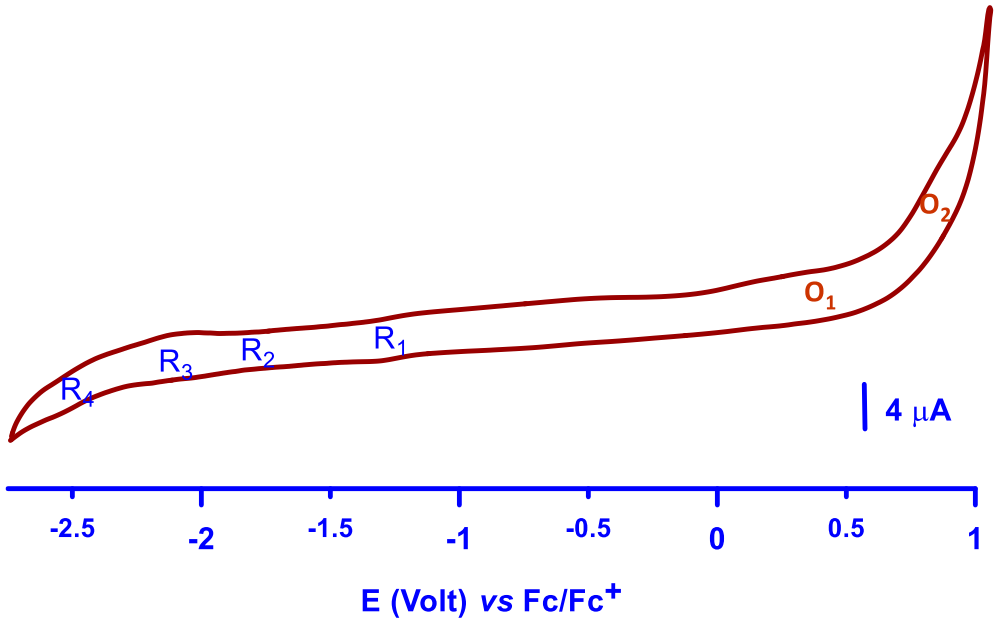

Appendix-19.7b: Cyclic voltammograms of ZnPc **(9g)** in DMF, scan rate 100 mV s^{-1}

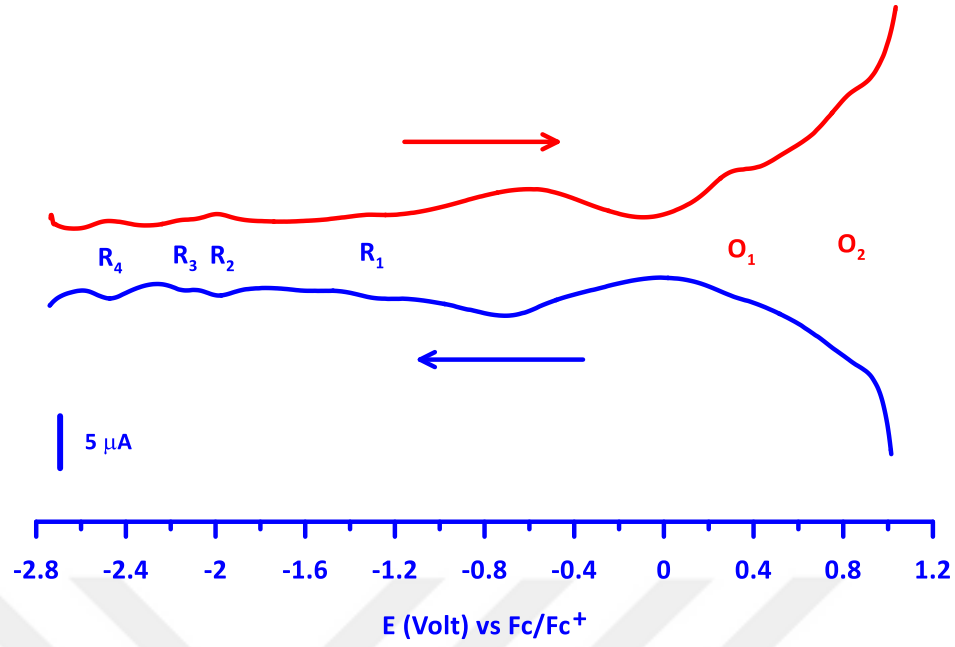

Appendix-20.1a: Square wave voltammograms of CrPc **(11a)**,10 Hz, pulse size 25 mV, scan directions shown by arrow.

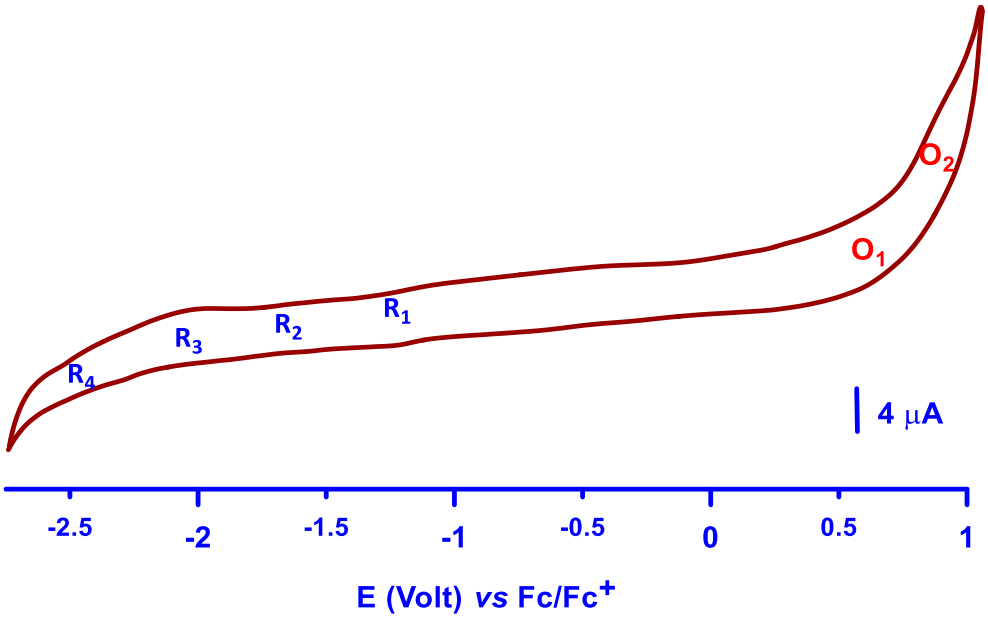

Appendix-20.1b: Cyclic voltammograms of CrPc **(11a)** in DMF, scan rate 100 mV s^{-1}.

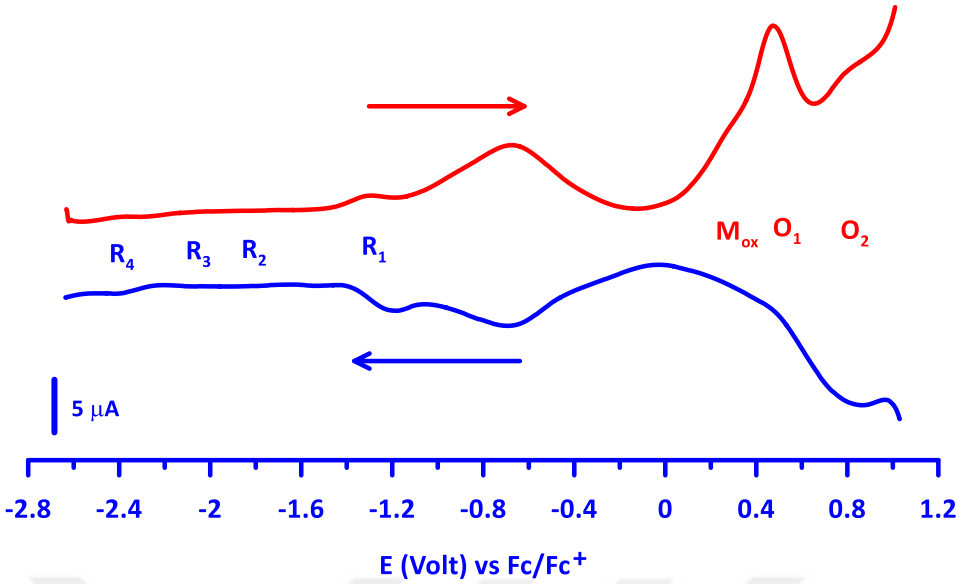

Appendix-20.2a: Square wave voltammograms of MnPc **(11b)**,10 Hz, pulse size 25 mV, scan directions shown by arrow.

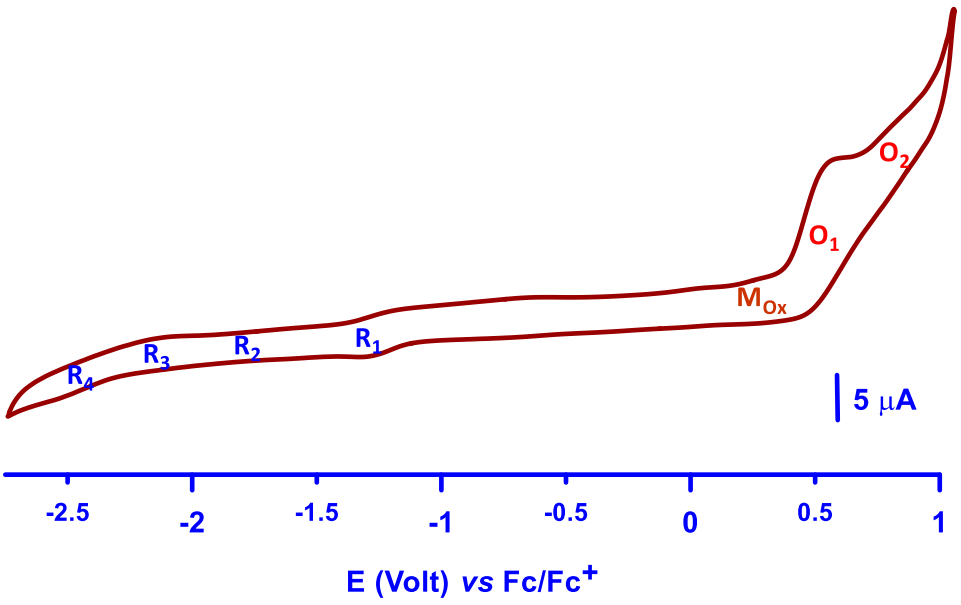

Appendix-20.2b: Cyclic voltammograms of MnPc **(11b)** in DMF, scan rate 100 mV s^{-1}.

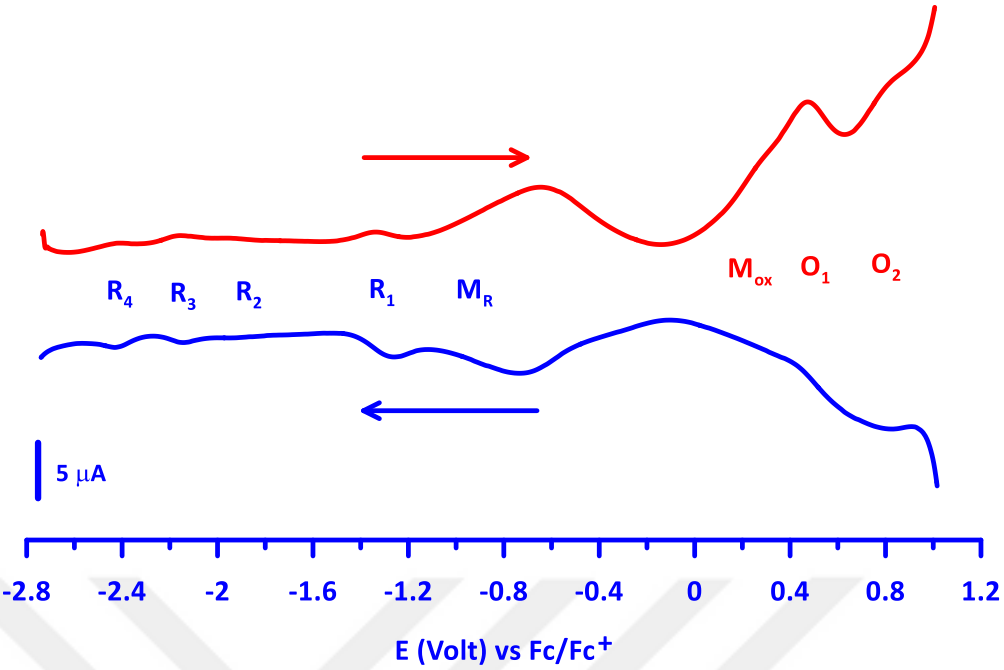

Appendix-20.3a: Square wave voltammograms of FePc **(11c)**,10 Hz, pulse size 25 mV, scan directions shown by arrow.

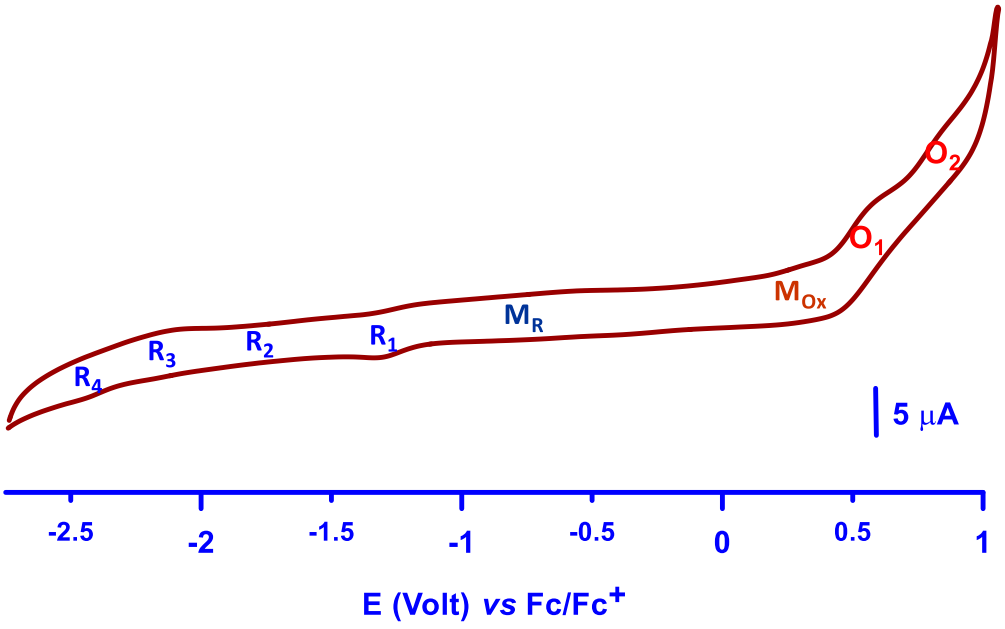

Appendix-20.3b: Cyclic voltammograms of FePc **(11c)** in DMF, scan rate 100 mV s^{-1}

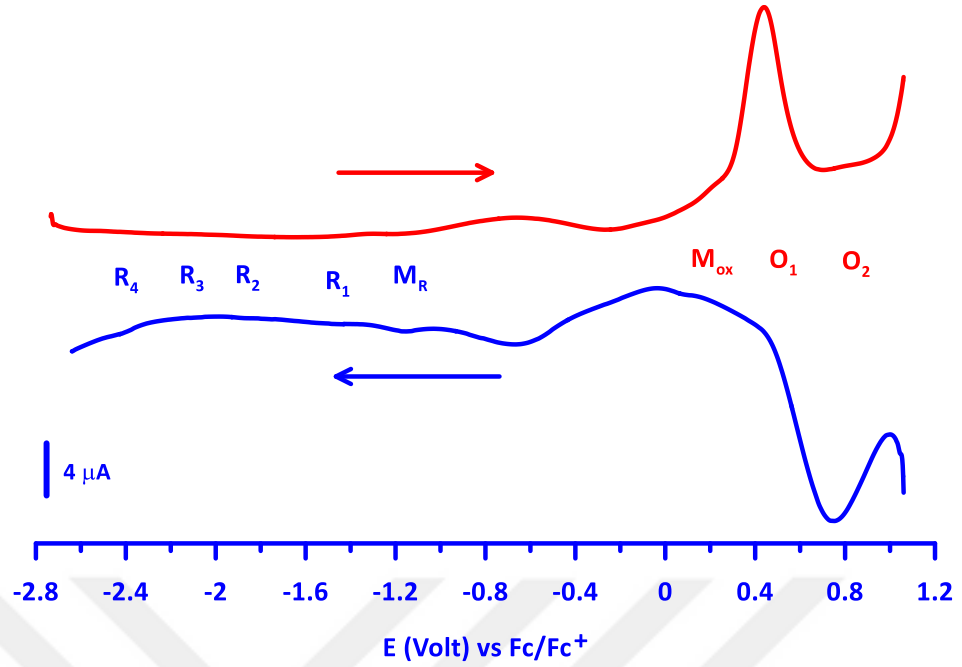

Appendix-20.4a: Square wave voltammograms of CoPc **(11d)**,10 Hz, pulse size 25 mV, scan directions shown by arrow.

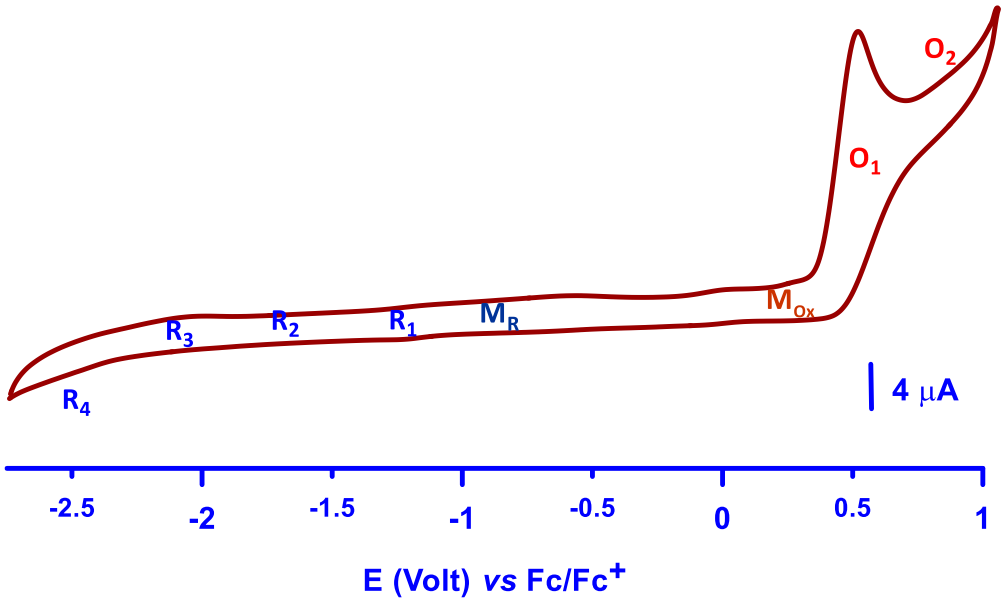

Appendix-20.4b: Cyclic voltammograms of CoPc **(11d)** in DMF, scan rate 100 mV s^{-1}.

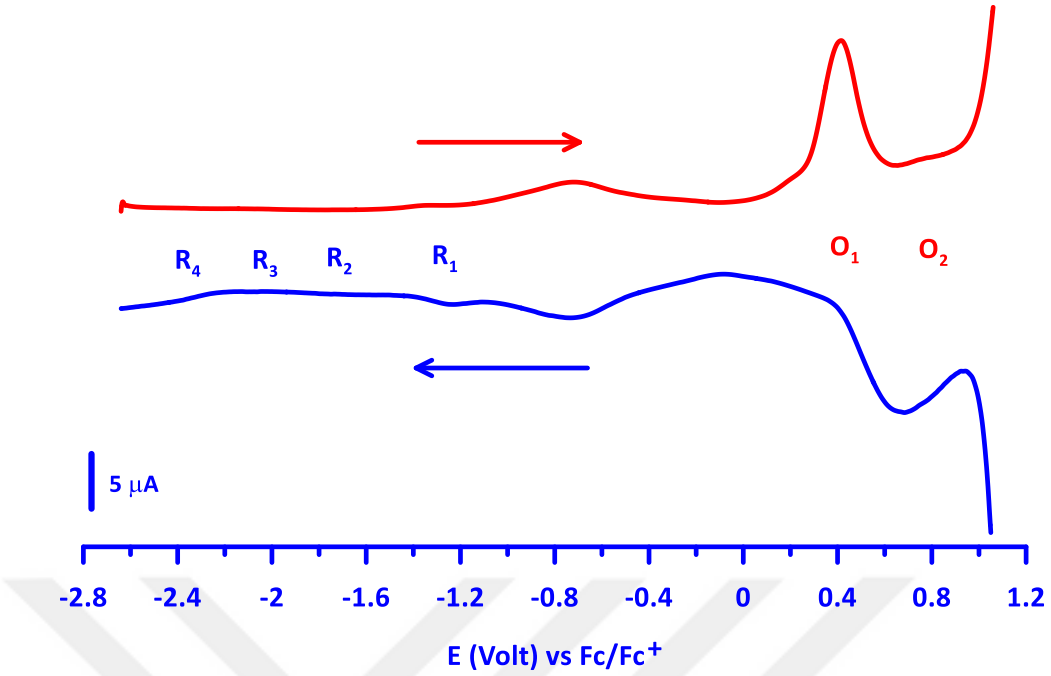

Appendix-20.5a: Square wave voltammograms of NiPc **(11e)**,10 Hz, pulse size 25 mV, scan directions shown by arrow.

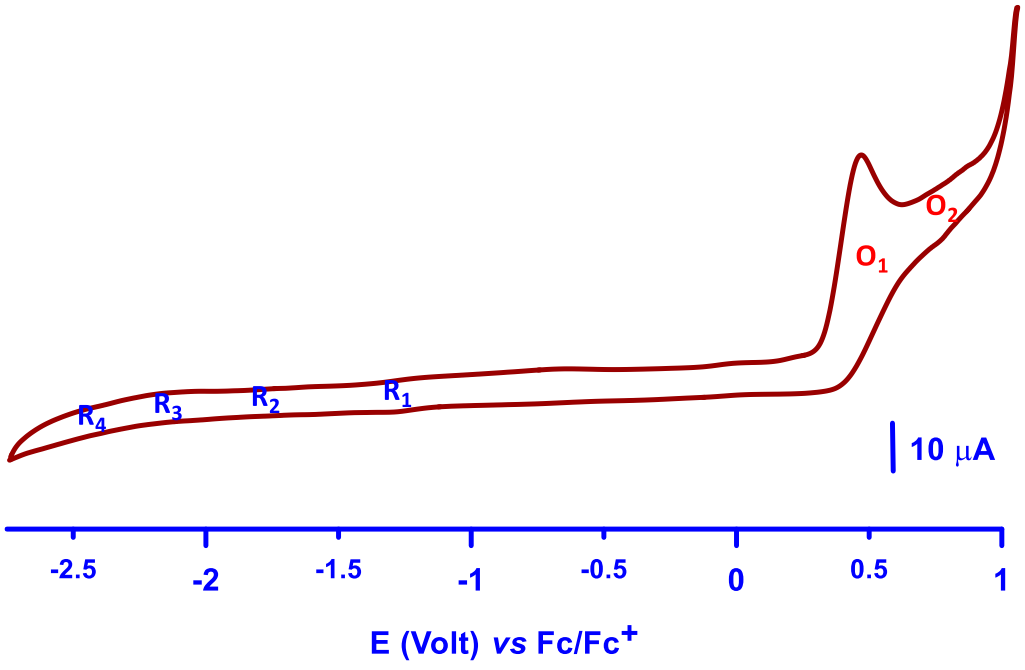

Appendix-20.5b: Cyclic voltammograms of NiPc **(11e)** in DMF, scan rate 100 mV s^{-1}

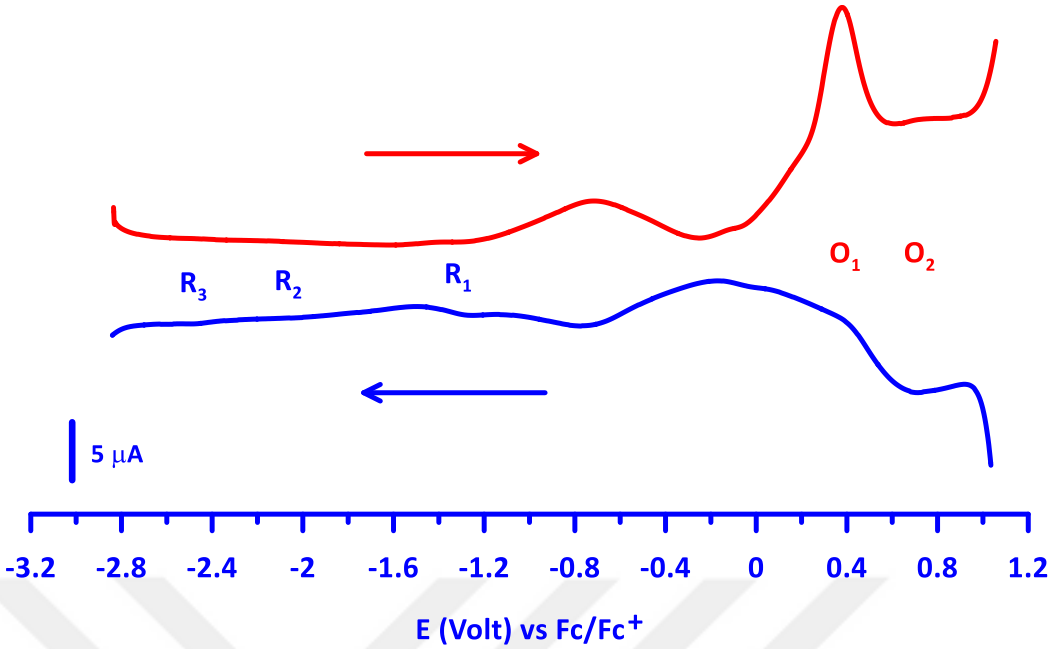

Appendix-20.6a: Square wave voltammograms of CuPc **(11f)**,10 Hz, pulse size 25 mV, scan directions are shown by arrow.

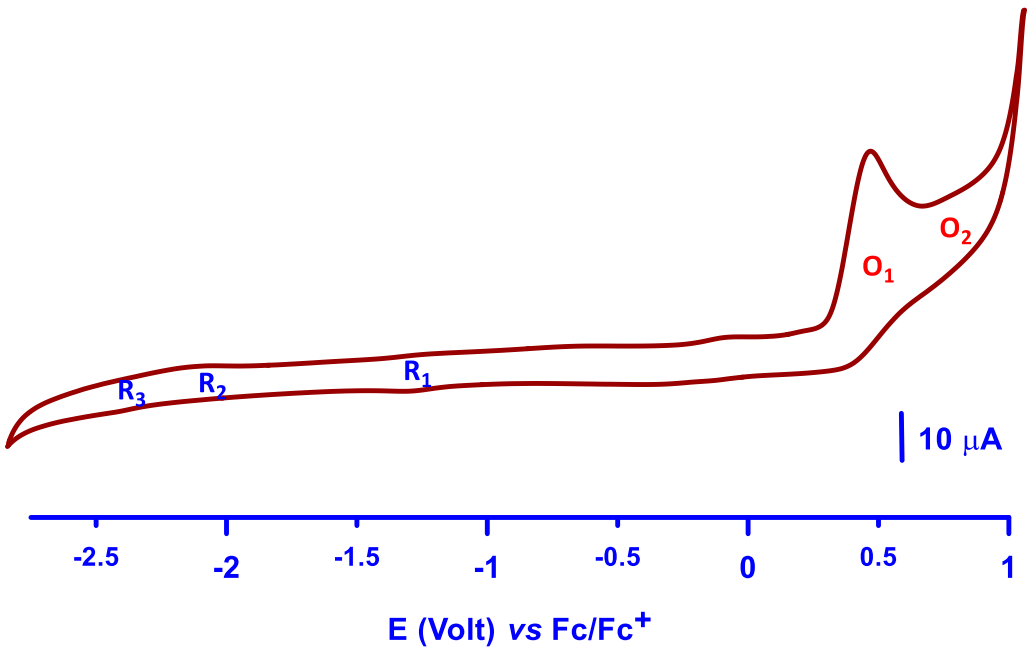

Appendix-20.6b: Cyclic voltammograms of CuPc **(11f)** in DMF, scan rate 100 mV s^{-1}.

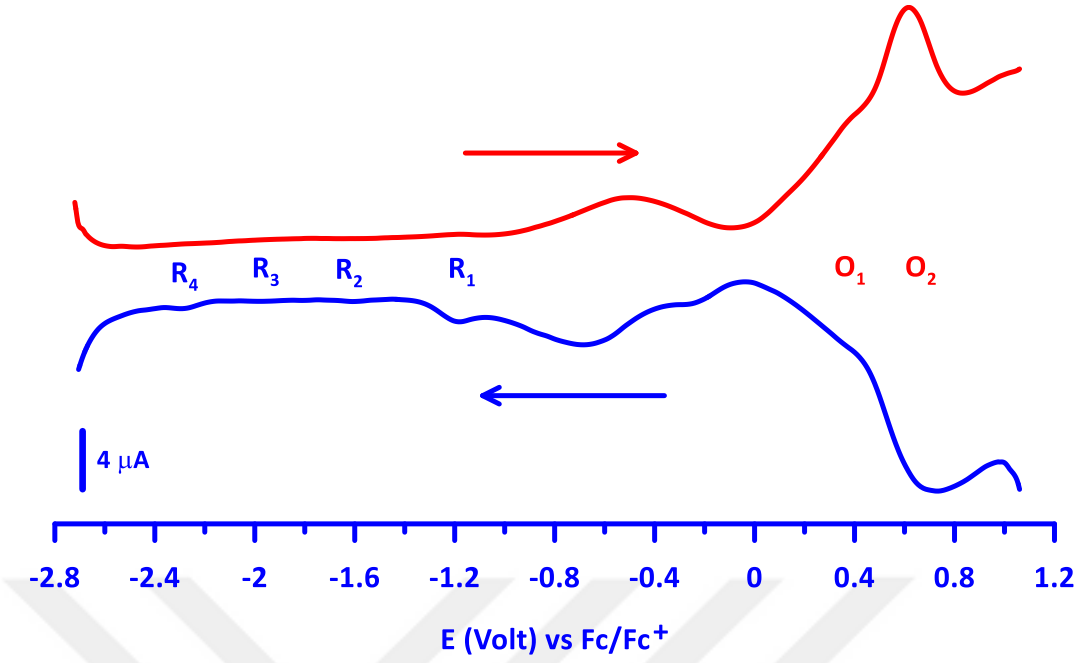

Appendix-20.7a: Square wave voltammograms of ZnPc **(11g)**,10 Hz, pulse size 25 mV, scan directions are shown by arrow.

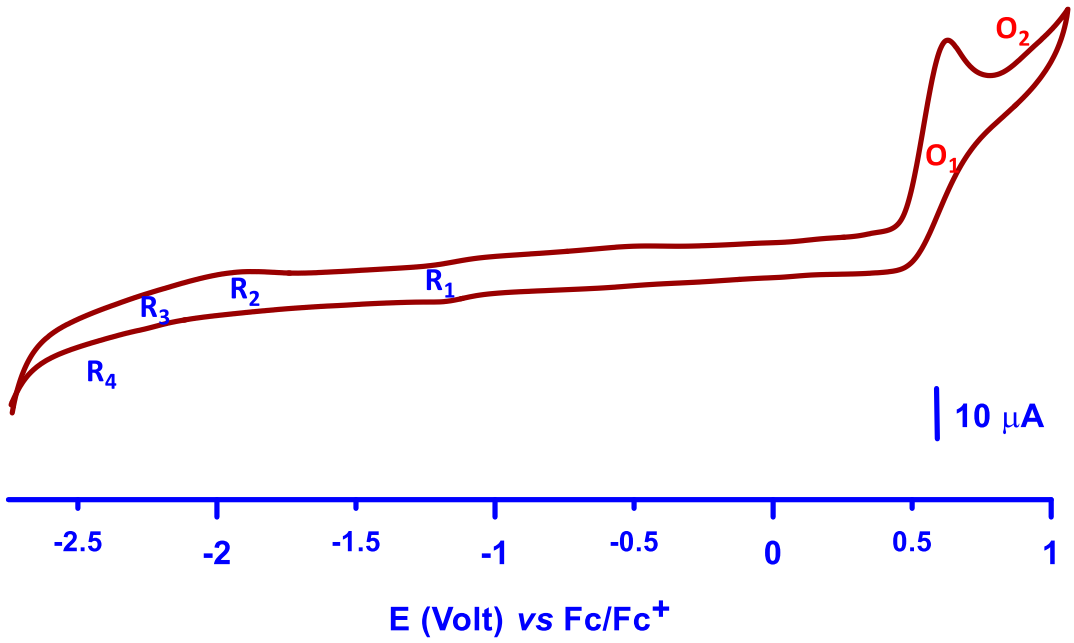

Appendix-20.7b: Cyclic voltammograms of ZnPc **(11g)** in DMF, scan rate 100 mV s^{-1}.

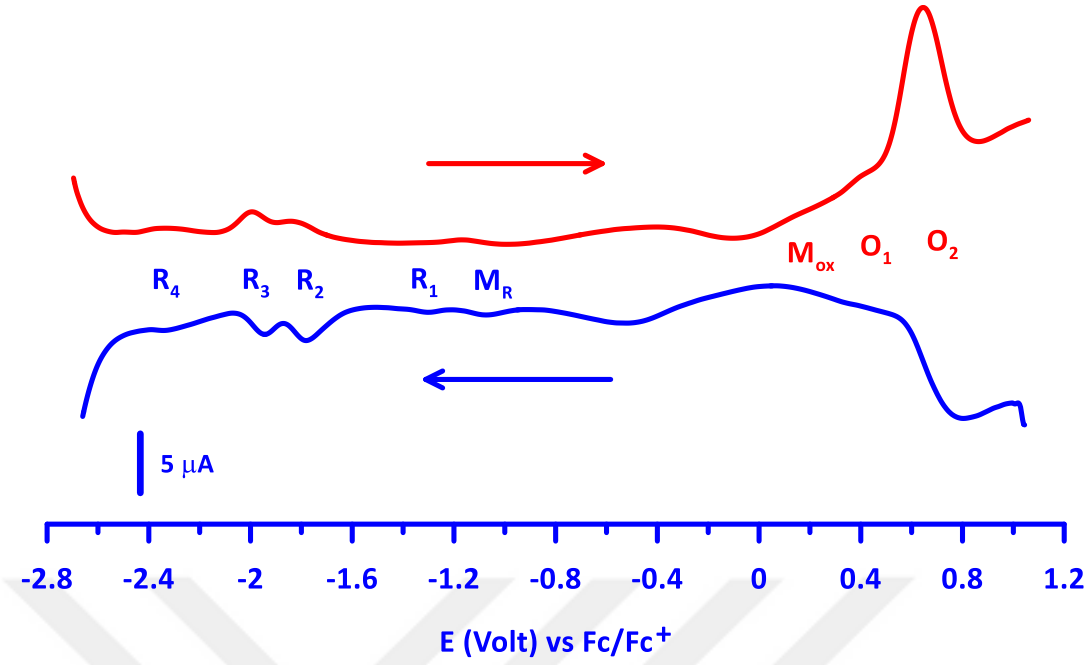

Appendix-21.1a: Square wave voltammograms of CrPc **(13a)**,10 Hz, pulse size 25 mV, scan directions shown by arrow.

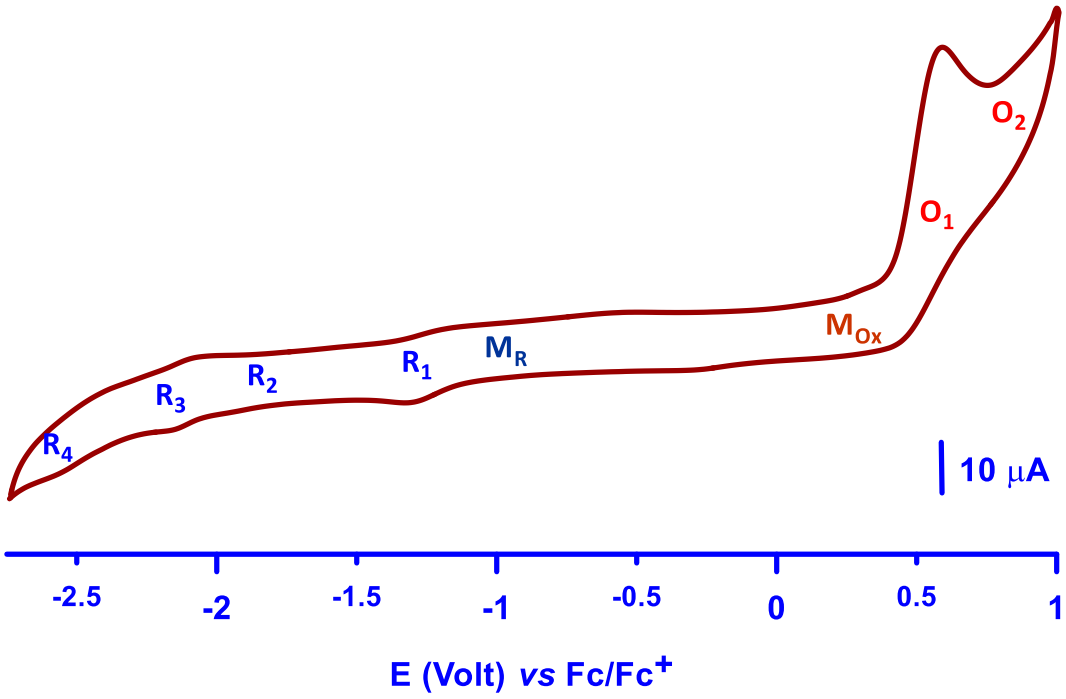

Appendix-21.1b: Cyclic voltammograms of CrPc **(13a)** in DMF, scan rate 100 mV s^{-1}.

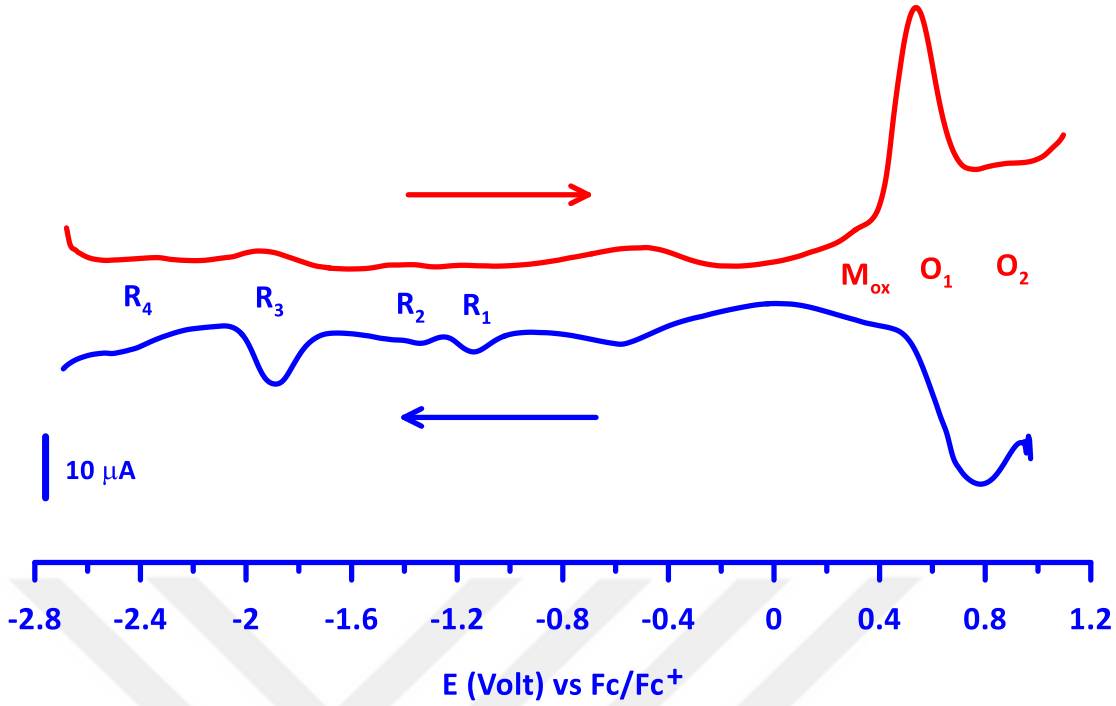

Appendix-21.2a: Square wave voltammograms of MnPc **(13b)**,10 Hz, pulse size 25 mV, scan directions shown by arrow.

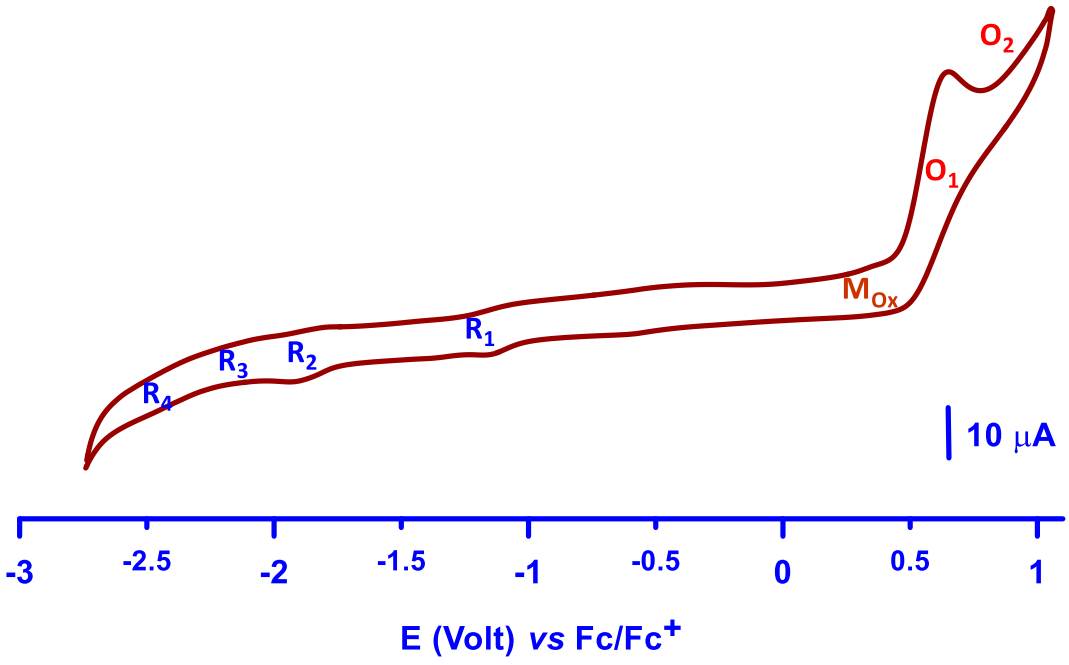

Appendix-21.2b: Cyclic voltammograms of MnPc **(13b)** in DMF, scan rate 100 mV s^{-1}.

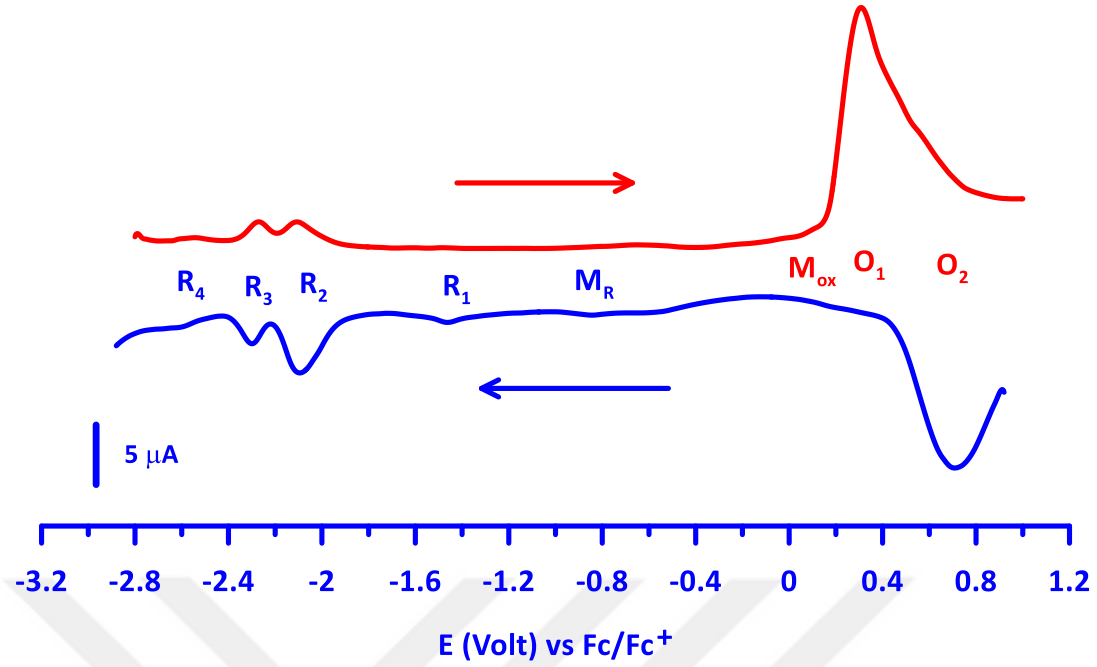

Appendix-21.3a: Square wave voltammograms of FePc **(13c)**,10 Hz, pulse size 25 mV, scan directions shown by arrow.

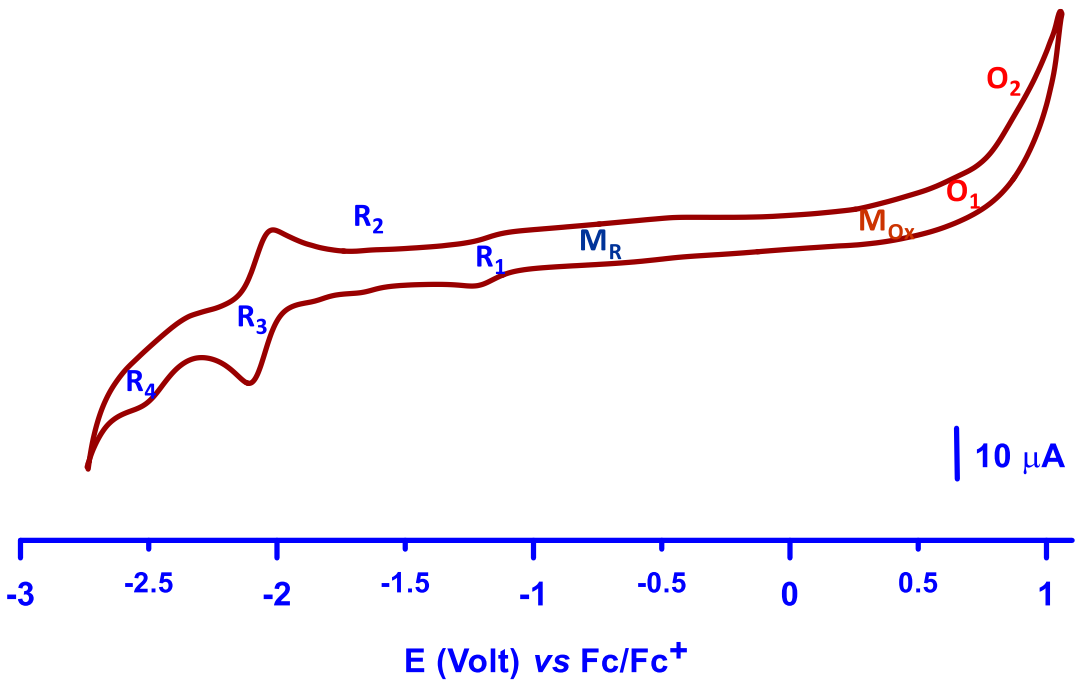

Appendix-21.3b: Cyclic voltammograms of FePc **(13c)** in DMF, scan rate 100 mV s^{-1}.

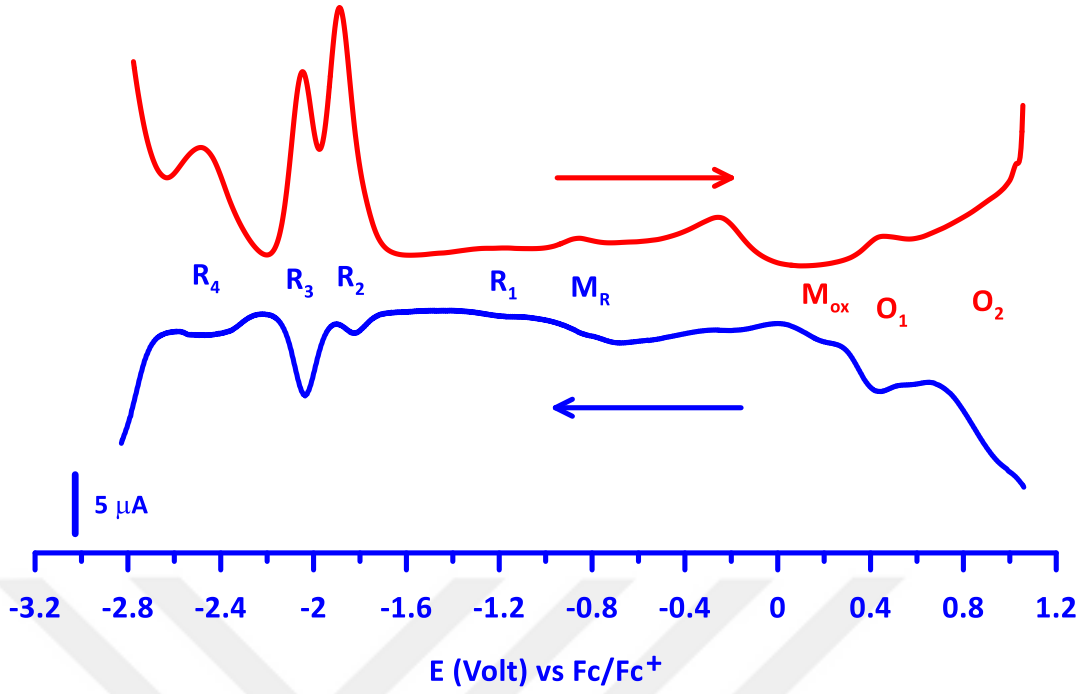

Appendix-21.4a: Square wave voltammograms of CoPc **(13d)**,10 Hz, pulse size 25 mV, scan directions shown by arrow.

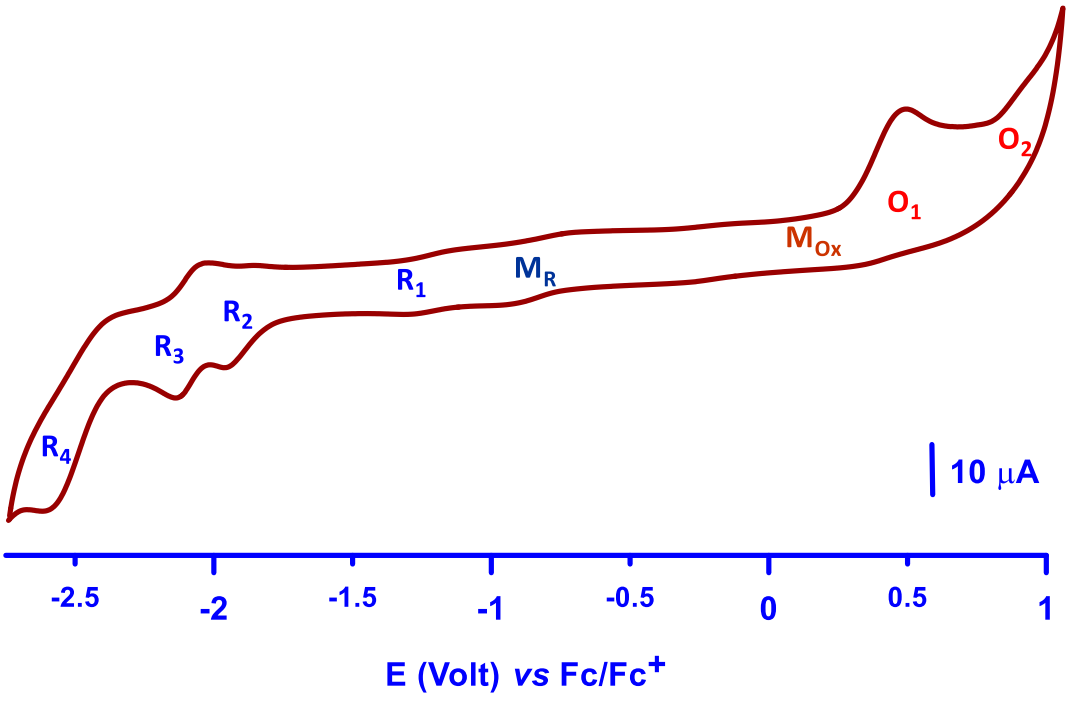

Appendix-21.4b: Cyclic voltammograms of CoPc **(13d)** in DMF, scan rate 100 mV s^{-1}.

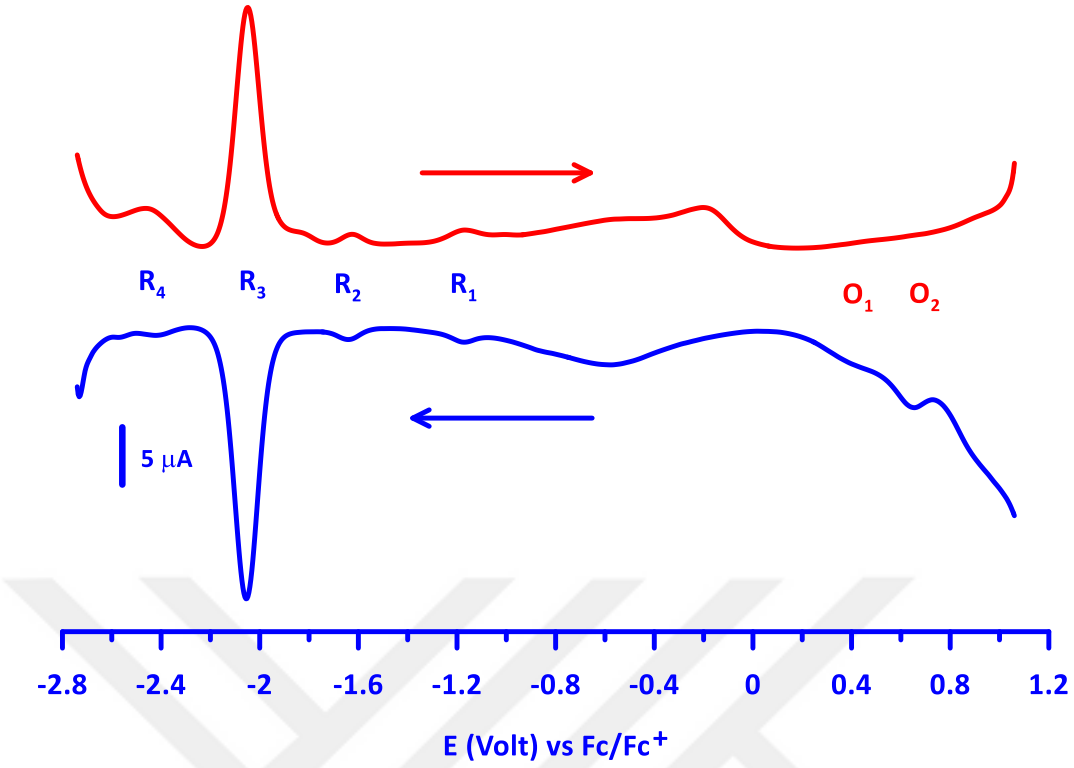

Appendix-21.5a: Square wave voltammograms of NiPc **(13e)**,10 Hz, pulse size 25 mV, scan directions are shown by arrow.

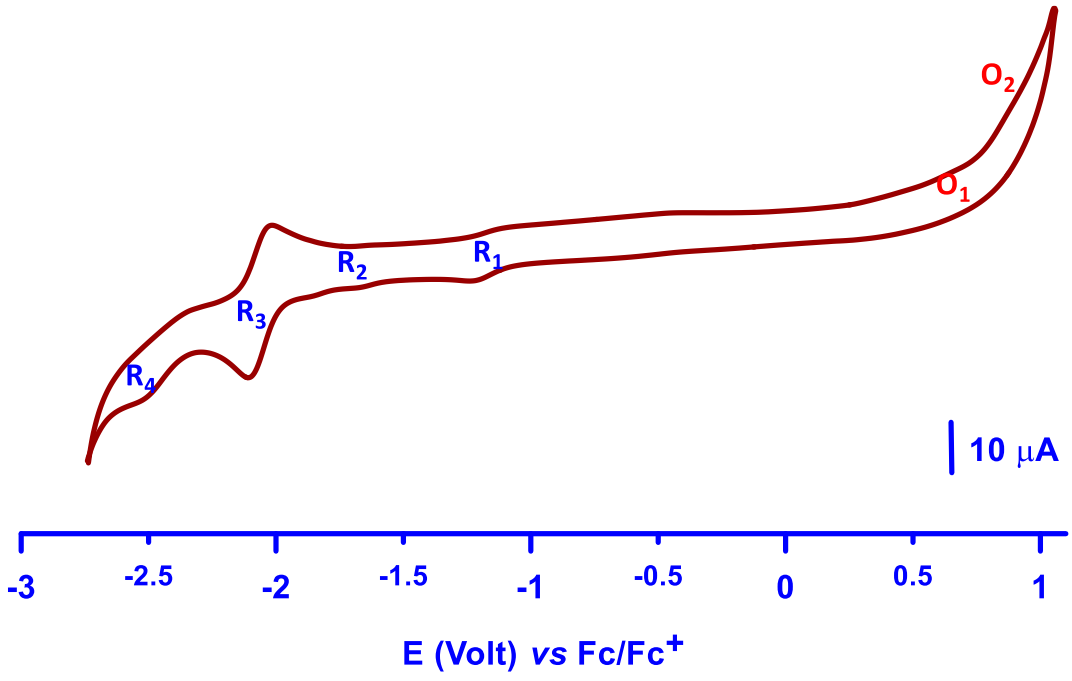

Appendix-21.5b: Cyclic voltammograms of NiPc **(13e)** in DMF, scan rate 100 mV s^{-1}.

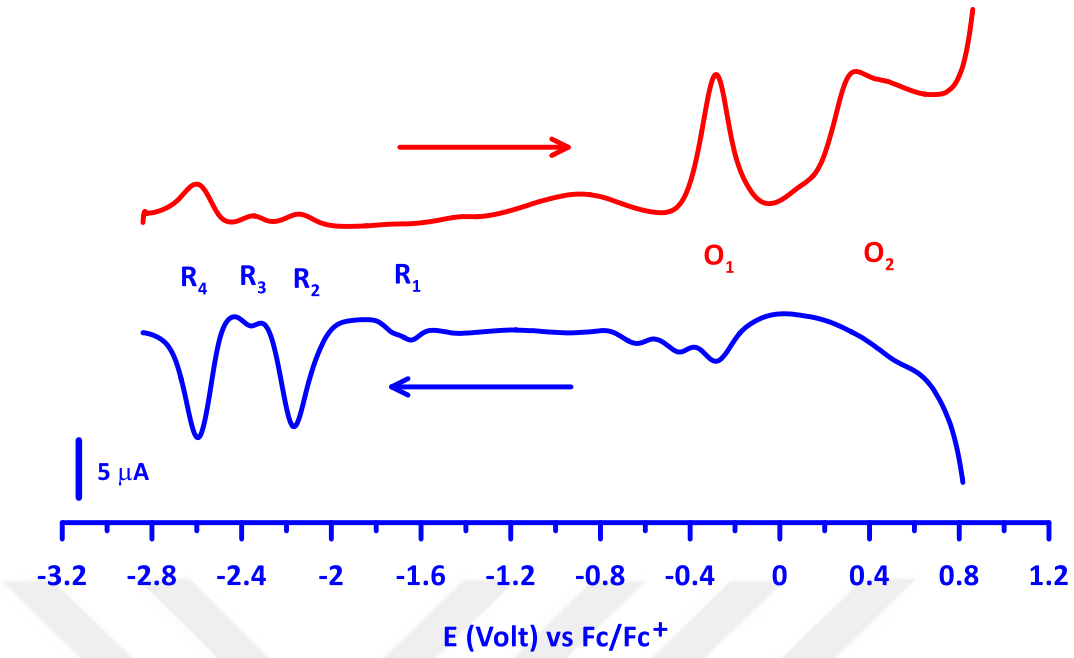

Appendix-21.6a: Square wave voltammograms of CuPc **(13f)**,10 Hz, pulse size 25 mV, scan directions are shown by the arrow.

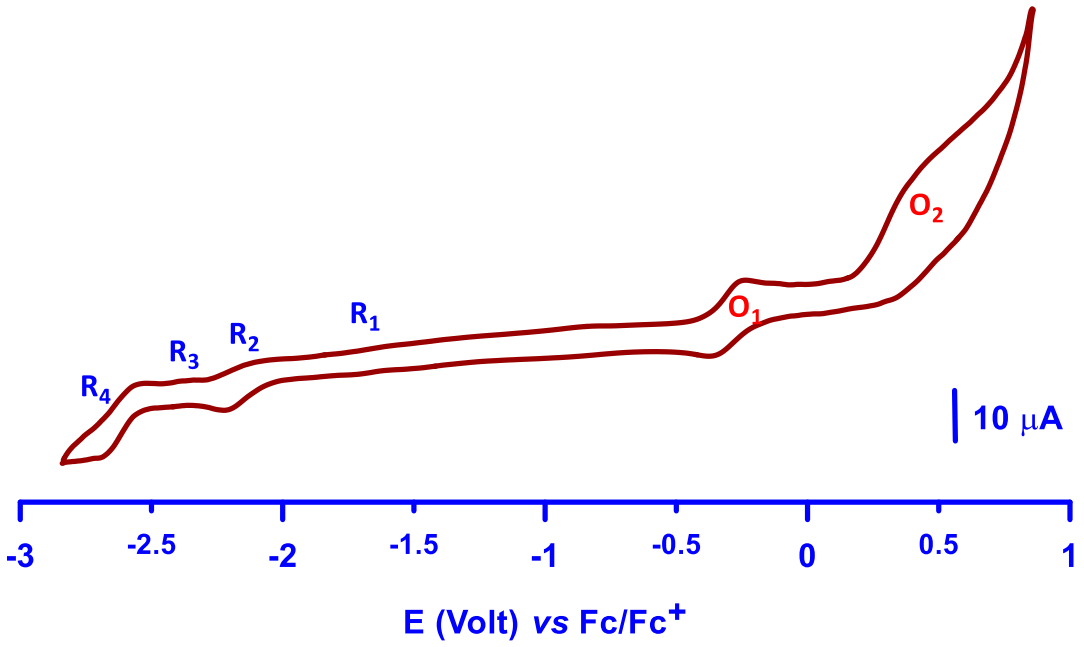

Appendix-21.6b: Cyclic voltammograms of CuPc **(13f)** in DMF, scan rate 100 mV s^{-1}.

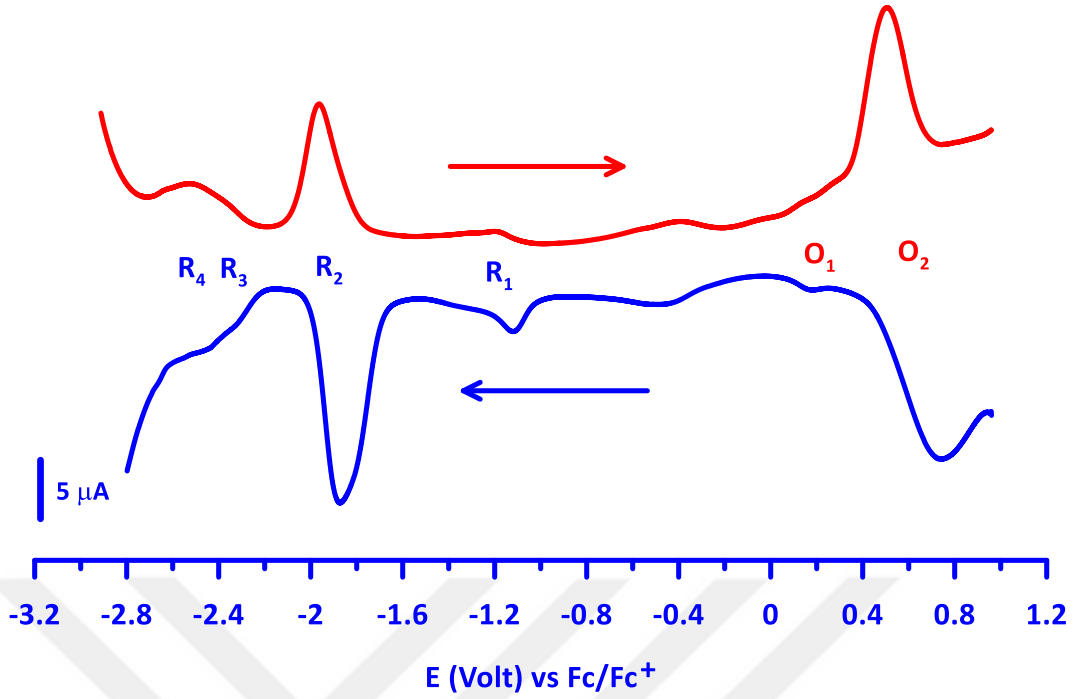

Appendix-21.6a: Square wave voltammograms of ZnPc **(13g)**,10 Hz, pulse size 25 mV, scan directions are shown by the arrow.

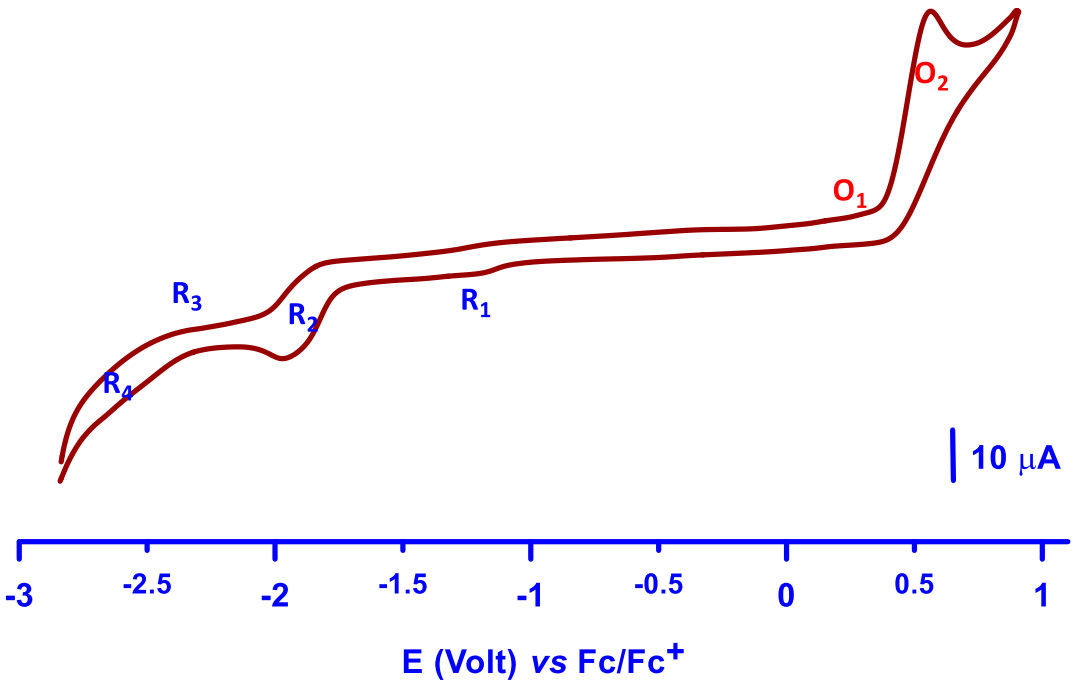

Appendix-21.6b: Cyclic voltammograms of ZnPc **(13g)** in DMF, scan rate 100 mV s^{-1}.

CURRICULUM VITAE

Sunusi IDRIS

[redacted]

ACADEMIC ACTIVITIES

Paper:

1. Idris, S.; Ndukwe, G.; Gimba, C. (2009). Preliminary phytochemical screening and antimicrobial activity of seed extracts of *Persea americana* (avocado pear). *Bayero Journal of Pure and Applied Sciences*, 2(1), 173-176. doi:10.4314/bajopas. v2i1.58538.

2. Tijjani, A; Sallau, M.S.; Sunusi, I. (2011). Synergistic Activity of Methanolic Extract of *Adenium obesum* (Apocynaceae) Stem-Bark and Oxytetracycline against Some Clinical Bacterial Isolates. *Bayero Journal of Pure and Applied Sciences*, 4(1), 79-82. doi:10.4314/bajopas. v4i1.18

3. Sunusi, I. (2014). In-vitro synergistic activity of *Euphorbia balsamifera* root extract and Ampiclox against some pathogenic bacterial isolate. *Journal of Emerging Trends in Engineering and Applied Sciences*, 5(8), 227-229.

4. Idris, S., E. Çalışkan, and S. SAYDAM, (2024): Synthesis, Thermal and Electrochemical Properties of Dipeptide Substituted Metallo-Phthalocyanine Complexes. *MW Journal of Science*, 2024. 1(3): p. 25-40.

5. Isah Nasidi, I., Muhammad, A., Idris, S. (2024). A Computational Study to Explore the Possibility of Doping in Ascorbic to Increase Its Efficiency: A Theoretical Study. *MW Journal of Science*, 1(2), 27–40. https://doi.org/10.5281/zenodo.13350136

Proceedings:

1. I., Sunusi; Sunusi, Y. H.; U., Nura (2013): Synergistic activity of methanolic extract of *Euphorbia balsamifera* Root and Ampiclox against some pathogenic bacteria isolation. 36th Annual International Conference, Workshop and Exhibition Niger, 2013, *Chemical Society of Nigeria (CSN)*: 16th - 20th September 2013, Justice Legbo Kutigi International Conference Centre, Minna, Niger state, Nigeria

2. S. Y., Hussaini, I., Sunusi, S., Sani. (2013): Synthesis, analysis, and antimicrobial activities of Schiff base derived from Salicylaldehyde and aniline. 36th Annual International Conference, Workshop and Exhibition Niger, 2013, *Chemical Society of Nigeria (CSN)*: 16th - 20th September 2013, Justice Legbo Kutigi International Conference Centre, Minna, Niger state, Nigeria.